ÉCOLE DE TECHNOLOGIE SUPÉRIEURE
UNIVERSITÉ DU QUÉBEC

MANUSCRIPT-BASED THESIS PRESENTED TO
ÉCOLE DE TECHNOLOGIE SUPÉRIEURE

IN PARTIAL FULFILLMENT OF THE REQUIREMENTS FOR
THE DEGREE OF DOCTOR OF PHILOSOPHY
Ph.D.

BY
Marc-Antoine FORTIN

ROBUSTNESS TECHNIQUES FOR GLOBAL NAVIGATION SATELLITE SYSTEMS (GNSS) RECEIVERS

MONTREAL, NOVEMBER 6, 2015

BOARD OF EXAMINERS

THIS THESIS HAS BEEN EVALUATED

BY THE FOLLOWING BOARD OF EXAMINERS

Mr. René Jr Landry, Thesis Supervisor
Department of Electrical Engineering at École de technologie supérieure

Mrs. Ruxandra Botez, President of the Board of Examiners
Department of Automated Manufacturing at École de technologie supérieure

Mr. David Bensoussan, Member of the jury
Department of Electrical Engineering at École de technologie supérieure

Mr. Olivier Julien, External Evaluator
École Nationale de l'Aviation Civile

THIS THESIS WAS PRESENTED AND DEFENDED

IN THE PRESENCE OF A BOARD OF EXAMINERS AND THE PUBLIC

ON SEPTEMBER 11, 2015

AT ÉCOLE DE TECHNOLOGIE SUPÉRIEURE

FOREWORD

Averna's Universal Receiver Tester (URT) is an instrument used to test telecommunications products with analog or digital protocols for audio, video or a combination thereof. To better suit the automotive industry requirements, the URT was expanded to satellite positioning as well as Traffic Message Channel (TMC) over Radio Data System (RDS). In the context of an industrial partnership with Averna, I started a Ph. D. at the "Laboratoire des technologies Spatiales, Systèmes Embarqués, Navigation et Avionique" (LaSSENA), under the supervision of Prof. René Jr Landry, in the field of satellite navigation.

Indeed, Global Positioning System (GPS) was evolving into Global Navigation Satellite System (GNSS), encompassing many international initiatives for new and modernized constellations for global, regional, augmentation and restricted services. This planned service availability led to international cooperation and agreements to favour signals interoperability and compabitility. On the other hand, patent requests have be submitted on the signals definition, which could have compromised deployment efforts. There was also struggles in terms of out-of-band interferences and bandwidth usage.

To add even more to this technologic turmoil, most of the initial satellite launch schedules slipped, delaying new signals availability to a point where the European Galileo came close to lose its broadcasting right in one of its assigned bands. The American GPS modernized signals deployment was also delayed due to a longer life expectancy of its current satellites. In the case of the Chinese BeiDou (also known as COMPASS) and Russian GLONASS, some signal definitions are still pending confirmation and public disclosure for their third phase.

Changes have also impacted my initial plans, taking advantage of many opportunities, such as spending a semester at the Universität der Bundeswehr München in Germany, participating to the International GNSS Summer School, attending different conferences, workshops and trainings, presenting papers and posters as well as giving classes to graduates as a junior lecturer at École de technologie supérieure (ÉTS). I was also deeply involved in a patent application, which was granted.

I was also involved in migrating the Graphical User Interface from Visual Basic 6.0 to .Net, automating the measurements reporting, configuring the receiver into different operation modes, decoding the different navigation messages, designing and implementing a GLONASS software only simulator, introducing a multipath characterization method, which are not further presented herein.

I am grateful for the richness brought by all these experiences, although I may have spent longer in completing my degree.

ACKNOWLEDGEMENTS

Accepting a new challenge always comes with a set of unknowns... Mainly, one knows when it starts, but not always when it ends! Hence, for having coped with my constraining occupation over the past years, I would like to thank my girlfriend, who throughout the process became my wife and the mother of my children.

Undertaking such a challenge is greatly facilitated with the financial support from the Industrial Innovation Scholarship - BMP Innovation FQRNT-NSERC with the participation of Averna. I would like to especially thank Yanique Martin and Dominique Fortin, who have been very supportive and comprehensive. I am grateful for all the opportunities that were made available to me. I would also like to thank Iurie Ilie and Stéphane Hamel, whom I have been corroborating my ideas with.

At the laboratory, my experience was very stimulating thanks to colleagues such as Jean-Christophe Guay and Dave Côté, as well as Kaveh Mollaiyan, Philippe Lavoie, Nick Liu, Guillaume Lamontagne, Thomas Delaporte and Bruno Sauriol, with whom I have closely worked with. I would also like to thank Jérôme Leclère for his valuable feedback in finalizing my thesis and defense presentation and many other students during their work terms, especially Francis Bourdeau. Together, we have taken the receiver where it had never been before!

Finally, but not least, I would like to thank my thesis director for providing me with all the latitude I needed to 1) develop, test and integrate new functionalities; 2) organize, manage and lead other students; 3) publish, present and defend my findings as well as to review those of others and 4) popularize technical notions, describe them through academic examples, assess and evaluate knowledge. Otherwise, I would not be who I became.

The whole experience had a significant impact on my academic and professional lives in terms of both technical and commercial knowledge acquisition, as well as of meeting with an important network of worldwide known experts in complementary fields, a few of which I have also been collaborating with.

TECHNIQUES DE ROBUSTESSE DES RÉCEPTEURS POUR LES SYSTÈMES GLOBAUX DE NAVIGATION SATELLITAIRE (GNSS)

Marc-Antoine FORTIN

SUMMARY

Depuis plusieurs années, le monde de la navigation satellitaire connait une évolution constante. Son engouement a connu un fort essor au tournant du siècle, donnant lieu à une multitude d'applications automatisées, tant aux niveaux commercial qu'industriel et ce, dans des domaines aussi variés que l'agriculture, la construction, la sécurité et les transports de tout genre. Grâce à l'intégration avec des technologies complémentaires et à des seuils atteints de précision toujours plus petits, la navigation parvient aussi à percer des marchés initialement incompatibles tels que dans des environnements hostiles et des endroits confinés (p. ex. au milieu de canyons urbains, à l'intérieur de bâtiments, sous la canopée, etc.). En effet, les récentes avancées technologiques et algorithmiques permettent d'atténuer, voire résoudre, les limitations traditionnelles du GPS, soient la disponibilité, l'intégrité, la précision et la résistance aux interférences.

Avec autant de variété et de changements, une approche universelle et flexible est préconisée comme structure de base d'un récepteur de géopositionnement. Les présents travaux portent donc sur des architectures universelles de tels canaux, en passant par différents modules matériels composant un récepteur de navigation par satellites. Bien qu'indispensables, les modules radiofréquence en amont et logiciels en aval de ces canaux excèdent la portée de cet ouvrage.

À la suite d'une revue exhaustive des spécificités de chacun des signaux de géopositionnement, une liste des techniques de poursuite de ces signaux est classifiée. Ces informations imposent les requis d'architecture des canaux universels visés, qui sont morcelés en trois et répartis en autant d'articles : 1) acquisition dans le domaine fréquentiel, 2) poursuite par corrélation avec une réplique local fidèle et 3) augmentation de la solution avec corrections différentielles. Viennent ensuite différents outils d'analyse et de configuration du récepteur pour en faire une plate-forme de développement flexible et efficace, dont le décodage des messages de navigation, différentes approches du calcul du rapport de signal à bruit et un niveau variable de quantification du signal entrant.

Puisque le projet est ambitieux, la validation est basée sur de l'expérimentation avec des signaux réels, évitant ainsi le recours à l'élaboration additionnelle de simulateurs complexes de différentes constellations multifréquentielles. Les impacts et retombées de cette recherche gratifiée d'un brevet sont considérables, surtout avec la croissance exponentielle du marché de l'électronique mobile et portable.

Cet ouvrage s'ouvre sur une vieille problématique renouvelée, à savoir la sélection de signaux (plutôt que celle des satellites). Celle-ci est ravivée par la mise à profit des canaux universels pour minimiser le temps d'acquisition tout en maximisant la robustesse de la solution par le passage progressif des anciens signaux aux plus récents. De surcroît, cette flexibilité des canaux pave la voie des récepteurs cognitifs et tactiques en leur permettant de s'adapter à leur environnement ou condition fréquentielle.

Mots clés: GNSS, Acquisition, Poursuite, Augmentation

ROBUSTNESS TECHNIQUES FOR GLOBAL NAVIGATION SATELLITE SYSTEMS (GNSS) RECEIVERS

Marc-Antoine FORTIN

ABSTRACT

The world of satellite navigation has known a constant evolution for several years. At the turn of the century, its craze resulted in a multitude of automated applications being released in both the commercial and industrial markets. All this occurred in areas as diverse as agriculture, construction, security and transport of all kinds. Through integration with complementary technologies and ever smaller achieved accuracy thresholds, geopositioning also managed to break through initially incompatible markets, such as hostile environments and confined spaces (e.g. in urban canyons, inside buildings, under the canopy, etc.). Indeed, recent technological and algorithmic advances can now mitigate or solve the traditional limitations of GPS, namely availability, integrity, accuracy and resistance to interference.

With so much variety and changes, a universal and flexible approach is best suited as a basic structure of a satellite navigation receiver. The work herein therefore focuses on universal architectures for such channels, through various hardware modules forming the receiver. Although indispensable, upstream radio frequency modules and downstream software in navigation receivers are beyond the scope of this thesis.

Following a comprehensive review of the specificities of each satellite signal, a list of their associated tracking techniques is classified. This information sets the stage for the architecture requirements of the targeted universal channels, which are broken up into three and divided into as many papers: 1) frequency domain acquisition, 2) match filter tracking and 3) solution augmentation with differential corrections. Various analyses and receiver configuration tools enabling a flexible and efficient development platform are then presented, including the decoding of navigation messages, different approaches to compute the signal to noise ratio and the quantification level of the incoming signal.

Since the project is ambitious, validation is based on experimentation with real signals, thus avoiding the additional development of complex multifrequency simulators for different constellations. Impacts and benefits of this patent-rewarded research are considerable, especially with the exponential growth of the market for mobile and wearable electronics.

The thesis opens with a renewed old problem, namely the signal selection (rather than the satellite selection). It is revived by leveraging the universal channels to minimize the acquisition time with old signals, while maximizing the robustness of the solution by the gradual transition to modernized and new signals. In addition, this channel flexibility paves the way for cognitive and tactical receivers, enabling them to adapt to their environment or frequency conditions.

Keywords: GNSS, Acquisition, Tracking, Augmentation

TABLE OF CONTENTS

Page

INTRODUCTION 1

CHAPTER 1 SIGNAL MODULATION AND AUTO-CORRELATION FUNCTION BACKGROUND FOR TRACKING LOOPS 13
1.1 BPSK Correlation 13
1.2 BOC Correlation 16
1.3 Early-Late Processing 19
1.4 Code Phase Jitter 29
1.4.1 Coherent EML 32
1.4.2 Non-Coherent EMLP 34
1.4.3 Non-Coherent DP 37
1.5 Modulations and Auto-correlation Summary 39

CHAPTER 2 SURVEY OF GNSS SIGNALS 41
2.1 GPS Constellation 41
2.1.1 GPS L1 C/A 46
2.1.2 GPS L1C 51
2.1.3 GPS L2C 54
2.1.4 GPS L5 57
2.1.5 GPS summary 58
2.2 GLONASS Constellation 59
2.2.1 CDMA-compliant modernized GLONASS signals 63
2.2.2 GLONASS Summary 64
2.3 Galileo Constellation 64
2.4 BeiDou Constellation 67
2.5 GNSS Civil Signals Summary 69

CHAPTER 3 PROPAGATION MEDIUM AND SIGNAL PROCESSING IMPACTS ON NAVIGATION SIGNALS 73
3.1 Propagation Medium Error Sources 73
3.1.1 Atmosphere Impacts 73
3.1.1.1 Ionosphere 74
3.1.1.2 Troposphere 76
3.1.2 Multipath 76
3.1.3 RF Interference 77
3.1.4 Propagation Model 78
3.2 Receiver Error Sources 80
3.2.1 Receiver Front-End 80
3.2.2 Receiver Tracking Channels 83
3.2.3 Signal and Noise Quantification 83

3.2.3.1 Calibration channel 85
3.2.3.2 Real Signal - Complex Noise 88
3.2.3.3 Beaulieu 88
3.2.3.4 Signal to Noise Variance 89
3.2.3.5 Moment Method 89
3.2.3.6 Narrowband-Wideband Power Radio 89
3.2.3.7 Variance Summing Method 90
3.2.3.8 Weighted Bandwidths Ratio 90
3.2.3.9 Methods Comparison 93
3.3 Signal Impairment Sources Summary 93

CHAPTER 4 EXISTING TRACKING ARCHITECTURES LITERATURE REVIEW 95
4.1 BPSK-like 96
4.2 Multi-correlators 96
4.3 Code Correlation Reference Waveforms 98
4.4 Sub-Carrier Correlation Cancellation 102
4.5 Side Peak Cancellation 103
4.6 Multi-Loops 106
4.7 Frequency-Domain 108
4.8 BOC Tracking Architectures Summary 109

GENERAL CONCLUSION 111

APPENDIX I PAPER #1: FORTIN *ET AL.* (2015) 117

APPENDIX II PAPER #2: FORTIN AND LANDRY (2016) 137

APPENDIX III PAPER #3: FORTIN *ET AL.* (2014) 165

BIBLIOGRAPHY 180

LIST OF TABLES

Page

Table 2.1 GNSS Constellations 70

Table 2.2 SBAS Constellations 71

Table 2.3 Regional Navigation Satellite Systems constellations 71

Table 2.4 GRANSS Open Signals on L1/G1 72

Table 3.1 Typical Pseudorange Error Sources [m] Taken from Trimble Navigation Limited (2007) 80

LIST OF FIGURES

Page

Figure 0.1 GNSS Application Fields 1

Figure 0.2 GNSS Weaknesses 4

Figure 0.3 GNSS Aid 6

Figure 0.4 Navigation Solution Concepts 11

Figure 1.1 Bandwidth Effect on a Square Chip Shape 14

Figure 1.2 Coherent Bandwidth-Limited Normalized ACF of a Square Chip 15

Figure 1.3 Normalized Spectral Representation of a BPSK(1) Modulation 16

Figure 1.4 Auto-Correlation Function of a BOC(1,1) Modulated Spreading Code of Length $N = 10\,230$ and Signal Amplitude $A = 2$ 17

Figure 1.5 Normalized Spectral Representation of a BOC(1,1) Modulation 19

Figure 1.6 Bandwidth Effect on a Square BOC(1,1) Chip Shape 20

Figure 1.7 Coherent Bandwidth-Limited Normalized ACF of a Square BOC(1,1) Chip 20

Figure 1.8 BPSK Tracking Loop PLL [blue], DLL [red], Data [green] 21

Figure 1.9 Non-Coherent (Power) Bandwidth-Limited Normalized BPSK(1) ACF of a Square Chip 23

Figure 1.10 Non-Coherent (Power) Bandwidth-Limited Normalized BOC(1,1) ACF of a Square Chip 23

Figure 1.11 Coherent Infinite Bandwidth BPSK(1) Early Minus Late Normalized Discriminator S-curve Details 25

Figure 1.12 Coherent Infinite Bandwidth BPSK(1) Early Minus Late Normalized Discriminator Curves 26

Figure 1.13 Non-Coherent Bandwidth-Limited BPSK(1) Early Minus Late Power Normalized Discriminator S-curves 26

Figure 1.14 Non-Coherent Bandwidth-Limited BOC(1,1) Early Minus Late Power Normalized Discriminator S-curves 27

Figure 1.15 Non-coherent Infinite-bandwidth BPSK(1) Early Minus Late Power Normalized Discriminator Curves 28

Figure 1.16 Non-coherent Infinite-bandwidth BOC(1,1) Early Minus Late Power Normalized Discriminator Curves 28

Figure 2.1 GNSS Signals 42

Figure 2.2 Ground Track of a GPS Satellite over 24 h Taken from Barmettler (2015) 45

Figure 2.3 GPS Satellite ECEF Position [m] over 1 Ground Track Period 45

Figure 2.4 ACF of a Rectangular NRZ Spreading Code with Length $N = 1023$ and Signal Amplitude $A = 2$ 48

Figure 2.5 Power Spectral Densities of GPS L1 C/A 49

Figure 2.6 Zoom on the Power Spectral Densities of GPS L1 C/A 49

Figure 2.7 TMBOC Pilot Sub-Carriers Assignation Pattern Adapted from ARINC Engineering Services (2013, Figure 3.3-2) 52

Figure 2.8 MBOC Definition Through its Spectrum 53

Figure 2.9 TMBOC Impact on ACF Taken from Ávila Rodríguez (2014) 53

Figure 2.10 Spectral Representation of the GLONASS L1 FDMA Modulation Scheme 62

Figure 2.11 ACF Shape Modulated by Cosine Wave with $g \cdot \frac{562.5}{511}$ period/chip, after Frequency Shifting the Local Code 63

Figure 2.12 Ground Track of COMPASS-M1 MEO Satellite over 24 h Taken from Barmettler (2015) 68

Figure 3.1 RF Amplification and Splitting of a Single Antenna Adapted from Côté and Andrianarison (2013, Figure 2) 82

Figure 3.2 RF to IF Down-Conversion Stage Adapted from Côté and Andrianarison (2013, Figure 5) 82

Figure 4.1 Bump and Jump Tracking Loop Overhead (red dashed lines) over BPSK 97

Figure 4.2 Code Correlation Reference Waveforms Tracking Loop Delta (red dashed lines) vs. BPSK 100

Figure 4.3 CCRW Prompt and Discriminator Replicas 100

Figure 4.4 BOC$(1,1)$ ACF Sub-Carrier Correlation Cancellation Taken from Sauriol (2008, Figure 4.10) 103

Figure 4.5 Side Peak Cancellation Principle 105

Figure 4.6 Autocorrelation Side-Peak Cancellation Technique Tracking Loop Delta (red dashed lines) vs. BPSK 105

Figure 4.7 Dual Estimator Complementary Estimates 107

Figure 4.8 Triple Loop Dual Estimator Tracking Loop Overhead (red dashed lines) vs. BPSK 107

Figure 4.9 Symmetric Phase-Only Matched Filter Loop Overhead (red dashed lines) vs. BPSK 109

Figure 4.10 Symmetric Phase-Only Matched Filter Loop Overhead (red dashed lines) vs. BPSK 109

LIST OF ABREVIATIONS

ABAS	Aircraft Based Augmentation Systems
ACF	Auto-Correlation Function
ADAS	Advanced Driving Assistance Systems
ADC	Analog to Digital Converter
AESS	Aerospace and Electronic Systems Society
AGC	Automatic Gain Control
APME	A-Posteriori Multipath Estimation
ARNS	Aeronautical Radio Navigation Services
ASIC	Application Specific Integrated Circuit
ASZ	Autocorrelation Sidelobe Zero
BCH	Bose, Chaudhuri, and Hocquenghem
BL	Beaulieu
BOC	Binary Offset Carrier
BPSK	Binary Phase Shift Keying
BW	BandWidth
CASI	Canadian Aeronautics and Space Institute
cBOC	cosine BOC
CBOC	Complex BOC
CC	Convolutional Coding

CCF	Cross-Correlation Function
CCRW	Code Correlation Reference Waveforms
CDMA	Code Division Multiplexing Access
CELP	Coherent Early-Late Processing
CGCS	China Geodetic Coordinate System
CL	Civilian Long
CM	Civilian Moderate
CNAV	Civil NAVigation message
CPC	Code Plus Carrier
CTRS	Conventional Terrestrial Reference System
CRC	Cyclic Redundancy Check
CWI	Continuous Wave Interference
C/A	Coarse Acquisition
C/N_0	Carrier power to Noise density
DBZP	Double Block Zero Padding
DD	Double Delta
DLL	Delay Lock Loop
DGPS	Differential GPS
DoD	Department of Defense
DoP	Dilution of Precision

DME	Distance Measurement Equipment
DP	Dot Product
ECEF	Earth Centered Earth Fixed
EFIS	Electronic Flight Instrument System
EGNOS	European Geostationary Navigation Overlay Service
EMLP	Early Minus Late Power
Eq	Equation
ÉTS	*École de technologie supérieure*
EU	European Union
FASF	Fast Ambiguity Search Filter
FARA	Fast Ambiguity Resolution Approach
FDMA	Frequency Division Multiplexing Access
FEC	Forward Error Correction
FFT	Fast Fourier Transform
FT	Fourier Transform
FMS	Flight Management System
FOC	Full Operational Capability
FPGA	Field-Programmable Gate Array
GAGAN	GPS Aided Geo Augmented Navigation
GBAS	Ground-Based Augmentation System

GEO	GEostationary Orbit
GIOVE	Galileo IOV Element
GIS	Geographic Information System
GNSS	Global Navigation Satellite System
GPS	Global Positioning System
GPU	Graphics Processing Unit
GRANSS	Global, Regional and Augmentation Navigation Satellite Systems
GRAPHIC	Group and Phase Ionosphere Correction
GRAS	Ground-based Regional Augmentation System
GSO	GeoSynchronous Orbit
GTRF	Galileo Terrestrial Reference Frame
GUI	Graphical User Interface
HCS	High-Cut S-curve
HEAD-Start	Highly Efficient Acquisition Degree Start
HEO	Highly Elliptical Orbit
HRC	High Resolution Correlators
ICD	Interface Control Document
ICRS	International Celestial Reference System
IF	Intermediate Frequency
IFFT	Inverse Fast Fourier Transform

IGSO	Inclined GSO
iid	independent and identically distributed
ION	Institute of Navigation
IOV	In-Orbit Validation
IEEE	Institute of Electrical and Electronics Engineers
IERS	International Earth Rotation Service
INS	Inertial Navigation System
IRM	IERS Reference Meridian
IRNSS	Indian Regional Navigational Satellite System
IS	Interface Specification
ITRS	International Terrestrial Reference System
ITU	International Telecommunication Union
LAAS	Local Area Augmentation System
LAMBDA	Least-squares AMBiguity Decorrelation Adjustment
LaSSENA	Laboratoire des technologies Spatiales, Systèmes Embarqués, Navigation et Avionique
LBS	Location Based Services
LDPC	Low Density Parity Check
LFSR	Linear Feedback Shift Register
LNA	Low Noise Amplifier
LO	Local Oscillator

LoS	Line of Sight
LSAST	Least-Square Ambiguity Search Technique
MBOC	Multiplexed BOC
MEO	Medium Earth Orbit
ML	Maximal Length
MLE	Maximum Likelihood Estimate
MM	Moment Method
MSAS	Multi-functional Satellite Augmentation System
MTTA	Mean Time To Acquire
NBP	Narrow Band Power
NC	Narrow Correlators
NCO	Numerically Controlled Oscillator
NELP	Non-coherent Early-Late Processing
NF	Noise Figure
NRZ	Non-Return to Zero
NWPR	Narrowband-Wideband Power Radio
OS	Open Service
PC	Personal Computer
PLL	Phase Lock Loop
POCS	Projection Onto Convex Sets

PPP	Precise Point Positioning
PPS	Precise Positioning Service
PRN	Pseudo Random Noise
PSD	Power Spectral Density
PVT	Position Velocity and Time
PZ	*Parametrop Zemp* or *Parametri Zemli*
QZSS	Quasi-Zenith Satellite System
RAIM	Receiver Autonomous Integrity Monitoring
RDS	Radio Data System
RF	Radio Frequency
RFI	Radio Frequency Interference
RHCP	Right Hand Circular Polarization
RMS	Root-Mean-Square
RNSS	Radio Navigation Satellite Services
RSCN	Real Signal - Complex Noise
RTK	Real-Time Kinematics
RSS	Received Signal Strength
SA	Selective Availability
sBOC	sine BOC
SBAS	Satellite-Based Augmentation System

SCPC	Sub-Carrier Phase Cancellation
SCS	S-Curve Shaping
SCM	Side-lobe Cancellation Method
SDCM	System of Differentional Correction and Monitoring
SDR	Software Defined Radio
SLL	Sub-carrier Lock Loop
SNAS	Satellite Navigation Augmentation System
SNR	Signal to Noise Ratio
SNV	Signal to Noise Variance
SoL	Safety of Life
SPOMF	Symmetric Phase-Only Matched Filter
SV	Satellite Vehicle
SVN	Satellite Vehicle Number
TEC	Total Electron Content
TK	Teager-Keaser
TLDE	Triple-Loop Dual Estimator
TMBOC	Time Multiplexed BOC
TMBPSK	Time Multiplexed BPSK
TOA	Time Of Arrival
TDOA	Time Difference Of Arrival

TMC	Traffic Message Channel
IUCAF	Inter-Union Commission on Frequency Allocation
UERE	User Equivalent Range Error
URT	Universal Receiver Tester
UTC	Universal Time Coordinated
UTO	Unambiguous Tracking Offset
VCO	Voltage Controlled Oscillator
VE	Very Early
VHF	Very High Frequency
VL	Very Late
VOR	VHF Omnidirectional Range
VSM	Variance Summing Method
WAAS	Wide Area Augmentation Systems
WBP	Wide Band Power
WBR	Weighted Bandwidths Ratio
WGS	World Geodetic System
XOR	eXclusive OR

LIST OF SYMBOLS AND UNITS OF MEASUREMENTS

A	amplitude
b_P	receiver carrier phase instrumental delay
b_P^k	satellite k carrier phase instrumental delay
b_{MP}	bias caused by multipath
B_L	single sided loop bandwidth
c	speed of light
C	carrier power
d	navigation data bit
dB	decibel
dBm	logarithmic milliwatt
dBW	logarithmic watt
D	Discriminator
E	Early
f	frequency
f_c	chipping rate
f_r	reference chipping rate
f_s	sub-carrier rate
f_S	sampling rate
F	noise factor

$\mathscr{F}$	Fourier transform
g	frequency slot number
G	gain
G_x	spectrum of x
h	hour
$H()$	transfer function
i	index
I	In-phase
I_0	modified first type Bessel function of order 0
Im	Imaginary
$\imath$	complexe unitary vector
i, j, k	indices
K	discriminator gain
km	kilometer
L	Late
m	meter
m	slope
M	wide and narrow bandwidth power ratio
min	minute
MP	multipath

ms	millisecond
n	BOC modulation rates ratio
N^k	phase cycles integer ambiguity
N	FFT samples or correlator outputs count
o	correlator complex outputs
p	first sub-carrier rate factor
P	Prompt
P_x	power of x
q	chipping rate factor
Q	Quadrature phase
r	geometric distance
r	second sub-carrier rate
$R()$	correlation
Re	Real
s	second
s	symbol
S	sample
sfu	solar flux units
S_η	noise power spectral density
T_c	chip period

T_s	sub-chip period
T_P	pre-processing integration time
V	volt
v_r	relative motion
w	wind-up factor
X	random variable
x	first component of an orthogonal coordinates system
y	second component of an orthogonal coordinates system
z	third component of an orthogonal coordinates system
α	correlator weight
$^\circ$	degree
ϕ	carrier phase
β_{fe}	front-end bandwidth
δ	half correlator spacing
Δ	correlator spacing (E - L)
Δb	satellite clock error
$\Delta\phi$	phase difference between incoming and replicate signals
ε	code tracking error
b_u	user clock bias
$\mathscr{F}$	Fourier transform

η	noise
ρ	measured pseudorange
ρ^T	true pseudorange, i.e. from user to satellite
ϕ	carrier phase measurement
ΔD	satellite position error effect on the range (i.e. along LoS)
ΔI	ionospheric delay error
ΔT	tropospheric delay error
Δv	relativistic time correction
v	receiver measurement noise error
λ	signal wavelength
μ_2	Rice's second moment
$\mathbb{R}$	Real numbers
υ	signal
σ^2	variance
τ	chip code delay
$\langle X \rangle$	expected value of X
$\bar{X}$	mean value of X
*	complex conjugate
∞	infinity
$\not{X}$	simplification of X to 1
$\not\not{X}$	simplification of X to 0

INTRODUCTION

Human kind has forever seeked for means to find its way to get “there and back again”. Lack of vital resources has further drawn people to explore beyond their known territories, striving to improve their life conditions. In today’s demanding context, being at the right place, at the right time has never been so critical. To meet and overcome these common expectations, satellite-based synchronized communications have opened the way to time-based wireless and autonomous positioning, leading to the automation of many repetitive tasks...

Until recently, navigation receivers based on open civil signals were limited to GPS L1 Coarse Acquisition (C/A). Initially, these signals were only intended for the acquisition of the more precise, but encrypted, P(Y) signals used by the U.S. military and their allies. Over the last decade, the use of GPS has spread into unforeseen applications. This increasingly popular trend has led to the integration of GPS receivers into everyday-life products in fields as varied as transportation, communications, tourism, emergency services and many more, as seen in Figure 0.1.

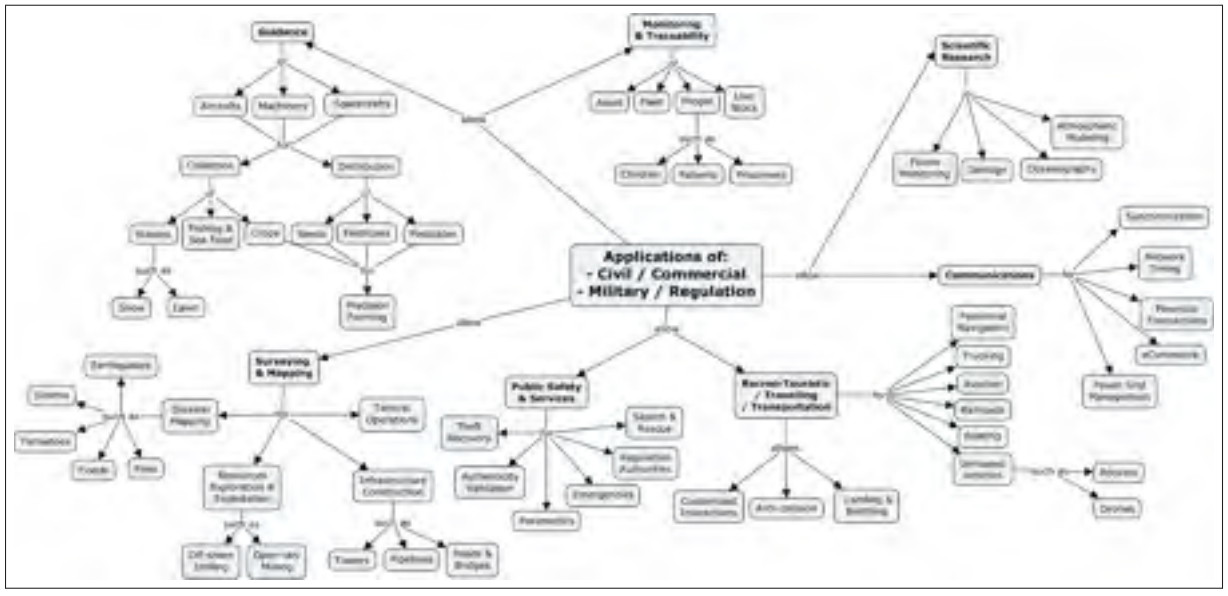

Figure 0.1 GNSS Application Fields

This development took place while GPS modernization had barely started and the GLONASS constellation was still not usable. Today, civil users can take advantage of a full dual-frequency GLONASS constellation as well as differential GPS through Satellite-Based Augmentation System (SBAS). SBAS includes Wide Area Augmentation System (WAAS) signals available on L1 (and the yet to be officially approved L5) in North America and the European Geostationary Navigation Overlay Service (EGNOS). Within the next few years, the sky (and what it bares) will dramatically change with the ongoing deployment of Galileo and BeiDou signals, both mostly sharing the same signals definition. All these signals are grouped under the Global Navigation Satellite Systems (GNSS) nomenclature. Moreover, regional and other augmentation systems are being defined, designed and deployed. Further information on the signals in space is provided in Chapter 2.

GPS has been reliably working under nominal conditions for the last decades (Gibbons, 2012). Nevertheless, as detailed in Figure 0.2, accumulated evidences have thus helped establishing current GPS limitations (Civil Aviation Authority, 2003), which can be expressed as:

Continuous availability: the capability of the system to maintain its operations when requested, without unintended interruption, delay nor degradation within its period of operation. It can also be seen as the system usability ratio, considering any shortage, no matter their origin. It is worth noting that, in the case of GPS, a non-uniform satellites distribution among each orbital plane could affect the consistency of the availability, especially at low Satellite Vehicles (SV) number, where some territories could have lower coverage.

Integrity: the capability of the system to comply to its specifications on a given period, which affects the confidence level of the system outcome, including its capacity to warn users of any anomaly within a reasonable delay. Receiver Autonomous Integrity Monitoring (RAIM) warn its users when integrity issues are detected; it provides the ability to detect and remove erroneous observations by exploiting the redundancy of the system. Integrity may also be associated with reliability.

Resistance to interferences: the capability of the system to maintain operation despite electromagnetic interferences (either intentional or not).

Precision: the finess of the system in providing an estimation close to a long series of equivalent estimations. It is typically quantified in terms of standard deviation. According to Benedicto *et al.* (2000), Dilution of Precision (DoP) and User Equivalent Range Error (UERE) as well as the signal characteristics may be used to predict a position precision.

Accuracy: the capability of the system in providing an estimation close to its true value. It is typically quantified in terms of the bias of the measurements average.

In severe environments, all types of interference have an undeniable impact on receiver tracking loops with increased in-band noise levels, and thus in noisier raw measurements. Not only does this impede the positioning accuracy, but may also compromise signal tracking due to noisier loop discriminator feedback, which could become so large as to cause loss of lock. Moreover, any interference is a potential source of navigation message (or even signal) loss, compromising receiver positioning, especially at early tracking stages. As a result, new modulation schemes offer great potential in terms of increased precision, higher sensitivity and greater protection against interferences. In fact, navigation in severe environments, such as under a forest canopy, within an urban canyon or even indoors, requires an even greater receiver robustness. More precisely, canopy tends to attenuate signals, while closely-located sky-scrapers result in multiple signal reflections (a.k.a. multipath) as well as signal blocking below what is called an elevation mask, all of which may significantly compromise signal reception.

These limitations represent a true problem for GPS-enabled automated applications. In this context, robustness is defined as the degree to which a system operates correctly in the presence of exceptional inputs or stressful environmental conditions (C/S2ESC - Software & Systems Engineering Standards Committee, 1990). Hence, several strategies have been (and continue to be) investigated to further extend modernized GNSS signals usability, beyond current GPS weaknesses. They can be grouped into the following trends:

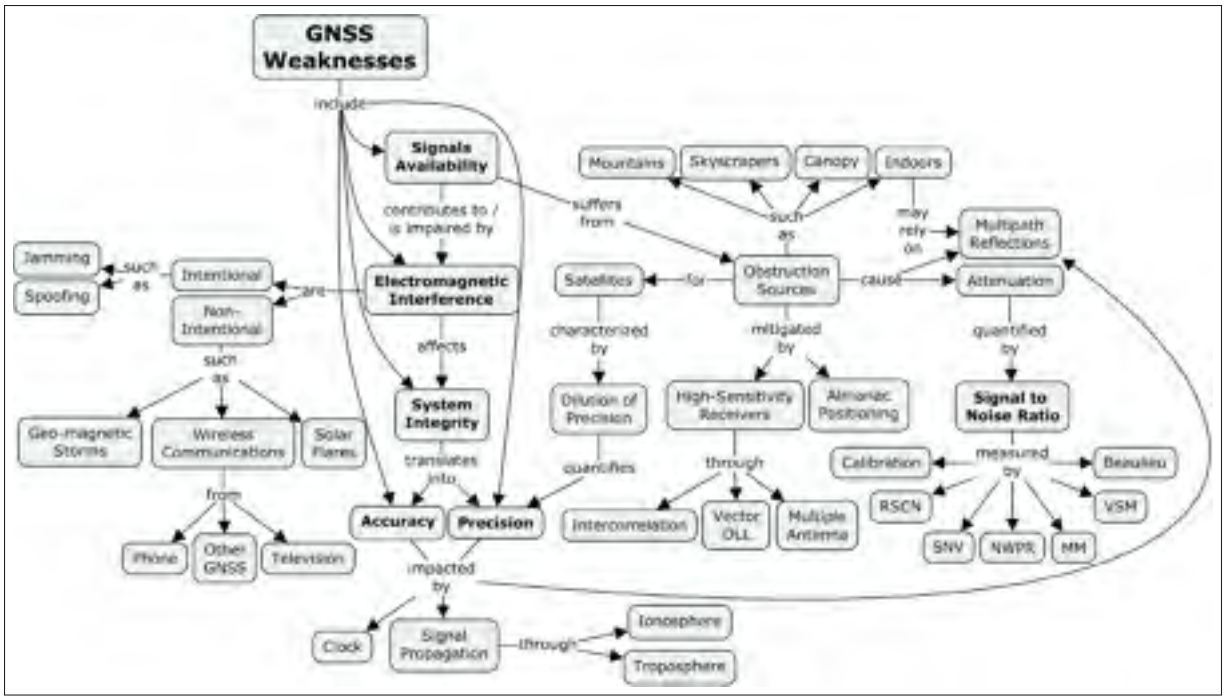

Figure 0.2 GNSS Weaknesses

Differential: relative measurements (compared to one or more reference base stations) allows eliminating common errors (cf. Chapter 3), thus achieving a position with improved accuracy and precision. Alternatively, applying corrections to decoded data allows improving the measurement accuracy.

Sensor fusion: integration of complementary raw measurements to improve the navigation solution.

External aiding: transmission of satellite-related data through an alternate medium, such as a mobile connection, thus facilitating acquisition by targeting visible satellites with valid Doppler estimates, eventually through longer integration periods through data wipe-off and precise positioning through corrected ephemerides.

Signal specification: satellite signal conditions receiver architectures in terms of modulation type, chipping rate, secondary code and data encryption, allowing increased positioning performances.

Receiver architecture: improving any module architecture may improve its outcome. Such areas may include correlators (standard, narrow, vision, Strobe, vector tracking loops, etc.), data/pilot combination, demodulation approach, sequential vs. parallel acquisition, filtering, super-heterodyne vs. direct RF sampling, RF front-end and much more.

Signal processing: signal processing strategies may improve receiver sensitivity and robustness through long coherent integrations with data wipe-off, non-coherent integrations, carrier smoothing, cycle slip management, multi-frequency measurements, ...

Algorithms: software may help harvesting observations without artefacts such as multipath mitigation techniques, RAIM, ...

Data fusion: inter-constellation data fusion allows autonomously correcting for certain errors and increasing availability and integrity.

These trends have achieved promising results, although some may depend on additional sensors (or even on external systems or networks). Indeed, GPS is often complemented through Inertial Navigation Systems (INS), which integrates linear and angular acceleration measurements from Inertial Measurement Units (IMU), respectively obtained through accelerometers and gyroscopes of different grades and sizes. Loosely, tightly or deeply coupled integrations define whether absolute GPS measurements reset the drifting relative inertial measurements or if the stable inertial measurements smooth jerkier GPS pseudoranges or positions. As opposed to GPS, IMU is immune to signal jamming/blocking. Another method consists in Real-Time Kinematic (RTK), also available in post-processing without a direct communication link requirement. It computes relative corrections on a reference receiver (i.e. base) against its known fixed position. These differential corrections are then applied onto the measurements of a mobile receiver (i.e. rover). These corrections remain valid in a short to medium range (i.e. 20 to 40 km (Delaporte, 2009)), based on the assumption that the Line of Sight (LoS) between each satellite is perceived with a parallel direction onto both receivers and is thus similarly impacted by the atmosphere through which their signals travel. The algorithm solves the integer carrier cycles ambiguity through double-differentiation and thus uses smooth, un-

ambiguous carrier phase measurements, leading to sub-millimetric accuracies, assuming 1 % measurement error. Also, Precise Point Positioning (PPP) post-processes raw measurements against precise ephemerides and clock information available on the web, such as through the International GNSS Service (IGS). Such external dependencies are making these solutions intrinsically not as widely accessible as through a standalone receiver on its own, on which many new applications are being developed. Figure 0.3 presents some available and planned navigation assistance methods.

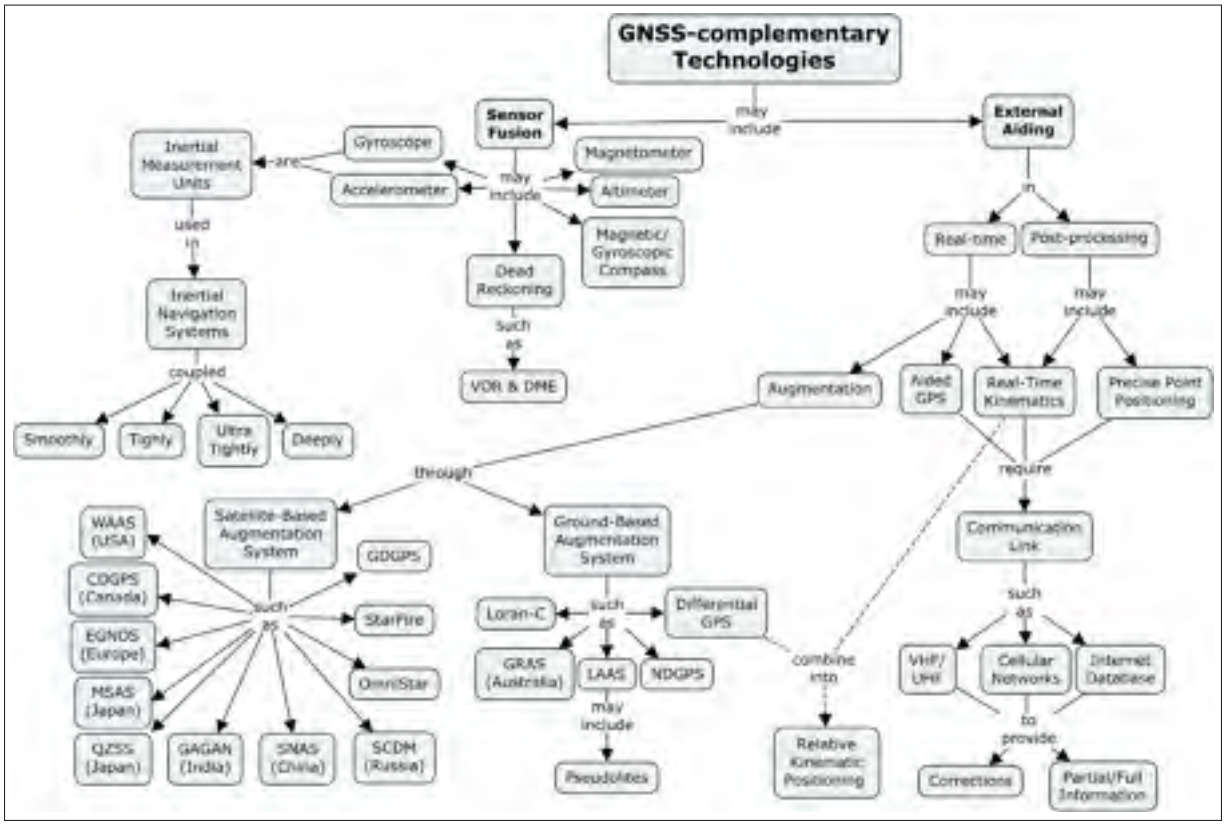

Figure 0.3 GNSS Aid

Although new GNSS signals are still too few in number to be independently integrated into a Position Velocity and Time (PVT) solution, GNSS receiver design has been, and continues to be, a very flourishing domain with an exponential growth. Lots of efforts are invested into fast acquisition, robust tracking and solution hybridization in order to harvest all the available signal power. For example, Stanford University has proposed a hybrid PVT by combining 2

GPS L1/L5 and all 3 WAAS L1/L5 signals, where the ephemerides are downloaded from L1 and the iono-free pseudoranges are obtained through the combination of L1/L5 (Chen *et al.*, 2011).

In the presented work, the main goal pursued aims at ensuring continuous availability of GNSS positioning via a universal receiver architecture capable of easily adapting to any GNSS civil signal available, this is expecially interesting as new and modernized constellations deployment will spread over a decade. Moreover, in a world driven by the economy, increasingly characterized by miniaturization and ecological trends, smart resource management becomes critical. In fact, this thesis general research problematic aims at extending standalone (i.e. without any form of external aiding) GNSS receiver performances beyond traditional dead zones of GPS by targeting all existing civil GNSS signals and those to come.

Indeed, a remedy to the root cause of these symptomatic behaviors lies in the robustness of stand-alone GNSS receivers, with its ability to harvest all the signals potential. This objective is twofold: 1) taking advantage of the GNSS compatibility has been at the heart of the study of universal acquisition and tracking channels, allowing for a very flexible solution running on a low consumption, embeddable, hardware implementation, and 2) processing different modulation types, spreading codes, data encryption, data structure, atmospheric models, time management as well as geodetic systems as an important underlying prerequisite for GNSS data fusion.

In order to achieve this, the following sub-objectives are formulated:

a. Current routines optimization to allow for more computationally demanding signal types.

b. Existing GPS L1 C/A tracking channel generalization to account for all civil GNSS (i.e. GPS, GLONASS, Galileo and BeiDou) on all bands, as well as their regional and augmentation counterparts.

c. Design paradigm change to allow for a common raw measurements extraction method for the different GNSS systems.

d. Raw measurements modeling in terms of noise.

The first step allowed getting familiarized with the previous work conducted by Sauriol (2008). In parallel, a thorough GNSS civil signals study led the path to the second step, through a collaboration with Guay (2010). While integrating GLONASS signals, which uses different timing and geodetic systems than those used by GPS, a new generic approach was devised to manage reception time stamps on the PC rather than in the embedded processor. Finally, theoretical analysis (step d.) allowed comparing against receiver performances.

The included research results are deemed original first in terms of the universal nature of the proposed tracking channel. Since many signals are still being defined or refined, these tracking channel need to be flexible enough to be considered future-compliant and claimed as universal. Furthermore, a receiver based on such universal channels faces a whole new set of challenges: 1) the system front-end architecture and its sampling frequency must account for every civil signal bandwidth on different carrier frequencies; 2) many loop controls must be made variable and automatically configured depending on the targeted signal definition and 3) the old satellite selection problem must be re-visited as a much more complex signal selection problem in order assign the most valuable signal to the next universal tracking channel available. This, on top of the navigation data fusion from different geodetic, timing and atmospheric modeling, all of which is transmitted in different frame structure, coding and modulation.

Considering that previous work included an already implemented GPS L1 C/A receiver prototype, the research conducted was directly applied and implemented into this prototype, which now has become a configurable GNSS receiver supporting augmentation services. To remain efficient, Matlab proof of concepts were developed and tested, when applicable, prior to final implementation. The characterization was then conducted with real signals, based on WAAS augmented navigation solutions involving data decoding, differential corrections and PVT accuracy assessments. In fact, no simulator, other than the Spirent GSS 7700 supporting GPS L1 C/A and WAAS L1, was readily available in-house. With signals in constant evolution, maintaining an in-house simulator would have required a considerable amount of work (Lavoie,

2013). In any case, without questioning its added-value, a simulator can never be fully representative of real signals.

VHDL test benches were realized to validate basic behaviors and to save massive amounts of compilation time. Signal modulation details, including primary and secondary spreading codes, were predefined in memory through matlab scripts. The host DLL was migrated from C to C++ with the help of Lavoie (2012), while the Graphical User Interface (GUI) was migrated from VB6 to VB.Net by Côté (2010). These two optimizations were very valuable in terms of testability, modularity, coding flexibility and source code documentation. Automatic post-analysis Matlab scripts were defined to generate standardized reports to improve feedback on applied modifications (Chapron, 2010; Romain, 2012).

As an outcome, changing the receiver paradigm from many dedicated channels to only a few universal ones allows minimizing its electrical consumption and thus maximizing its portability. In an era of mobile and wearable technologies gathering the greatest share of the electronics market, this becomes a very valuable asset... Especially with Russia and China recent law reinforced decision that any receiver sold on their territories shall use their respective constellation. In fact, the proposed architecture also complies with military receivers who typically transit from Coarse Acquisition (C/A) signals to the precise and robust P(Y) ones. Moreover, the proposed architecture allows on-the-fly signals definition updates, making the receiver upgrades very easy, even for those already in the field.

With such a flexible architecture, the controlling logic of a universal channel should also determine which signal should be tracked. This could be achieved in terms of geometrical coverage metrics, such as the traditional Dilution of Precision (DoP), as well as frequency diversity and signal robustness. All these features widely open the path to cognitive receivers.

In terms of scientific contributions, this research includes work in the GNSS fields of Multipath (Guay *et al.*, 2008; Fortin *et al.*, 2009a), WAAS (Fortin *et al.*, 2014), Signal to Noise Ratio (SNR) computations, Fast Fourier Transform (FFT) acquisition (Narbaïts-Jauréguy, 2009; Bourdeau, 2011; Fortin *et al.*, 2015), Universal Acquisition/Tracking for which a patent has

been accepted (Landry *et al.*, 2010) supported by a conference (Fortin *et al.*, 2009b) and a paper (Fortin and Landry, 2016), data demodulation (Thibodeau, 2010; Ducharme, 2010; El Hatimi, 2011; Dussart, 2012; Pivel, 2012) and signal selection (Liu *et al.*, 2009) on top of other collaboration (Ilie *et al.*, 2008, 2009b,a; Fortin *et al.*, 2010). Several undergrad students, involved in these projects under the author's technical supervision, as well as a few colleagues contributions helped making this receiver a true success with many features at hand.

In the presented work, unless specified otherwise, the spectral representations refer to power spectrums. This thesis is further partitioned into several chapters. The literature review spans from the satellite down to the receiver, over four chapters. The signal modulation background in Chapter 1 allows describing the signals in space in Chapter 2. Chapter 3 then glances through signal error sources, both external and internal to the receiver, while Chapter 4 reviews existing tracking channels approaches and their associated limitations. These lay down the basis for three peer-reviewed journal papers with contributions to improve receiver robustness. These are presented in Appendices, located after the conclusion. Hence, this thesis contribution core resides in three concepts required to achieve a corrected navigation solution in a stand-alone receiver (as represented in Figure 0.4):

a. a generic parallel-code **FFT-based acquisition channel** allows locking the receiver loops onto available satellite signals (cf. Appendix I),

b. a sequential acquisition and **universal tracking channel** allows decoding the navigation message as well as providing raw measurements (cf. Appendix II derived from the granted patent # US 8401546 B2), both of which are required to resolve the navigation solution, and

c. an **augmentation** solution overlay allows integrating differential correction to improve the achieved navigation solution (cf. Appendix III).

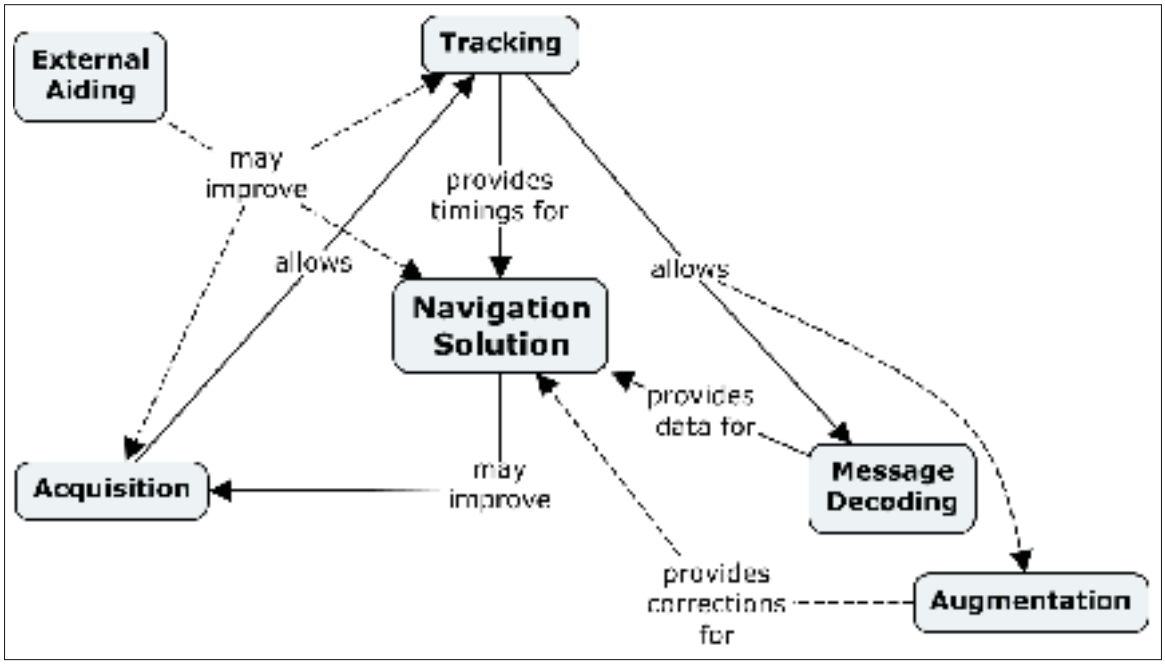

Figure 0.4 Navigation Solution Concepts

CHAPTER 1

SIGNAL MODULATION AND AUTO-CORRELATION FUNCTION BACKGROUND FOR TRACKING LOOPS

Navigation signals acquisition and tracking is fundamentally based on the Auto-Correlation Function (ACF) of the incoming signal with its locally generated replica. It can be thought of as a convolution of the two signals, but without flipping the second sequence from end to start. Hence, from the Convolution Function:

$$\{f \star g\}(\tau) \triangleq \int_{-\infty}^{\infty} f(t) \cdot g(\tau - t)\, dt \tag{1.1}$$

one can derive the general Correlation Function (with the complex conjugate operator *):

$$R_{fg}(\tau) = \{f(t) \star g^*(-t)\}(\tau) = \int_{-\infty}^{\infty} f(t) \cdot g^*(t - \tau)\, dt \tag{1.2}$$

Thus, the ACF of a real function (i.e. where $f^*() = f()$) becomes, when applied over a finite time interval T_P:

$$R_{ff}(\tau) = \int_{0}^{T_P} f(t) \cdot f(t - \tau)\, dt \tag{1.3}$$

A simplified analysis is first conducted for the traditional Binary Phase Shift Keying (BPSK) modulation whereas most new civil, commercial and regulated modernized signals are based on a more recent modulation scheme known as the Binary Offset Carrier (BOC) family of modulations, which are both further detailed in the following sections, before introducing discriminator function, correlator spacing and phase jitter.

1.1 BPSK Correlation

A pseudo-random spreading code is a sequence mimicking white gaussian noise, where “0” and “1” represent the sign (i.e. $\pm$) of a series of successive square pulses (i.e. the chips). The independent and identically distributed (iid) chips of a misaligned pair of the same spreading

code would be equal about half of the time, the matching chips being canceled out by those opposed in sign, resulting in a close to zero sum. For example, a 1023 chip-long code would have 511 matching chips as well as 511 chips in sign opposition, leaving 1 chip not being canceled out by the ACF with any offset. However, from partial (i.e. when the sequences are aligned within a fraction of a chip) to perfect code alignment, the correlation result will ramp up from 0 to the number of chips – or the length of the sequence – N and back down to 0, generating an isoceles triangular shape with a 2 chip-wide base. In these terms, one can simplify the code ACF analysis to that of a single chip. The most important factor for this peak shape is the incoming signal admitted bandwidth; the local signal bandwidth is deemed to be infinite, provided the sampling frequency is high enough. Indeed, at a conceptual level, filtering will have a direct impact on the supposedly square incoming chip, as depicted in Figure 1.1 where a 1.023 MHz rated chip is filtered down to $\pm 12, \pm 8, \pm 4$ and ± 2 MHz. The resulting normalized ACF will therefore also be impacted by the incoming signal shape, as shown in Figure 1.2. Obviously, a higher rated spreading code will suffer more from a given bandwidth, as would be the case for GPS L5, whose chipping rate is 10 times that of GPS L1 C/A.

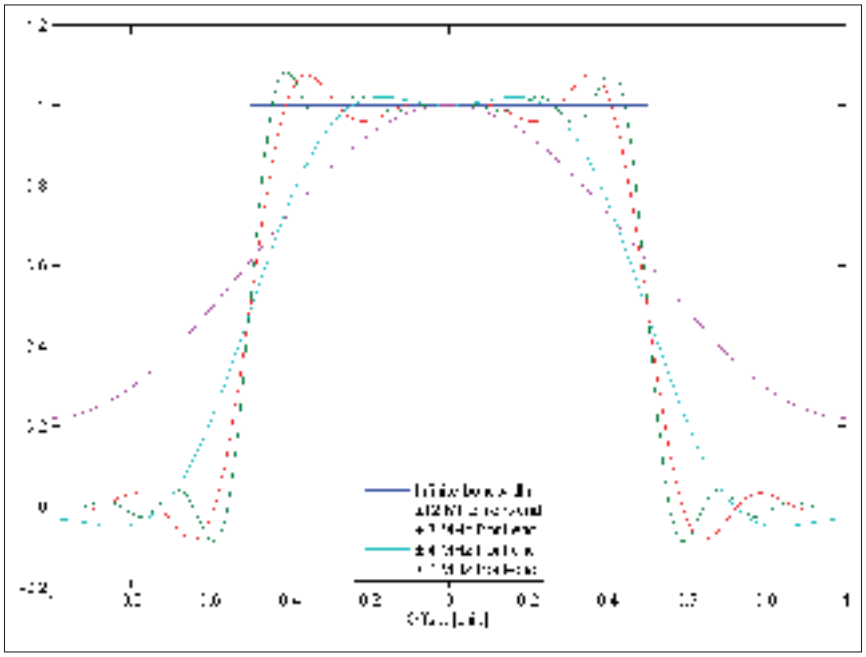

Figure 1.1 Bandwidth Effect on a Square Chip Shape

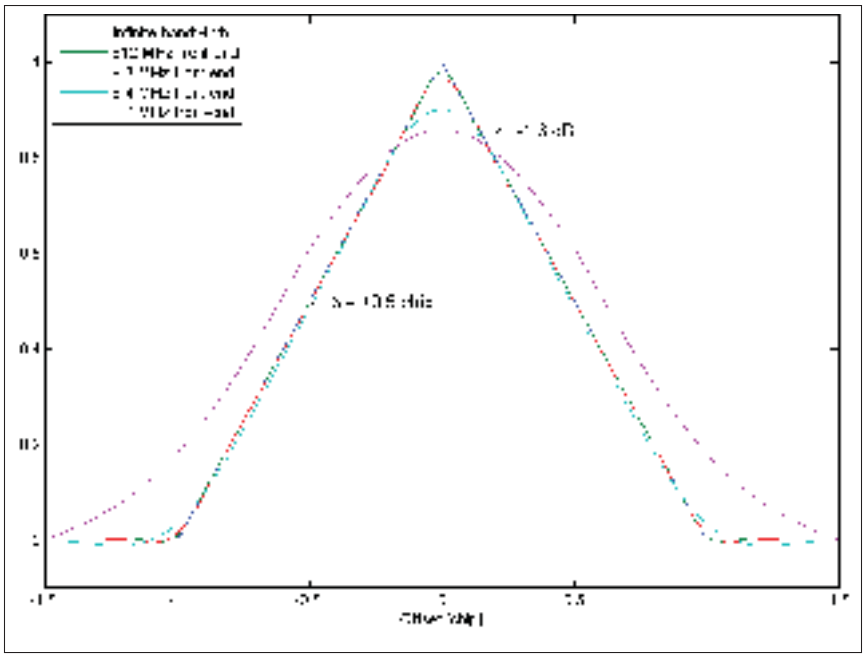

Figure 1.2 Coherent Bandwidth-Limited Normalized ACF of a Square Chip

Using the reference chipping rate f_r = 1.023 MHz, the resulting modulation may be expressed as BPSK(1), "1" being the ratio of the chipping rate f_c to f_r. Assuming that the spreading code iid values are equally likely (actually, there is one more "1" than there are "0"), this modulation implies a power spectrum that may be approximated by (with the amplitude A):

$$\begin{aligned} G_{\mathrm{BPSK}(f_c)}(f) &= \frac{|\mathscr{F}\{\mathrm{BPSK}\}|^2}{A^2 \cdot T_c} \\ &\cong \frac{f_c}{A^2} \frac{\tan\left(\frac{\pi \cdot f}{f_c}\right) \cdot \cos\left(\frac{\pi \cdot f}{f_c}\right)^2}{\pi \cdot f} \cong \frac{f_c}{A^2} \left\{ \frac{\sin\left(\frac{\pi \cdot f}{f_c}\right)}{\frac{\pi \cdot f}{f_c}} \right\}^2 \\ &\cong \frac{f_c}{A^2} \cdot \mathrm{sinc}^2\left(\frac{\pi \cdot f}{f_c}\right) \ [\mathrm{Hz}] \end{aligned} \tag{1.4}$$

Its graphical representation may be seen in Figure 1.3, where this theoretical approximation is superposed onto the Fourier Transform (FT) $\mathscr{F}$ of the spreading code. Note that in this simulation, an oversampling was used to better illustrate the spectrum. From the figure, one can notice that the balanced (i.e. iid) spreading code draws the DC spectral component to $\sim$0

(i.e. in the middle of the main lobe), as well as for all side lobes center frequency. It can also be seen that the side lobes width corresponds to the chipping frequency (f_c), while the main lobe has twice this bandwidth (i.e. 2.046 MHz).

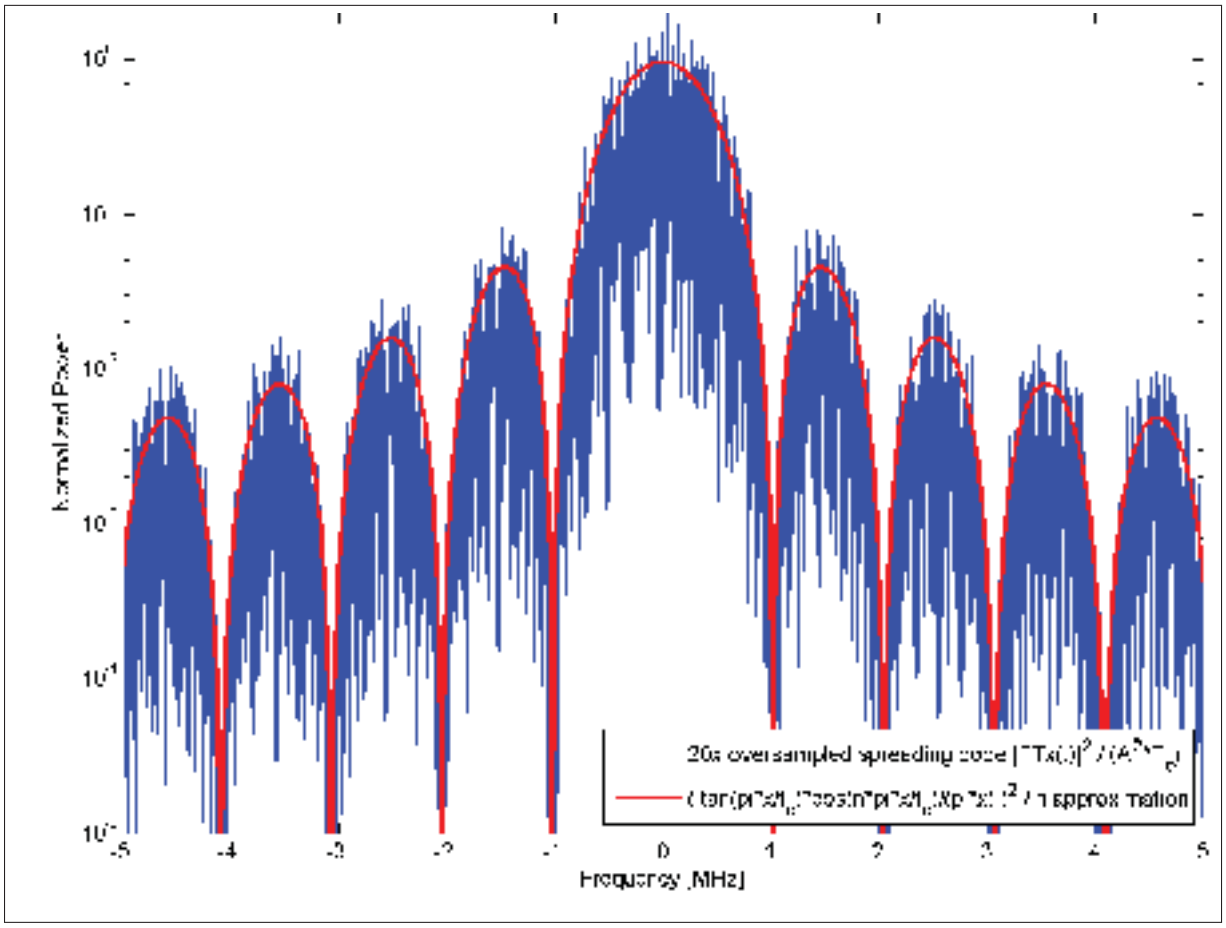

Figure 1.3 Normalized Spectral Representation of a BPSK(1) Modulation

1.2 BOC Correlation

The BOC modulation, introduced to the GNSS field by Betz (2001), addresses the fundamental issue of adding new signals to the already crowded L1 band. In fact, BOC is defined in terms of its square sub-carrier frequency f_s and of its chipping frequency f_c. In order to facilitate GNSS receivers operation, these frequencies are chosen as multiples of the reference frequency f_r =

1.023 MHz. BOC modulation can hence be defined as BOC(p,q), where:

$$\begin{aligned} f_s &\triangleq p \cdot f_r \\ f_c &\triangleq q \cdot f_r \end{aligned} \tag{1.5}$$

Similarly, BPSK can be defined as BPSK(q).

In the case of BOC$(1,1)$, the sub-carrier inverts the chip value at half its length, resulting in a Manchester-like spreading code, doubling the Gabor bandwidth (cf. Figure 1.5) (Spilker and Parkinson, 1996):

$$\mathrm{BW}_{\mathrm{Gabor}} = \sqrt{\int_{-\mathrm{BW}}^{\mathrm{BW}} f^2 \mathrm{PSD}_{\mathrm{S}}(f)\, df} \tag{1.6}$$

and thus requiring narrower correlators (cf. Figure 1.4).

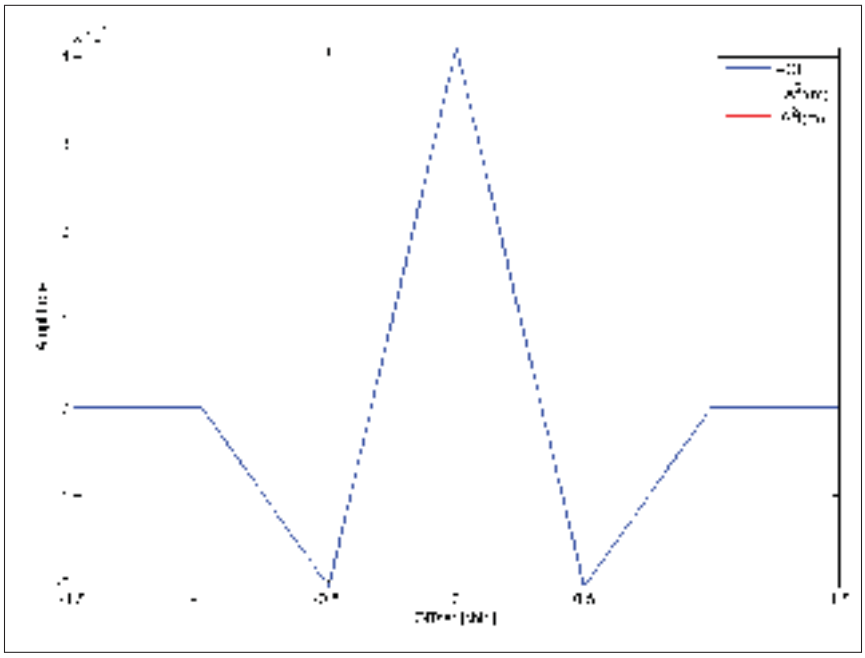

Figure 1.4 Auto-Correlation Function of a BOC$(1,1)$ Modulated Spreading Code of Length N = 10 230 and Signal Amplitude A = 2

Another parameter is twice the BOC ratio n of these two frequencies, defined as:

$$n \triangleq 2 \cdot \frac{f_s}{f_c} = 2 \cdot \frac{p}{q} \tag{1.7}$$

By symmetrically splitting and offsetting the spectrum away from the carrier frequency, BOC thus becomes complementary to the traditional BPSK in terms of spectral usage, as seen in Figure 1.5.

$$\begin{aligned} G_{\mathrm{BOC}(f_c)}(f) &\cong \frac{f_c}{A^2} \frac{\tan\left(\frac{\pi \cdot f}{f_c}\right) \cdot \cos\left(\frac{n\pi \cdot f}{f_c}\right)^2}{\frac{\pi \cdot f}{n}} \leftarrow \text{odd } n \\ &\cong \frac{f_c}{A^2} \frac{\tan\left(\frac{\pi \cdot f}{f_c}\right) \cdot \sin\left(\frac{n\pi \cdot f}{f_c}\right)^2}{\frac{\pi \cdot f}{n}} \leftarrow \text{even } n \end{aligned} \tag{1.8}$$

Compared to BPSK(1), BOC$(1,1)$ filtering has a stronger impact on its narrower chip shape and thus on its ACF[1], as illustrated in Figures 1.6 and 1.7. A ± 2 MHz input bandwidth barely admits both 2.046 MHz wide main lobes of BOC$(1,1)$, as seen in Figure 1.5. The resulting advantage of the BOC modulation is to increase the signal Root Mean Square (RMS) bandwidth, which is reflected in the correlation peak sharpness. In other words, the high frequency components contribute in producing sharper edges and clear discriminator zero-crossing, which allows more accurate code tracking.

It is worthwhile noting that, depending on the relative phase between the sub-carrier and the code, sine-BOC (sBOC) and cosine-BOC (cBOC) are defined, with slightly different spectrums. In this text, BOC refers to sBOC, as all GNSS open signals use this modulation. In fact, the only signals using cBOC are Galileo E1A and E6A, which are respectively regulated and commercial services, requiring the knowledge of their publicly undisclosed spreading sequences.

[1] Given a chip width dictated by the chipping rate, the square sub-carrier for $n = 2$ induces a level transition in the middle of a chip, doubling the occupied spectrum.

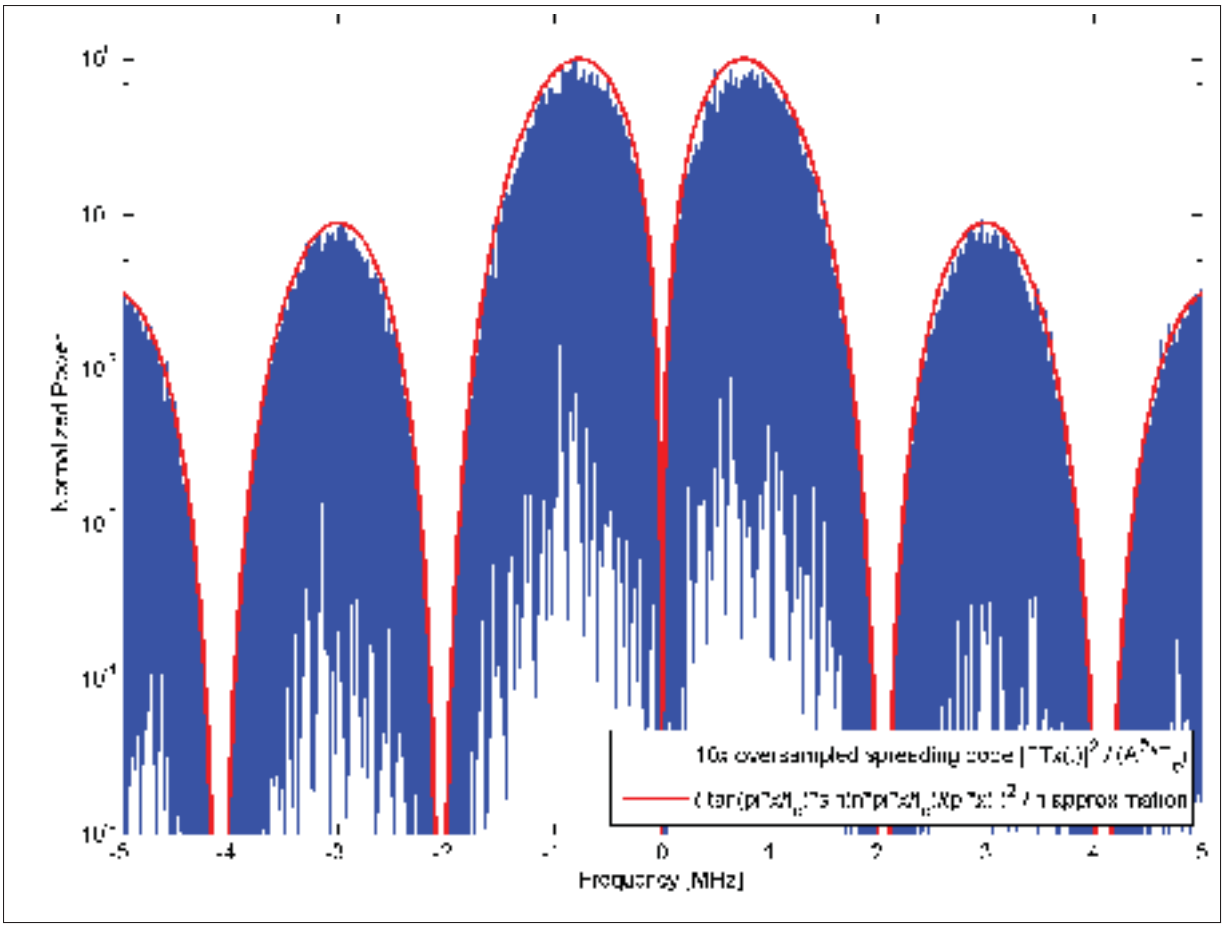

Figure 1.5 Normalized Spectral Representation of a BOC$(1,1)$ Modulation

1.3 Early-Late Processing

In order to achieve and maintain alignment on the input signal, a receiver channel may use different tracking loop modules: Frequency Lock Loop (FLL), Phase Lock Loop (PLL) and Delay Lock Loop (DLL), the latter two being represented in Figure 1.8. More precisely, the blue PLL uses *cos* and *sin* multipliers to wipe off the Intermediate Frequency (IF) from the input signal, resulting in the baseband complexed discrete branches I and Q. The carrier phase alignment is maintained via a loop feedback onto its Numerically Controlled Oscillators (NCO). Similarly, the red DLL uses differently delayed instances of the local code replicate, i.e. Early (E), Prompt (P) and Late (L), to compute the code phase error. In both cases, after integration, the correlator outputs are used by the discriminators, whose filtered error output (the code error

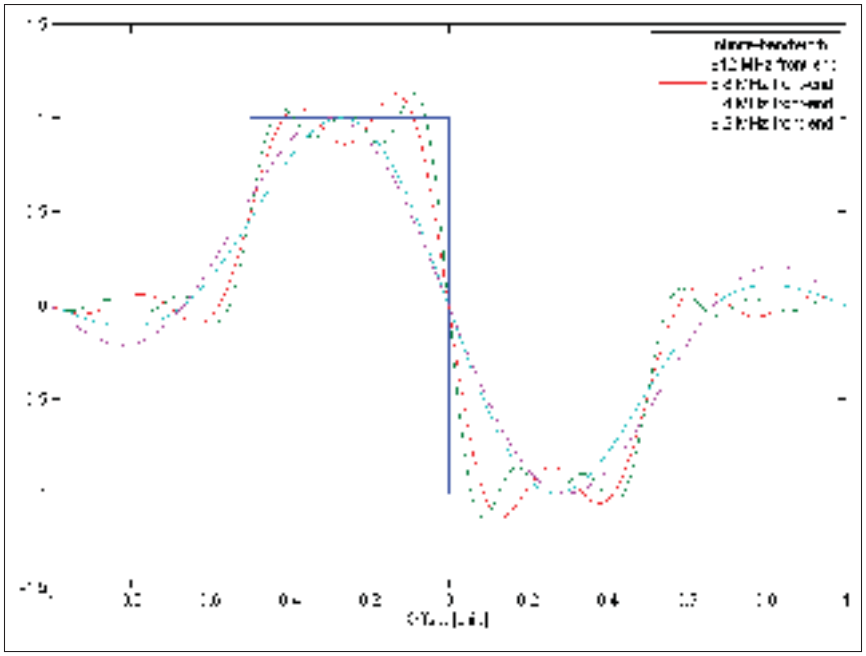

Figure 1.6 Bandwidth Effect on a Square BOC(1, 1) Chip Shape

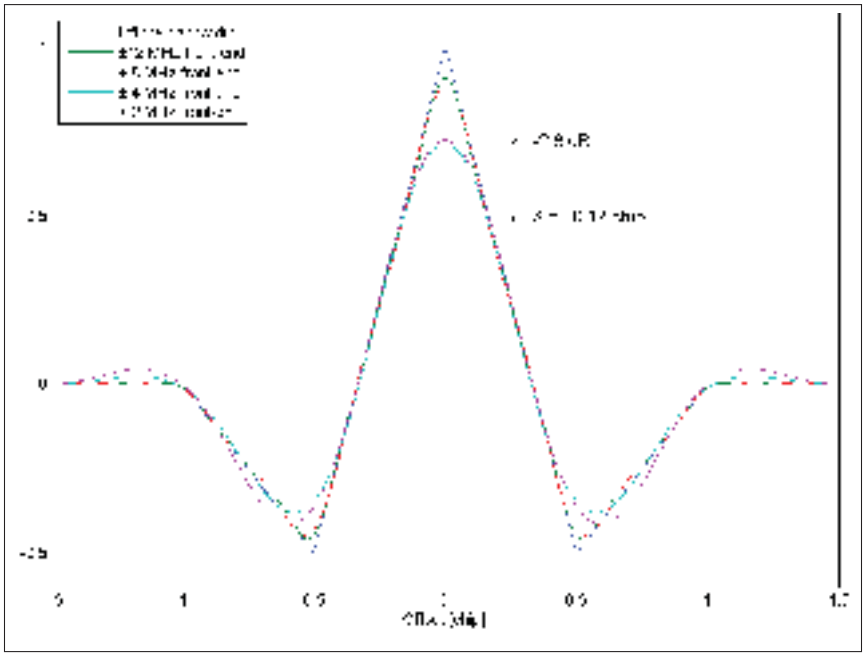

Figure 1.7 Coherent Bandwidth-Limited Normalized ACF of a Square BOC(1, 1) Chip

$\varepsilon = I_E - I_L$ and the carrier phase error $\varphi = \text{atan}\left(\frac{Q_P}{I_P}\right)$ for example) adjusts the rate of the corresponding loop NCO. These NCO counters are respectively used to provide carrier phase and code raw measurements.

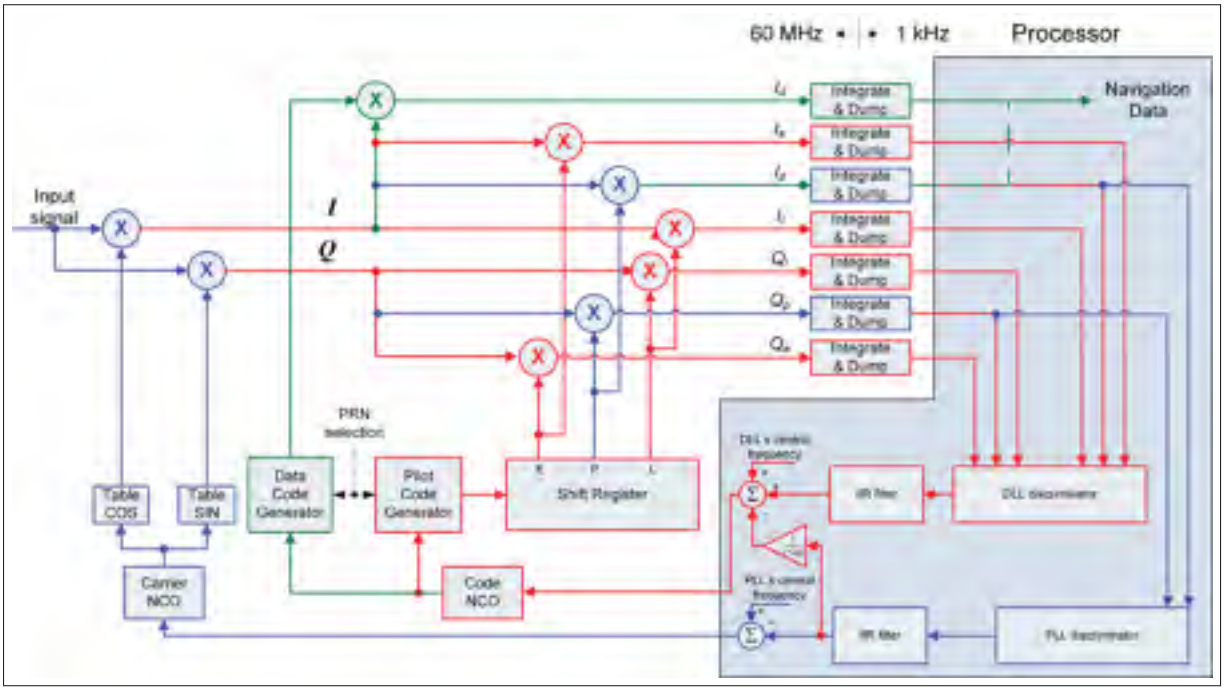

Figure 1.8 BPSK Tracking Loop
PLL [blue], DLL [red], Data [green]

Discriminators have traditionally been using Early Minus Late (EML) type of approaches. Two types of processing exist: Non-coherent Early-Late Processing (NELP) and Coherent Early-Late Processing (CELP). The former involves the squared magnitude – or alternatively the absolute value (not used herein) – of the code Cross-Correlation Function (CCF) and requires no knowledge of the incoming signal phase. The fact of combining the In-phase (I) and Quadrature-phase (Q) correlators, by summing their squared values, introduces squaring losses. It is thus more robust, but less sensitive compared to the latter, which uses only the I correlators and assumes the Phase Lock Loop (PLL) is perfectly aligned with the reference signal (Betz and Kolodziejski, 2000). Therefore, with a CELP Delay Lock Loop (DLL) discriminator, there is a loss of lock as soon as the PLL hangs. To sum up, if the carrier phase is

ignored, then the search is called non-coherent tracking. On the other hand, a coherent DLL discriminator requires that the PLL be locked so that $\Delta\theta \approx 0$. Hence, NELP are generally preferred.

On top of BOC multipath mitigation potential associated with its larger occupied bandwidth, its sub-carrier introduces polarity inversions in the correlation function, thus leading to peak detection ambiguity. In the case of BOC$(1,1)$ and assuming the inversion caused by the navigation message data bits is considered, a coherent discriminator should still be able to identify the single extrema (cf. Figure 1.7). However, in the case of non-coherent discriminators, the squared correlation function is characterized by several local maxima, referred to as the BOC ambiguity.

Anyhow, because of the phase uncertainty of the PLL, it is important to consider both in-phase I and quadrature Q branches, combined by summing their squared magnitudes in non-coherent discriminators in order to provide more robust tracking. Furthermore, in presence of weak signals, non-coherent discriminators may be required to correlate over longer periods without being affected by spreading codes sequence inversion due to navigation bit or secondary chip transitions.

From Figures 1.2 and 1.9, one clearly sees that the traditional BPSK correlation function (coherent or not) has a single peak. This fact remains, no matter how high its chipping rate gets. On the other hand, the correlation function of BOC presents $2n-1$ positive and negative peaks separated by the sub-carrier half period (Cf. Figure 1.7):

$$T_s = \frac{1}{2 \cdot f_s} \tag{1.9}$$

resulting in $2n-1$ positive peaks in the case of non-coherent processing, as seen in Figure 1.10. Hence, the BOC ambiguity increases with higher n ratios (Betz, 2001). It is also worth noting that without noise, as is the case of the presented figures, the non-coherent combining of powers does not introduce noise: Figures 1.2 and 1.9 display a -1.3 dB correlation amplitude loss (affecting the tracking loops sensitivity) for the same ± 2 MHz input bandwidth.

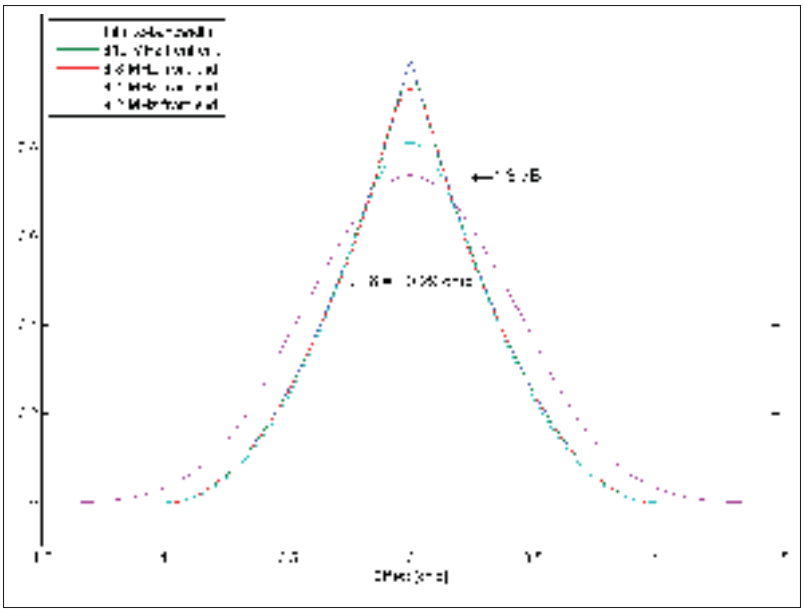

Figure 1.9 Non-Coherent (Power) Bandwidth-Limited Normalized BPSK(1) ACF of a Square Chip

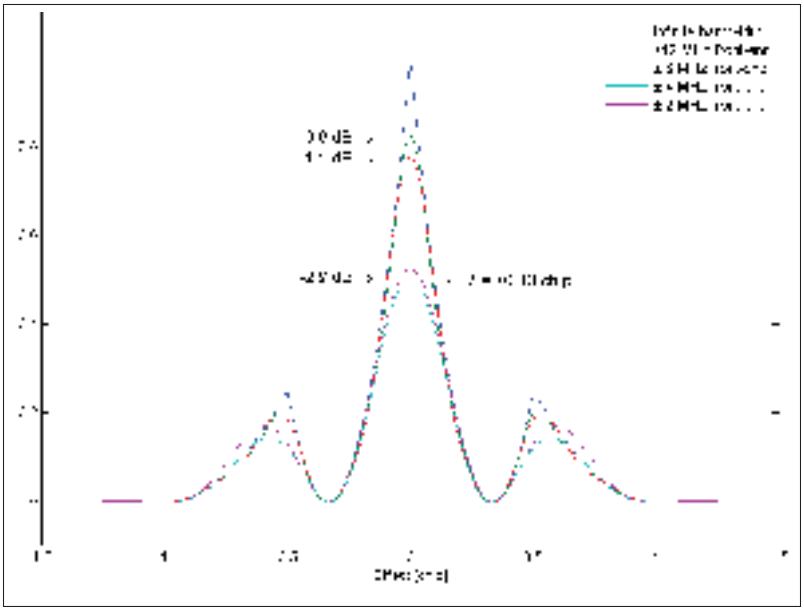

Figure 1.10 Non-Coherent (Power) Bandwidth-Limited Normalized BOC(1,1) ACF of a Square Chip

The resulting EML discriminator curve takes the form of a "tilted S" and is hence often referred to as the S-curve[2]. In fact, it results from subtracting the amplitude of the correlation function of the Early (E) and Late (L) correlators, equally spaced from the Prompt (P) correlator. Note that the Early replica is generated in advance with respect to the Prompt, hence its correlation with the incoming code also appears in advance. Similarly, the Late replica is lagging the incoming code. The EML discriminator hence has a positive slope. As seen in Figures 1.11 and 1.12, the BPSK discriminator (whether it is coherent or not) with ± 0.5 chip-spaced correlators has several characteristics:

a. A central *linear zone* with a zero amplitude at zero-crossing, whose slope is twice the correlator slope. The linear zone varies according to the discriminator function. In the case of infinite front-end bandwidth EML, it is equal to the E to L correlator spacing Δ. Narrower front-end filtering could slightly extend the linear zone by rounding off its ACF extrema, as shown in Figures 1.13 and 1.14. Also, the minimum pre-detection bandwidth is imposed by the chipping and sub-carrier rates to allow encompassing the modulation main lobes. Also, the pre-detection bandwidth is highly related to the PLL noise and to the external carrier aid provided. Nevertheless, one can expect a very short linear region for bandwidth limited Narrow Correlators (NC).

b. A *pull-in zone* (or validity range, i.e. the bipolarity extent of the discriminator). Above this range, the DLL loses lock whether because of a no-lock condition or of an inverted feedback, pushing the estimated error away from the actual error.

c. A *discriminator bipolarity* can be said of a discriminator function that is 1) non-negative for positive chip offsets, and 2) non-positive for negative chip offsets.

d. A *single code tracking point*, which is the stabilized position of the discriminator output. In fact, it corresponds to the zero-crossing of a positive slope. Multiple tracking points

[2] The resulting discriminator curve may also look like a reversed tilted S (i.e. a rounded tilted Z), depending on the Earle and Late convention with respect to the Prompt.

lead to biased tracking, also known as the BOC ambiguity problem, as displayed in Figure 1.14.

e. A *positive slope*, which should ideally be unitary to prevent infinite oscillation between $\pm\varepsilon$ with a slope of 2. To avoid this behaviour, the feedback may be low-pass filtered (i.e. integrated) before affecting the code phase delay of the replica.

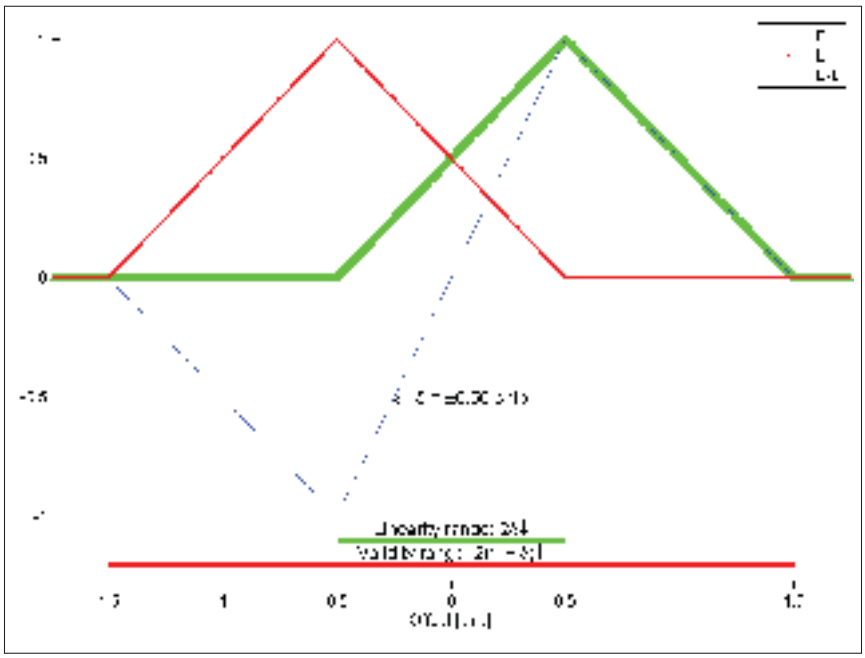

Figure 1.11 Coherent Infinite Bandwidth BPSK(1) Early Minus Late Normalized Discriminator S-curve Details

Moreover, since the main peak of the BOC ACF is narrower than that of BPSK, it requires narrower correlators to preserve a given attenuation (say -3 dB) to maintain tracking sensitivity. However, in order to have narrower correlators, the front-end bandwidth must be higher to avoid rounding of the resulting correlation function (van Dierendonck *et al.*, 1992). In fact, considering the infinite bandwidth signal auto-correlation, one sees that BOC main peak has a slope of $1.5n$ (cf. Figure 1.7). However, non-coherent processing steepens these slopes, which results approximatly in $2n$ between the peak and the zero-amplitude level (cf. Figure 1.10). Note that with a correlation spacing $\delta \geq \pm\frac{1}{n}$ chip, an inversion of the S-curve would compro-

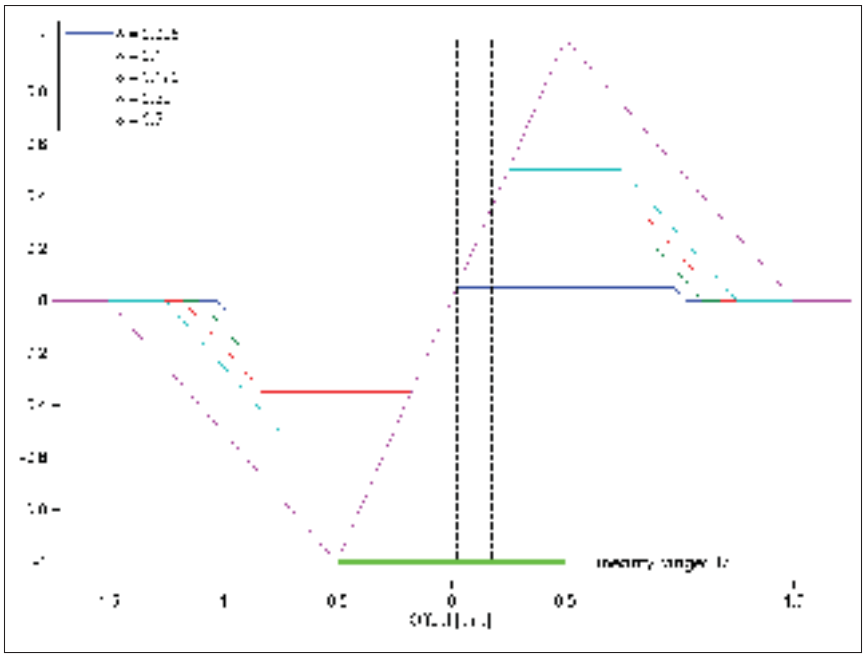

Figure 1.12 Coherent Infinite Bandwidth BPSK(1) Early Minus Late Normalized Discriminator Curves

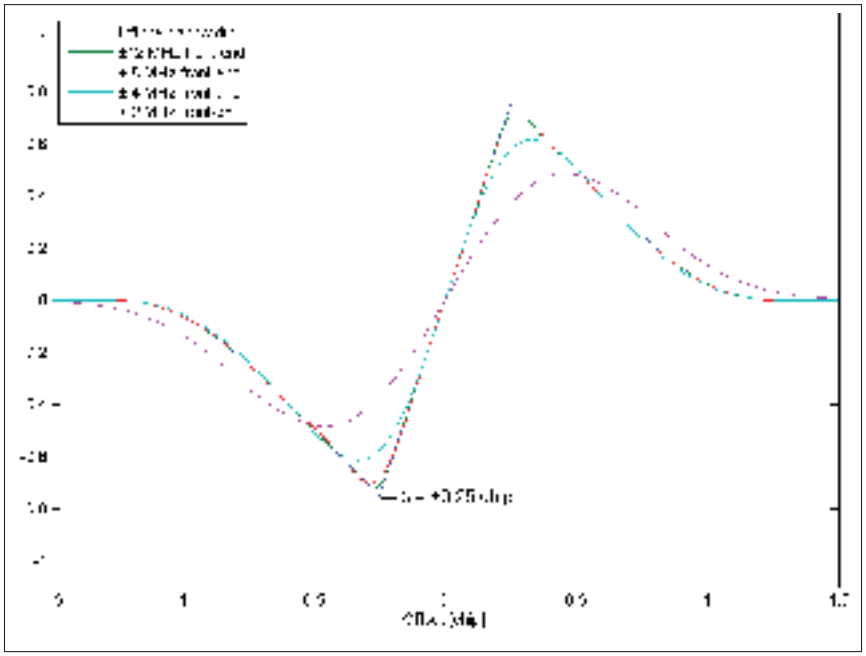

Figure 1.13 Non-Coherent Bandwidth-Limited BPSK(1) Early Minus Late Power Normalized Discriminator S-curves

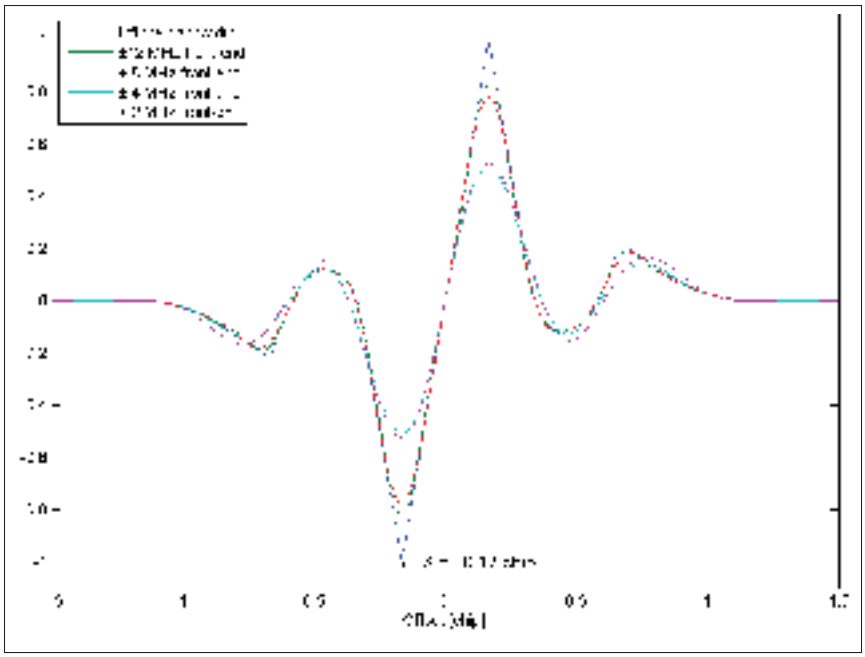

Figure 1.14 Non-Coherent Bandwidth-Limited BOC$(1,1)$
Early Minus Late Power Normalized Discriminator S-curves

mise the DLL behaviour (i.e. amplifying the error), as seen in Figure 1.16 (Betz, 2000). One should notice that coherent processing reaches plateaus while in non-coherent processing bare single-point maxima.

Figures 1.15 and 1.16 display the effect of chip spacing on the discriminator function for both BPSK and BOC$(1,1)$: the narrower the E-L correlators, the smaller the resulting maximum amplitude of the discriminator. In the latter, one can see that the resulting pull-in zone is thinner. In fact, the limits are now represented by a maximum correlator spacing of $\pm\frac{1}{n}$ chip, which also translates into a reduction of the linear zone. As mentioned earlier, greater correlator distance would induce an inversion of the S-curve slope. Moreover, the bipolarity characteristic is lost, due to the oscillations of the sub-carrier. Furthermore, Figure 1.16 clearly identifies $2\cdot(n-1)$ side S-curves, corresponding to the squared BOC$(1,1)$ correlation function side peaks of Figure 1.7. These false-locks imply a biased discriminator output. If these secondary S-curves were to be replaced by null lines, tracking would become impossible due to no-lock.

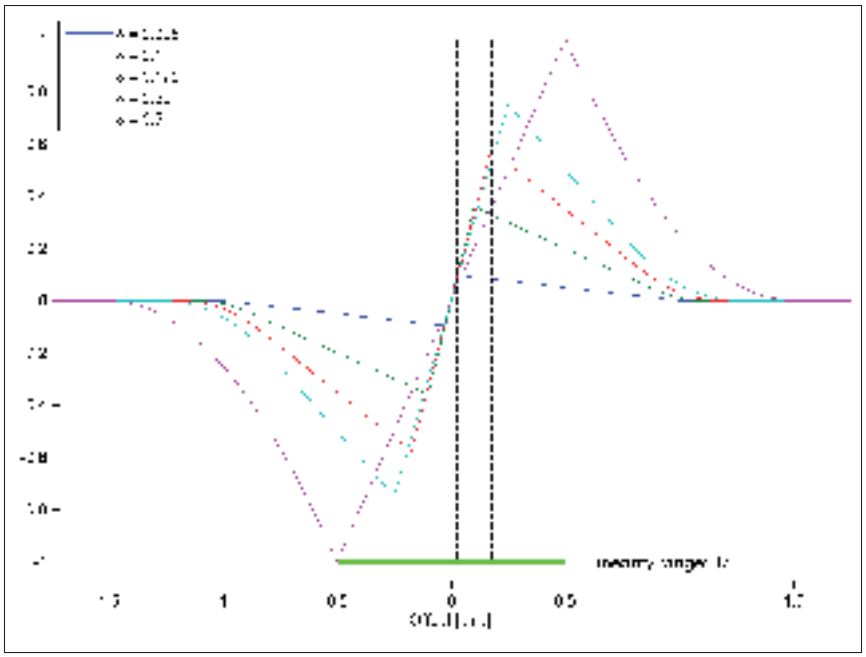

Figure 1.15 Non-coherent Infinite-bandwidth BPSK(1)
Early Minus Late Power Normalized Discriminator Curves

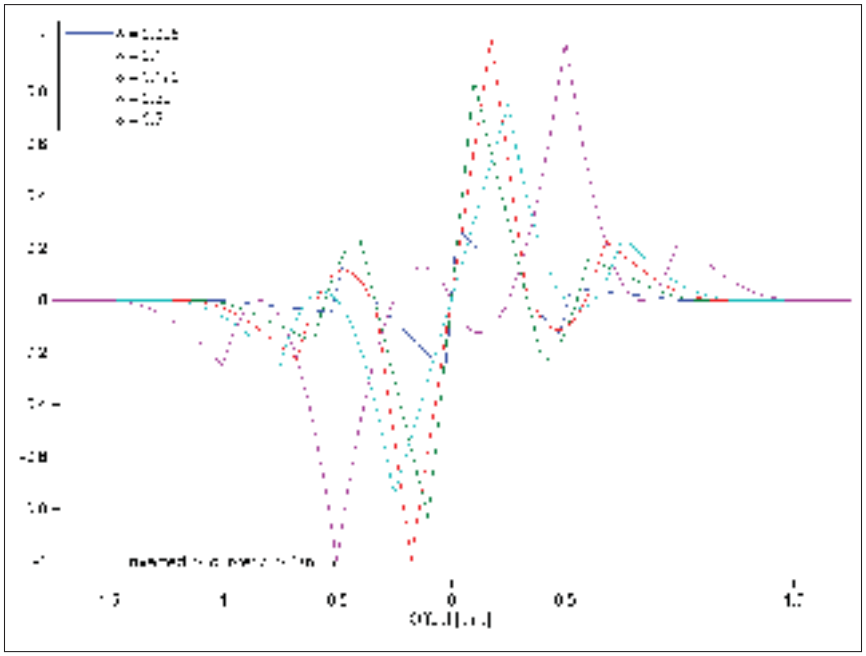

Figure 1.16 Non-coherent Infinite-bandwidth BOC(1,1)
Early Minus Late Power Normalized Discriminator Curves

Also, stick points are referred to as where the discriminator curve has small or near zero gain outside the linear zone.

1.4 Code Phase Jitter

In a tracking channel, one common performance metric is its code phase jitter. This section expands the equations from the traditional BPSK to the BOC modulation for the main discriminator functions. The computation thereof implies a few concepts.

First, the random variable $X = \upsilon + \eta$ is split into the useful signal υ and the noise η. Its variance is defined as:

$$\sigma^2 \triangleq \left\langle \left(X - \overline{X}\right)^2 \right\rangle = \left\langle (X - \upsilon)^2 \right\rangle = \left\langle \eta^2 \right\rangle \tag{1.10}$$

with the expected values denoted by $\langle X \rangle$, the mean value referred to by $\overline{X}$. The expected value is defined as the mean value of a random variable, i.e. the sum of the weighted probability of every possible output, the weight being the outcome value. In other words, expected value cancels out the noise of the (first degree) equation. Being independent, different branches (i.e. I and Q) of noise are not correlated, except for EML noise on a given branch, which results from combining different correlator outputs. Moreover, the expected value of odd powers of noise is null.

Also, steady-state implies vanishingly small frequency, carrier phase and code delay errors, which are neglected. When such code tracking errors are small so that a linearized analysis applies, the variance of the code tracking error [s^2] can be derived from van Dierendonck *et al.* (1992, appendix), Betz and Kolodziejski (2000) and Betz (2000), the code tracking performances of Ries *et al.* (2002) and Lee (2002) for multipath. It is well known that code phase jitter performance depends on the slope of the discriminator curve (i.e. better performances for

higher slopes or gain K). In fact, the code phase error ε variance can be defined as:

$$\sigma_\varepsilon{}^2 = \int_{\mathbb{R}} |H(f)|^2 \cdot \frac{S_\eta(f)}{K^2} df \approx \frac{[2 \cdot B_L] \cdot S_\eta(0)}{K^2} \tag{1.11}$$

with the loop transfer function $H(f)$ and the post-correlation noise Power Spectral Density (PSD) $S_\eta(f)$, further detailed in Eq. 1.15. This approximation is valid as long as the unilateral noise equivalent bandwidth B_L:

$$B_L = \frac{1}{2} \int_{\mathbb{R}} |H(f)|^2 df \tag{1.12}$$

remains small compared to the front-end complex bandwidth β_{fe}. This effective noise bandwidth is the bandwidth that an ideal filter (i.e. brick-wall), providing infinite rejection in the stop bands, would admit the same amount of noise as in the currently used non-ideal filter. It is obtained by integrating the total available noise power under the response curve for frequencies ranging from 0 to infinity. The power spectrum averaged over time typically reveals a flat noise floor, the height of which is proportional to B_L. It can also be determined from the z-transform of the loop filter transfer function $H(z)$ with the pre-integration time T_P [s] as reported by Pany and Eissfeller (2004):

$$B_L = \frac{1}{2\pi T_P} \int_0^\pi \left[\frac{T_P \cdot H(z)}{T_P \cdot H(z) + (z-1) \cdot \left(1 - \frac{T_P}{2} H(z)\right)} \right]^2 d\theta, \text{ with } \mathrm{z} = \mathrm{e}^{\mathrm{j}\theta} \tag{1.13}$$

The gain K of the discriminator output D at chip offset τ is defined as:

$$K = \frac{\langle D \rangle|_{\tau \to 0}}{\tau} \tag{1.14}$$

The post-correlation noise PSD S_η [W/Hz] is given by:

$$S_\eta = T_P \cdot R_\eta(0) \tag{1.15}$$

which corresponds to the noise correlation output at every T_P period. Note that the PSD of any signal corresponds to its squared spectrum over time. The noise correlation $R_\eta(\tau)$ at $\tau = 0$ is

defined as:

$$R_\eta(0) = \left\langle \eta^2 \right\rangle\Big|_{\tau=0} \tag{1.16}$$

Hence, by combining Eq. 1.12 to 1.16 into Eq. 1.11, the closed loop noise error variance [chip^2] is given by:

$$\sigma_\varepsilon^2 \cong \frac{2 \cdot B_L \cdot T_P \cdot R_\eta(0)}{K^2} = \frac{2 \cdot B_L \cdot T_P \cdot \left\langle \eta^2 \right\rangle\Big|_{\tau=0}}{\left(\langle D \rangle / \tau \right)^2} \tag{1.17}$$

This leads to the 1-sigma error [m] with the speed of light c:

$$\sigma_\varepsilon \approx c \cdot T_c \sqrt{\frac{2 \cdot B_L \cdot T_P \cdot R_\eta(0)}{K^2}} \tag{1.18}$$

with the speed of light c and the chip period T_c.

In the case of EML discriminators with a total spacing of Δ [chip], a rule of thumb imposes, neglecting dynamic stress error (Kaplan and Hegarty, 2006, Chapter 5)

$$3 \cdot \sigma_\varepsilon < \frac{\Delta}{2} \tag{1.19}$$

Hence, considering bandwidth limitations, the pseudo-linear zone $(\pm\Delta/2)$ should be made wide enough to encompass six times the code tracking jitter due to thermal noise. As an example for the closed loop noise jitter, the two widely used forms of EML non-coherent discriminators are considered: Early Minus Late Power (EMLP) and Dot Product (DP). With the in-phase I and quadrature-phase Q branches at iteration k, the incoming signal down-converted to baseband can be written as:

$$\begin{aligned} I_k &= \sqrt{C} \cdot T_P \cdot R(\tau_k) \cdot d_k \cdot \cos(\Delta\phi_k) + \eta_k^I \\ Q_k &= \sqrt{C} \cdot T_P \cdot R(\tau_k) \cdot d_k \cdot \sin(\Delta\phi_k) + \eta_k^Q \end{aligned} \tag{1.20}$$

with the data bit d, the noise η^I and η^Q associated with each branch and the received signal power over infinite bandwidth C [W]. Note that it is assumed that the PLL is locked, so that the phase bias $\Delta\phi$ is small. Assuming the Early and Late correlators fall onto the ACF main

peak (i.e. $|\tau| < \frac{1}{2n} - \frac{\Delta}{2}$ chip), the normalized Early and Late correlations $R\left(\tau \pm \frac{\Delta}{2}\right)$ are estimated by the main peak positive $(\tau < 0)$ and negative $(\tau > 0)$ slopes: $\left\{1 + m\left(\tau - \frac{\Delta}{2}\right)\right\}$ and $\left\{1 - m\left(\tau + \frac{\Delta}{2}\right)\right\}$ with a chip code delay τ with EML correlators spaced by $\Delta = 2\delta$ chip.

The noise jitter is derived below for one coherent (with the BOC main peak slope $m \approx 1.5n$ with an infinite front-end bandwidth) and two non-coherent (with $m \approx 2n$) discriminators, i.e. EML, EMLP and DP, where $\not{X}$ simplifies to 1, while $\not\not{X}$ is null and $\not{X}^{\infty}$ represents infinity.

1.4.1 Coherent EML

The EML discriminator output may be expressed as:

$$\begin{aligned} D_{EML} &= I_E - I_L \\ &= \left\{\sqrt{C} \cdot T_P \cdot d \cdot R\left(\tau - \frac{\Delta}{2}\right) \cdot \cos(\Delta\phi) + \eta_E^I\right\} \\ &- \left\{\sqrt{C} \cdot T_P \cdot d \cdot R\left(\tau + \frac{\Delta}{2}\right) \cdot \cos(\Delta\phi) + \eta_L^I\right\} \end{aligned} \tag{1.21}$$

The expected value of the discriminator output is thus:

$$\begin{aligned} \langle D_{EML} \rangle &= \overline{I_E} - \overline{I_L} \\ &= \sqrt{C} \cdot T_P \cdot d \cdot \left[R\left(\tau - \frac{\Delta}{2}\right) - R\left(\tau + \frac{\Delta}{2}\right)\right] \cdot \cancel{\cos(\Delta\phi)} \\ &\cong \sqrt{C} \cdot T_P \cdot d \cdot \left[\left\{1 + m\left(\tau - \frac{\Delta}{2}\right)\right\} - \left\{1 - m\left(\tau - \frac{\Delta}{2}\right)\right\}\right] \\ &\cong \sqrt{C} \cdot T_P \cdot d \cdot [2m \cdot \tau] \end{aligned} \tag{1.22}$$

Leading to its gain K, which depends on the navigation data bit d:

$$K \cong 2 \cdot \sqrt{C} \cdot T_P \cdot d \cdot m \tag{1.23}$$

The noise correlation R_η may be computed as the discriminator variance when $\tau \to 0$ and may be expressed as:

$$\begin{aligned} \sigma^2_{D_{EML}} &= \left\langle \left(D_{EML} - \overline{D_{EML}}\right)^2 \right\rangle \Big|_{\tau=0} \\ &= \left\langle \left[\left(I_E - \overline{I_E}\right) - \left(I_L - \overline{I_L}\right) \right]^2 \right\rangle \Big|_{\tau=0} \end{aligned} \tag{1.24}$$

Based on Eq. 1.24 and applying a flat noise power density N_0, the correlated noise can be shifted from $\pm\delta$ to $0-\Delta$, giving:

$$\begin{aligned} \sigma^2_{D_{EML}} &\cong N_0 \cdot T_P \cdot [\{1\} - \{1 - m \cdot \Delta\}] \\ &\cong N_0 \cdot T_P \cdot [m \cdot \Delta] \end{aligned} \tag{1.25}$$

These partial results combine into the closed loop noise error variance:

$$\begin{aligned} \sigma^2_{\tau_{EML}} &\cong \frac{2 \cdot B_L \cdot T_P \cdot R_\eta(0)}{K^2} \\ &\cong \frac{2 \cdot B_L \cdot T_P \cdot \{N_0 \cdot T_P \cdot [m \cdot \Delta]\}}{\left\{2 \cdot \sqrt{C} \cdot T_P \cdot d \cdot m\right\}^2} \\ &\cong \frac{B_L \cdot \Delta}{2 \cdot \dfrac{C}{N_0} \cdot m} \end{aligned} \tag{1.26}$$

1.4.2 Non-Coherent EMLP

The EMLP discriminator output non-coherently combines both I and Q branches and may be expressed as:

$$\begin{aligned} D_{EMLP} &= I_E^2 - I_L^2 + Q_E^2 - Q_L^2 \\ &= \left\{\sqrt{C}\cdot T_P \cdot d \cdot R\left(\tau - \frac{\Delta}{2}\right)\cdot\cos(\Delta\phi) + \eta_E^I\right\}^2 \\ &- \left\{\sqrt{C}\cdot T_P \cdot d \cdot R\left(\tau + \frac{\Delta}{2}\right)\cdot\cos(\Delta\phi) + \eta_L^I\right\}^2 \\ &+ \left\{\sqrt{C}\cdot T_P \cdot d \cdot R\left(\tau - \frac{\Delta}{2}\right)\cdot\sin(\Delta\phi) + \eta_E^Q\right\}^2 \\ &- \left\{\sqrt{C}\cdot T_P \cdot d \cdot R\left(\tau + \frac{\Delta}{2}\right)\cdot\sin(\Delta\phi) + \eta_L^Q\right\}^2 \end{aligned} \tag{1.27}$$

As an intermediate step, the squared correlation results give:

$$\begin{aligned} R^2\left(\tau - \frac{\Delta}{2}\right) &= 1 + m^2\left(\tau^2 - \tau\cdot\Delta + \frac{\Delta^2}{4}\right) + 2m\left(\tau - \frac{\Delta}{2}\right) \\ &= 1 + m^2\tau^2 - m^2\tau\cdot\Delta + \frac{m^2\Delta^2}{4} + 2m\cdot\tau - 2m\frac{\Delta}{2} \\ R^2\left(\tau + \frac{\Delta}{2}\right) &= 1 + m^2\left(\tau^2 + \tau\cdot\Delta + \frac{\Delta^2}{4}\right) - 2m\left(\tau + \frac{\Delta}{2}\right) \\ &= 1 + m^2\tau^2 + m^2\tau\cdot\Delta + \frac{m^2\Delta^2}{4} - 2m\cdot\tau - 2m\frac{\Delta}{2} \end{aligned} \tag{1.28}$$

Their difference simplifying to:

$$\begin{aligned} R^2\left(\tau - \frac{\Delta}{2}\right) - R^2\left(\tau + \frac{\Delta}{2}\right) &= -2m^2\tau\cdot\Delta + 4m\cdot\tau \\ &= 2m\cdot\tau(2 - m\cdot\Delta) \end{aligned} \tag{1.29}$$

The expected value of the discriminator gives (omitting first order noise terms):

$$\begin{aligned}\langle D_{EMLP}\rangle &= \overline{I_E^2}-\overline{I_L^2}+\overline{Q_E^2}-\overline{Q_L^2}\\ &= C\cdot T_P^2\cdot \cancel{d^2}\cdot\left[R^2\left(\tau-\frac{\Delta}{2}\right)-R^2\left(\tau+\frac{\Delta}{2}\right)\right]\cdot\cancel{\left(\cos^2(\Delta\phi)+\sin^2(\Delta\phi)\right)}\\ &\cong C\cdot T_P^2\cdot[2\cdot m\cdot\tau(2-m\cdot\Delta)]\end{aligned} \tag{1.30}$$

Leading to its gain K:

$$K \cong 2\cdot C\cdot T_P^2\cdot m\cdot[2-m\cdot\Delta] \tag{1.31}$$

On the other hand, the discriminator variance at $\tau\to 0$ can be expressed (where $\langle D_{EMLP}\rangle$ cancels out) as:

$$\begin{aligned}\sigma^2_{D_{EMLP}} &= \left\langle\left(D_{EMLP}-\overline{D_{EMLP}}\right)^2\right\rangle\Big|_{\tau=0}\\ &= \left\langle\begin{pmatrix}\left[I_E^2-\overline{I_E^2}\right] & - & \left[I_L^2-\overline{I_L^2}\right]+\\ \left[Q_E^2-\overline{Q_E^2}\right] & - & \left[Q_L^2-\overline{Q_L^2}\right]\end{pmatrix}^2\right\rangle\Bigg|_{\tau=0}\\ &= \left\langle\begin{pmatrix}2\cdot\sqrt{C}\cdot T_P\cdot d\cdot\cancel{\cos(\Delta\phi\to 0)}\cdot\begin{bmatrix}R\left(-\frac{\Delta}{2}\right)\cdot\eta_E^I-\\ R\left(+\frac{\Delta}{2}\right)\cdot\eta_L^I\end{bmatrix}+\eta_E^{I2}-\eta_L^{I2}+\\ 2\cdot\sqrt{C}\cdot T_P\cdot d\cdot\cancel{\sin(\Delta\phi\to 0)}\cdot\begin{bmatrix}R\left(-\frac{\Delta}{2}\right)\cdot\eta_E^Q-\\ R\left(+\frac{\Delta}{2}\right)\cdot\eta_L^Q\end{bmatrix}+\eta_E^{Q2}-\eta_L^{Q2}\end{pmatrix}^2\right\rangle\end{aligned} \tag{1.32}$$

Taking advantage of $R\left(-\frac{\Delta}{2}\right)^2=R\left(+\frac{\Delta}{2}\right)^2$, of $\cancel{\langle\eta^{\text{odd}}\rangle}$, and of correlated noise in a given EML discriminator branch, $\sigma^2_{D_{EMLP}}$ can be further simplified by assuming equivalent noise levels on both I and Q branches, i.e. $\langle\eta_x^2\rangle=N_0\cdot T_P\cdot R_x(0)$ where the noise correlation is shifted from

$\pm\frac{\Delta}{2}$ to $0-\Delta$ on any given branch.

$$\begin{aligned}
\sigma^2_{D_{EMLP}} &\cong 4\cdot C\cdot T_P^2\cdot R^2\left(\frac{\Delta}{2}\right)\cdot\left\langle \eta_E^{I2}-\eta_L^{I2}\right\rangle+\left\langle\left(2\eta_E^{I2}-2\eta_L^{I2}\right)^2\right\rangle \\
&\cong 4\cdot C\cdot T_P^2\cdot\left\{1-m\left(\frac{\Delta}{2}\right)\right\}^2\cdot\{N_0\cdot T_P\cdot[R(0)-R(\Delta)]\} \\
&+ 4\left\langle \eta_E^{I2}\cdot\eta_E^{I2}-2\eta_E^{I2}\cdot\eta_L^{I2}+\eta_L^{I2}\cdot\eta_L^{I2}\right\rangle \\
&\cong C\cdot T_P^2\cdot\{2-m\cdot\Delta\}^2\cdot\{N_0\cdot T_P\cdot[\{1\}-\{1-m\cdot\Delta\}]\} \\
&+ 4\left[\{N_0\cdot T_P\cdot R(0)\}^2-\{N_0\cdot T_P\cdot R(\Delta)\}^2\right] \\
&\cong C\cdot N_0\cdot T_P^3\cdot m\cdot\Delta\cdot\{2-m\cdot\Delta\}^2+4\cdot N_0^2\cdot T_P^2\cdot m\cdot\Delta[2-m\cdot\Delta] \\
&\cong C\cdot N_0\cdot T_P^3\cdot m\cdot\Delta\cdot\{2-m\cdot\Delta\}^2\cdot\left[1+\frac{4}{\frac{C}{N_0}\cdot T_P\{2-m\cdot\Delta\}}\right]
\end{aligned} \tag{1.33}$$

Finally, we get:

$$\begin{aligned}
\sigma^2_{\tau_{EMLP}} &\cong \frac{2\cdot B_L\cdot T_P\cdot R_\eta(0)}{K^2} \\
&\cong \frac{2\cdot B_L\cdot T_P\cdot\left\{C\cdot N_0\cdot T_P^3\cdot m\cdot\Delta\cdot\{2-m\cdot\Delta\}^2\cdot\left[1+\frac{4}{\frac{C}{N_0}\cdot T_P\{2-m\cdot\Delta\}}\right]\right\}}{\left\{2\cdot C\cdot T_P^2\cdot m\cdot[2-m\cdot\Delta]\right\}^2} \\
&\cong \frac{B_L\cdot\Delta}{2\cdot\frac{C}{N_0}\cdot m}\cdot\left[1+\frac{4}{\frac{C}{N_0}\cdot T_P\{2-m\cdot\Delta\}}\right]
\end{aligned} \tag{1.34}$$

1.4.3 Non-Coherent DP

The Dot-Product discriminator output D_{DP} is defined as:

$$\begin{aligned} D_{DP} &= I_{EML} \cdot I_P + Q_{EML} \cdot Q_P \\ &= \left\{ \sqrt{C} \cdot T_P \cdot d \cdot \left[R\left(\tau - \frac{\Delta}{2}\right) - R\left(\tau + \frac{\Delta}{2}\right) \right] \cdot \cos(\Delta\phi) + \eta_{EML}^{I} \right\} \cdot \\ &\quad \left\{ \sqrt{C} \cdot T_P \cdot d \cdot R(\tau) \cdot \cos(\Delta\phi) + \eta_P^I \right\} \\ &+ \left\{ \sqrt{C} \cdot T_P \cdot d \cdot \left[R\left(\tau - \frac{\Delta}{2}\right) - R\left(\tau + \frac{\Delta}{2}\right) \right] \cdot \sin(\Delta\phi) + \eta_{EML}^{Q} \right\} \cdot \\ &\quad \left\{ \sqrt{C} \cdot T_P \cdot d \cdot R(\tau) \cdot \sin(\Delta\phi) + \eta_P^Q \right\} \end{aligned} \tag{1.35}$$

Its expected value is:

$$\begin{aligned} \langle D_{DP} \rangle &= \overline{I_{EML} \cdot I_P} + \overline{Q_{EML} \cdot Q_P} \\ &= C \cdot T_P^2 \cdot \left[R\left(\tau - \frac{\Delta}{2}\right) - R\left(\tau + \frac{\Delta}{2}\right) \right] \cdot R(\tau) \cdot \cancel{\left(\cos^2(\Delta\phi) + \sin^2(\Delta\phi) \right)} \\ &= C \cdot T_P^2 \cdot [2 \cdot m \cdot \tau] \cdot \{1 - m \cdot |\tau|\} \end{aligned} \tag{1.36}$$

With the gain, whose dependence on τ may be neglected:

$$K \cong 2 \cdot C \cdot T_P^2 \cdot m \cdot \cancel{\{1 - m \cdot |\tau|\}} \tag{1.37}$$

The noise variance being:

$$
\begin{aligned}
\sigma^2_{D_{DP}} &= \left\langle \left(D_{DP} - \overline{D_{DP}}\right)^2 \right\rangle \Big|_{\tau=0} \\
&= \left\langle \begin{pmatrix} I_{EML}\cdot I_P & - & \overline{I_{EML}\cdot I_P} + \\ Q_{EML}\cdot Q_P & - & \overline{Q_{EML}\cdot Q_P} \end{pmatrix}^2 \right\rangle \Bigg|_{\tau=0} \\
&= \left\langle \begin{pmatrix} \sqrt{C}\cdot T_P \cdot d \cdot \cancel{\left[R\left(-\frac{\Delta}{2}\right) - R\left(+\frac{\Delta}{2}\right)\right]} \cdot \cancel{\cos(\Delta\phi)} \cdot \eta^I_P + \\ \sqrt{C}\cdot T_P \cdot d \cdot \cancel{R(0)} \cdot \cancel{\cos(\Delta\phi)} \cdot \eta^I_{EML} + \eta^I_{EML}\cdot\eta^I_P + \\ \sqrt{C}\cdot T_P \cdot d \cdot \cancel{\left[R\left(-\frac{\Delta}{2}\right) - R\left(+\frac{\Delta}{2}\right)\right]} \cdot \cancel{\sin(\Delta\phi)} \cdot \eta^Q_P + \\ \sqrt{C}\cdot T_P \cdot d \cdot \cancel{R(0)} \cdot \cancel{\sin(\Delta\phi)} \cdot \eta^Q_{EML} + \eta^Q_{EML}\cdot\eta^Q_P \end{pmatrix}^2 \right\rangle \\
&= \left\langle \left(\sqrt{C}\cdot T_P \cdot d \cdot \eta^I_{EML} + \eta^I_{EML}\cdot\eta^I_P + \eta^Q_{EML}\cdot\eta^Q_P\right)^2 \right\rangle \\
&= \left\langle C\cdot T_P^2 \cdot \eta^{I2}_{EML} + \eta^{I2}_{EML}\cdot\eta^{I2}_P + \eta^{Q2}_{EML}\cdot\eta^{Q2}_P \right\rangle \\
&= C\cdot T_P^2 \cdot \left\langle \eta^{I2}_{EML}\right\rangle + 2\cdot\left\langle \eta^{I2}_{EML}\cdot\eta^{I2}_P\right\rangle \\
&= C\cdot T_P^2 \cdot \{N_0\cdot T_P\cdot[\{1\} - \{1 - m\cdot\Delta\}]\} \\
&+ 2\cdot\{N_0\cdot T_P\cdot[\{1\} - \{1 - m\cdot\Delta\}]\}\cdot\{N_0\cdot T_P\cdot\{1\}\} \\
&= C\cdot N_0\cdot T_P^3\cdot m\cdot\Delta\cdot\left[1 + \frac{2}{\frac{C}{N_0}\cdot T_P}\right]
\end{aligned}
\tag{1.38}
$$

Finally, we get:

$$\begin{aligned}
\sigma^2_{\tau_{DP}} &\cong \frac{2 \cdot B_L \cdot T_P \cdot R_\eta(0)}{K^2} \\
&\cong \frac{2 \cdot B_L \cdot T_P \cdot \left\{ C \cdot N_0 \cdot T_P^3 \cdot m \cdot \Delta \cdot \left[1 + \dfrac{2}{\dfrac{C}{N_0} \cdot T_P} \right] \right\}}{\left\{ 2 \cdot C \cdot T_P^2 \cdot m \cdot \left\{ 1 - \cancel{m \cdot |\tau|} \right\} \right\}^2} \\
&\cong \frac{B_L \cdot \Delta}{2 \cdot \dfrac{C}{N_0} \cdot m} \cdot \left[1 + \frac{2}{\dfrac{C}{N_0} \cdot T_P} \right]
\end{aligned} \tag{1.39}$$

In such non-coherent discriminators, squaring losses is due to squaring, cancelling the ± 1 data bit while doubling the noise. Hence, non-coherent processing is usually 3 dB less sensitive than coherent processing. This squaring loss was isolated in square brackets in the code noise jitter equations above. Hence, in non-coherent discriminators, the associated code noise may have a larger variance, but preserves the same null mean.

The above tracking architectures should offer a code tracking improvement of m in BOC over BPSK. Also, code noise variance and maximum multipath errors are proportional to the correlator spacing in an EML DLL. On the other hand, the noise performance decreases as the distance of the tracking point from the correlation peak increases. This is a good example for the necessity of a trade-off between a good multipath performance and an acceptable noise performance, which is further assessed in Appendix II.

1.5 Modulations and Auto-correlation Summary

In this chapter, the fundamentals of receiver tracking loops have been presented, with an emphasis on the PLL and DLL parts of its high level block diagram.

It has been shown that the spreading code characteristics influence the DLL complexity and expected performances. For example the traditional BPSK(q) modulation and corresponding

ACF has a wider linear range than in the case of BOC(p,q), for a given chipping rate and front-end bandwidth. This is due to the introduction of a square sub-carrier superposed onto the square chips of a spreading code. The resulting local ACF minima introduce tracking false locks, a main concern called the BOC ambiguity. Finally, different coherent and non-coherent code discriminator have been compared in terms of noise theoretical assessment.

The next chapter presents a survey of GNSS signals, whose definition is based on the modulations introduced herein.

CHAPTER 2

SURVEY OF GNSS SIGNALS

Current concerns regarding signals coexistence in an already crowded spectrum are defined in terms of interoperability and compatibility. “Compatibility” refers to the ability of two or more systems to perform their functions, while sharing the same environment (C/S2ESC - Software & Systems Engineering Standards Committee, 1990). Hence, the ability of multiple satellite navigation systems to co-exist and be used separately (or jointly), without interfering with one another, has lead to international regulation initiatives. On the other hand, “interoperability” refers to the ability of two or more systems to exchange information and use it (C/S2ESC - Software & Systems Engineering Standards Committee, 1990). Thus, in order to allow open services of multiple satellite navigation systems to be jointly used (providing improved user capabilities over those from single service), these systems should be derived from common design principles to simplify user equipment, such as GNSS receivers.

In order to design a universal channel consuming as few resources as possible, an assessment of the GNSS civil signal characteristics, highlighted in Figure 2.1 must first be performed. Hence, the following material will lay down the basis for the design of a universal navigation acquisition/tracking channel. In an attempt to clarify the different aspects of all signals, this survey will proceed by constellations, from the oldest (in terms of full compliance) to the ones to come, i.e. GPS, GLONASS, Galileo and BeiDou, detailed in their corresponding sections.

This chapter provides a summary of satellite navigation systems and associated signals.

2.1 GPS Constellation

The Global Positioning System (GPS) results from many prior efforts in mastering satellite communications. It was designed by the Department of Defense (DoD) and first intended for military applications. After reaching Full Operational Capability (FOC) in April 1995 and being declared available to civil users in 1996, the Coarse Acquisition (C/A) signal on L1 soon

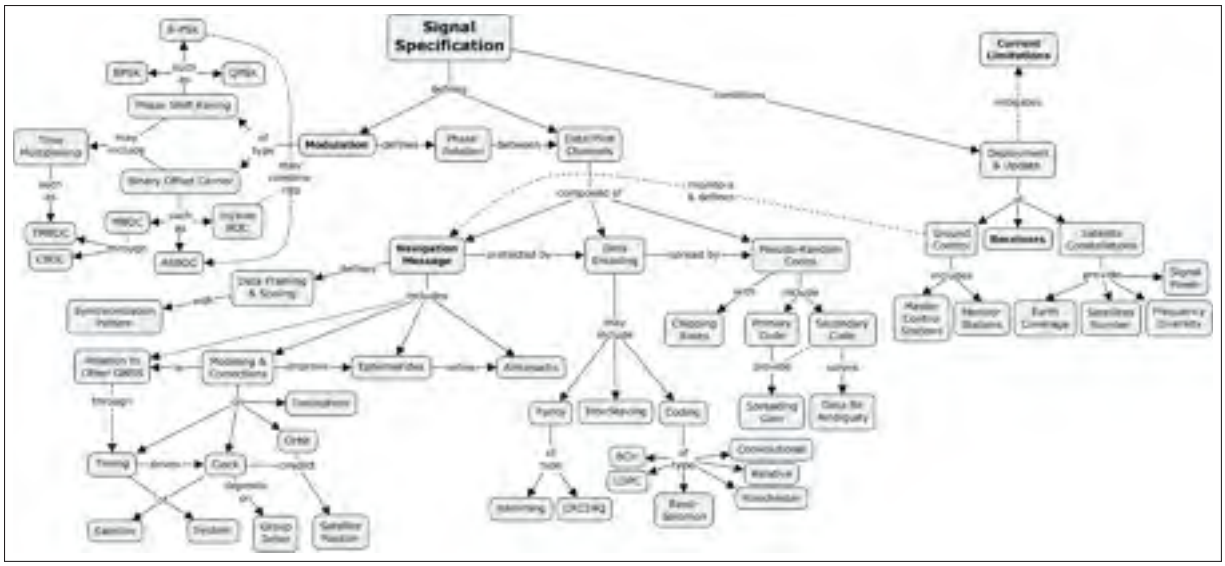

Figure 2.1 GNSS Signals

became widely used in civil applications, despite the fact that its Selective Availability (SA) provided a User Equivalent Range Error (UERE) of ± 25 m, until it was deactivated on May 1st, 2000 (National Coordination Office for Space-Based Positioning Navigation and Timing, 2001). This political decision was partly motivated by the fact that the induced pseudo-random phase noise could be removed through differential systems. The fact that the European Union (EU) was laying down the basis of a new public navigation system might also have influenced the decision, as mentionned by PosiTim (2010):

> Selective Availability (SA), the denial of full accuracy, is accomplished by "manipulating" navigation message orbit data (epsilon) and/or the satellite clock frequency (dither). So far, only the satellite clock frequency has been manipulated. With this dithering process the GPS satellite clocks are artificially degraded by adding a signal with an unknown frequency and amplitude to the known clock behavior. This is done to degrade the performance of GPS for the "normal" users. Both, the frequency and amplitude of the added signal, change rapidly over time. The amplitude of this "clock dithering" is of the order of 0.3 microseconds (which corresponds to roughly 100 meters) and the frequency is of the order of only a few minutes. This SA clock dithering limits the accuracy of real time position estimates to 25 meters RMS. Selected (military) users possess special "keys" to remove the SA-effect in real time giving them access to the full navigation potential of GPS, i.e., one meter real time absolute point positioning.

As a proof of this commitment, GPS block IIF and newer satellites will not offer the SA option anymore (U.S. Department of Defense, 2007).

The GPS constellation is composed of nominally 24 satellites distributed over 6 orbits equally spaced along the Equator (i.e. a right ascension of the ascending node separation of 60°) and inclined by 55° with respect to it. Nevertheless, as of January 2015, there are 30 healthy satellites, plus another in commissioning phase or in maintenance. During year 2014, 7 block IIA still valid satellites were forced into retirement, relegated to an outer orbit (National Coordination Office for Space-Based Positioning Navigation and Timing, 2015a).

Since the DoD has a satellite replacement philosophy based on orbiting satellite failures as opposed to new satellites availability on ground, some instances (Coursey, 2009) were worried that the constellation would soon be outperformed by emerging constellations with aggressive launch rates. Nevertheless, at the ION GNSS 2011 conference discussion panel on GNSS signals, representatives of Galileo and BeiDou both predicted a FOC by 2020, leaving plenty of time for GPS to pursue with its progressive satellite replacement plan.

But more importantly, this approach almost caused them to lose the right to broadcast on L5. The International Telecommunication Union (ITU) had granted the Department of Defense (DoD) the right of broadcasting on L5, within the protected Aeronautical Radio Navigation Services (ARNS) band, under the condition that a first satellite transmissions were to happen before a specified deadline. In order to meet this requirement, a IIR-M satellite launched at the end of 2010 was upgraded with a preliminary L5 payload. The Satellite Vehicle Number (SVN) 49, well known for its unrepairable phase incoherence between L1 and L5, has been decommissioned on May 6th, 2011, now that more satellites are broadcasting on L5, i.e. PRNs 1 and 25 (Gibbons, 2009).

Because of the orbit inclination of the GPS satellites, their ground track[1] is limited to latitude below 55°, as depicted by Figure 2.2. The orbits are posigrade, meaning the satellites move along with the Earth rotation. GPS satellites travel along an almost perfectly circular orbit

[1] A ground track represents the projection of the satellite position onto the surface of the Earth.

of 26 560 km average radius (i.e. a 20 180 km altitude) at a ∼3900 m/s linear speed. Their revolution period lasts 11 h 58 min 2 s, thus introducing a ground track drift of 4 minutes per solar day. Indeed, during the first satellite revolution of almost half a day, the Earth has performed a 180° rotation (the satellite would thus not be visible). Nevertheless, after two such revolutions, the Earth has performed a full rotation[2], making the satellite visible again at approximately the same time the following day.

In Figure 2.2, the green circle shows the satellite position, and its area of visibility for the requested time. The ground track (red/orange) is plotted for the time interval covering 2.3 orbital period(s), where red is before, and orange after this time. A thin satellite ground track and footprint outline indicates the satellite is in the shadow of Earth and not visible by optical means. The yellow dot is the position with the Sun directly overhead, and the green cross is your position.

The resulting Earth Centered Earth Fixed (ECEF) position of a satellite is displayed in Figure 2.3. Hence the period of visibility of a GPS satellite is at most six hours (assuming horizon visibility for a static observer over which the satellite will reach zenith) every 24 h period. However, if the satellite orbit does not reach zenith over an observer, its visibility period may be split into shorter periods, the sum of which should still cumulate to six hours. Furthermore, the satellites among any given orbit are not equidistant from one another, but rather strategically located to ensure a better coverage of the DoD's coverage zones of interest (National Coordination Office for Space-Based Positioning Navigation and Timing, 2015a).

Although military signals could be used through the well known technique of semi-codeless tracking[3], they will not be described herein since, on May 16, 2008, the Office of Space Commercialization announced its plan to phase out codeless and semi-codeless access to GPS by

[2] The sidereal day (i.e. a 360° rotation of the Earth about itself, with respect to a distant star) lasts 23 h 56 min 4.091 s, only a few minutes away from the ground track period of 24 h.

[3] Semi-codeless tracking makes it possible to track signals, even without knowledge of their encrypted spreading codes, where the unknown 500 chip/s Y code is modulo-2 added onto the known 1 week long P spreading code rated at 10.23 Mchip/s, resulting in the spoofing resistant P(Y) code. It takes advantage of the fact that the "encrypted" P(Y) code is synchronously transmitted on both L1 and L2 frequencies. Hence, correlating a frequency-compensated version of one band signal with that of the

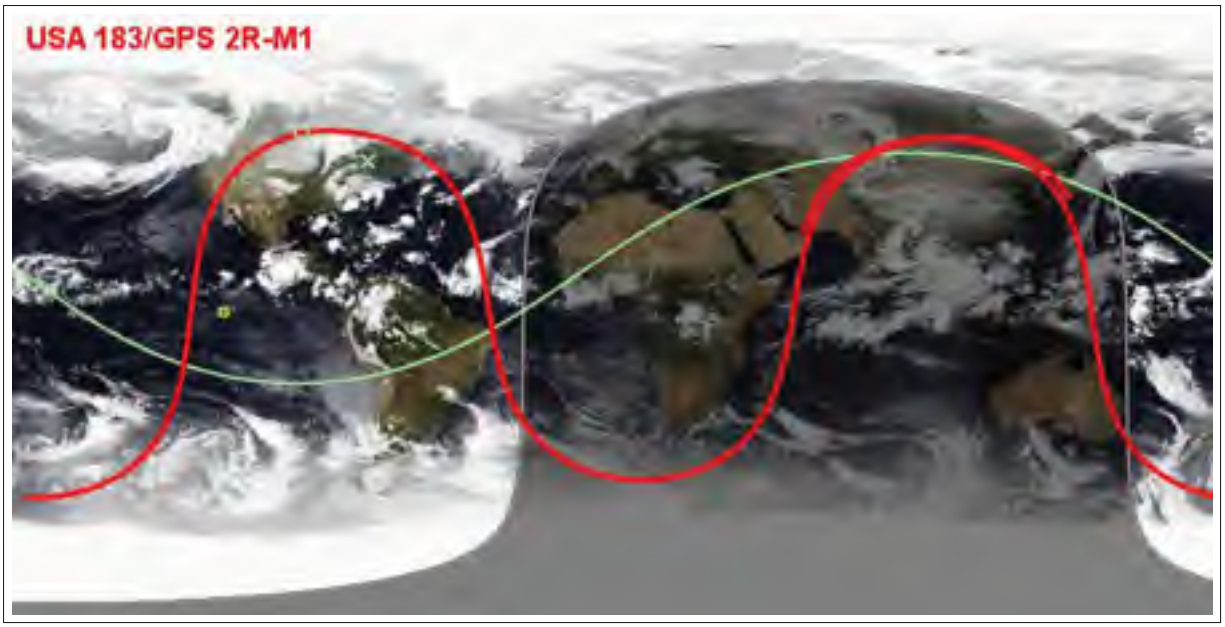

Figure 2.2 Ground Track of a GPS Satellite over 24 h
Taken from Barmettler (2015)

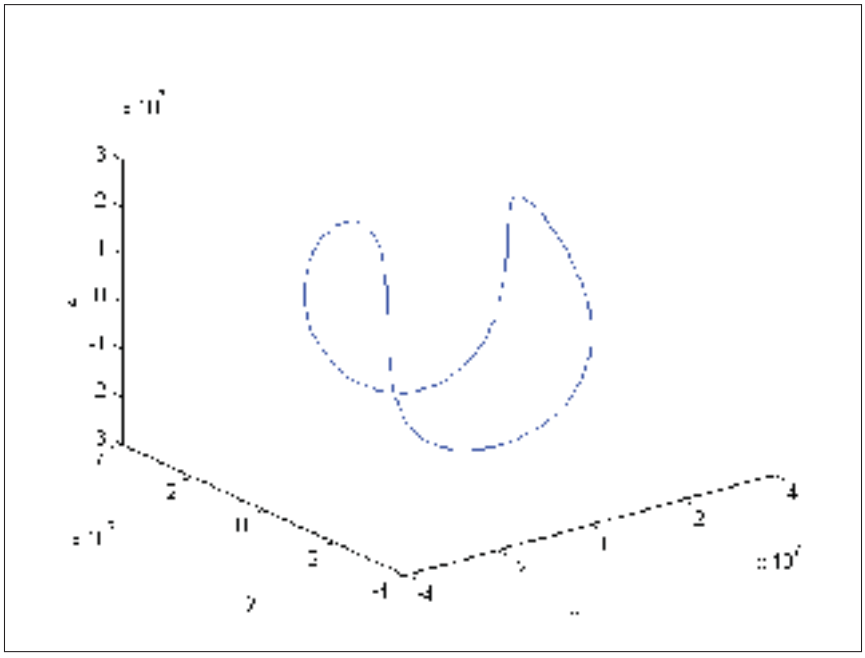

Figure 2.3 GPS Satellite ECEF Position [m] over 1 Ground Track Period

second frequency successfully removes the unknown code. This strategy allows one to make high precision phase measurements (Montenbruck *et al.*, 2006).

December 31, 2020 (Office of Space Commercialization, 2008), encouraging GPS receiver manufacturers to favor the new civil signals L2C and L5 for their dual/triple frequency measurements, although unlike L1 and L5, L2 cannot be used for aviation as it falls out of ARNS bands. L5 offers a military-like signal to civilians, although it suffers from multiple interference sources such as Distance Measurement Equipment (DME) and Very High Frequency (VHF) Omnidirectional Range (VOR).

The following subsections will describe current (initial and modernized) as well as future civil signals definition amongst the three 24 MHz wide transmission frequency bands (i.e. L1, L2 and L5), starting with the most widely used GPS L1 C/A.

2.1.1 GPS L1 C/A

GPS L1 C/A is the Coarse Acquisition signal on the L1 ARNS band, whose center frequency is located at f_{L1} =1575.42 MHz, which is an integer multiple (i.e. 154) of the 10.23 MHz reference clock on-board the satellites. As defined in the Interface Control Document (ICD) (Global Positioning System Wing (GPSW) Systems Engineering & Integration, 2013), its spreading codes are 1023 chip-long Gold codes (Gold, 1967). The chipping rate being $f_c = 1.023$ MHz, the code period is 1 ms long, assuming it is not affected by Doppler. The Doppler phenomenon refers to the relative motion v_r between the transmitter and the receiver in the direction of the Line of Sight (LoS).

$$\Delta f = \frac{v_r}{\lambda} \tag{2.1}$$

For example, a reducing LoS induces both a code length contraction and a frequency increase of the received signal, such as the siren of an approaching police car.. Considering a light speed of 299 792 458 m/s, a chip length represents $\frac{c}{T_c} \approx 291.3$ m. Assuming a typical DLL performance with a resolution of 1 % of a chip (based on the chip transition detection), the best achievable pseudo-distance estimate would then be in the range of $\sim$3 m. The resulting PVT solution, based on a Least-Mean-Square approach minimizing these measurement residuals, would have

a standard deviation that would also depend on the constellation geometry, measured as the DoP.

Moreover, since there is no secondary code, an integer ambiguity ($c \cdot 1$ ms ≈ 300 km) remains between the periods of the code and of the navigation data bit. Since the 50 bit/s navigation data bit (without any channel encoding) lasts 20 ms, 20 consecutive spreading codes are transmitted for every navigation data bit. Also, from a modulation stand point, the GPS L1 C/A signal is of the simplest form, i.e. BPSK. More precisely, the $2^m - 1$ chip-long Gold codes are balanced independent and identically distributed (iid) sequences, where the number of digital "1" and "0" only differ by one, leading to close to null frequency component at 0 Hz. Moreover, the preferred subset of 37 Pseudo Random Noise (PRN) codes misaligned auto-correlation product may only take the values: $\{-1, -t(m), t(m) - 2\}$ with $(m = 10)$:

$$t(m) = \begin{cases} 2^{\frac{m+1}{2}} + 1 \leftarrow \text{odd } m \\ 2^{\frac{m+2}{2}} + 1 \leftarrow \text{even } m \end{cases} \tag{2.2}$$

Note that the digital spreading sequence ("0" and "1") must be translated into a bipolar, i.e. a rectangular Non-Return to Zero (NRZ), sequence of "± 1" in order to achieve these figures. According to Kaplan and Hegarty (2006, Table 4.7), the typical misaligned autocorrelation level isolation is proportional to the spreading code length.

The GPS L1 C/A spreading Gold codes used by GPS (the last five being reserved for ground applications, only 32 could initially be assigned to a satellite... this will be expanded to 63 with block III satellites (Global Positioning System Wing (GPSW) Systems Engineering & Integration, 2013)) are specified to have a cross-correlation protection around 21 dB (considering the summed effect of all 32 satellites) (Kaplan and Hegarty, 2006, table 4.9). As depicted in Figure 2.4, the lowest CCF measured is 20.55 dB between any two codes, which is slightly worse than the theoretical value, i.e. $20 \cdot \log_{10}\left(\frac{N}{t(m)}\right) = 23.94$ dB, in agreement with Kaplan and Hegarty (2006, table 4.8).

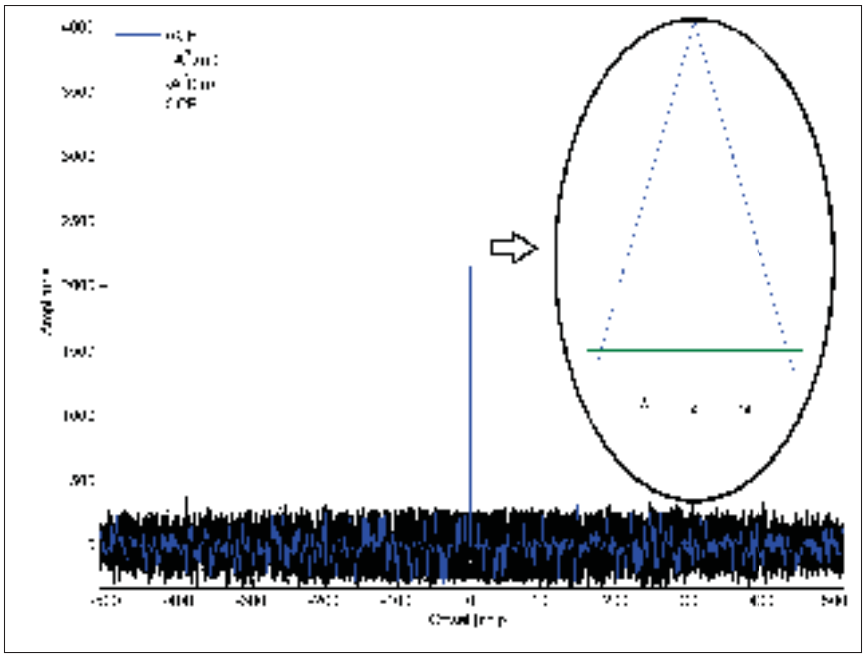

Figure 2.4 ACF of a Rectangular NRZ Spreading Code with Length $N = 1023$ and Signal Amplitude $A = 2$

Knowing that the Power Spectral Density (PSD) of a signal is given by the Fourier Transform (FT) of its Auto-Correlation Function (ACF), a square pseudo-random sequence with a chipping period T_c and amplitude A has a PSD given by $A^2 T_c \text{sinc}^2(\pi f T_c)$. For example, in the case of GPS L1 C/A, the PSD of the 50 bit/s navigation data displays a greater maxima than that of its 1.023 Mchip/s spreading code, leading to the spreading gain:

$$10 \cdot \log_{10} \frac{\text{chipping rate}}{\text{data rate}} = 10 \cdot \log_{10} \frac{1\,023\,000}{50} = 43.1 \text{ dB} \tag{2.3}$$

More precisely, assuming a signal power received at ground level of -160 dBW (i.e. 10^{-16} or a corresponding amplitude $A = 10^{-8}$), the maximal PSD of the data would be $A^2 T = 2 \cdot 10^{-18}$ W/Hz or equivalently -177 dBW/Hz or -147 dBm/Hz. Similarly, a 1 Mchip/s spreading code PSD is approximately -190 dBm/Hz, 43 dB lower than that of the navigation data. At room temperature (i.e. $T^\circ = 300$ K), the noise is known to have a DSP of $N_0 = k_B \cdot T^\circ = -174$ dBm/Hz. So, the spreading code PSD is below the noise floor, but not that of the data, as displayed in Figures 2.5 and 2.6.

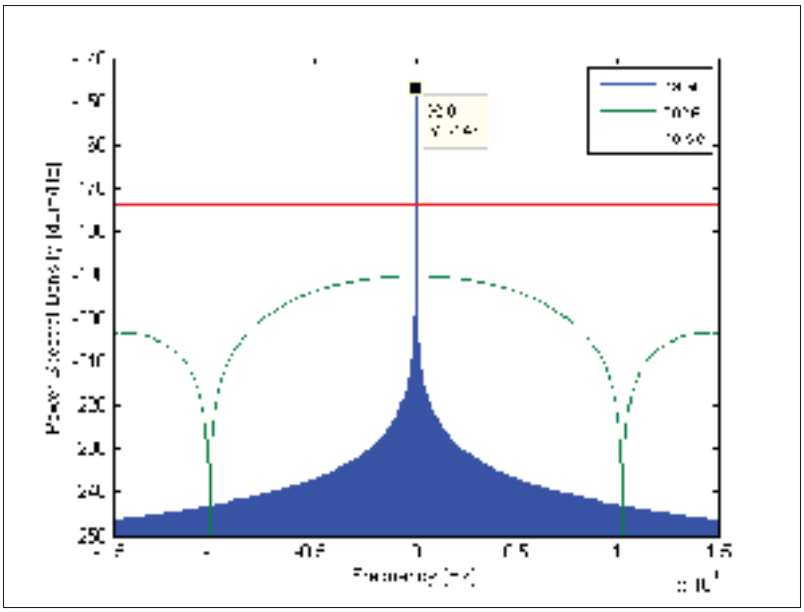

Figure 2.5 Power Spectral Densities of GPS L1 C/A

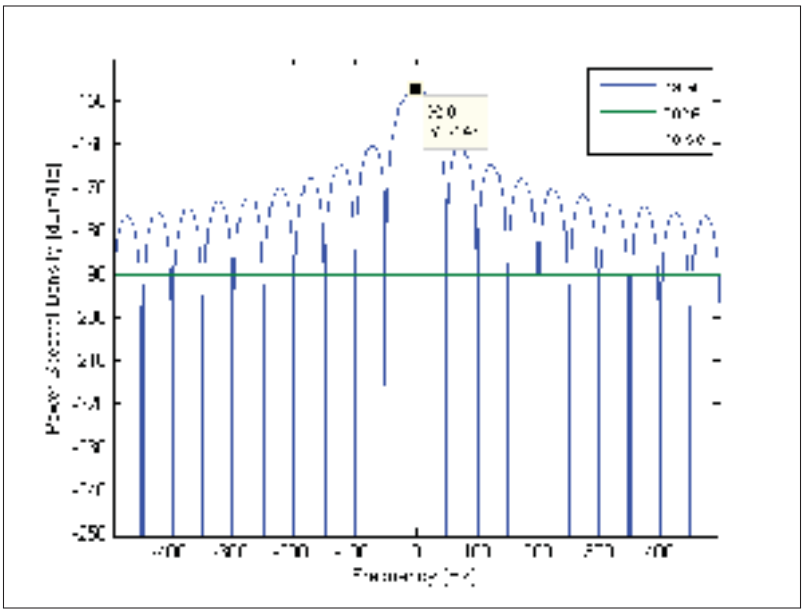

Figure 2.6 Zoom on the Power Spectral Densities of GPS L1 C/A

Nevertheless, the power is what really matters. In the current implementation of the development platform (named *RxGNSS*), a 22.3 MHz wide 3 dB bandwidth is admitted, as specified

by Sauriol (2008, p. 89), leading to the front-end noise power $\eta_{\text{front-end}}$:

$$\begin{aligned} \eta_{\text{front-end}} &= -174 \text{ dBm/Hz} + 10 \cdot \log_{10}(22.3 \text{ MHz}) \\ &= -174 + 73.48 = -100.52 \text{ dBm} \end{aligned} \tag{2.4}$$

The GPS L1 C/A signal is typically received with a power greater than -158.5 dBW (or equivalently -128.5 dBm) (Global Positioning System Wing (GPSW) Systems Engineering & Integration, 2013), making it impossible to observe at the front-end.

$$\text{SNR}_{\text{front-end}} = -128.5 - -100.52 \not\geq 10 \text{ dB} \tag{2.5}$$

Where the above 10 dB is a conservative SNR threshold enabling proper PLL behaviour (Blanchard, 1976).

However, the post-correlation bandwidth may be reduced to say 1 kHz (after 1 ms integration, i.e. post-correlation filtering). The noise power then becomes:

$$\begin{aligned} \eta_{\text{Post-correlation}} &= -174 \text{ dBm/Hz} + 10 \cdot \log_{10}(1 \text{ kHz}) \\ &= -174 + 30 = -144 \text{ dBm} \end{aligned} \tag{2.6}$$

This leads to a $\text{SNR}_{\text{Post-correlation}} = -128.5 - -144 = 15.5$ dB. The post-correlation SNR thus depends on the integration time (and the resulting noise bandwidth).

When comparing receiver sensitivity, a common metric used is the Carrier power to Noise density ratio (C/N_0) to make abstraction of the post-correlation bandwidth. In the case of the GPS L1 C/A signal, the minimal expected ratio (without additional sources of noise) would be:

$$\frac{C}{N_0} = -128.5 \text{ dBm} - -174 \text{ dBm/Hz} = 45.5 \text{ dB-Hz} \tag{2.7}$$

In fact, C/N_0 and SNR are related by the post-correlation bandwidth:

$$\frac{C}{N_0} = \text{SNR} + 10 \cdot \log_{10}(\text{BW}) \tag{2.8}$$

2.1.2 GPS L1C

With an increasing demand for commercial navigation applications with improved performances, GPS is undergoing a modernization phase. Indeed, the Block III generation of satellites will introduce a new civil signal, namely the GPS L1C, with improvements over the legacy signal L1 C/A to help users compute their position more reliably. This additional civil signal on L1 first needed to coexist with its predecessor, i.e. compatibility. Hence, its spectrum was split into two via the BOC modulation, which introduces a square sub-carrier.

To summarize, L1C has the following main characteristics:

- A 10 230 chip-long spreading memory code composed of a Weil code (i.e. a 10 223 chip-long unique Legendre Sequence xor'ed with itself with a specified relative shift) to which a 7 chip fixed sequence is inserted at a specified index. These primary codes provide a cross-correlation isolation of ~ 28 dB.

- A data component (I) is modulated with BOC$(1,1)$, which preserves the same chipping rate as for L1 C/A, but doubles its occupied bandwidth due to its 1.023 MHz square sub-carrier. Its period lasts 10 ms. Since the encoded data (i.e. symbol) rate is 100 symbols/s, there is no code period ambiguity, as was the case with the legacy signal. Its typical ground level power is -163 dBW.

- A data-less component allows users to perform unlimited coherent integration, without requiring data wipe-off through an external aid. This *pilot* component (Q) is in phase quadrature with its data counterpart (I). The pilot has the same chipping rate, but its sub-carrier alternates between $1 \cdot 1.023$ and $6 \cdot 1.023$ MHz frequencies in a 29 to 4 ratio; i.e. 29 predetermined slots out of 33 are BOC$(1,1)$ while the remaining 4 slots are BOC$(6,1)$, achieving a Time Multiplexed BOC (TMBOC), as depicted in Figure 2.7.

- Considering that the pilot component has 75 % of the of the total L1C signal power (i.e. $10 \cdot \log(3) = 4.77$ dB higher than its data counterpart, with a nominal ground-level power of -158.25 dBW), it can be thus demonstrated that the Multiplexed BOC (MBOC) spectrum

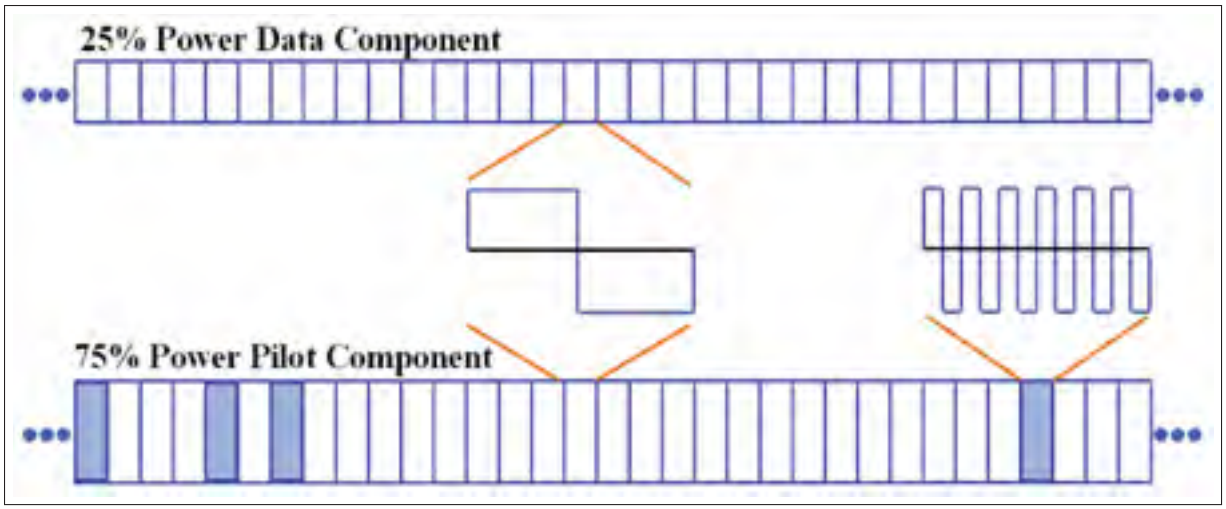

Figure 2.7 TMBOC Pilot Sub-Carriers Assignation Pattern
Adapted from ARINC Engineering Services (2013, Figure 3.3-2)

requirement is fulfilled, as per its definition (the impacts on spectrum and ACF are depicted in Figures 2.8 and 2.9):

$$G_{\mathrm{MBOC}}(f) = \frac{10}{11} G_{\mathrm{BOC}(1,1)}(f) + \frac{1}{11} G_{\mathrm{BOC}(6,1)}(f) \tag{2.9}$$

Nevertheless, according to van Dierendonck (2014), RTCA and EUROCAE MOPS do not require $\mathrm{BOC}(6,1)$ tracking; the associated low signal loss may not justify its added tracking implementation complexity.

- A 1800 chip-long secondary code is superposed onto the pilot primary code, where one secondary chip lasts a full primary code period. If a receiver tracking loop is not anchored to this secondary code, it acts as an unknown data message, limiting the coherent integration time to the 10 ms primary code period. Synchronizing a 1.8 s long code is quite a demanding task unless the search space is reduced by estimating the Satellite Vehicle (SV) transmission time and the pseudo-range. All signal components are synchronized on-board the satellite, hence the current secondary chip index may be extrapolated.

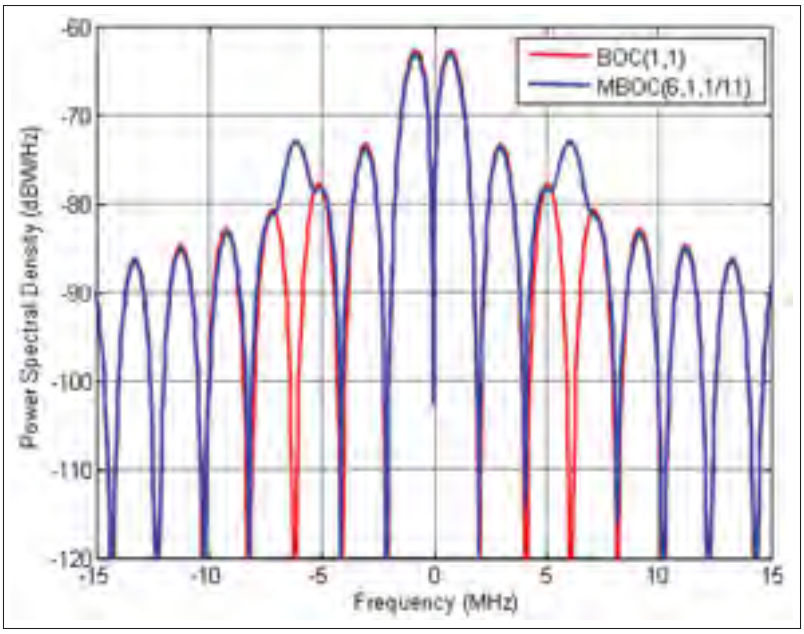

Figure 2.8 MBOC Definition Through its Spectrum

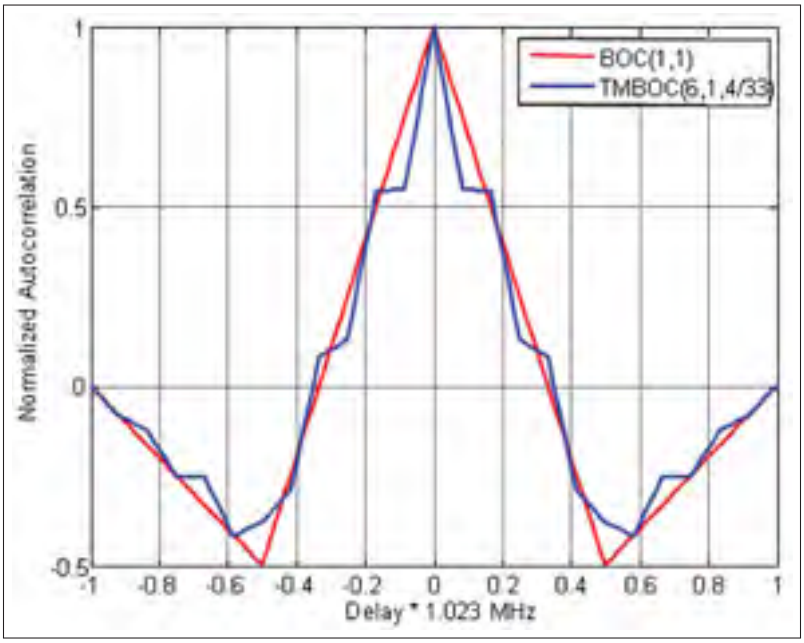

Figure 2.9 TMBOC Impact on ACF
Taken from Ávila Rodríguez (2014)

- The navigation message subframes 2 and 3 are encoded with Low Density Parity Check or LDPC($\frac{1}{2}$) on top of Cyclic Redundancy Check (CRC) on 24 bits, while subframe 1 is encoded with Bose, Chaudhuri, and Hocquenghem (BCH).

Hence, receivers with lower sampling rates should still acquire and track the signal by only processing the data component, but would suffer a power loss of $10 \cdot \log_{10}(\frac{1}{4}) = 6$ dB by only taking advantage of 25 % of the available signal power. A better compromise would consist of only processing the BOC$(1,1)$ modulation part of the complex signal, leading to a $10 \cdot \log_{10}(\frac{1}{4} + \frac{3}{4} \cdot \frac{29}{33}) = 10 \cdot \log_{10}(\frac{40}{44}) \approx 0.4$ dB theoretical loss, although requiring twice the hardware to process both I and Q signal components. Equivalently, as per the MBOC definition, dropping the BOC$(6,1)$ components of the complex signal represents a power loss of $\frac{1}{11}$ resulting in a admitted signal power of $\frac{10}{11} \sim 0.4$ dB loss, as seen above.

The future L1C signal will build over the modernized civil signals putting forward a navigation message called CNAV-2, composed of 1800-symbol long frames (including Forward Error Correction or FEC) transmitted at 100 symbols/s. Its frames contain 9 bits of timing information, 600 bits allocated to clock and ephemeris and 274 bits of variable payload packets.

2.1.3 GPS L2C

Since its beginning, GPS satellites have been broadcasting encrypted military signals P(Y) for Precise Positioning Service (PPS) on both L1 and L2 frequencies, respectively at integer ratios of 154 and 120 times the 10.23 MHz on-board reference clock. The advantage of dual-frequency receivers is to compensate for ionospheric delays, which are proportional to the carrier frequency. Although this compensation outperforms any single-frequency model (e.g. Klobuchar), it can be reliably approximated through ionospheric corrections provided by Wide Area Augmentation Systems (WAAS) over the North American territory (Guay, 2010), although intense solar activity can cause error reaching tens of meters (Enge and van Diggelen, 2014), where a multi-frequency receiver might have outperformed augmentation performances. While the L5 signal was being defined, GPS went ahead with a second civil signal to rapidly provide dual-frequency signals for civil users. Indeed, the satellites payload was expanded to include a civil signal on an already available frequency (i.e. L2), rather than on a third one (i.e. L5).

A downside to L2C is that is lies on a frequency band open to all sorts of Radio Navigation Satellite Services (RNSS), which includes more potential interferences than the ARNS, employed by civil aviation applications, such as with L1 an L5 bands. Although, 15 GPS satellites are now broadcasting L2C, thanks to the Air Force CNAV uploads since December 31st, 2014, it is still considered pre-operational and should be used at the user's risk (National Coordination Office for Space-Based Positioning Navigation and Timing, 2015b).

Here are L2C most important characteristics:

- A 10 230 chip-long Civilian Moderate (CM) length spreading code obtained by a Galois sequence[4] is transmitted at 511.5 kchip/s and lasts 20 ms. Since the secondary code length matches that of a navigation bit, integer code ambiguity may be avoided. In the GPS constellation, the propagation time varies between 66 ms (at zenith) and 80 ms (at horizon). A code period of 20 ms thus avoids the integer code ambiguity problem.

- This CM code is time-multiplexed with a 767 250 chip-long Civilian Long (CL) spreading code obtained through the same polynomial. It is also transmitted at a 511.5 kchip/s chipping rate. It therefore lasts $\frac{767\,250}{511.5\times10^3} = 1.5$ s. Its offers a substantial correlation suppression (~ 44 dB) (Gernot *et al.*, 2007).

- The spreading code resulting from alternating the CM and CL codes is thus transmitted at a combined rate of 1.023 Mbit/s, leading to a modulation specified as Time-Multiplexed BPSK or TMBPSK($\frac{1}{2}, \frac{1}{2}$).

- The merged spreading code (i.e. the L2C code) can be expected at -160 dBW at ground level (and eventually at -158.5 dBW in Block III satellites) (Global Positioning System

[4] In order to generate the same output sequence than a Fibonacci sequence, the shift register taps (which may also be defined by a code generator polynomial) of a Galois sequence are computed in the inversed order of those of a conventional Linear Feedback Shift Register (LFSR). Furthermore, the eXclusive OR (XOR) operations are performed on the output of the feedback and that of the previous register in the chain; the computation time of such a structure is thus reduced as it is easily programmed in parallel, rather than computing the feedback as the XOR of all the taps at once. Note that the internal state of both LFSR sequences (namely Fibonacci and Galois) is not necessarily the same.

Wing (GPSW) Systems Engineering & Integration, 2013). Nevertheless, during initial acquisition would suffer a 3 dB loss by only correlating with the CM code. Compared to L1 C/A code, this yields a longer albeit less probable acquisition, given 4.5 dB weaker harvested signal.

- The navigation message follows a new GPS standard named Civil NAVigation message (CNAV), which is also used by the GPS L5-I signal. Its Forward Error Correction (FEC), identical to that of WAAS L1 signal, allows detecting and correcting errors. This margin allows receivers to collect data only once before using it, as opposed to twice the GPS L1 C/A data (van Dierendonck, 2014). Furthermore, its slower 25 bit/s navigation message rate becomes 50 symbols/s, thus perfectly overlaying onto the 20 ms long CM code.

In the case of strong signals, L1 C/A assisted L2 CM acquisition is desirable as it reduces the CM code search space[5]: Lim *et al.* (2006) proposed to aid L2C acquisition with CM code phase and frequency offset estimation through L1 C/A; Psiaki (2004) developed a frequency-domain acquisition scheme to acquire L2 CM and CL codes under weak signal conditions; Yang (2005) compared acquisitions approaches on L2 CM alone, L2 CL alone and on joint CM/CL codes.

L2C has 2.7 dB greater data recovery and 0.7 dB greater carrier-tracking compared to L1 C/A, even if its transmission power is 2.3 dB weaker. Also, its modernized navigation message contains a GPS-to-GNSS time offset, allowing for interoperability with other global time systems. Moreover, the system is designed to support 63 satellites, compared to only 32 in the original L1 NAV message. When using L2C signal alone, a user should expect 65 % more position uncertainty than with the L1 signal as the ionosphere impact becomes more important at lower frequencies.

[5] L1 C/A has a 10 times shorter code, that lasts 1 vs. 20 ms. Nevertheless, both codes are synchronized at the satellite and their Doppler ratio corresponds to their carrier frequency ratio.

2.1.4 GPS L5

GPS L5 (located at $115 \cdot 10.23 = 1176.45$ MHz) is the second GPS signal in the ARNS band, making it possible for civil aviation to use dual-frequency GPS measurements. Nonetheless, this band is shared with other RF sources on the surface of the Earth, which would not impact flying aircrafts as other ground receivers. Apart from the early launch of a satellite SVN49 with the L5 payload rushed in (so that the granted transmission frequency band could be preserved, but still ended up being discarded when later replaced by a healthy one), there are now 8 GPS satellites broadcasting this new civil signal and the ninth planned for March 2015 (U.S. Department of Homeland Security, 2015).

In order to withstand all the interference caused by other aviation measurement equipment, such as DME and VOR, within the same frequency band, the L5 signal needs a large bandwidth. Hence, its chipping rate was set to 10.23 Mchip/s; its QPSK(10) modulation leading to a 20.46 MHz wide main lobe. Both signal components (data and pilot) in phase quadrature with one another are publicly available, making it possible for civil users to benefit from the same precision U.S. military and their allies have been using for years with the encrypted P(Y) code. Another benefit of L5 is its Safety of Life (SoL) integrity messages.

One great advantage of L5 over L2C is its primary code period of 1 ms (i.e. 10 230 chips rated at 10.23 Mchip/s). A sequential search can thus easily be performed on consecutive ~ 1 ms worth of incoming signal, correlated by a local code shifted by one additional chip every iteration. Hence, in cold start, the worst acquisition time would be 10.23 s times the amount of Doppler bins considered.

Another advantage over L2C is that its dataless pilot component, overlayed with a 20 ms long secondary code (unique to all SVs), can be integrated over longer periods, once synchronized with the secondary code. The resulting code has a total period of 20 ms, thus avoiding the integer code ambiguity (caused by a 66-80 ms long propagation time). The data counterpart also has a 10 ms long secondary code overlaying onto the primary one, thus avoiding the 100 symbols/s data symbol ambiguity.

The transmitted power dedicated to L5 is -157.9 dBW (in Block IIF satellites, but eventually -157 dBW with Block III) for each signal component, leading to a total currently available power of -154.9 dBW, which is more than twice the power for GPS L1 C/A.

Just as for L2C, its navigation message is based on CNAV, although there are some slight differences between the two: namely Integrity Status and L2C Phasing flags in Message Type 10.

In the CNAV message, the preamble is also continuously encoded, without any reset. Fortunately, the 8-bit preamble is followed by the 6-bit PRN. Hence, the synchronization may be achieved without prior decoding by searching for the encoded 28 symbols resulting from the 14 bits above. Given a coding constraint length of 7, one can conclude that any symbol will depend on the previous 6 bits. Therefore, the last 16 symbols out of 28 are searched for with a periodicity of 500 symbols. Once this first synchronization step is achieved, we can spend the decoding effort with great chances of success. This approach dramatically reduces the CPU effort.

2.1.5 GPS summary

Naturally, military signals on L1 and L2 have also been modernized through the addition of the military M code, which is modulated with a sBOC$(10,5)$. Theoretically its two main lobes use up to $2\cdot(10+5)\cdot 1.023 = 30.69$ MHz. Thus, the 24 MHz transmission bandwidth granted by ITU encompasses 70 % of the signal power (Barker *et al.*, 2000). One noticeable advantage of this split spectrum lies in the fact that civil signals could be jammed, while US allies could still use the military M code. This signal not being publicly disclosed, it will not be further described herein.

The RNSS bandwidths for GPS signals is 24 MHz on the L1, L2 and L5 bands (only L1 and L5 being ARNS), leaving plenty of room for low chip rates, typically used for civil signals. For military and L5 signals, the chipping rate reaches 10.23 Mchip/s. In order to remain compliant with ITU regulations, the signals have to be attenuated in such a way as to prevent a specified

interference level outside the allocated bands, on adjacent frequency bands; 24 MHz partially including the secondary lobes of the BPSK(10) and QPSK(10) modulations. A concern has been the addition of new signals in an already crowded spectrum, in order to ensure both interoperability and compatibility. In this sense, the BOC modulation family was well suited to complement the legacy bandwidth usage.

In terms of frequency variations, there cannot be true frequency diversity as different messages are used on all civil signals. Also, if a single civil signal were to be used, a compromise would need to be achieved in terms of signal power (evolving from one satellite block to another) vs. ionospheric delay magnitude (inversely proportional to the carrier frequency).

Upcoming block III satellites weight will increase from 1 to 2 tons, mostly accountable for on-board clock shielding from radiations, for improved system performances.

2.2 GLONASS Constellation

Over the years, the GLONASS constellation has undergone several problems. Initially, the launched satellites had a very short life expectancy (4 years), thus requiring an aggressive launch plan in order to fulfill and maintain the nominal 24 satellite constellation in orbit, which became problematic with the collapse of the Russian economy. Indeed, it almost led to the disappearance of the constellation, i.e. only six satellites were left in 2001. Under the demilitarization process, the constellation management was transferred to the Russian Federation's civilian space agency Roscosmos. Nowadays, GLONASS satellites generation M have a greater life expectancy than their first generation equivalents, none of which remains. By the end of 2011, despite Russia's earlier failed launches (Finck, 2011), GLONASS became the first dual-frequency civil constellation available worldwide with 28 satellites in orbit, of which 24 are operational (Federal Space Agency - Information-analytical centre, 2010). Another reason for the increased interest in GLONASS receivers is that all satellite-based navigation receivers sold in Russia must be GLONASS compliant.

GLONASS is also undergoing a modernization phase, especially with the upcoming satellites of generation K, bringing a fundamental change to its broadcast signals: GLONASS legacy signals on L1 and L2 are based on Frequency Division Multiplexing Access (FDMA), as opposed to all other GNSS signals based on Code Division Multiplexing Access (CDMA). One particularity of FDMA is that the same spreading code may be used for all its satellites, since they are spatially separated in frequency. Up until 2005, L1 transmissions extended over $1610.6 - 1613.8$ MHz, which dramatically degraded radio astronomical observations. Now that these frequencies have been dropped, GLONASS is left with only 14 (-7 to $+6$) different frequency slots g. As agreed with the Inter-Union Commission on Frequency Allocation (IUCAF), frequency slots $+5$ and $+6$ should be used only for orbital insertion, or during periods of exceptional circumstances (PosiTim, 2010)[6]. Assuming only one out of two antipodal satellites can be tracked by any receiver located at low altitudes, a total of 28 satellites may share this FDMA scheme, whereas the constellation is designed for 24. Indeed, as opposed to a custom location of a satellite within its orbit for strategic coverage as is the case with GPS, GLONASS (and Galileo) propose equidistant satellites among any given orbital plane, i.e. with an argument of latitude displacement of 45°. Furthermore, the navigation message must be decoded during at most 30 s to confirm the right satellite PRN is being tracked in the case of cold acquired signals, as two SVs share the same frequency slot g.

More specifically, three equidistant orbits at a 19 100 km altitude (i.e. a radius of 25 480 km) and an inclination 64.8°[7], composed of 8 satellites, fulfilling the 24-satellite constellation. An orbit revolution takes 11 hours 15 minutes and 44 seconds, leading to a ground track periodicity of eight sidereal days, as opposed to one sidereal day in the case of GPS. According to the Russian System of Differentional Correction and Monitoring (SDCM) data in 2010, a positioning precision of $4.46 - 7.38$ m can be expected with $7 - 8$ GLONASS satellites in view, as opposed to $2.00 - 8.76$ m with $6 - 11$ GPS satellites in view. These performances are expected

[6] Glonass-M satellites are equipped with filters to attenuate unwanted emissions in the frequency ranges: $(1610.6 - 1613.8)$ MHz and $(1660.0 - 1670.0)$ MHz (Russian Institute of Space Device Engineering, 2008).

[7] This greater inclination provides a better coverage of northern regions, typical of the Russian territory

to improve to 2.8 m by 2015. Nevertheless, civil GLONASS is slightly less accurate than GPS, although on northern latitudes, GLONASS accuracy is better due to the orbits characteristics.

On top of having its own timing reference based on Universal Time Coordinated (UTC), GLONASS system also has its own geodesic system, which was updated to PZ-90.02 in 2007 to become compliant with ITRF2000, also used by GPS WGS 84 geodesic reference system. GLONASS and GPS coordinates systems now differ by less than 40 cm in any given direction.

Another difference with GPS is the on-board reference frequency of 5 MHz, of which is derived a 511 kHz code clock for the civil signals. Their modulation being BPSK, they are referred to as BPSK($\sim \frac{1}{2}$), where $\sim \frac{1}{2}$ refers to 511 instead of 511.5 kbps. The unique spreading code is obtained through a nine stage LFSR, providing a Maximal Length (ML) code with $2^9 - 1 = 511$ chips; its period is therefore 1 ms. Although the occupied bandwidth by a single satellite signal is half that required for GPS L1 C/A, the total GLONASS bandwidth is much larger when considering the 14 frequency slots, as detailed below.

The navigation message is identical on L1 and L2. The navigation message stream is not encoded for error correction, although an 8-bit Hamming code parity check is added before relative coding is applied. It is then followed by a Manchester encoding (referred to as a Meander code in the ICD), which doubles its throughput. The resulting 100 symbols/s therefore leaves an integer code ambiguity; the navigation data symbols last 10 ms, during which 10 identical spreading codes are transmitted. The minimal power level received at ground level is -161 dBW on L1. While older satellites broadcast L2 signals with a minimal power level of -167 dBW at the Earth surface, newer satellites should provide a power increase to match that of L1. The main difference between the civil signals on L1 and L2 will reside in the frequency slot separation, i.e. 562.5 kHz on L1 and 437.5 kHz on L2, leading to a greater main lobes overlap on L2, allowing for frequency diversity as with GPS P(Y). As a result, the minimal front-end bandwidth required by a receiver is $(0.5 + 14 + 0.5) \cdot 0.5625 = 8.4375$ MHz on L1 (as shown in Figure 2.10), while it is only $15 \cdot 0.4375 = 6.5625$ MHz on L2, both cases significantly greater than the GPS L1 C/A main lobe of 2.046 MHz bandwidth. This pays off with a greater

cross-correlation isolation of the spreading code from one slot to another simulated to reach a minimum protection of 30.8 dB, overachieving the theoretical Cross-Correlation protection of $20 \cdot \log_{10}\left(\frac{N}{t(m)}\right) = 23.798139$ dB with $N = 511$ and $m = 9$. Another important factor to consider is the frequency wipe-off associated to the slot number. Indeed, shifting the local code replica to align it with the incoming signal (offset by a multiple of 562.5 kHz on top of Doppler shift), as proposed in some acquisition and tracking approaches, introduces unnecessary zeros in the ACF as depicted in Figure 2.11, which could cause detection misses. A full carrier wipe-off on the incomming signal is thus necessary, and comes at no extra cost when directly performed on the incoming signal, prior to correlation.

The reader should note that GLONASS signals naming convention refers to: “O” for Open signals (standard precision) or “S”: for obfuscated Secure signal (high precision); “F” for FDMA or “C” for CDMA. The frequency slot number g can take the values -7, -6, ..., 0, ..., $+6$.

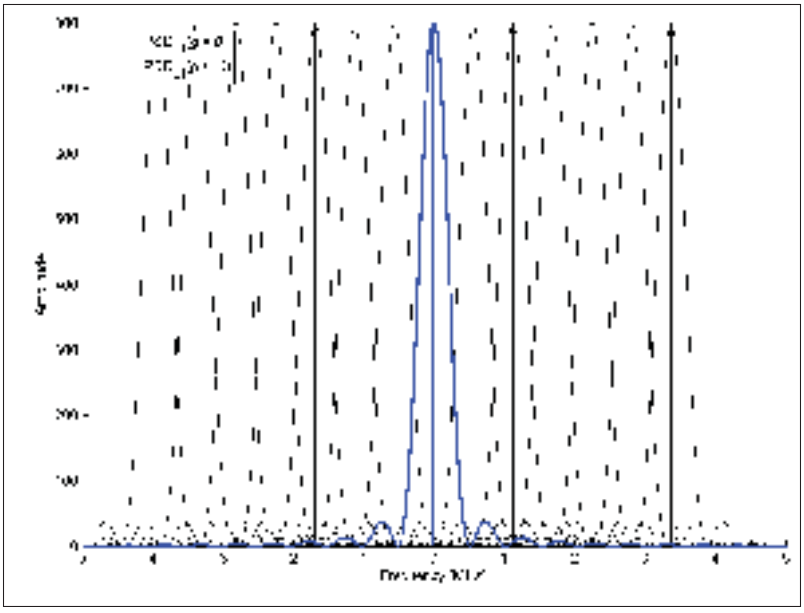

Figure 2.10 Spectral Representation of the GLONASS L1 FDMA Modulation Scheme

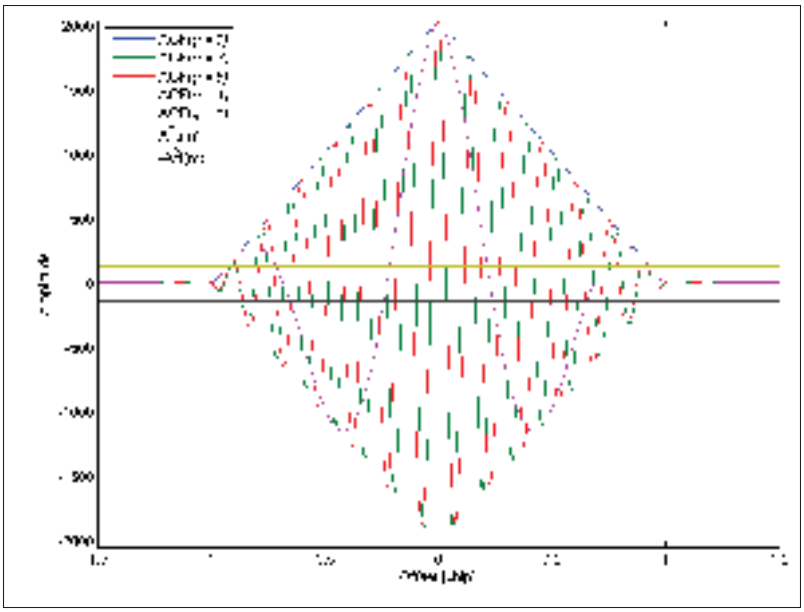

Figure 2.11 ACF Shape Modulated by Cosine Wave with $g \cdot \frac{562.5}{511}$ period/chip, after Frequency Shifting the Local Code

2.2.1 CDMA-compliant modernized GLONASS signals

Only little has been published about the CDMA-based GLONASS signals to come. References differ from BOC$(1,1)$ vs. BOC$(2,2)$ on L1 centered on 1575.42 MHz and BOC$(4,4)$ on L5 at 1176.45 MHz and another signal on L3 (Urlichich *et al.*, 2011; European Space Agency, 2012a). In fact, modernization frequencies and modulations are still being defined. Nevertheless, two GLONASS-K1 (launched on February 26$^{\text{th}}$, 2011 and November 30$^{\text{th}}$, 2014) broadcast a test CDMA signal on L3, for which the spreading and modulation schemes have been defined. They are comparable to GPS L5, although centered on 1202.025 MHz (i.e. $117.5 \cdot 10.23$). According to van Dierendonck (2014), Russians need to move their frequencies to other GNSS frequency bands to be interoperable rather than an aviation antenna issue. GLONASS-K2 satellites will rather be centered on 1207.140 MHz ($118 \cdot 10.23$). Anyhow, a third GLONASS frequency is available to civil users, although it still cannot be used by the navigation solution. Data and pilot components are in phase quadrature, leading to a QPSK(10)

modulation, where the 10 230 chip long truncated Kasami[8] code has a period of 1 ms with a -40 dB cross-correlation protection. Secondary codes are used, as well as Convolutional Coding (CC) at a $\frac{1}{2}$ rate for the navigation message (Russian Institute of Space Device Engineering, 2008).

2.2.2 GLONASS Summary

With the 24$^{\text{th}}$ satellite activation on December 8$^{\text{th}}$ 2011, the GLONASS constellation offered full global coverage with eight healty SVs on all three orbital planes. In fact, FOC was first established in 1995, after which budget cuts (occuring after fall of the Soviet Union) prevented its maintenance: by 2001, a handful of satellites were still functioning. Concerning GLONASS third signal on L3, broadcasted by GLONASS-K1 SVs (Urlichich *et al.*, 2011):

> There are two well-known methods of signal multiplexing – time multiplexing and amplitude equalizing. The time multiplexing technique is used for the GPS L2C signal, while the amplitude equalizing method is used for the *Composite BOC (CBOC)* signals in the Galileo L1 band and the Alternative BOC (AltBOC) signals in E5 band. This method has the disadvantage of 10 to 16 % loss of the transmitter power on the equalization. However, it has an advantage: simple user equipment architecture and, more importantly, the possibility of step-wise implementation of the multicomponent signal. The step-wise approach is compatible with older receivers. New user equipment will be able to track both old and new signal components, as well as a combined signal consisting of old and new components. [...] Even with six components, losses are lower than about 16 %, but it is possible to avoid any loss using time multiplexing. That is why the final decision about future GLONASS signals has not yet been made.

2.3 Galileo Constellation

Galileo is a European civil system open to all users, while GPS is an American military system that provides higher accuracy signals to US military users only. Since GPS has the capability to block civil signals while still using the military signals, a primary motivation for the Galileo project was this international concern where users could be denied access to GPS during political disagreements.

---

[8] Kasami sequences are binary sequences of length $2m-1$ where m is an even integer. The Gold codes used for GPS L1 C/A are a special case of Kasami codes.

Hence, Galileo was the first public, non-military, system that was put forward. After a thorough analysis, its released signals specification was inspired by that of GPS on many aspects, such as a 10.23 MHz reference frequency and the resulting transmission center frequencies and chipping rates. Shortly after the European Union (EU) intention to design a public satellite-based navigation system was revealed, GPS was made more accessible to civil users through the deactivation of Selective Availability (SA). Despite this stronger competition, the project went on, although its public funding mechanism has long been unclear.

Composed of three orbits equally spaced by 120° at the Equator and inclined by 56°, each orbit will consist of nine satellites equally spaced by 40°, and a spare (inactive) satellite; the total constellation will thus account for 30 satellites at an altitude of 23 222 km (29 601 km semi-major axis). The resulting revolution period lasts 14 h 7 min, making the ground-track repeat itself after 17 revolutions over 10 solar days ($10 \cdot 24/14.117 \approx 17$) (European Space Agency, 2015).

One critical characteristic of the Galileo Signals In Space (SIS) is that the signals will be compatible and inter-operable with GPS, hence increasing signal availability for GNSS receivers, while minimizing interferences with one another. Satellites will broadcast different services (open, commercial, regulatory and SoL) over a combination of their signals, found on L1, L2 (different from that of GPS) and L5 (partly shared by GPS). As opposed to GPS and GLONASS, Galileo commercial signal has guaranteed service, which is especially useful for commercial airliners.

Over the past decade, the only open signal on L1 has undergone many revisions, according to international collaboration of the EU responsibles with their GPS homologues. Indeed, an initial modulation scheme considered was the BOC$(1,1)$ in order to minimize interference with the "not so robust" legacy GPS L1 C/A signal while maintaining a high level of inter-interoperability by sharing the same 1575.42 MHz carrier frequency. This collaboration then needed to also consider the modernized GPS L1C signal to come, leading to the MBOC spec-

trum to be implemented by all new signals on L1 (BeiDou should use it too, while GLONASS has not yet decided on what their L1OC signal would look like).

In order to secure the Galileo frequency allocations by providing a signal in space, a first Galileo In-Orbit Validation Element (GIOVE) satellite named GIOVE-A was launched in 2005. It transmitted an open signal on L1 with BOC$(1,1)$ modulation and a navigation message of its own. The second satellite launched in 2008 (GIOVE-B) first introduced the MBOC spectrum and offered continuous transmissions over all three frequency bands, with the navigation message as described in the official ICD or SIS documents. Both GIOVE have been silenced in 2012, leaving the sky to 4 In-Orbit Validation (IOV) launched in 2011-2012 and 2 FOC, launched on a bad orbit in August 2013, but recovered in December 2014 and March 2015 into a suitable corrected orbit (European Space Agency, 2014, 2015). Finally, two more satellites were launched on March 27$^{\text{th}}$, 2015.

The Galileo E1 B&C signal is modulated by a 4092-chip long memory code at a 1.023 Mchip/s rate with a 4 ms period. These memory codes were only released as sequences without their generation mechanism. They were nevertheless analyzed by Gao (2008), who had developed a unique method to crack undisclosed signal characteristics. The MBOC spectrum is implemented through the Complex BOC (CBOC) modulation scheme, where the data and pilot components are in phase opposition. CRC is appended to data streams, before being encoded by a $\frac{1}{2}$ Convolutional Coder. The resulting 250 symbols/s perfectly overlays onto the spreading code period, avoiding the code integer ambiguity. Since both data and pilot components are combined in counter-phase, with the same -160 dBW power, their summed modulations comply with the MBOC definition:

$$\begin{aligned}
\Phi_{\text{Data}}(f) &= \text{CBOC}(6,1,\tfrac{1}{11},+) &&= \sqrt{\tfrac{10}{11}}\text{BOC}(1,1)+\sqrt{\tfrac{1}{11}}\text{BOC}(6,1)\\
\Phi_{\text{Pilot}}(f) &= \text{CBOC}(6,1,\tfrac{1}{11},-) &&= \sqrt{\tfrac{10}{11}}\text{BOC}(1,1)-\sqrt{\tfrac{1}{11}}\text{BOC}(6,1)\\
\text{MBOC} &= \Phi^2_{\text{Data}}+\Phi^2_{\text{Pilot}} &&= 2\cdot\left(\tfrac{10}{11}\text{BOC}^2(1,1)+\tfrac{1}{11}\text{BOC}^2(6,1)\right)
\end{aligned} \tag{2.10}$$

The fact that its spreading code is four times longer would offer a ~ 6 dB cross-correlation theoretical gain over GPS L1 C/A $20\log_{10}\left(\frac{N}{t(m)}\right)$, assuming Gold codes. Indeed, GPS P has $10\cdot$

$\log(10\,230 \cdot 1000 \cdot 3600 \cdot 24 \cdot 7) = 127$ dB cross-correlation isolation as per Kaplan and Hegarty (2006), in agreement with its code length. Although this approximation may not hold considering that a pair of 50 random (a.k.a. memory) codes, optimized for their Autocorrelation Sidelobe Zero (ASZ) property, are used (Wallner *et al.*, 2007). Moreover, the synchronization pattern is not encoded, simplifying the data extraction preliminary steps, i.e. frame alignment.

The Galileo E5 signal offers a combined signal with a constant amplitude through the Alternate BOC (AltBOC) modulation scheme, combining its two complex signals E5a and E5b (each one can be processed as QPSK(10)) into a single one of the form BOC$(15, 10)$. Nevertheless, the SoL I/NAV message is broadcast on E5b and E1 only, while E5a bares the Open Service (OS) F/NAV message. A dual-frequency receiver tracking both E1 and E5b I/NAV data stream will download the full data twice as fast as the full data frame on each frequency is offset by half a frame.

2.4 BeiDou Constellation

COMPASS (also known as BeiDou) is a navigation system put forward by China. After having built its own demonstration (BeiDou-I) and regional (BeiDou-II) systems, BeiDou is expected to evolve into Phase III, with a different signal definition, including navigation message and frequency plan. The final system should include 30 Medium Earth Orbit (MEO) and Inclined GeoSynchronous Orbit (IGSO) and five GeoSynchronous Orbit (GEO) satellites positioned across China at longitudes specified in Table 2.3 (China Satellite Navigation Office, 2013). As of May 2014, the current Phase II regional system (operational since 2012) includes five GEOs, four MEOs (plus the partially operable IOV M1) broadcasting B1 and B2 civil signals, and five IGSOs. Its accuracy is not as good as that of GPS, mainly because orbit modelling and on-board clocks, causing greater drifts, which need to be compensated for by more frequent updates. That is to say that in the short term, only the four MEOs could be tracked from North American countries given their ground track will cover all regions of the globe (within $\pm 55.5^\circ$ latitudes) at some point during their 7 sidereal days revolution period, as seen in Figure 2.12. Moreover, these four MEO satellites may never all be visible to a user at any given time, if

they are evenly distributed around the Earth upon full deployment to provide a better coverage (which would prevent a PVT solution solely based on these satellites).

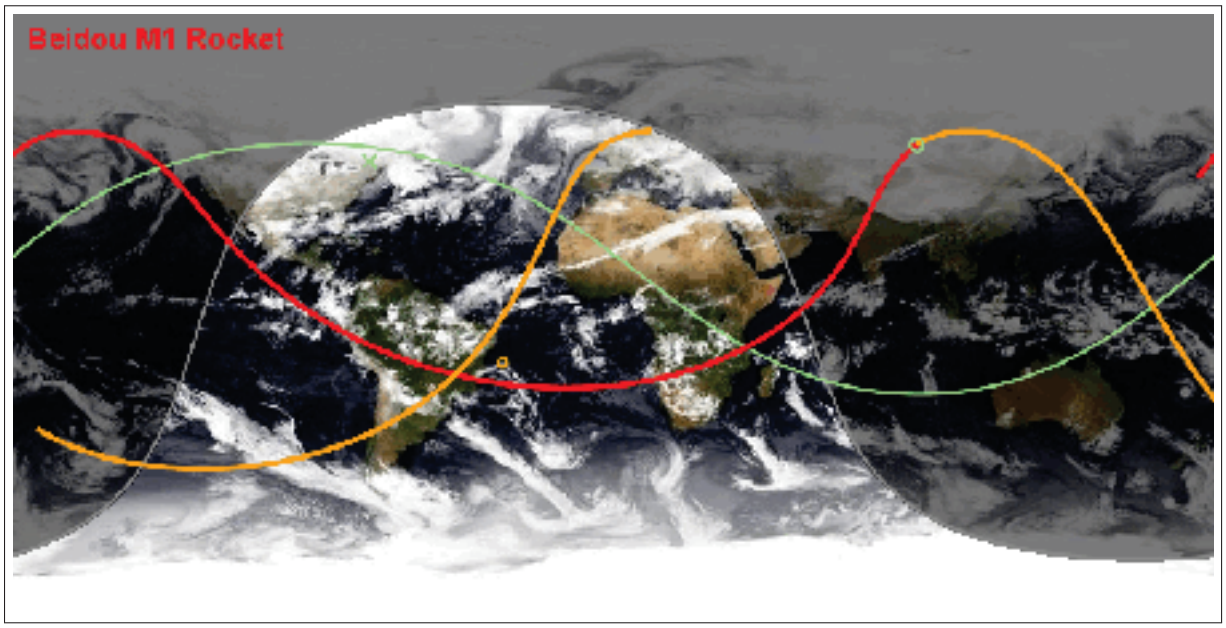

Figure 2.12 Ground Track of COMPASS-M1 MEO Satellite over 24 h
Taken from Barmettler (2015)

In 2007, Stanford University succeeded in breaking down the undisclosed spreading code (as well as its generation mechanism) and modulation scheme of the first broadcasting MEO, known a Compass-M1, thanks to their tracking station based on a 1.8 m steerable parabolic antenna dish providing an additional 25 dB gain over standard patch antennae (Chen *et al.*, 2007).

More specifically, the MEO orbit is nearly circular at an altitude of 21 150 km, with an inclination of 55.5° (PosiTim, 2010). As of December 2011, a first "test version" of an official ICD has been released providing an overview of the B1 signal (centered on 1561.098 MHz) of the Phase II regional system, although it completely lacks any description of the navigation message, which were disclosed in December 2012 in the ICD version 1 (China Satellite Navigation Office, 2013). From this source, it has been established that SVN#30 matches the previously cracked spreading code sequence. Note that only the civil in-phase branch of the

QPSK modulation is publicly released, as the quadrature component of the signal is reserved for military applications. It has a 2046 chip-long spreading code rated at 2.046 Mchip/s with a bandwith twice as large as for GPS L1 C/A, hence complying with a 1 ms primary spreading code period. Its 20 chip-long secondary code is laid over the primary one (with one secondary bit per primary code), for a total duration of 20 ms which, combined with a 50 bit/s navigation message, eliminates the integer ambiguity threat.

On a longer horizon, the future Phase III global system should become operational by year 2020. It is expected that it should comply with the modulation and carrier frequencies first put forward by Galileo, hence favoring compatibility. Yet it remains unknown as to what characteristics from Phase II will be kept for Phase III...

The BeiDou Time (BDT) system defines its zero time-point at 00:00 UTC on January 1st, 2006 and is specified to preserve a ± 100 ns tolerance within 1 s. Moreover, China's Geodetic Coordinate System 2000 (CGCS2000) is defined such that its origin is located at the Earth center of mass with its Z-axis in the direction of the North Pole while its X-axis points towards the International Earth Rotation Service (IERS) Reference Meridian (IRM). The CGCS2000 ellipsoid is superposed onto this coordinates system with the following parameters:

a. Semi-major axis: $a = 6378137.0$ m

b. Geocentric gravitational constant (including the Earth mass): $GM = 398600.4418 \times 10^9 \frac{\mathrm{m}^3}{\mathrm{s}^2}$

c. Flattening: $f = \frac{1}{298.257222101}$

d. Earth rate of rotation: $\Omega = 7.2921150 \times 10^{-5}$ rad/s

2.5 GNSS Civil Signals Summary

As described above, all global constellations are located in MEO, while augmentation services are broadcast from geosynchronous satellites at higher altitudes, or Highly Elliptical Orbits (HEO) in the case of higher targeted latitudes.

These four global systems are synthesized in Table 2.1. As a complementary information, a broader survey of Augmentation and Regional Navigation Satellite Systems (ANSS and RNSS) is presented in Tables 2.2 and 2.3. As can be seen, the same carrier frequencies are used to ensure compatibility, simplifying receiver architecture.

Table 2.1 GNSS Constellations

System	GPS	GLONASS	Galileo	BeiDou
Orbit	6 MEO	3 MEO	3 MEO	3 MEO 3 IGSO 1 GEO
Orbit inclination [°]	55	64.8	56	55.5; 55.5; 0
Orbit altitude [km]	20 180	19 130	23 222	21 150 35 816 35 816
Revolution period	11:58:00	11:15:44	14:07:00	12:53:00
Ground track [day]	1 sidereal	8 sidereal	10 solar	7 sidereal
In-orbit satellites	32/24	27/24	4+2/27	4/24; 5; 5
Spare satellites	8 active	3 active	3 planned	3; 0; 0 planned
Ref. geodesic system	WGS-84	PZ-90.02	GTRF	CGCS2000
Ref. time system	UTC + 16s	UTC + 3h	UTC + 16s	UTC $\pm$100 ns
Center frequencies (bandwidth) [MHz]	L1: 1575.42 (24) L2: 1227.60 (24) L5: 1176.45 (24)	G1: 1602.000 (18) G2: 1246.000 (16) G3: 1202.025 (20)	E1: 1575.420 (33) E6: 1278.750 (41) E5: 1191.795 (51.15)	B1: 1575.420 (—) B3: 1268.520 (24) B2: 1191.795 (51.15)

A general description of WAAS L5 signal particularities was provided by Langley and Rho (2009).

On top of those listed in the table, commercial satellite-based augmentation systems such as StarFire operated by John Deere (Sharpe *et al.*, 2000) and OmniStar operated by Fugro (Trimble Navigation Limited, 2014), available worldwide, are said to outperform SBAS (Sharpe *et al.*, 2000).

Table 2.4 summarizes most common L1 signals, whether they are Global, Regional or Augmentation Navigation Satellite Systems (GRANSS). Note that BeiDou-II B1-I signal is not shown, as BeiDou-III is expected to evolve close to Galileo signals definition.

Table 2.2 SBAS Constellations

System	WAAS	SDCM	EGNOS	SNAS	MSAS	QZSS	GAGAN
Corrections for GNSS:	GPS	GPS GLONASS	GPS GLONASS Galileo		GPS	GPS Galileo MSAS	GPS
In-orbit satellites	3/3 GEO	1/3 GEO	3/3 + 0/3 GEO		2/2 GEO	1/3 HEO, 40-53°	0/1 GEO
Longitude [°]	−98.0 −107.3 −133.0	−16.0 +95.0 +167.0	−15.5 +21.5 +25.0 +5.0 +31.5 +64.5		+140.0 +145.0	[0, 2]·120	
Orbit altitude [km]	35 816	35 816	35 816	35 816	35 816	[32, 40]10^3	35 816
Center frequency [MHz]	L1 L5	L1	L1 L5		L1	L1 L2, E6 L5	L1 L5

Table 2.3 Regional Navigation Satellite Systems constellations

System	BeiDou-II	IRNSS
In-orbit satellites	4/4 MEO 5/5 IGSO 5/5 GEO	0/3 GEO 0/4 IGSO, 29°
Longitude [°]	+58.75, +80, +110.5, +140, +160	+34, +83, +132 +55(·2), +111(·2)
Orbit altitude [km]	35,816	35,816 250–24,000
Center frequencies (bandwidth) [MHz]	L1: 1575.42 (24.0) L5: 1176.45 (24.0)	L1: 1575.42 (24.0) L5: 1176.45 (24.0) S: 2492.028 (16.5)

From Table 2.4, it can be observed that most new or modernized GNSS signals using parity check are based on the Cyclic Redundancy Check (CRC) defined on 24 bits, as proposed by Qualcomm. Moreover, apart from GPS L1C, most FEC approaches refer to the same two polynomials defining the convolutional encoding scheme: in fact, Galileo E1-B uses –133o instead of +133o for its second polynomial. Hence, the same Viterbi decoder may be used for all signals, provided every second bit of E1-B is first inverted. Since only few details are

Table 2.4 GRANSS Open Signals on L1/G1

Signals / Characteristics	GPS C/A	GPS L1C$_I$	GPS L1C$_Q$	GLONASS L1OF	Galileo E1-B	Galileo E1-C	SBAS
Spreading code							
Primary Type	Gold	Weil	Weil	ML	mem	mem	Gold
Primary Length [chip]	1023	10 230	10 230	511	4092	4092	1023
Primary Rate [Mchip/s]	1.023	1.023	1.023	0.511	1.023	1.023	1.023
Primary Duration [ms]	1	10	10	1	4	4	1
Secondary Type	—	—	11-reg. LFSR	—	—	mem	—
Secondary Length [chip]	—	—	1800	—	—	25	—
Secondary Rate [chip/s]	—	—	180	—	—	250	—
Secondary Duration [ms]	—	—	10	—	—	100	—
Cross-Correlation [dB]	20.55	27.9	28.4	30.8	26.0	25.5	20.46
Navigation data							
Bit Rate [bit/s]	50	50	—	50	125	—	250
Error Management	6 Hamming	24Q	—	8 Hamming	24Q	—	24Q
Encoding	—	BCH-LDPC($\frac{1}{2}$)	—	Relative-Manchester	+171o −133o	—	+171o +133o
Symbol Rate [symbol/s]	50	100	—	100	250	—	500
Data bit duration [ms]	20	10	10-∞	10	4	4-∞	2
Data Ambiguity	20	1	—	10	1	—	2
Carrier							
Modulation Scheme	BPSK(1)	BOC(1,1)	TMBOC $(6,1,\frac{4}{33})$	BPSK($\sim\frac{1}{2}$)	CBOC $(6,1,\frac{1}{11},+)$	CBOC $(6,1,\frac{1}{11},-)$	BPSK(1)
Gabor Bandwidth [MHz]	2.046	4.092	14.332	1.022	14.332	14.332	2.046
Min. Ground Power [dBW]	−158.50	−160.00	−158.25	−161.00	−160.00	−160.00	−161.00
Phase Relationship [°]	90	0	0	90	0	180	90

publicly available for commercial, regulated and military signals, they are simply not displayed to enhance readability.

To sum up GNSS signal characteristics, the reader should bare in mind that coherent integration time is limited by the navigation message in a standalone receiver (i.e. without external aid). On the other hand, the data-free pilot component of newer signals solves this issue. Similarly, secondary spreading codes simplify the transmission integer ambiguity, although not being synchronized onto it has the same limiting effect than the navigation message, even on the pilot component.

CHAPTER 3

PROPAGATION MEDIUM AND SIGNAL PROCESSING IMPACTS ON NAVIGATION SIGNALS

Prior being broadcast by through their satellite antenna, signals defined in Chapter 2 are impaired by system integrity (such as the accuracy of ephemerides data modelling their orbit), by on-board clock and amplifier. Civil GPS positioning receivers have known a wide commercial interest, especially after 2000 when the GPS Selective Availability (SA) was deactivated. The Standard Positioning Service (SPS) accuracy had then improved from roughly 30 to 5 m, thus making atmospheric delays and multipath the most important error sources to overcome. When activated, SA intentionally induced jitter onto the publicly available L1 C/A signal in a pseudo-random way, making civil navigation less interesting without the required correction.

Signals out of the satellite antenna propagate through the underlying medium before reaching the receiver antenna and being further processed. This chapter aims at providing an overview of these different sources of perturbation, both external and within the receiver.

3.1 Propagation Medium Error Sources

As GNSS signals propagate from the satellite to the receiver through the atmosphere, they may be impeded by the medium itself as well as by interferences and multipath. This section shortly reviews the different error sources external to the receiver. Some numerical values may be found in Table 3.1.

3.1.1 Atmosphere Impacts

As signals transit through all the atmosphere layers, they are impacted by two of them. The ionosphere is part of the upper atmosphere, in altitudes ranging from 50 to 1000 (or more) km. Moreover, the troposphere induces an error due to its high level of humidity, which can be realistically be modelled through both its dry and wet components.

3.1.1.1 Ionosphere

Radio propagation solely depends on electron density, not on temperature nor ionic composition. Since gaseous density lowers with altitude, the ionosphere is typically quantified as accumulated ions along a given path as the Total Electron Content (TEC). In fact, this part of the atmosphere is so thin that free electrons can temporarily exist before being captured by recombination with surronding positive ions, resulting in a plasma of neutral heated gas, which affects radio propagation. Furthermore, solar activity (sunspot, solar flares, solar winds, etc.) affects Earth geomagnetic field. Hence, the ionosphere polarizes the waves, delaying the code offset, but advancing the carrier phase measurements of approximately the same magnitude (Xu, 2007).

From a receiver perspective, the LoS of a satellite at horizon crosses a larger path through ionoshere than at zenith. Hence, the ionosphere impacts may be modelled in terms of geometrical relative positioning of the satellites on top of the considered receiver location and altitude, time of day (affected by solar activity) and season of the year (influenced by Earth inclination) and phase of the 11-year long sunspot cycle (Hathaway, 2010), whose most recent peak occurred in 2013 was the lowest in a century (Gannon, 2013).

The ionosphere delays are proportional to the squared carrier frequency, allowing accurate characterisation through frequency diversity, as described in Eq. 3.1. Indeed, dual frequency receivers can benefit from measurements taken on two bands by combining the observations on two frequencies from a same satellite (i.e. geometry-free measurement), achieveing a better combined measurement to be used to obtain a solution. The iono-free pseudorange of a receiver tracking both L1 and L5 signals can be obtained as:

$$\rho = \frac{\left(f_{L1}^2 \cdot \rho_{L1}\right) - \left(f_{L5}^2 \cdot \rho_{L5}\right)}{f_{L1}^2 - f_{L5}^2} \tag{3.1}$$

with the pseudorange ρ and the radio frequency f.

This pre-processing reduces the computational complexity of the solution and provides a smoother (i.e. less noisy, more accurate) position. GLONASS is the only constellation to provide a full dual-frequency constellation. At the time these lines were written, the GPS constellation includes a few IIR-M and IIF satellites with L2C and L5 signals, whose respective navigation message are not yet operational (GPS World, 2014). From the denominator of Eq. 3.1, it can be said that the greater the frequency difference, the greater the correction impact. The best corrections would then be achieved by combining L1 and L5 signals. Since both bands are ARNS, their use in navigation makes more sense, at the cost of a higher sampling frequency f_S to accommodate the higher chipping rate of L5.

Geometry- and ionosphere-free measurements allow further code and phase corrections through ambiguity resolution and multipath mitigation group delay estimations, as described by Simsky (2006).

Alternatively, in single-frequency measurements, Code-Plus-Carrier (CPC), formerly known as Group and Phase Ionosphere Correction (GRAPHIC), requires a long convergence time (20 to 30 min) to get precise coordinates and achieve an accurate solution (Diessongo *et al.*, 2012), based on the averaged measurements:

$$\frac{\rho+\phi}{2} = r - \frac{\lambda}{2}\cdot N + \Delta T + MP + \eta_{CPC} \tag{3.2}$$

with the pseudorange measurement ρ, the carrier phase measurement ϕ in units of distance, the geometric distance r, the wavelength λ, the ambiguity N, the tropospheric delay ΔT, the multipath MP and the additional code and carrier phase noises η_{CPC}. This approach eliminates the ionospheric *slant* delay, which is added to the range measurement, but substracted from the carrier phase measurement.

Luckily for single frequency receivers, different models are broadcasted by the global constellations, e.g. Klobuchar in the case of GPS and BeiDou B1, whereas a the Galileo navigation message broadcasts a second degree polynomial based on solar flux units (sfu) to account for 70

% of the ionosphere delays, namely the NeQuick ionospheric model (European Space Agency, 2012b).

Finally, Differential GPS (DGPS) allows an alternative communication link through RF, WiFi, internet or Radio Data System (RDS), providing additional corrections computed from base receivers with known position (Aarmo *et al.*, 1996; Lanigan *et al.*, 1990). One such transmission link consists in SBAS, providing a regional coverage from GEO broadcasts, e.g. WAAS in North America (as further discussed in Appendix III), EGNOS in Europe and Quasi-Zenith Satellite System (QZSS) in Japan to name a few. Alternatively, Ground-Based Augmentation System (GBAS) rely on a network of DGPS towers, mostly found in Australia, and in airports, namely the Local Area Augmentation System (LAAS).

3.1.1.2 Troposphere

The troposphere is the lowest portion of the atmosphere and contains approximately 80 % of the atmosphere mass and 99 % of its water vapor. Its composition is essentially uniform, apart for the water vapor resulting from evaporation and transpiration (humidity ratios may change rapidly). As temperature decreases with altitude, the water vapor amount decreases, along with the atmosphere pressure. The troposphere reaches up to 7-20 km of altitude, varying from polar to equatorial latitudes in summer, while remaining more uniform during winter. The overall Earth heat balance results from the absorption of the Sun energy at ground (heating the lower atmosphere) while the radiation of the heat at the top of the atmosphere cools the Earth.

3.1.2 Multipath

Multipath results from the reflection of the direct LoS signal onto surfaces surrounding the receiver, such as natural landscape (mountains, trees) and man-made infrastructures such as in urban canyons. Basically, two types of reflections are considered depending on the reflective surface: specular and diffuse (Bickerstaff *et al.*, 2006). More precisely, every signal reflection is characterized by an amplitude attenuation, as well as time and phase delays. Hence, many

attenuated carrier phase- and code-delayed versions of the LoS are constructively (or destructively depending on the relative phase of the reflection) superposed at the receiver antenna. The resulting ACF is then composed of the sum of the triangular-shaped ACF – in the case of BPSK signals – of each incoming version of the LoS, as shown in (Guay *et al.*, 2008). A single LoS reflection delayed by a duration corresponding to more than two chips would appear as a distinct triangle.

In order to mitigate Multipath, a few approaches have been proposed, including narrow correlator (van Dierendonck *et al.*, 1992), Strobe correlator (Sousa *et al.*, 2006), Teager-Keaser (TK) and Projection Onto Convex Sets (POCS) (Lohan *et al.*, 2006), and A-Posteriori Multipath Estimation (APME) (Siala and Gibert, 1999). But sometimes, multipath are the only signals available. Indeed, the successful GPS system falls short of expectations when it comes to indoor areas, which present a highly destructive RF environment for already weak GPS signals. Previous measurement campaigns performed at the University of Leeds, UK, has determined that in urban canyon and indoor locations, the attenuation of GPS signals can be as high as 27 dB, although more typical levels should remain in the 15-20 dB range (Ioannides *et al.*, 2006); equivalent figures can be expected for Galileo signals. Due to this fact, a number of different methods have been developed for indoor localization and tracking. The most commonly used methods are Time Of Arrival (TOA), Time Difference Of Arrival (TDOA) and Angle Of Arrival (AOA) (Bensky, 2008, Chapters 7-8) .

3.1.3 RF Interference

RF Interferences (RFI) may be intentional or not. In the former case, jamming would prevent use of the targeted bandwidth through different types of RF sources, ranging from simple, yet effective, Continuous Wave Interferences (CWI) to wide band interferences. Cheap electronic gadgets may be successful in denying GNSS signals usability, which is forbidden by law. Another, more subtil intentional interference approach is to mislead a receiver into a bad position, a.k.a. spoofing, a serious threat to airplanes for example. In the latter case, natural events such as solar flares and geomagnetic storm may cause rare outages, but bad spectrum

usage may cause more harm. For example, the GNSS bands of interest may be polluted by adjacent frequency bands overflow, lower bands harmonics, as well as other equipment sharing the same spectrum, such as Distance Measurement Equipment (DME) in L5. These issues require international regulations on bandwidth allocation and usage, through the International Telecommunication Union (ITU).

New GNSS signals with larger bandwidths (as a consequence of higher chipping rates) will help resist to interferences by diluting the impact of narrow CWI over a wider bandwidth. These signals should also provide better positioning accuracy and resistance to multipath since the chip period is shorter, requiring smaller correlator spacings and thus higher sampling rates.

3.1.4 Propagation Model

The pseudorange measurements (evaluated as the propagation time between emission t_e and reception t_r times) from at least four satellites (k) can be used to solve the system of equations (required to solve for user position in x, y, z and time Δt, using the speed of light c and the known satellite position x_k, y_k, z_k):

$$\rho^k = c \cdot (t_{r_k} - t_{e_k}) = \sqrt{(x_k - x)^2 + (y_k - y)^2 + (z_k - z)^2} + c \cdot \Delta t \tag{3.3}$$

Each measurement is known to be affected by the error sources above, which can be accounted for in (Tsui, 2005):

$$\begin{aligned} \rho^k &= \rho^{kT} + \Delta D^k \\ &- c \cdot \left(\Delta b^k - b_u\right) \\ &+ c \cdot \left(\Delta T^k + \Delta I^k + v^k + \Delta v^k\right) \\ &+ \lambda \left(N^k + w + b_P - b^{P^k}\right) \\ &+ b_{MP} \end{aligned} \tag{3.4}$$

where:

ρ^k is the measured pseudorange

ρ^{kT} is the true pseudorange, i.e. from user to satellite k

ΔD^k is the satellite position error effect on the range (i.e. along LoS)

Δb^k is the satellite clock error

b_u is the user clock bias

ΔT^k is the tropospheric delay error

ΔI^k is the ionospheric delay error

v^k is the receiver measurement noise error

Δv^k is the relativistic time correction

λ is the signal wavelength

N^k is the integer ambiguity of phase cycles

w is the wind-up effect [1] factor

b_P is the receiver carrier phase instrumental delay

b_P^k is the satellite k carrier phase instrumental delay

b_{MP} is the bias caused by multipath

These error sources may be approximated as (for the GPS L1 C/A signal): Alternatively, Kaplan and Hegarty (2006, Table 7.4) and Borre (2001) provide slightly different figures, computed for 1σ probabilities.

To achieve better performances, carrier phase measurements (with a $\frac{c}{f_{L1}} \approx 0.19$ m wavelength) may be considered, although their integer ambiguity must be resolved. Several methods exist

[1] A 360 °rotation applied on a fixed position receiver antenna, introduces a variation of one wavelength in the phase-obtained measurement of apparent distance between the receiver and the satellite (European Space Agency, 2013).

Table 3.1 Typical Pseudorange Error Sources [m]
Taken from Trimble Navigation Limited (2007)

Error Source	Standard GPS	Differential GPS
Satellite Clocks	1.5	0
Orbit Errors	2.5	0
Ionosphere	5.0	0.4
Troposphere	0.5	0.2
Receiver Noise	0.3	0.3
Multipath	0.6	0.6

those exposed by Liang and Jie (2012), such as Fast Ambiguity Resolution Approach (FARA), Least-Square Ambiguity Search Technique (LSAST), Fast Ambiguity Search Filter (FASF) and Least-squares AMBiguity Decorrelation Adjustment (LAMBDA), as well as the Modified LLL (Zhou, 2006) and the Modified Cholesky Decomposition (Fang and O'Leary, 2006),

3.2 Receiver Error Sources

Once satellite signals have reached the receiver, they are still subject to other error sources, i.e. those baring within the receiver. These error sources are highlighted herein, from antenna to digitization, prior being process in the tracking channels.

3.2.1 Receiver Front-End

The receiver antenna plays an important role in the processed signal quality. For example, an antenna matching the Right Hand Circular Polarization (RHCP) signals would allow rejecting odd multipath reflections characterized by inferted polarity. The antenna phase center may induce a common delay on received signals, which is then removed when computing the navigation solution. However, an independent delay is induced by every broadcasting satellite antenna center, contributing to pseudoranges error.

For Noise Figure (NF) sake, it is important to provide gain early in the transmission chain, as dictated by the budget link (Constantinescu, 2007), especially for passive antennae. The Friis formula dictactes the resulting noise factor F from cascading the stages (identified with the

subscript number) with gain G:

$$F = F_1 + \frac{F_2 - 1}{G_1} + \frac{F_3 - 1}{G_1 \cdot G_2} + \cdots + \frac{F_N - 1}{G_1 \cdot G_1 \cdot \ \cdots \ \cdot G_{N-1}} \tag{3.5}$$

Eq. 3.5 highlights the importance of Low Noise Amplifier (LNA) being located as close as possible to the antenna before cascading the N path components.

The front-end continues with the frequency down-conversion stage, found in two approaches. First, super-heterodyne architecture consist of at least two down-converting stages with as many Local Oscillator (LO), mixers and filters. The signal is then converted numerically. On the other hand, direct RF sampling, described in (Lamontagne, 2009), is based on under-sampling, folding the RF signal back into Intermediate Frequency (IF) as dictated by the Nyquist-Shannon theorem: the sampling frequency not only imposes the processed bandwitdh, but also the many points where the signal is folded. One should be aware that each of these folding steps induces signal attenuation, which could limit a receiver sensitivity.

The receiver reference clock is thus important in synchronizing down-conversion and digitizing components, although its bias from the navigation system clock is resolved as part of the navigation solution. In order to limit the clock bias multiplication, satellites are equiped with high quality reference clocks, on top of being modelled with a polynomial, broadcasted as part of navigation messages. The receiver clock jitter will also contribute to sampling noise.

In the current implementation of the development platform, namely the *RxGNSS*, each RF front-end has been quantified to admit signals bandwidth ranging from -15 to +7 MHz around the specified RF center frequency, once down-converted to IF, i.e. the digitized signal is comprised between 0 and 22.3 MHz (3 dB bandwidth) (Sauriol, 2008). A first down-conversion stage is customized to take the GNSS band of interest down to a common second stage from 70 MHz, before translating the signal further down to a 15 MHz IF through a 55 MHz oscillator. The 60 MHz sampling frequency allows processing a 30 MHz bandwidth centered on IF. However, filtering at 70 MHz reduces the effective bandwidth. As described in Chapter 2, the GNSS signals are spread over several radio frequencies, which are supported by three

Voltage Controlled Oscillator (VCO), i.e. one per band (i.e. L1, L2 and L5). The different RF paths in these three front-ends could impact the phase alignment between signals on different frequency, which is not quantified in this research effort. The resulting RF front-end is represented in Figures 3.1 and 3.2.

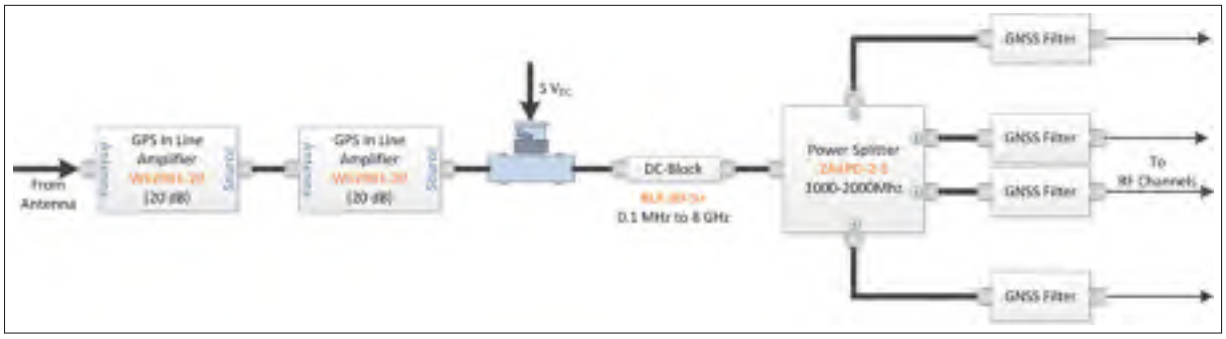

Figure 3.1 RF Amplification and Splitting of a Single Antenna
Adapted from Côté and Andrianarison (2013, Figure 2)

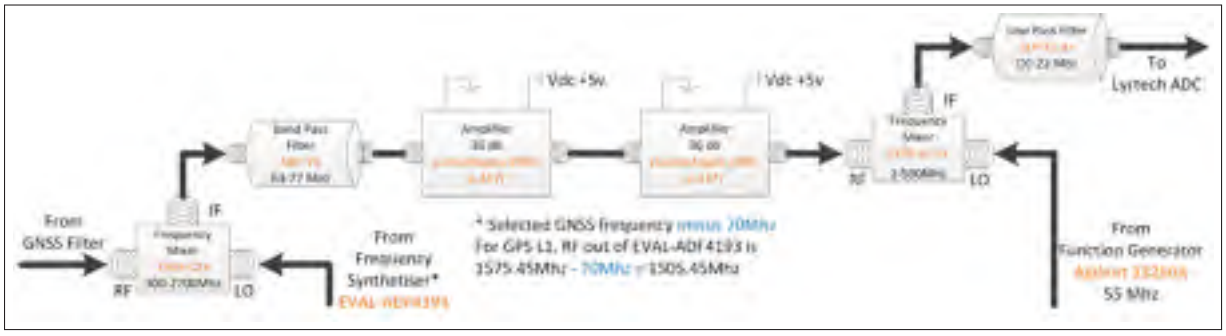

Figure 3.2 RF to IF Down-Conversion Stage
Adapted from Côté and Andrianarison (2013, Figure 5)

GNSS signals having different center frequencies, note that it is possible that several RF front-end stages may be assigned to L1. For example, one is needed for GPS/Galileo L1 at 1575.42 MHz, a second is required for GLONASS L1 at 1602 MHz while more front-ends would have been needed for BeiDou L1 at 1561.098 and 1589.74 MHz if they had not decided to change their frequency plan to comply with those of existing constellations. A more interesting alternative would be to admit larger bandwidths rather than dedicating a channel to each signal

spectral component, making it possible to admit commercial signals such as Galileo E1-A, spanning $\pm(15 + 2.5)$ MHz around 1575.42 MHz.

3.2.2 Receiver Tracking Channels

The tracking channel represents the main signal processing component of a receiver, where the signal is extracted from the noise through correlation. As a matter of fact, sampling rate imposes an upper limit on the admitted signal bandwidth, as well as a lower limit on the half correlator spacing δ, thus admitting greater multipath biases according to the EML discriminator approach. Also, its internal channel architecture (input and processing quantization levels, correlators and discriminators) affects signal acquisition and tracking sensitivity. Finally, the embedded algorithms set the robustness of the solution in presence of satellite blockage, interferences or any integrity issue.

Coherent integration provides better post-correlation SNR than non-coherent ones, introducing squaring losses, while removing the navigation message stream. That is to say that the navigation bit period limits the coherent integration time, thus imposing a lower limit on receiver sensitivity (Chibout *et al.*, 2007).

Satellite navigation being increasingly widely used, potential applications are now looking into indoors as well as in other hostile environments characterized by low SNR. To address this issue, most new signals will include a data-free pilot component on top of the traditional data one, where the integration times will be only limited by its secondary code and Doppler effect, which alters the measured frequency according to the user-satellite LoS dynamics (Misra and Enge, 2006).

3.2.3 Signal and Noise Quantification

In a receiver, the most widely used metric is C/N_0, a generalization of the well known Signal to Noise Ratio (SNR), requiring both signal and noise measurements. The signal quantification process has a direct impact on the receiver architecture; Proakis and Manolakis (2007) demon-

strated that the RMS value should be set to accomodate the digitized span. Quantification can be performed on linear or logarithmic scales with their respective losses (van Diggelen, 2009, p. 154), although single-bit quantification also exists. The number of quantification bits imposes bus sizes within the tracking channels. In the current implementation, 1-4 linear bits of quantification are supported. Up to 8 distinct Automatic Gain Control (AGC) maximize the digital signal whose gain is continuously adjusted by detecting over- and under-flows. The theoretical noise floor density is -174 dBm/Hz. In a 22.3 MHz bandwidth (BW), this corresponds to a level of -100.5 dBm, which should be constant for all Analog to Digital Converters (ADC) on the *RxGNSS* development platform.

In the original implementation of the receiver development platform, a single channel was used to quantify the noise floor level for GPS and GIOVE signals on L1. If we now think of a GNSS receiver baring universal channels, the need for such a dedicated channel must be revisited, as the "calibration" channel would need to be duplicated for each admitted frequency band and eventually each chipping rate. The paragraphs below describe the theory behind the initial approach, as well as that of all the considered replacement methods. These methods were empirically compared, proving their correct implementation and integration into the development platform. Finally, the Beaulieu method was selected to replace the calibration channel for its theoretical accuracy and its low real-time implementaiton complexity, thus freeing resources initially dedicated to the calibration channel.

The reader should bare in mind that the correlation of the incoming signal υ with its local replicate leads to the correlation R outputs, i.e. the accumulation of samples indices i (on I and Q branches):

$$\begin{aligned} I_{ACC} &= \frac{1}{f_S \cdot T_P} \sum_{i=1}^{f_S \cdot T_P} I_i \\ Q_{ACC} &= \frac{1}{f_S \cdot T_P} \sum_{i=1}^{f_S \cdot T_P} Q_i \end{aligned} \tag{3.6}$$

3.2.3.1 Calibration channel

According to Sauriol (2008), an independent calibration channel, whose sole purpose is to assess the noise power in an independent channel, may be used to evaluate the SNR. To avoid any signal correlation power, both frequency and PRN codes are changed at every 1 ms epoch. That is to say that it is configured to perform random frequency hopping on a spreading code built from different PRN partial sections (from all 32 GPS gold codes) in order to minimize overall cross-correlation without knowledge of which PRN are being tracked in the standard tracking channels. Actually, using the 1 week long P code with the same frequency hopping scheme every ms would have provided an improved cross-correlation isolation. Its noise power measurement is further smoothed over 10 s via non-coherent accumulation of 10 000 epochs, thus allowing for reliable noise measurement. Nevertheless, its chipping rate should match that of the signal of interest. Also, such a calibration channel is required for every frequency band of every antenna used. In a multi-GNSS receiver, this approach becomes thus less interesting.

The SNR computation approach is based on the fact that when actually tracking a satellite signal, the correlator complex outputs o follow a Ricean probability distribution:

$$f(o\,|\upsilon,\eta) \;=\; \frac{o}{\eta^2} e^{-\left(\frac{o^2+\upsilon^2}{2\eta^2}\right)} \cdot I_0\left(j\frac{o\cdot\upsilon}{\eta^2}\right) \tag{3.7}$$

where:

- o $= \sqrt{I_{ACC}^2 + Q_{ACC}^2}$ is the non-coherent sum of both branches accumulated results I_{ACC} and Q_{ACC}, thus making the SNR measurement robust against carrier phase noise error and allows for QPSK signal SNR measurements.
- υ^2 represents the channel signal power
- η^2 represents the channel noise power
- I_0 is the modified first type Bessel function of order 0

When no signal υ is present, o follows the Rayleigh's noise distribution, with the Maximum Likelihood Estimate (MLE):

$$f(o\,|\eta\,) \;=\; \frac{o}{\eta^2}e^{-\left(\frac{o^2}{2\eta^2}\right)} \Rightarrow \eta^2\big|_{\text{MLE}} = \frac{1}{2N}\sum_{j=1}^{N} o_j^2 \tag{3.8}$$

with every epoch j summed over the correlator outputs number N used to produce one averaged noise estimate. According to the Central Limit theorem, the average of a sufficiently large number of observations will be distributed according to the normal distribution, regardless of their underlying distribution. The calibration channel accounts for $N = 1000$ to 10 000 independent and identically distributed (iid) Rayleigh random variables (i.e. successive measurements).

Rice's second moment μ_2 then allows isolating the signal power:

$$\mu_2 \;=\; 2\cdot\eta^2+\upsilon^2 \Rightarrow \upsilon^2\big|_{\text{MLE}} = \frac{1}{N}\sum_{j=1}^{N}\left(o_j^2\right) - 2\cdot\eta^2 \tag{3.9}$$

The SNR may then be computed as:

$$SNR\big|_{\text{calib}} \;=\; \frac{\upsilon^2}{\eta^2} = \frac{\frac{1}{N}\sum_{j=1}^{N}\left(I_{ACC,j}^2+Q_{ACC,j}^2\right) - 2\cdot\left\{\frac{1}{2N}\sum_{j=1}^{N}\left(I_{ACC,j}^2+Q_{ACC,j}^2\right)\Big|_{\text{calib}}\right\}}{\left\{\frac{1}{2N}\sum_{j=1}^{N}\left(I_{ACC,j}^2+Q_{ACC,j}^2\right)\Big|_{\text{calib}}\right\}} \tag{3.10}$$

The numerator should measure the variance of the signal while the denominator considers noise-only variance. In order to use calibration channel variance as an assessment of noise power, the chipping rate and the ADC should be the same as those of the tracking channel of interest. The former would provide similar accumulation conditions, while the latter would account for different antennae being characterized by different noise environment and NF. Assuming the channel is perfectly synchronized (i.e. all signal – with noise – is on the I branch while only noise is on Q, with the same amount of noise on both branches), the noise

could be assessed from the Q branch. It could also be estimated using the I accumulator if the mean value of the de-spread signal were accounted for. If a receiver were to display different I and Q variances (noise powers) that would be an indication of a phase noise problem with the receiver.

Hence, the correlator outputs o should provide, after accumulating over $f_S \cdot T_P$ samples[2]: $I_{ACC} \approx (f_S \cdot T_P) \cdot \overline{d} \cdot \frac{\sqrt{2 \cdot C}}{2} + \overline{\eta}$ with the sinusoidal carrier power C. And thus, $\overline{I_{ACC}^2} \approx (f_S \cdot T_P)^2 \cdot \frac{C}{2}$ where every correlated sample S has an RMS amplitude of $\sqrt{2 \cdot C}$, the resulting half of which is due to the rejection of the high-frequency term by filtering. The code being despread and the data being squared, only the carrier remains (even powers of noise being null): $C \approx 2 \frac{\overline{I_{ACC}^2}}{(f_S \cdot T_P)^2}$. Similarly, for noise with each sample index i, $Q_{ACC}|_{\text{calib}} = \sum_{i=1}^{f_S \cdot T_P} \eta_i \Rightarrow \overline{Q_{ACC}^2} = \left\langle Q_{ACC}^2 \right\rangle = \left\langle \left(\sum_{i=1}^{f_S \cdot T_P} S_i \right)^2 \right\rangle = \sum_{i=1}^{f_S \cdot T_P} \left\langle S_i^2 \right\rangle = f_S \cdot T_P \left(\eta_S^2 \right)$.

The assumption that the noise samples are uncorrelated is valid given that the choice of sampling rate is appropriate for the noise bandwidth of the intermediate filter, assuming all noise samples are uncorrelated. However, as pointed out by van Diggelen (2009), with larger f_S, adjacent noise samples end up being the same, increasing noise power and thus eating up on the SNR. Since $N_0 = \frac{\sigma_\eta^2}{\text{BW}} = \frac{\sigma_I^2 + \sigma_Q^2}{\text{BW}} = \frac{2 \cdot \sigma_Q^2}{\text{BW}} = \frac{2 \cdot \frac{\overline{Q^2}}{f_S \cdot T_P}}{\text{BW}}$, the signal to noise density is:

$$\left. \frac{C}{N_0} \right|_{\text{calib}} = \frac{2 \cdot \frac{\overline{I_{ACC}^2}}{(f_S \cdot T_P)^2}}{\frac{2 \cdot \overline{Q_{ACC}^2}}{(f_S \cdot T_P)}} = \underbrace{\frac{1}{2} \cdot \frac{\overline{I_{ACC}^2}}{\overline{Q_{ACC}^2}}}_{\approx SNR|_{RSCN}} \cdot \frac{2 \cdot \text{BW}}{f_S \cdot T_P} = \frac{\overline{I_{ACC}^2} \cdot \text{BW}}{\overline{Q_{ACC}^2} \cdot f_S \cdot T_P} \tag{3.11}$$

where RSCN is detailed in paragraphs below.

In the development platform *RxGNSS*, the signal correlation power and noise variance are independently computed, the ratio thereof being multiplied by 1 kHz (T_P = 1 ms) leading to $\frac{2 \cdot 30 \times 10^6}{60 \times 10^6 \cdot 1 \times 10^{-3}} = 1000$.

[2] The high-frequency term is assumed to be filtered out by the accumulation process over 1 ms epochs.

However, the true IF bandwidth should have provided $\frac{2\cdot \mathrm{BW}}{f_S \cdot T_P} = \frac{2\cdot 22.3\times 10^6}{60\times 10^6 \cdot 1\times 10^{-3}} = 743.\overline{3}$. This bandwidth difference could have been overlooked if $f_S = 2\cdot \mathrm{BW}$.

3.2.3.2 Real Signal - Complex Noise

The Real Signal - Complex Noise (RSCN), described by Badke (2009), is an intuitive approach that relies on the fact that similar noise levels should be present whether or not signal is present, i.e.

$$SNR|_{RSCN} = \frac{P_{\text{total}} - P_\eta}{P_\eta} \tag{3.12}$$

With noise $P_\eta = \frac{2}{N}\sum_{j=1}^{N}\left(o_{j,\mathrm{Im}}\right)^2$ and total $P_{\text{total}} = \frac{1}{N}\sum_{j=1}^{N}\left(o_j\right)^2$ powers. That is to say:

$$\begin{aligned} SNR|_{RSCN} &= \frac{\frac{1}{N}\sum_{j=1}^{N}\left(I_{ACC,j}^2 + Q_{ACC,j}^2\right) - \left\{\frac{2}{N}\sum_{j=1}^{N} Q_{ACC,j}^2\right\}}{\left\{\frac{2}{N}\sum_{j=1}^{N} Q_{ACC,j}^2\right\}} \\ &\approx \frac{\overline{I_{ACC}^2} - \cancel{\overline{Q_{ACC}^2}}}{2\cdot\overline{Q_{ACC}^2}} \end{aligned} \tag{3.13}$$

Assuming N is high enough – typically on the order of a few hundreds of epochs – to prevent any additional estimation bias due to an insufficient number of observations.

3.2.3.3 Beaulieu

Beaulieu *et al.* (2000) proposes to estimate the noise power $P_{\eta,j} = \left(\left(o_{j,\mathrm{Re}}\right) - \left(o_{j-1,\mathrm{Re}}\right)\right)^2$ as the difference between successive samples, while the signal of interest power $P_{\upsilon,j} = \frac{1}{2}\left(o_{j,\mathrm{Re}}^2 + o_{j-1,\mathrm{Re}}^2\right)$ is rather characterized by the sample to sample consistency, both leading to the Beaulieu (BL) method:

$$SNR|_{BL} = \left[\frac{1}{N}\sum_{j=1}^{N}\frac{P_{\eta,j}}{P_{\upsilon,j}}\right]^{-1} \tag{3.14}$$

3.2.3.4 Signal to Noise Variance

The Signal to Noise Variance (SNV), described and tested in (Falletti *et al.*, 2010), appears to be complementary to the RSCN method, where the signal power is removed from the total power to evaluate noise

$$SNR|_{SNV} = \frac{P_\upsilon}{P_{\text{total}} - P_\upsilon} \tag{3.15}$$

With the signal power $P_\upsilon = \left[\frac{1}{N}\sum_{j=1}^{N}\left(o_{j,\text{Re}}\right)\right]^2$ and the total power $P_{\text{total}} = \frac{1}{N}\sum_{j=1}^{N}\left(o_j\right)^2$.

3.2.3.5 Moment Method

The Moment Method (MM), also described and tested in (Falletti *et al.*, 2010), uses the second and forth moments of the correlated signals $M_2 = \frac{1}{N}\sum_{j=1}^{N}\left(o_j\right)^2$ and $M_4 = \frac{1}{N}\sum_{j=1}^{N}\left(o_j\right)^4$ to compute signal $P_\upsilon = \sqrt{2M_2^2 - M_4}$ and noise $P_\eta = M_2 - P_\upsilon$ powers, leading to the ratio:

$$SNR|_{MM} = \frac{P_\upsilon}{P_\eta} \tag{3.16}$$

3.2.3.6 Narrowband-Wideband Power Radio

The Narrowband-Wideband Power Radio (NWPR) method (Falletti *et al.*, 2010) computes the Wide Band Power (WBP) and Narrow Band Power (NBP):

$$\begin{aligned} WBP_k &= \sum_{j=1}^{M}\left(o_{kM+j}\right)^2 \\ NBP_k &= \left(\sum_{j=1}^{M}\left|o_{kM+j,\text{Re}}\right|\right)^2 + \left(\sum_{j=1}^{M}\left|o_{kM+j,\text{Im}}\right|\right)^2 \end{aligned} \tag{3.17}$$

With the steps $k = \left[0, \left(\frac{N}{M} - 1\right)\right]$ and the ratio $M = \frac{WBW}{NBW}$ between wide and narrow bandwidth powers, leading to: $\left.\frac{C}{N_0}\right|_{NWPR} = \frac{1}{T_P}\cdot\frac{\mu_{NP}-1}{M-\mu_{NP}}$ with $\mu_{NP} = \frac{M}{N}\sum_{k=0}^{\frac{N}{M}-1}\frac{NBP_k}{WBP_k}$.

3.2.3.7 Variance Summing Method

Psiaki *et al.* (2005) describes the Variance Summing Method (VSM), which allows performing a C/N_0 estimation by non coherently averaging the squared magnitude of the complex prompt correlator. Squaring removes all dependencies to the navigation data bit polarity, provided j is 1 ms worth of accumulation.

$$\overline{o} \;=\; \tfrac{1}{N}\sum_{j=1}^{N}\left(o_j\right) \;=\; \tfrac{1}{L}\sum_{j=1}^{L}\left(I_{ACC,j}^2+Q_{ACC,j}^2\right) \tag{3.18}$$

The correlator output variance $\sigma_o^2=\frac{1}{N-1}\sum_{j=1}^{N}\left(o_j-\overline{o}\right)^2$ can be isolated the signal from the accumulation power statistical estimate $\left(\frac{N\cdot A}{2}\right)^2=\sqrt{\overline{o}^2-\sigma_o^2}$, as well as the variance of the accumulation noise terms on I and Q, i.e. $\sigma_{IQ}^2=\dfrac{1}{2}\left(\overline{Z}-\sqrt{\overline{Z}^2-\sigma_Z^2}\right)$. The signal to noise density ratio may then be computed as:

$$SNR|_{VSM} \;=\; \frac{\left(\frac{N\cdot A}{2}\right)^2}{2\sigma_{IQ}^2} \tag{3.19}$$

3.2.3.8 Weighted Bandwidths Ratio

Landry (1997, section 3.1) proposed a Weighted Bandwidths Ratio (WBR) method involving the smoothing of the signal over differents bandwidths, where the signal is known to be present or not. In the case of the GPS L1 C/A signal bound by a 20 ms navigation data bit duration,

the signal of interest can be found within ±50 Hz:

$$
\begin{aligned}
SNR|_{50\text{ Hz}} &= \underbrace{\frac{E_{50\text{ Hz}} - \frac{1}{10}\left(E_{1000\text{ Hz}} - E_{500\text{ Hz}}\right)}{\frac{1}{10}\left(E_{1000\text{ Hz}} - E_{500\text{ Hz}}\right)}}_{\text{weighted bandwidths}} \\
&= \underbrace{\frac{\frac{o_{20\text{ ms}}}{20} - \frac{1}{10}\left(o_{1\text{ ms}} - \frac{o_{2\text{ ms}}}{2}\right)}{\frac{1}{10}\left(o_{1\text{ ms}} - \frac{o_{2\text{ ms}}}{2}\right)}}_{\text{correlation measurements averaged on 1 ms}} \\
&\approx \underbrace{\frac{o_{20\text{ ms}} - \left|2o_{1\text{ ms}} - o_{2\text{ ms}}\right|}{\left|2o_{1\text{ ms}} - o_{2\text{ ms}}\right|}}_{\substack{\text{simplified equation with} \\ \text{positive noise and correlation signals}}}
\end{aligned}
\tag{3.20}
$$

Where:

- E is the signal energy in a given bandwidth
- o with the subscript x ms is the correlation result accumulated over an integration time of x ms

With non-coherent integrations, a 1 kHz window is processed.

$$
SNR|_{1000\text{ Hz}} \approx \underbrace{\frac{\sum_{j=1}^{20}\left|R_{1\text{ ms},j}\right| - \frac{\sum_{j=1}^{10}\left|R_{1\text{ ms},2j} - R_{1\text{ ms},2j-1}\right|}{10}}{\frac{\sum_{j=1}^{10}\left|R_{1\text{ ms},2j} - R_{1\text{ ms},2j-1}\right|}{10}}}_{\text{non coherent signal and noise accumulations}} \tag{3.21}
$$

For better results, a coherent integration with data synchronization would be desirable, although a compromise would be to accumulate the absolute value of the I and Q branches over

the required integration time before summing their squared values.

$$SNR|_{50\text{ Hz}} \approx \underbrace{\frac{R_{20\text{ ms}} - \frac{\sum_{j=1}^{10} \left|2R_{1\text{ ms},2j} - R_{2\text{ ms},2j-1}\right|}{10}}{\frac{\sum_{j=1}^{10} \left|2R_{1\text{ ms},2j} - R_{2\text{ ms},2j-1}\right|}{10}}}_{\text{coherent signal and noise accumulations}} \tag{3.22}$$

Special care must be taken to ensure the noise is always positive (from one j to another) since what matters here is the deviation from one ms to another. In order to reduce the SNR variations due to these 1 ms measurements, the 50 Hz SNR is averaged over every second. But this is not sufficient and not so representative as only 2 ms are considered to compute noise whereas 20 ms are used for the signal. Hence, the $\left|R_{1\text{ ms},j} - R_{1\text{ ms},j-1}\right|$ is averaged over 10 consecutive non-overlapping iterations j, i.e. once every 2 ms. This smoothing provides us with more reliable measurements, without altering the noise equivalent bandwidth, resulting in:

$$\text{SNR}|_{1\text{ s}} = \underbrace{\frac{\sum_{k=1}^{50} \text{SNR}_k}{50}}_{\text{smoothed SNR measurements}} \tag{3.23}$$

Conversion to Carrier to Noise density is performed as:

$$\begin{aligned} \left.\frac{C}{N_0}\right|_{WBR} &= 10 \cdot \log_{10}\left(\text{SNR}_{1000\text{ Hz}}|_{1\text{ s}} \cdot 1000\right) \\ &= 10 \cdot \log_{10}\left(20 \sum_{k=1}^{50} \frac{\sum_{j=1}^{20} R_{1\text{ ms},j} - \frac{\sum_{j=1}^{10} \left|R_{1\text{ ms},2j} - R_{1\text{ ms},2j-1}\right|}{10}}{\frac{\sum_{j=1}^{10} \left|R_{1\text{ ms},2j} - R_{1\text{ ms},2j-1}\right|}{10}}\right) \end{aligned} \tag{3.24}$$

3.2.3.9 Methods Comparison

As summarized by Falletti *et al.* (2010), for high values of $\frac{C}{N_0}$, the SNR estimates from the RSCN, SNV and NWPR methods remains valid only for vanishingly small phase noise. On the other hand, greater phase noise provide consistent estimates for low to medium $\frac{C}{N_0}$ levels. Falletti *et al.* (2010) found that the RSCN algorithm underestimates the $\frac{C}{N_0}$ by more than three decibels at all signal power levels. The RSCN method may thus not be suitable for GNSS receivers. The bias of the BL method remains negligible over typical phase noise values. The MM provides an accurate estimate of the true SNR. Hence, receiver designers should knowingly choose the method that best suits their needs.

3.3 Signal Impairment Sources Summary

This chapter dealt with the different sources of navigation signal impairment. First, the propagation medium was described in terms of its atmospheric impacts, multipath and RF interferences, resulting in a propagation model. Then, the receiver-bound sources were described, in terms of RF front-end, tracking channels and quantification, where the emphasis was put on several implemented SNR computation methods.

CHAPTER 4

EXISTING TRACKING ARCHITECTURES LITERATURE REVIEW

With all the enthusiasm brought up by the Global Navigation Satellite Systems (GNSS) being deployed or modernized, lots of efforts have been invested into successfully mitigating the different navigation error sources. Furthermore, over the past years, satellite positioning has known an increasing popularity across a variety of application fields, most of which are now consumer-based hand-held products (Blackroc Technology, 2015). Indeed, GPS receivers are now being included in Personal Device Assistants (PDA), wearables and smart phones through limited-resources hardware (HW) chips for consumer mobile applications.

Initially, receivers were confined to Application Specific Integrated Circuit (ASIC) due to high sampling clocks required for proper signal processing. Nowadays, Field-Programmable Gate Array (FPGA) offer a better development alternative in terms of gates capacity, computational power and price. Moreover, their programming ease reduces the time-to-market, an important commercial advantage in a very dynamic field. More recently, with the advent of increasingly more powerful Personal Computers (PC) with additional computational power on dedicated Graphics Processing Unit (GPU), Software Defined Radio (SDR) has become a mainstream research avenue.

In order to assess all the actually broadcasted signals, a flexible code tracking algorithm is required. With the objective of finding such a universal architecture, the existing code tracking algorithms are reviewed here. Since tracking is more complex for BOC than for BPSK signals, the emphasis is put on the first modulation.

The state of the art is mainly based on the Coherent and Non-coherent Early-Late Processing (CELP/NELP), as introduced in Chapter 1. Furthermore, most of BOC tracking architectures were developed, in a first attempt, to only track BOC$(1,1)$ signals (i.e. the simplest case). These architectures can be regrouped into six categories: A) BPSK-like, B) Multi-correlators C) Code Correlation Reference Waveforms, D) Sub-carrier Correlation Cancellation, E) Side

Peak Cancellation, F) Multi-loops and G) Frequency domain. The following paragraphs further describe each of these families.

4.1 BPSK-like

A first attempt to solve the BOC ambiguity is to independently process the BOC decentralized BPSK-like lobes. This requires severe filtering because of the proximity of side lobes, especially as the BOC ratio n decreases to 2. A first such technique only considers 1 lobe – Single Side Band (SSB) (Martin *et al.*, 2003) represented in Figure 1.8 — while another benefits from both lobes of BOC$(1,1)$ independently -– Double Side Band (DSB) (Heiries *et al.*, 2004). The latter approach offers a greater interference and multipath protection as twice the bandwidth is considered. A third variation of the BPSK-like method uses a weighted combination of the different side lobes — Partial Side Band (PSB) (Bello and Fante, 2005) -– to obtain a modified version of each lobe. However, precision and sensitivity loss due to filtering, even after combining both side lobes, is inevitable. With this approach, the BOC modulation advantages (e.g. narrower correlation peak providing greater precision) are lost. Because of their highlighted limitations, these architectures will not be further investigated.

4.2 Multi-correlators

In order to assess the problem of correlation peak ambiguity raised with the Traditional EML discriminator, additional Very Early (VE) and Very Late (VL) correlators were added to the traditional DLL structure. In fact, these extra correlators are positioned so that if a side peak is being tracked by the E, P and L correlators, then one of VE and VL correlators would track the main peak. This approach was named the Bump and Jump (BJ) (Fine and Wilson, 1999) technique depicted in Figure 4.1 and is recognized by the community as the BOC tracking reference to benchmark the performances of new algorithms. It is also worthwhile noting that their exact position must be determined according to the signal admitted front-end bandwidth, which affects the shape of the correlation function. Furthermore, because of noise, interference and multipath affecting the signal, multiple measurement iterations must be performed before

applying a correction (or jump). This statistical approach is hence long to react; it remains biased until the statistical computations confirm a wrong state. Although it has been validated in favourable environments, BJ rapidly reaches its limits in presence of weak signals with sudden changes (Irsigler and Hein, 2005).

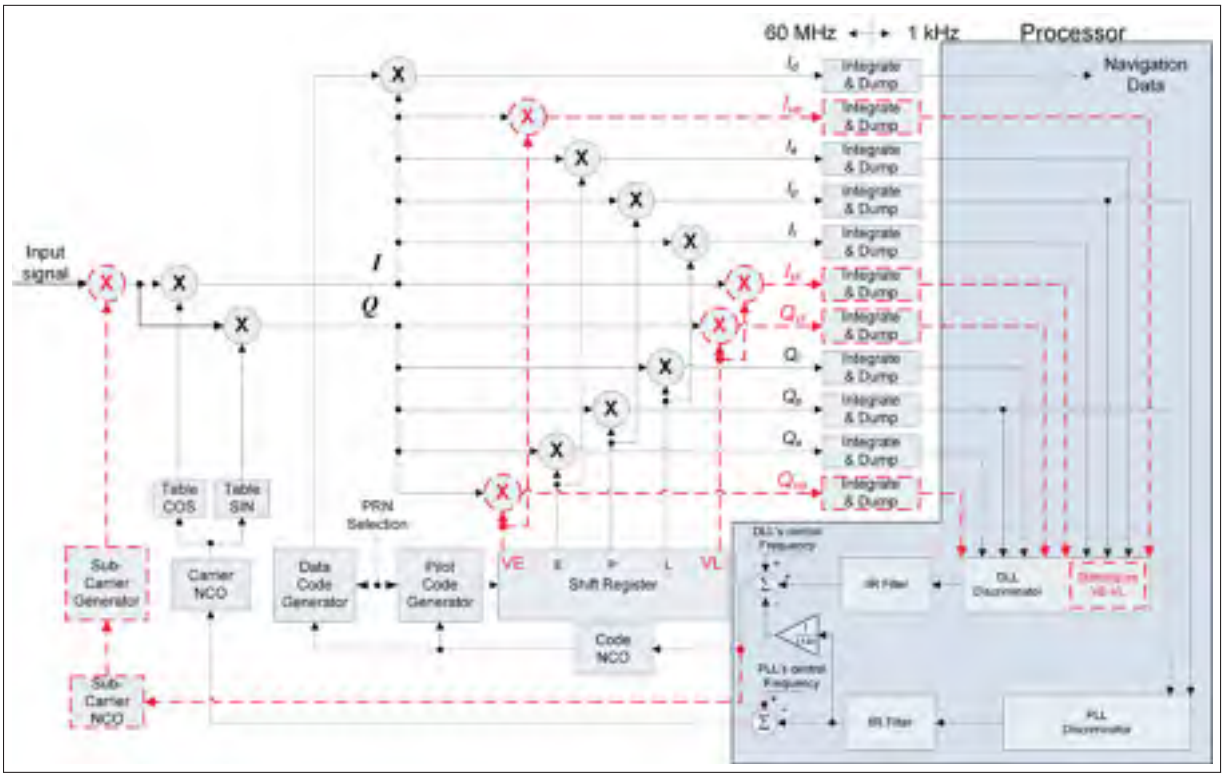

Figure 4.1 Bump and Jump Tracking Loop Overhead (red dashed lines) over BPSK

Other techniques require a lot more correlators, such as the Multiple Gate Delay (MGD) techniques. For example, the order of the discriminator is increased to N to obtain a linear combination of N weighted differences (requiring $2N$ correlators) (De Castro *et al.*, 2006). Furthermore, over 16 equidistant correlators are linearly combined by Fante (2003) to synthesize a linear zone over ± 3.5 chips, thus achieving a wide linear and pull-in range. It is capable of solving the BOC$(2q,q)$ correlation peak ambiguity, but its sensitivity decreases with the number of correlators. Below 12 correlators, the discriminator loses its monotony, although it would still be usable.

There are also other benefits in using multiple correlators, such as multipath mitigation. For more robustness, both slopes of the main peak can be measured to improve the discriminator response (Townsend and Fenton, 1994). In order to measure these slope, at least 2 correlators are required on both sides. An improvement of this technique has been suggested by Heiries *et al.* (2006). Similarly, some applications use up to 23 correlators, equally distributed over ± 3 chips (Bickerstaff *et al.*, 2006) to catch all ranges of multipath. Also, the Multipath Estimating DLL (MEDLL) method has been proposed by van Nee *et al.* (1994). This method is not based on a discriminator function, but estimates the multipath delays and attenuations in an iterative approach where a reference function is subtracted from the correlation function of the incoming signal (LoS and multipath) until only the LoS is left. This approach can also be used in open- and closed-loop. However, this approach has not really been used for BOC modulations. Nevertheless, the number of correlators monitoring the correlation shape of these methods could be reduced through a Variable Spacing Correlator (VSC), as presented by Guay *et al.* (2008).

Multi-correlators code tracking architectures may achieve interesting results in terms of multipath mitigation, but do not fully solve the BOC ambiguity, especially if different modulation rates are considered.

4.3 Code Correlation Reference Waveforms

The concept of Code Correlation Reference Waveforms (CCRW) has been introduced by Lee (2002). It basically involves two correlators. First, a prompt code replica is required to wipe-off the spreading code for the phase/frequency loops and to allow navigation message extraction. Second, a reference waveform is synthesized to directly produce a discriminator output, as illustrated in Figure 4.2. The simplest example of which, is the traditional EML: the E and L code replicas are combined into a single reference function (whether stored in memory or generated in real-time), which is then multiplied with the incoming signal and integrated in a single correlator. Such an example for BOC$(1,1)$ is shown in Figure 4.3. In the *RxGNSS*

development platform, such a CCRW could be a precomputed spreading code like any other, but would require more RAM, but less logic, making it an interesting alternative.

As a logic extrapolation of the EML comes the Narrow Correlators (NC) ^{TM}, initially intended for more robust BPSK tracking, as proposed by van Dierendonck *et al.* (1992). Applying this approach to BOC signals seems intuitive since BOC modulation causes the correlation function to narrow (i.e. get steeper), hence the need for narrowly spaced E and L correlators to preserve the same worst case attenuation in the DLL. Moreover, Garin *et al.* (1996) demonstrated that the multipath tracking error depends on the correlator spacing and on the correlation function slope, but not on the multipath delay as in standard EML tracking. Nevertheless, faced to a multi-peak correlation function, this technique is not sufficient, especially in a noisy environment, where a multipath could drag the tracking from the central peak to a side peak, thus introducing a tracking bias, resulting in $\sim$ 150 m error (i.e. half a chip bias at the speed of light) in the case of BOC$(1,1)$. That is to say that Narrow Correlators alone cannot track BOC signals reliably: there will always be uncertainty about the peak being tracked.

Another implementation of CCRW is the Double Delta (DD) technique (Morrissey *et al.*, 2006), which includes 2 pairs of High Resolution Correlators (HRC) spaced at 5 % and 10 % of the main correlation peak width to track BOC$(p,1)$ signals (Bhola *et al.*, 2006). One of the DD implementations is the strobe correlator proposed by Garin *et al.* (1996). It consists of gated correlator defined by McGraw and Braasch (1999) and reduces the correlation function non-zero width, thus isolating the main peak slopes from multipath to a certain limit. In this case, symmetric slopes can be used, thus reducing multipath error. This concept has also been extended to BOC(p,q) by altering the local code by a chain of bipolar asymmetric strobe pulses of specifically tailored duration and shape, as by Sousa *et al.* (2006). Moreover, the strobe correlator has been extended to MBOC (Sousa *et al.*, 2008). Even if tracking error due to multipath is greatly reduced, one of the drawbacks of these methods is that $n-1$ stick points (i.e. near-zero points where the discriminator could get confused) remain.

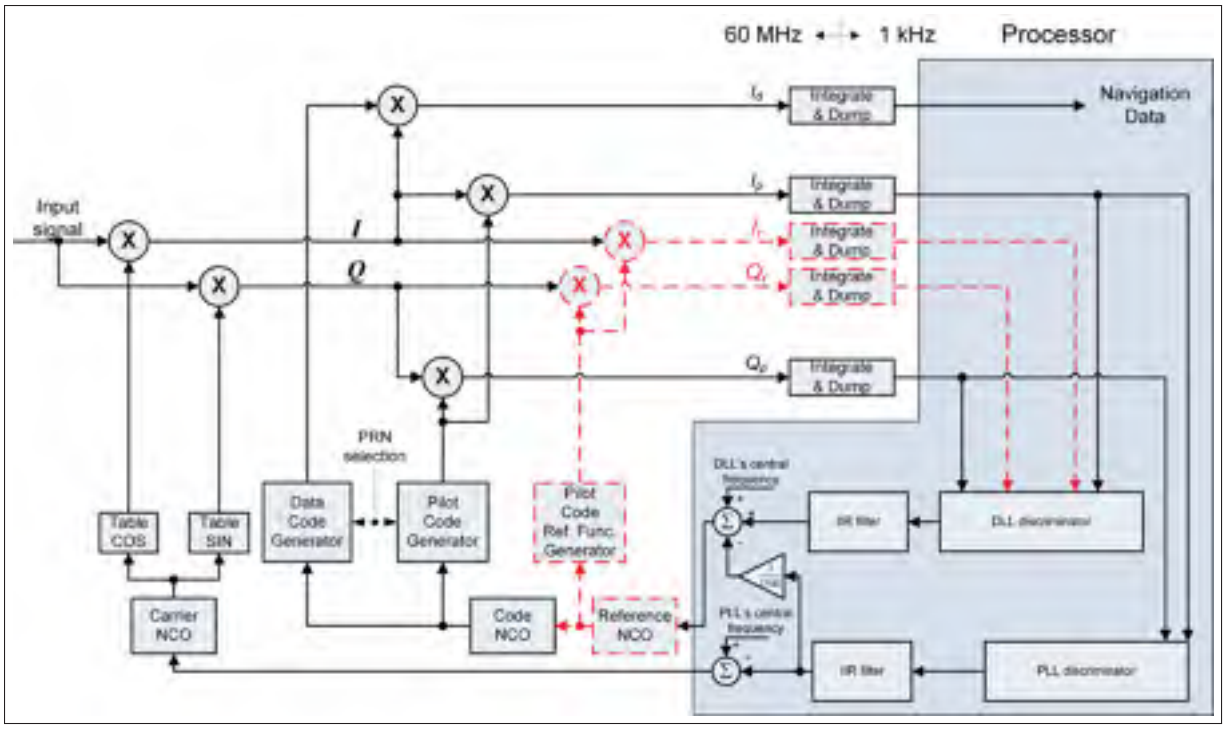

Figure 4.2 Code Correlation Reference Waveforms Tracking Loop Delta (red dashed lines) vs. BPSK

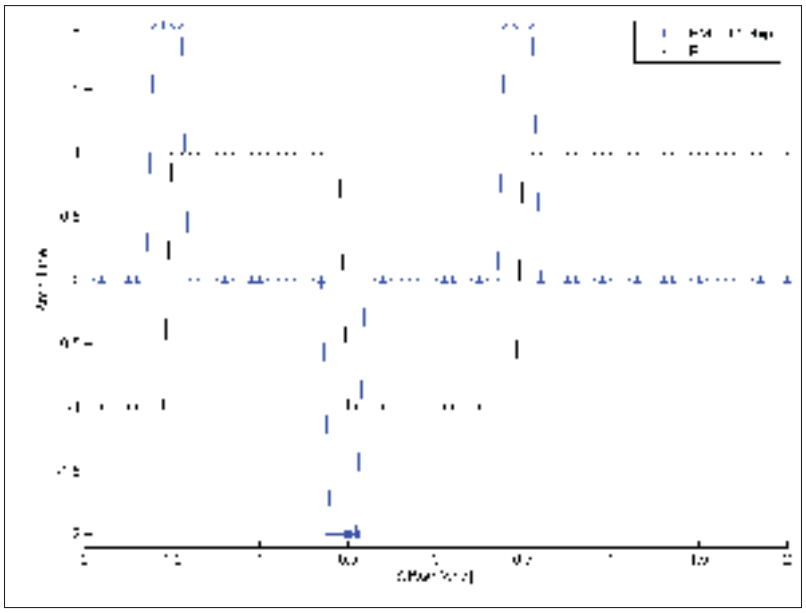

Figure 4.3 CCRW Prompt and Discriminator Replicas

The Shaping Correlator is introduced by Garin (2005). Arguing that each signal (whether received or replicated) transition creates a non-zero correlator response, $n+1$ T_s-distant reference Bipolar Waveforms are combined. The resulting P correlation being null outside the ± 1 chip range, a Dot-Product combination eliminates the E and L side components arriving beyond the ± 1 chip range. However, as pointed out by Kim *et al.* (2007), it only applies to BOC(p,p). Furthermore, the side-lobes are not completely removed, hence preserving a discriminator ambiguity, although attenuated.

Finally, S-Curve Shaping (SCS) proposes a weighted discrete multi-correlators approach that can also be synthesized into a single reference function. The method starts by defining an ideal S-curve; one that can solve the BOC ambiguity and mitigate multipath. More specifically, this ideal S-curve has four criteria:

a. Linearity zone;

b. Loss of lock outside pull-in region;

c. Unambiguous Tracking Offset (UTO) to avoid BOC ambiguity (bipolarity as previously defined) and to increase pull-in region and

d. High-Cut S-curve (HCS) to reduce maximum multipath errors. Note that this effect can also be obtained by gating the replica.

Once this ideal discriminator shape $\tilde{D}$ is determined, the equally-spaced correlator weights α are programmatically determined though Eq. 4.1 (Pany *et al.*, 2005):

$$\mathscr{F}\{\alpha\}(\Delta k) = \text{conj}\left(\frac{\mathscr{F}\left\{\tilde{D}\right\}(\Delta k)}{\mathscr{F}\{R\}(\Delta k)}\right) \tag{4.1}$$

With the correlation R calculated for every correlator. This method was extended to MBOC signals with enhanced multipath mitigation performances compared to NC and DD (Paonni *et al.*, Winter 2008-2009). Although the intuitive discrete approach could require several hundreds

of correlators, depending on the required performance, the continuous approach only imposes to store a reference waveform in memory (although a much higher sampling rate would lead to a greater accumulation depth), on top of the PRN (for prompt correlation). Obviously, as the resolution increases (or as the correlator spacing is reduced), the reference code cannot conceivably be reproduced in hardware and must be stored in memory. Nevertheless, the same basic approach can be used for any type of modulations.

4.4 Sub-Carrier Correlation Cancellation

To identify the main peak of the NC approach applied to BOC signals, Ward (2004) proposed a method requiring 12 correlators to remove the sub-carrier from the input signal, hence removing all the elements from the modulating chain on-board the satellites. Alternatively, Sauriol (2008) proposed a time-sharing optimization for the I and Q square sub-carriers, resulting in a non-coherent DLL discriminator. Assuming an infinite front-end bandwidth, it results in a plateau identifying the BOC central peak as represented in Figure 4.4. Although this approach may apply to different n ratios of BOC modulation (with $2n-1$ "ideal plateaus" resulting from the as many in-phase peaks), its performance rapidly degrades for bandwidth-limited signals. The cosine-BOC (quadrature) also shows slightly different characteristics than the sine-BOC (in-phase). These facts may lead to undesirable discriminator output, as argued by Blunt (2007).

Similarly, Sub-Carrier Phase Cancellation (SCPC) succeeds in removing the square sub-carrier by summing the squared in- and quadra-phased correlation products, resulting in a triangular-like correlation function of width $\pm T_c$ (Heiries *et al.*, 2004). Although considered as an interesting reduced-time acquisition technique – the searched bins width being greater than for the BOC$(1,1)$ correlation function – the provided accuracy is of $\pm T_c$, which is not enough to efficiently track the signal.

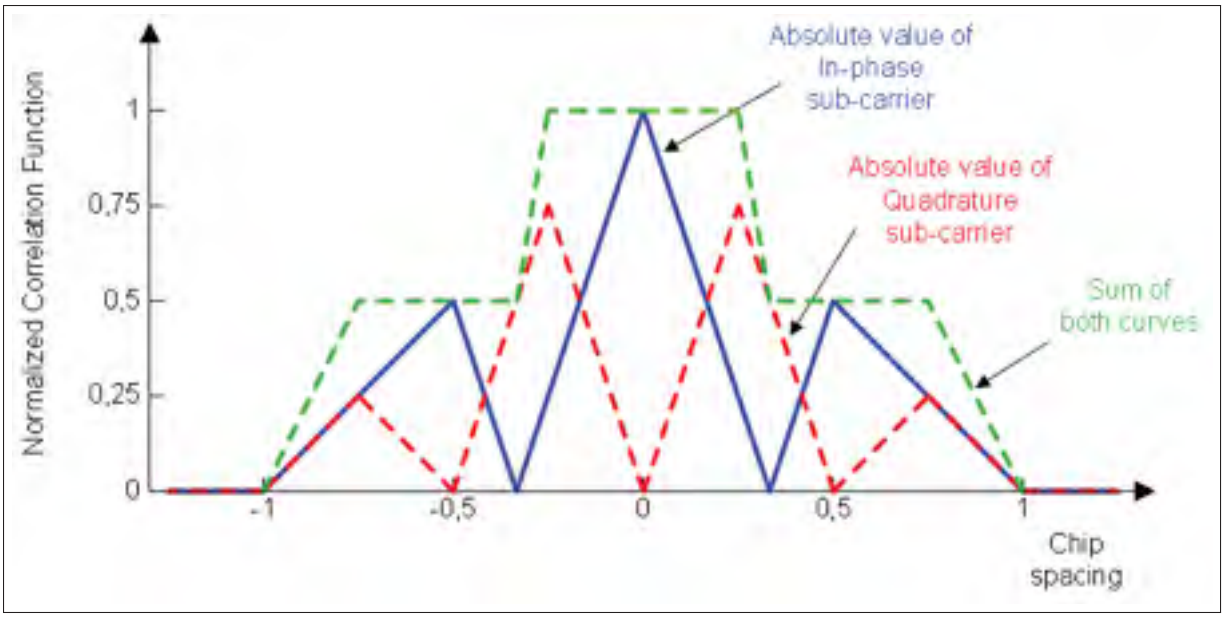

Figure 4.4 BOC$(1,1)$ ACF Sub-Carrier Correlation Cancellation
Taken from Sauriol (2008, Figure 4.10)

4.5 Side Peak Cancellation

The correlation function peak ambiguity problem introduced by the BOC modulation takes the form of side lobes. In order to avoid this ambiguity, some tracking architectures attempt to cancel the side peaks. Different approaches have been proposed (Kim *et al.*, 2007; Avellone *et al.*, 2007; Burian *et al.*, 2007; Julien *et al.*, 2007). These methods are based on the difference between two correlation products taken with the incoming signal to improve the correlation function shape (i.e. attenuate or completely remove the side lobes), while preserving the narrow central peak, as depicted in Figure 4.5.

In fact, Avellone *et al.* (2007) proposes a family of waveforms to achieve this goal. However, it only applies, to some extent, to sBOC(p,p) modulations. An improvement has been proposed as the Autocorrelation Side-Peak Cancellation Technique (ASPeCT) (Julien *et al.*, 2007), which removes the side lobes by subtracting the weighted squared cross-correlation of the incoming signal with the PRN only from the squared *standard* correlation function product,

as in Figure 4.6, achieved through:

$$R_{\text{ASPeCT}}(\tau) = \tilde{R}^2_{\text{BOC}}(\tau) - \beta \cdot \tilde{R}^2_{\frac{\text{BOC}}{\text{PRN}}}(\tau) \tag{4.2}$$

These operations require twice as many correlators to account for the second correlation product and result in a non-coherent discriminator that can be either of the Dot Product (DP) or the Early Minus Late Power (EMLP). The resulting discriminator has a reduced pull-in zone of only ± 0.83 chip, because false locks were replaced by no-locks. Furthermore, this method remains vulnerable to high dynamics with its reduced pull-in zone. Moreover, the weighting factor depends on the front-end bandwidth.

In Burian *et al.* (2007), five Side lobe Cancellation Methods (SCM) derived by combining and improving on existing methods (as above) are proposed. These methods have the advantage of being applicable to all (sine or cosine) BOC-modulated signals. The basic principle relies on a reference function modeling the side lobes that, as opposed to ASPeCT, are stored in memory. This reduces by half the number of required correlators. One such reference function exists per type of modulation. The resulting method is then combined to MEDLL for improved multipath mitigation: the side lobes reference function is removed for each main peak (that of LoS and multipath). The whole process is repeated a second time to implement a narrow EML discriminator or four times for the DD discriminator.

Another distinct approach directly uses the cross-correlation of the incoming signal with the PRN as the discriminator output (Dovis *et al.*, 2005), thus saving resources (fewer correlators and no code discriminator). Furthermore, gating the replica code (i.e. zeroing a portion of the code) emulates the smaller chip spacing of the NC approach. However, this method only works for BOC(p,p) signals and can only be used coherently.

To the author's knowledge, Side Peak Cancellation techniques are bound to BOC(p,p) tracking, unless combined with other techniques.

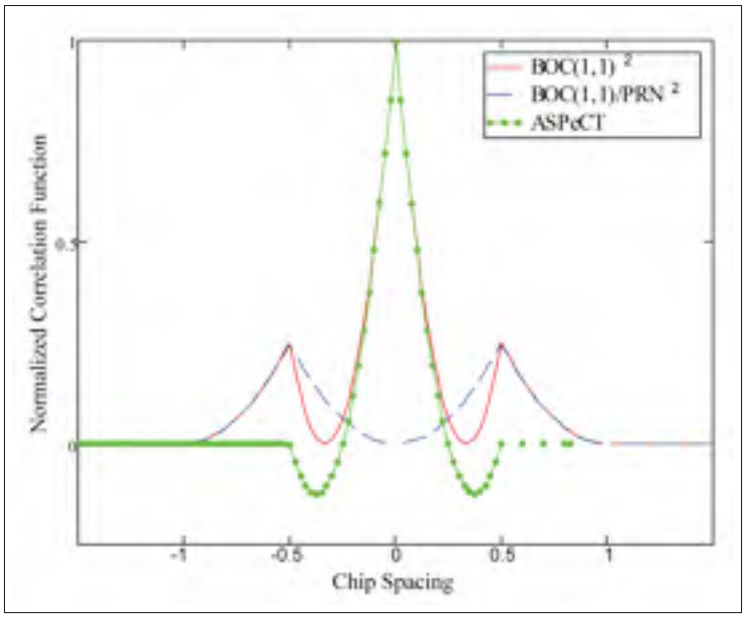

Figure 4.5 Side Peak Cancellation Principle

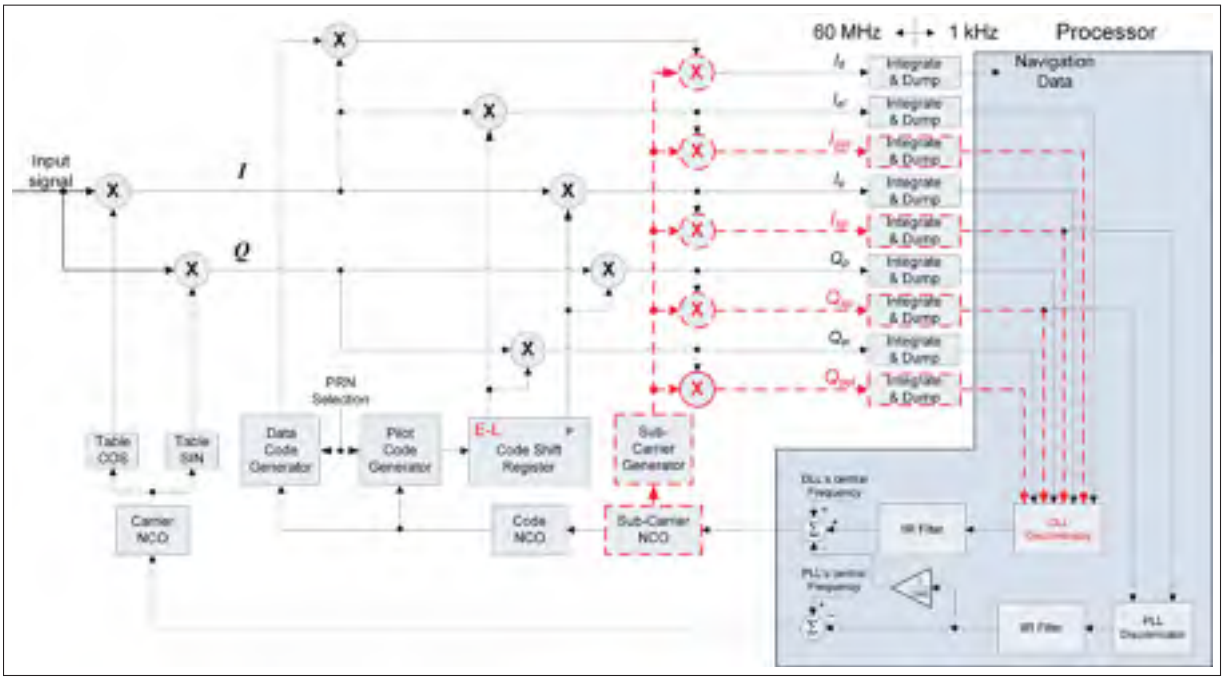

Figure 4.6 Autocorrelation Side-Peak Cancellation Technique Tracking Loop Delta (red dashed lines) vs. BPSK

4.6 Multi-Loops

Since BOC modulation is synthesized from three components (i.e. carrier, sub-carrier and code) the Triple-Loop Dual Estimator (TLDE) (Hodgart *et al.*, 2007) adds, to the traditional architecture of FLL/PLL and DLL, a third loop to track the sub-carrier. In the case of sine-BOC(kq,q), the sub-carrier is phase-synchronized with the code. The Numerically Controlled Oscillators (NCO), used in both Sub-carrier Lock Loop (SLL) and DLL, can then be controlled by a combined feedback. As a matter of fact, the SLL has an integer ambiguity (because the same square wave repeats itself over and over), but a greater resolution due to the greater sub-carrier rate compared to that of the code. The code by itself (i.e. without sub-carrier), however, has a no ambiguity, but a poor resolution (i.e. lower rate). Hence, by combining these two measurements, a better, ambiguity-free, estimate is obtained. This approach requires implementing all the additional components related to the additional loop, except for the shared discriminator. It could also be adapted to MBOC, provided that additional resources are made available for the BOC$(6,1)$ component of the signal. This method has recently been granted a patent (Hodgart and Blunt, 2015).

The Dual Estimator (DE) discriminator can be obtained through:

$$\hat{\tau}^{+} = \hat{\tau}^{*} + round\left(\frac{\hat{\tau} - \hat{\tau}^{*}}{T_S}\right) \times T_S \tag{4.3}$$

where:

$\hat{\tau}^{+}$ is the combined delay estimate

$\hat{\tau}^{*}$ is the sub-carrier delay estimate

$\hat{\tau}$ is the code delay estimate

T_S is the sub-carrier half-period

The resulting tracking loop architecture is represented in Figure 4.8.

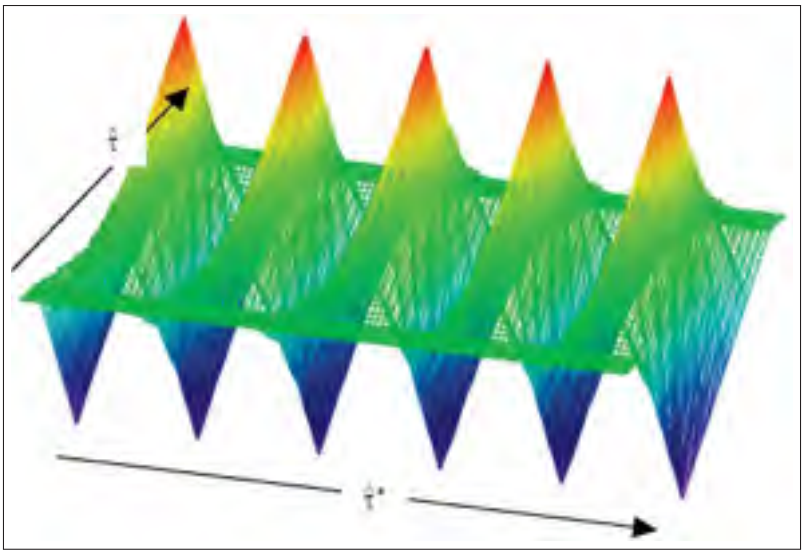

Figure 4.7 Dual Estimator Complementary Estimates

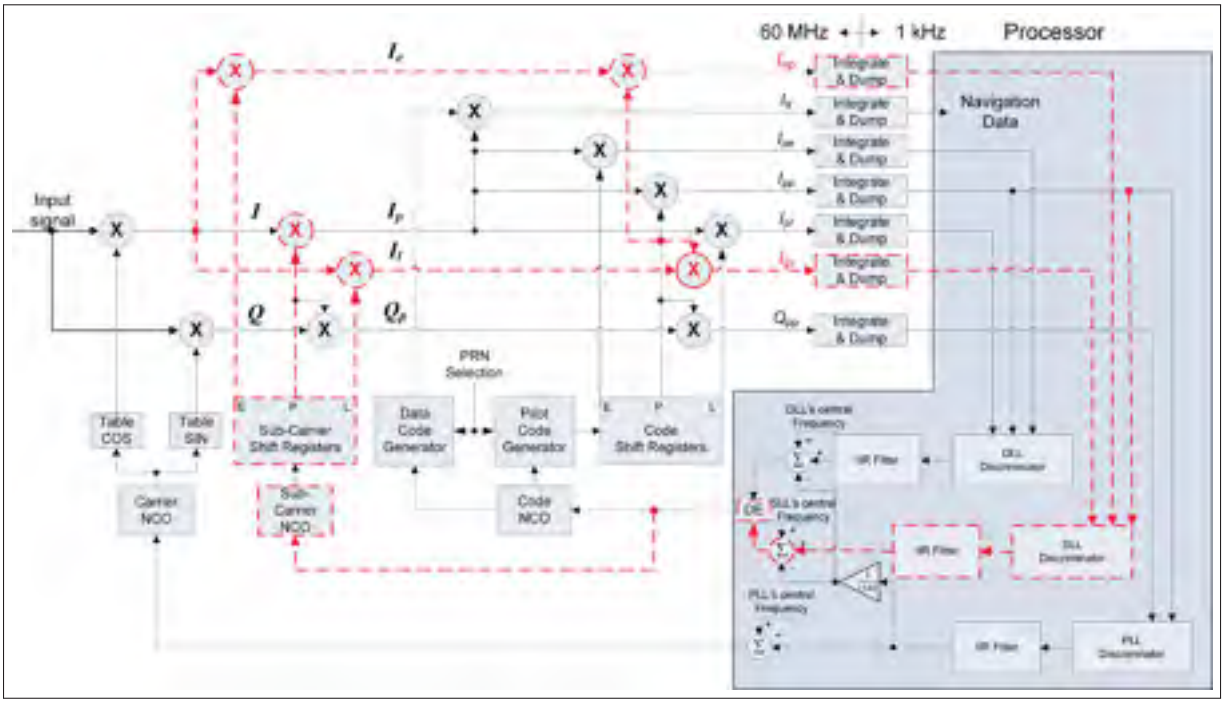

Figure 4.8 Triple Loop Dual Estimator Tracking Loop Overhead (red dashed lines) vs. BPSK

4.7 Frequency-Domain

This completely different type of approach takes advantage of the multiplication in the frequency-domain equivalence to the time-domain correlation, as more often seen in parallel acquisition algorithms. In fact, frequency-domain analysis is more flexible and precise (i.e. the corresponding correlation function takes the form of a Dirac function), no matter what the modulation is (Yang *et al.*, 2006). The narrower width triangular-shaped ACF makes it less sensitive to multipath, while other frequency-domain filtering allows for windowing, amplitude compensation and interference zeroing to name a few. It thus provides very precise pseudo-range measurements, whether through its impulse response (Yang and Miller, 2005) or a specialized Symmetric Phase-Only Matched Filter (SPOMF) (Miller *et al.*, 2006). These methods can be used in both open- and closed-loop for acquisition and tracking, respectively. The main drawback of these methods is the computational effort required for the transforms: a Fast Fourier Transform (FFT) for the incoming signal and for the local code (complex conjugated) per channel, per integration period. Another constraint is that these mathematical operations must be performed in real time, which limits the processed signal bandwidth. The Inverse FFT (IFFT) of the frequency-domain multiplication of these two spectrums represents their time-domain correlation. This last transform can be performed on a few points around the tracked peak only, reducing the computational effort. As depicted in Figure 4.9, a combined (Doppler & code) discriminator function is based on 3 delayed code replicates on 3 adjacent frequency bins to compute an improved joint estimate. The resulting frequency error is broken down into integer and fractional parts, as seen in Figure 4.10.

Such a method appears unpractical, especially for signals characterized by long spreading codes or complex modulation requiring FFT computations on a very large number of points, every 1 ms epoch, in every channel. The GPU computation power in recent copmuters could alleviate this potential limitation.

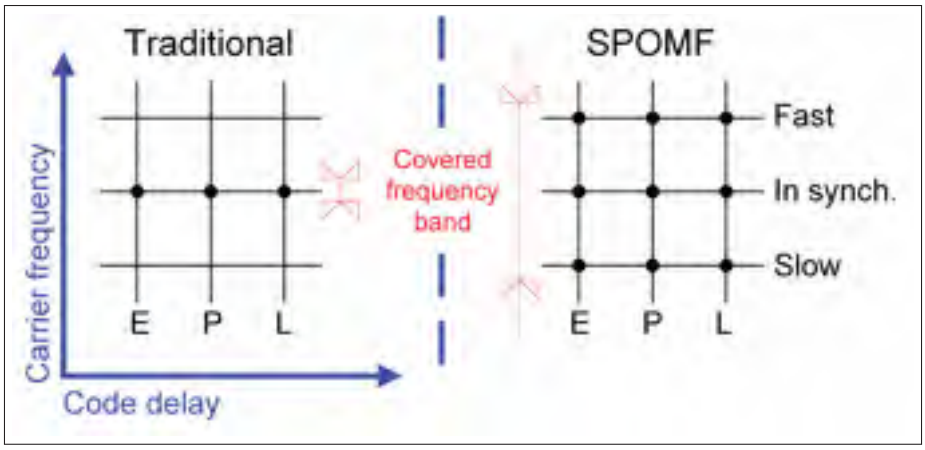

Figure 4.9 Symmetric Phase-Only Matched Filter Loop Overhead (red dashed lines) vs. BPSK

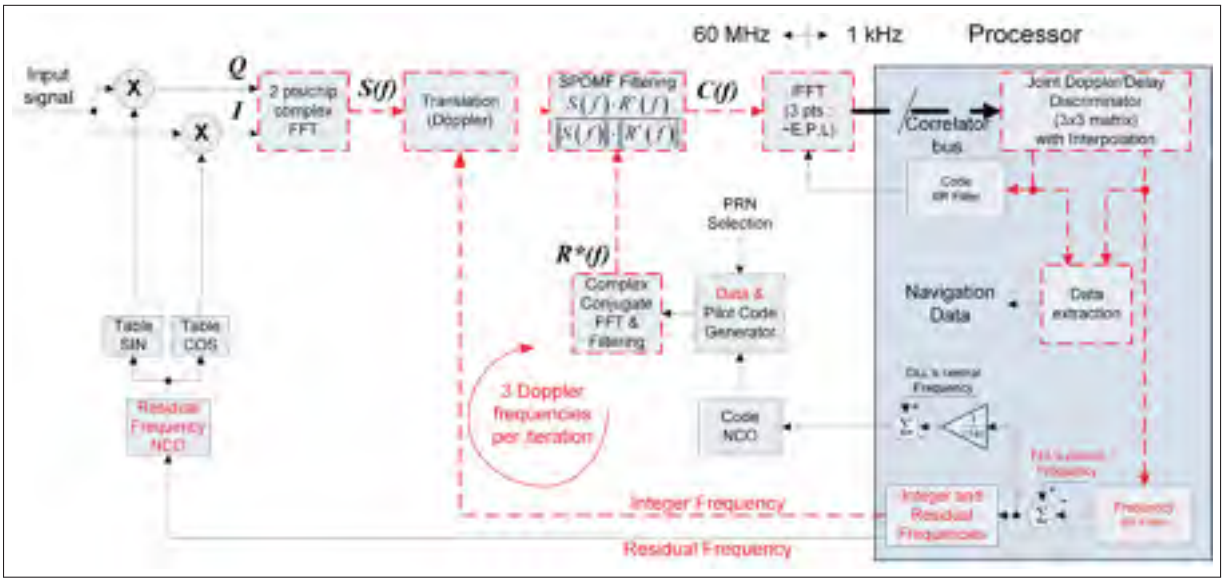

Figure 4.10 Symmetric Phase-Only Matched Filter Loop Overhead (red dashed lines) vs. BPSK

4.8 BOC Tracking Architectures Summary

In this chapter, different BOC tracking architectures have been introduced and compared against the BPSK architecture. Most of these distinctive approaches take advantage of 1-bit code replicate representations. Hence, none of them uses the "matched filter" approach, known as the

ideal correlator, which represents a core part of the innovative tracking channel presented in Appendix II.

In order to speed up signals locking by such tracking loops, Appendix I presents a resource-optimized FFT-based acquisition channel. Later, in Appendix III, these loops are further characterized through different scenarios involving WAAS-augmented solutions.

GENERAL CONCLUSION

The satellite navigation field continues along a constant evolution, leading receivers to break through initially incompatible markets, such as hostile environments and confined spaces; recent technological and algorithmic advances can now mitigate or solve the traditional limitations of GPS, namely availability, integrity, accuracy and resistance to interference. Amongst other, the flexibility of the universal tracking channel provides tools for robust receivers, enabling them to adapt to their environment or frequency conditions by harvesting the best available signals. By doing so, the current work meets objectives defined in the introduction, with foreseable positive impacts in both research and commercial domains. In order to appreciate the complexity of such work, this work has undergone vulgarizing the different aspects of navigation receivers.

Whereas the modulation schemes used are all derived from BPSK and BOC with their identified ACF characteristics and tracking challenges (cf. Chapter 1), GLONASS has still not disclosed its modernized frequency plan on L3 while Galileo and BeiDou-III constellations should be deployed by year 2020. By the end of this decade, the GPS constellation should also be updated with the up-coming block III satellites in order to provide the new civil signal L1C (cf. Chapter 2). All these particularities lay down the navigation receiver requirements, on top of which signals are impounded by their propagation medium as well as noise and limitations intrinsic to the receiver itself, as highlighted in Chapter 3. Different receiver tracking architectures are then assessed in Chapter 4.

These four chapters describe the context of receivers, whose core rely on acquisition, tracking and augmentation to achieve a navigation solution. These three cornerstone modules are further analysed in as many papers, included at the end of this work. Indeed, a generic FFT-based civil L1 signal acquisition modules is characterized in Appendix I. Once a signal is harvested from under the noise floor, universal tracking channels, synthesized in Appendix II, may be used to lock on the signals and provide raw measurements. These pseudoranges can then be improved through augmentation, as presented in Appendix III. Furthermore, various analyses and receiver configuration tools enabling a flexible and efficient development platform were

then outlined, including the decoding of navigation messages, different approaches to compute the signal to noise ratio and the quantification level of the incoming signal. In the future, the WAAS message on L5 will differ from that on L1, and should bring added value.

With all these observables, a navigation solution may be computed. Hence, the three implemented modules, namely acquisition and tracking VHDL channels and augmentation in C++, consist in the main resources found in a receiver. Being universal, they remain agnostic to the different signal specificities, thus making them future compliant. The impacts and benefits of this patent-rewarded research are considerable, especially with the blooming market for mobile and wearable electronics. Indeed, a unique microchip design may be reused in all products (and every generation thereof); the support for more or less signals then becomes only a matter of upgrading the configuration files associated to the signals of interest, assuming the RF front-end supports the navigation bands. Moreover, several instances of this microchip could be combined into a single product to increase the total number of channels.

Since the project is ambitious, validation was based on experimentation with real signals, thus avoiding the additional development of complex multifrequency simulators, for different constellations. Also, one should not minimize the complexity and the extra corner cases brought up by the different navigation systems integration. As a matter of fact, navigation data fusion is a totally different topic (Spirent Federal Systems, 2014), which falls outside of this work scope. A smaller challenge bares in the signal selection algorithm (rather than the older method for satellite selection), as described below.

Future Work

With the signals multiplication under way, the old satellite selection problem opens up a new research avenue: given a number of universal channels to which any GNSS signal may be assigned (Fortin and Landry, 2016; Landry *et al.*, 2010; Fortin *et al.*, 2009b), as described in Appendix II, it becomes of primary importance to determine the most efficient combination of GNSS signals to be tracked. This assessment should be performed in terms of geometric and frequency diversity, modulation robustness, signal quality. Furthermore, an up-to-date

replacement list of signals to acquire in case of loss of tracked signals (potentially caused by blockage or any type of interference) should be maintained and used at will to reduce as much as possible the measurements exclusion impacts on the solution, as proposed by Liu *et al.* (2009). Note that this list should be sorted in a multi-dimensional array to address a given signal loss according to its root cause. For example, simultaneously losing multiple signals on the same frequency may be caused by band interference. Hence, replacement signals transmitted on different frequencies should be used primarily (provided a multi-frequency front-end is available), until the assessed frequency threat is resolved. On the other hand, the algorithm should also answer the fundamental question of which signal should provide an improved solution (even in an ideal environment) in terms of Dilution of Precision (DOP) involving satellites from any constellation, of ionospheric corrections over frequency diversity from a satellite already being tracked or from a differential correction, provided it is available. This should open the path to "cognitive" and tactical receivers, a research domain where lots remain to be achieved.

Here is a high-level vulgarization of the traditional acquisition scheme, typically used for GPS L1 C/A signals.

Cold Start : Blindly perform a sequential (or parallel) search of all codes, for all chips and Doppler bins.

Warm Start : Apply knowledge of current time and almanac data to extrapolate current satellites position and determine which are visible based on the last known user position in order to reduce the three-dimensional search.

Hot Start : Apply knowledge of current time and ephemerides data to estimate visible satellites precise position with their associated Doppler based on the known user position (established not so long ago) to further refine the two-dimensional search grid of satellites expected to be visible.

The Highly Efficient Acquisition Degree (HEAD)-Start consists of obtaining a first position estimate based on the fastest signals to acquire. This initial step comes at no additional cost and provides a true real-time position estimate on which all subsequent steps are based. Then, signals providing the best GNSS solution in terms of accuracy and robustness gradually replace the ones currently being tracked. Hence, the algorithm undergoes the following few steps:

a. Reduced Time To First Fix (TTFF): All universal tracking channels are initially assigned to sequentially search and acquire GLONASS L1 because it has fewer chips than GPS L1 C/A to search for. More explicitly, the search space only includes 14 frequency indices (i.e. -7 to $+6$) of a 511-chip long code, compared to 32 1023-chip long codes in the case of GPS L1 C/A. Another advantage is that the ephemerides contained in the GLONASS navigation message are refreshed during the first 8 s of every 30-s long frame, compared to the first 18 s of every 30-s long frame in the case of GPS L1 C/A NAV data. Nevertheless, a single FFT channel remains a more efficient approach.

b. Parallel acquisition status update: A single universal Fast Fourier Transform (FFT) based parallel acquisition channel performs a smart search of known visible satellites, based on the current PVT achieved in the previous step as well as the receiver environmental metrics from its observables.

c. Optimum GNSS signals tracking: The replacement signals list would be used to gradually replace those currently being tracked, achieving more robustness in terms of:

    a. signal availability through a given elevation angle constraint;

    b. positioning accuracy through

        a. higher Gabor bandwidth achieved through both higher chipping and sub-carrier rates,

        b. frequency band diversity for better ionospheric correction,

        c. differential corrections or

        d. geometrical space diversity;

c. interference immunity through
    a. longer codes or
    b. non polluted frequency bands;
d. signal quality through
    a. Signal Quality Monitoring (SQM) and
    b. Receiver Autonomous Integrity Monitoring (RAIM);
e. higher sensitivity through long coherent integration times on signals pilot component.

As an outcome, it is expected that this GNSS signal selection algorithm based on a universal acquisition and tracking architecture would offer a low cost, compact size, highly efficient design for low power consumption commercial receivers embedded in widely used portable devices. Indeed, assigning a better signal (in terms of the environment assessed by the receiver) to a universal channel serves two goals: improving positioning quality using the same resources while reducing the computational load of the solution by only considering a limited number of high quality measurements. Moreover, the replacement signals list offers a reliable real-time backup to ensure enhanced robustness to any signal singularity. It could equally be used in certified high-end user equipment where a higher sampling frequency is used for better precision, at the cost of greater power consumption. The algorithm being scalable, it also seamlessly applies to airborne receivers and other Safety of Life (SoL) applications, where a greater number of universal acquisition and tracking channels are required to ensure absolute solution robustness, opening the way for reliable automated landing for example. Finally, a new metric assessing all these characteristics at once could be used in this signal selection algorithm.

APPENDIX I

PAPER #1: FORTIN *ET AL.* (2015)

This paper was published in the Journal of Navigation.

Fortin, Marc-Antoine, Francis Bourdeau and René Jr Landry. 2015. "Implementation Strategies for a Software-Compensated FFT-based Generic Acquisition Architecture with Minimal FPGA Resources". NAVIGATION: *Journal of The Institute of Navigation*, vol. 62, no 3, pp. 171–188. Available: http://onlinelibrary.wiley.com/doi/10.1002/navi.110/abstract

Implementation Strategies for a Software-Compensated FFT-based Generic Acquisition Architecture with Minimal FPGA Resources

MARC-ANTOINE FORTIN, FRANCIS BOURDEAU and RENÉ JR. LANDRY
École de Technologie Supérieure (Éts), Montréal, Canada

Received December 2014; Revised February 2015;

ABSTRACT: *A generic 2048-point FFT acquisition architecture is proposed to address L1 civil signals from all four GNSS constellations. After emphasizing hardware design criteria and their resulting design limitations, software compensation approaches are compared.*

A detailed validation methodology, involving a successive 1000-step Monte-Carlo study, was defined to optimally configure the acquisition channel, with new metrics to establish formal signal detection. The integration thereof results in a novel, minimalistic, yet generic, acquisition channel implementation, as well as a thorough validation method.

Execution time of one acquisition iteration is approximately 5 ms, in line with VHDL simulations and foreseen channel management overhead. Coarse/fine search increments and thresholds are based on extensive experimentation. A 41 dB-Hz acquisition sensitivity threshold was established to achieve >95 % detection rates for 1 ms integrations, while 15 ms non-coherent integrations are required for signal strengths down to 37 dB-Hz. These thresholds account for known implementation losses.

1 INTRODUCTION

The acquisition of a Global Navigation Satellite System (GNSS) signal consists of searching for a given satellite signal buried in noise. For a receiver to synchronize itself onto such a Pseudo-Random Noise (PRN) signal, it must approximate the spreading code time offset due to its propagation, as well as its Doppler frequency shift induced by the satellite Line Of Sight (LOS) variations, i.e., the relative movement of the satellite with respect to the receiver. During cold start, without *a priori* knowledge about a given satellite orbit, this two-dimensional (2-D) search may become a heavier processing burden as the code length increases. Indeed, one typically searches the best code delay with a half-chip resolution (for BPSK modulation) and parses a low user dynamic resulting in a ±5 kHz Doppler range with steps smaller than $2/(3T_I)$ [1], where T_I is the coherent integration time. Valid almanacs could lead to warm starts targeting satellites known to be visible with a Doppler coarse estimate, while valid ephemerides could even further narrow down the search space by providing expected Doppler and code offset estimations, provided the time, user location and speed are approximately known. This useful knowledge may be obtained by either tracking other satellites or through an external communication link such as in Assisted-GPS (A-GPS) [2].

Acquisition algorithms are typically based on signal autocorrelation properties. In satellite navigation, spreading codes are periodically repeated pseudo-random sequences allowing for multiple satellite signals access. Hence, spreading codes are truly deterministic, although exhibiting random signal properties to a GNSS receiver. Nevertheless, the correlation process indicates how well the received signal is aligned (in both time and frequency) with its locally generated replica. In the case of code offsets greater than one chip, the correlation product tends towards 0, whereas a Binary Phase Shift Keying (BPSK) modulated code alignment within ±1 chip would be located somewhere on the 2-chip wide isosceles triangular shaped correlation peak. More precisely, achieving a correlation normalized threshold of say 1/2 implies a partial (i.e., sub-chip) alignment of the input signal

with its replica. Moreover, the targeted carrier frequency (translated down to Intermediate Frequency or IF) must also be matched, at least coarsely, in order to prevent undesired signal losses (which could compromise the acquisition process altogether), as dictated by the signal linear correlation amplitude attenuation factor A (with the frequency offset Δf between input signal and replica):

$$A = \frac{\sin(\pi \cdot \Delta f \cdot T_I)}{(\pi \cdot \Delta f \cdot T_I)} = \mathrm{sinc}(\pi \cdot \Delta f \cdot T_I) \tag{1.1}$$

This potential loss reaches a peak when the incoming signal is exactly in between two Doppler bins, resulting in a maximum amplitude attenuation $A = \mathrm{sinc}\left(\pi \frac{2/(3T_I)}{2} T_I\right) = \mathrm{sinc}\left(\frac{\pi}{3}\right) = 0.827 \quad (-1.647\,\mathrm{dB})$, which is not nearly as bad as the complete signal attenuation when the argument of the *sinc* function tends towards an integer multiple of π ($sinc(\pi \cdot x) = 0, \forall x \in \mathbb{Z}^*$). This potential pitfall applies equally to all acquisition methods.

Acquisition sensitivity may be defined as the post-correlation Signal to Noise Ratio (SNR) – or equivalently the Carrier power to Noise Density (C/N_0) defined as the SNR normalized in a bandwidth (BW) of 1 Hz – threshold required for successful signal acquisition. In hostile environments and indoors, typically characterized by harmful perturbations and attenuated, distorted signals, this acquisition threshold is not as easily achieved as in clear open sky conditions. In the case of post-correlation SNR, one is interested in the correlation of the signal of interest s_x with the corresponding local replica r_x compared against an independent replica r_y.

$$SNR = \sum_{t=0}^{T_I} s_x[n] \cdot r_x[n] / \sum_{t=0}^{T_I} s_x[n] \cdot r_y[n] \tag{1.2}$$

$$\frac{C}{N_0} = \frac{SNR}{BW} \tag{1.3}$$

Acquisition (or re-acquisition of lost signals) is a crucial step in satellite navigation. More specifically, indoor navigation strongly relies on successive acquisitions as more robust tracking loops simply cannot work consistently in these signal-challenging conditions.

To improve acquisition sensitivity, longer integration periods can be used to accumulate incoming signal power. Coherent integration time is limited by the navigation bit length (or symbol length for encoded messages), unless properly wiped-off through external aiding and Doppler change, as well as by an unresolved overlaid secondary chip period, if applicable. Non-coherent integration overcomes these limitations at the cost of greater noise, known as squaring losses [3]. Furthermore, some signals now have the advantage of also being composed of a data-less pilot component, which may offer a signal strength gain and allow for longer coherent integration times. A combined data and pilot channels acquisition scheme would allow harvesting all the available signal power, thus achieving better acquisition performance, although with greater computational efforts and larger resource costs.

In all acquisition modes (cold to very hot starts with external aiding), finding the right code offset remains a time-consuming task. With the advent of longer codes, the expected Mean Time To Acquire (MTTA), without any *a priori* knowledge, becomes even greater. Considering the multitude of GNSS signal standards emerging and accounting for the previous considerations, a generic acquisition approach would appear to be of interest.

1.1 Acquisition Objectives

The blooming mobile device market is being driven towards minimal power/resource configurations, favoring more computationally efficient approaches. In this context, a minimalistic GNSS parallel acquisition channel design should accommodate all four GNSS constellations (i.e., GPS, GLONASS, Galileo, and BeiDou) while consuming minimal power. To alleviate the first requirement, at least one signal type per constellation must be successfully acquired. Indeed, the information obtained from one signal may then be extrapolated to other signals from the same satellite, minimizing their sequential acquisition effort. This knowledge is even more valuable than almanacs or ephemerides. Currently, the simplest and fastest signals to acquire are GPS L1 C/A, GLONASS L1OF, Galileo E1B/C, and BeiDou B1-I (characterized in Table 1–I), which also have the advantage of being on the same

Table 1—I: Characteristics of a Signal per GNSS Constellation

GNSS signal	RF carrier Frequency [MHz]	Primary code: Chipping rate [Mchip/s]	Primary code: Length [chip]	Primary code: Period [ms]	Data bit length [ms]	Modulation type
GPS L1 C/A [4]	1575.420	1.023	1023	1	20	BPSK
GLONASS L1 [5] [6]	1602.000 + 0.5625·[−7, 6]	0.511	511	1	10	BPSK
Galileo E1-B/C [7]	1575.420 ±1.023	1.023	4092	4	4	MBOC(6,1,11,±)
BeiDou B1-I [8]	1561.098	2.046	2046	1	1	BPSK

frequency band (provided the front-end Local Oscillator frequency can be adjusted to adapt to a slightly different RF carrier for GLONASS at 1602 MHz and BeiDou at 1561.098 MHz), thus conveniently simplifying the RF front-end required for demonstrating its implementation.

In GNSS signals, unsynchronized secondary code and unknown binary message (encoded whenever applicable) introduce phase inversions, thus limiting the coherent integration time. Even worse, the destructive effect reaches a maximum for a correlation straddling two different symbols; the correlation peak can be completely eluded if a phase inversion were to occur at 50% of the integration window. Luckily, the navigation message rates are low for GPS L1 C/A (50 Hz) and GLONASS L1 (100 Hz). However, this phase inversion would have a more frequent impact in the case of Galileo E1 as both secondary code (in the case of E1-C) and navigation symbol (in the case of E1-B) duration match their primary code duration. Nevertheless, the 50 Hz BeiDou B1-I navigation message is laid over a 1 kHz secondary code, making it the most challenging signal to acquire in terms of phase inversion probabilities.

Signal processing of these four signals by the simplest acquisition approach creates several challenges, including:

1. Different code generators;
2. Primary code lengths from 511 to 4092 chips with rates varying from 0.511 to 2.046 Mchip/s;
3. Secondary code or navigation bits introducing phase inversions with 1–20 ms intervals;
4. Code duration varying between 1–4 ms;
5. Multiple modulations including BPSK, BOC, and even MBOC;
6. RF band center frequencies ranging from 1561.098 to 1602.000 MHz; and
7. GLONASS FDMA plan requires the carrier wipe-off component to span over $[-7, +6] \cdot 562.5$ kHz.

Addressing these sub-objectives, a parallel acquisition architecture may be optimized in terms of resources, thus meeting the reduced resources (i.e., the second) requirement. After reviewing a few fundamental concepts and further describing the signals to be acquired, this paper details the proposed parallel GNSS acquisition channel and justifies the choices that have led to its design. Iterative software algorithms were developed to alleviate the limitations introduced by channel hardware reductions. New metrics are introduced to support the analysis of several trials in different conditions. Finally, the paper presents concluding remarks on the general performance of the proposed method, called HEAD-start for Highly Efficient Acquisition Degree (−start).

2 PARALLEL ACQUISITION ARCHITECTURES

Acquisition algorithms may be divided into two categories: sequential and parallel algorithms. The proposed algorithm is based on a parallel architecture, the literature thereof being outlined below, where it is assumed that T_I = 1 ms with 2 samples per chip.

Van Nee [9] has established that parallel algorithms based on Fast Fourier Transform (FFT) provide faster results through a reduced computation complexity $O(N \cdot \log(N))$ versus their sequential counterparts $O(N^2)$, where N is the correlated sequences length. There are two main types of 1-D parallel acquisition: Parallel Frequency and Parallel Code, both being repeated for each of their un-parallelized dimension; 2-D parallel acquisition combines both these 1-D acquisition types.

The *parallel search in the frequency domain algorithm* relies on the fact that perfectly wiping-off the code results in a sine wave, which can then be identified by a strong frequency coefficient at the FFT output [10].

$$D_n = \mathrm{FFT}\left\{ \left(s|_{\mathrm{baseband}}[n] \cdot c[n] \right)_{\mathrm{decimated}} \right\} \qquad (2.1)$$

where:

D_n	is the Doppler bin estimate for a particular code alignment
I/FFT	are the Inverse/Fast Fourier Transform operator
P_s	is the sampling period
$s[n]$	is the received signal with $s[n] = s(n \cdot P_s)$ and
$c[n]$	is the code replica.

The associated frequency resolution for ±5 kHz frequency search and 1 ms integration time impose:

$$Res_D \le \frac{BW_{\mathrm{FFT}}}{N_{\mathrm{FFT}}} \Rightarrow 667 \le \frac{2 \cdot \left(5 \cdot 10^3\right)}{N_{\mathrm{FFT}}} \Rightarrow N_{\mathrm{FFT}} \ge 15 \qquad (2.2)$$

where:

Res_D	is the Doppler frequency resolution
BW_{FFT}	is the searched signal Doppler frequency span, and
N_{FFT}	is the number of FFT points, typically a power of 2.

An increased coherent integration time T_I requires narrower Doppler bin spacing and therefore greater FFT lengths, as per (2.2). To avoid computation of a large number of different code offset iterations, van Nee proposes to rather apply parallelism on the code search. To do so, the *parallel search in the code domain algorithm* must resolve the following equations [9]:

$$\begin{aligned} C[f] &= \mathrm{FFT}(c[n]) \\ S[f] &= \mathrm{FFT}(s[n]) \\ R_{cs}[n] &= \mathrm{IFFT}(C^*[f] \cdot S[f]) \end{aligned} \qquad (2.3)$$

where:

$S[f]$	is the received signal Fourier coefficients
$C[f]$	is the replica Fourier coefficients
*	is the complex conjugate operator, and
R_{cs}	is the correlation between the input signal s and corresponding code replica c.

Here, the frequency-domain correlation must be computed for each tested Doppler bin. One way to remove a frequency offset consists of multiplying the time-domain signal by a complex exponential $(s'[n] = s[n] \cdot e^{-j\omega n P_s})$. Alternately, one can multiply the real code time-domain replica by a complex exponential to add a corresponding Doppler frequency offset $(c'[n] = c[n] \cdot e^{+j\omega n P_s})$. A computationally optimized approach consists of circularly shifting the frequency-domain replica (i.e., $C[f]$) to reproduce discrete approximations of different Doppler shifts, thus greatly reducing the number of FFT computations at the cost of signal sensitivity losses due to lower frequency resolution. For each Doppler alignment tested, an Inverse FFT (IFFT) is performed on the complex product, producing a time-domain cross-correlation product at every sample. Further details, such as signal correlation and Doppler side lobes as well as artefacts resulting from zero-padding may be found in [1, 11].

2.1 Parallel Acquisition Architectures Comparison

Compared to the parallel *frequency* algorithm, the parallel *code* algorithm requires fewer operations, as seen in Table 2–I. Indeed, considering the GPS L1 signal with two samples per chip, the former requires 1 FFT and 2046 multiplications for each tested chip offset. In its most complex implementation, the latter requires 1 code FFT and 16 signal FFTs, 15 of which are prior compensated in frequency (2046 complex multiplications), followed by 2048 complex multiplications and an IFFT for each of the 16 iterations.

If the baseband real code replica were multiplied by a real exponential to induce a Doppler frequency shift, some computations would be saved at the cost of reduced accuracy. Nevertheless, circular shifting the frequency coefficients of the replica comes at no hardware cost and saves 15 FFT computations, achieving the best resources per computation ratio. Such an injected Doppler frequency offset may be quantified as:

$$\Delta f_D = \frac{f_s}{N_{\text{FFT}}} \cdot N_{shift} \tag{2.4}$$

where:

$f_{\text{s,avg}}$ is the sampling frequency of the signal at the input of the FFT module.

Thus, the parallel code phase search appears to be the most computationally efficient acquisition method, but requires more resources because of its greater algorithm complexity, where the sampling frequency is set at twice the chipping rate. However, if the three Fast Fourier transforms (two direct and one inverse) are done sequentially through a single I/FFT module, the parallel code algorithm becomes even more interesting, as it allows for keeping the iterations count equal to the Doppler bins, no matter how large the spreading codes get, while also keeping the resources low through sharing. In this paper, the parallel *code* (i.e., 1-D) with circular shifting approach is chosen and further analyzed, after an outline of similar work in literature.

2.2 Other Parallel Frequency Domain Acquisition Approaches

FFT-based acquisition was first introduced by Van Nee and Coenen [9]. Later, Double Block Zero Padding (DBZP), also known as Circular Correlation by Partition and Zero Padding, was proposed by Tsui, as summarized in [1]. Recently, a lot of efforts were invested in a weak signals acquisition trend. Although this paper favors low complexity over high sensitivity, their work (often based on longer integration time) is outlined herein.

In [11], Ziedan proposed the Circular Correlation with Multiple Data Bits (CCMDB) and the Modified Double Block Zero Padding (MDBZP), which was further developed in [12]. Another optimization of the DBZP method is available in [13], where

Table 2—I: Five GPS L1 Acquisition Methods Computational Complexity carriage return (assuming 2 real samples/chip for both signal and code replica)

Acquisition method	Addition	Real multiplication	16-point FFT	2048-point FFT	2048-point IFFT	Computational order O()
Sequential (i.e., traditional correlator)	16·2046·2046	16·2046·2046	0	0	0	$16 \cdot 2046^2$
Parallel Frequency	2046·2046	2046·2046	2046	0	0	$2046 \cdot [2046 + 16 \cdot \log_2(16)]$
Parallel Code with complex exponential (Doppler injection & FFT product)	2·16·2048	2·15·2046 + 4·16·2048	0	15 + 2	16	$33 \cdot [2048 \cdot \log_2(2048)] + 30 \cdot 2046 + 64 \cdot 2048$
Parallel Code with real sine wave (Doppler injection & FFT product)	2·16·2048	15·2046 + 4·16·2048	0	15 + 2	16	$33 \cdot [2048 \cdot \log_2(2048)] + 15 \cdot 2046 + 64 \cdot 2048$
Parallel Code with circular shifting (Doppler injection & FFT product)	2·16·2048	4·16·2048	0	2	16	$18 \cdot [2048 \cdot \log_2(2048)] + 64 \cdot 2048$

Complete Correlation Results (CCR), rather than Partial ones (PCR), allow a 1.3 dB processing gain. Mollaiyan proposed a Pre-Correlation Accumulation (PCA) method, also derived from DBZP [14].

Other high sensitivity acquisition approaches are referred to in [15], although these are beyond the scope of this paper. Instead, a theoretical investigation of the proposed architecture performance is highlighted in Section 6 to serve as benchmark against its experimental results.

3 ACQUISITION CHANNEL IMPLEMENTATION DETAILS

The acquisition channel presented in this paper targets a Xilinx Virtex IV FPGA implementation. The synthesis tool provides built-in and configurable entities such as RAM, Digital Signal Processing on 48-bit (DSP48) slices, and I/FFT cores. Furthermore, a GNSS receiver has already been implemented [16–19], which cannot afford enough dedicated resources for all available GNSS civil signals. The system is composed of a computer host, the above mentioned FPGA in which a programmable processor is synthesized. In the current implementation, the same 60 MHz sampling frequency $f_s = 1/P_s$ and a 15 MHz Intermediate Frequency (IF) are used from the existing GNSS receiver development platform, regardless of which GNSS signal is being processed, hence allowing for a generic architecture.

The 60 Msample/s sampling frequency leads to an unmanageable 65 536 samples/ms FFT radix-2 sizes. Hence, the signal first needs to be down-sampled. To determine an appropriate FFT length (considering GPS L1 signal in a first attempt), many factors need to be considered, including the Nyquist sampling theorem to avoid aliasing [10] while still harvesting 90% of the signal power located within ±1.023 MHz.

$$f_{s,\,\mathrm{avg}} \geq 2f_c = 2 \cdot 1.023 \cdot 10^6 = 2.046\ \mathrm{Msample/s} \qquad (3.1)$$

Note that considering square chips with chipping rate f_c, a single sample per chip would allow for complete code reconstruction, but with lower expected performances. Then, the Doppler frequency and code resolution conditions must be considered. Assuming a 1023 chip long code sampled at 2 Msample/s during 1 ms, slightly below what is prescribed in (3.1), we get:

$$\begin{aligned} Res_D &\leq \frac{BW_{\mathrm{FFT}}}{N_{\mathrm{FFT}}} \Rightarrow 500 \leq \frac{2 \cdot 10^6}{N_{\mathrm{FFT}}} \Rightarrow N_{\mathrm{FFT}} \geq 4000 \\ Res_C &\leq \frac{N}{N_{\mathrm{FFT}}} \Rightarrow 0.5 \leq \frac{1023}{N_{\mathrm{FFT}}} \Rightarrow N_{\mathrm{FFT}} \geq 2046 \end{aligned} \qquad (3.2)$$

where:

- Res_D is the Doppler frequency resolution
- Res_C is the chip resolution
- BW_{FFT} is the bandwidth at the FFT input
- N is the spreading code length in chips, that of GPS L1 C/A being used in (3.2), and
- N_{FFT} is the FFT length.

With the objective of minimizing hardware resources, the constraint on the Doppler frequency resolution is relaxed to 1 kHz rather than $500 < 667$ Hz in (3.2), reducing the first constraint to $N_{FFT} \geq 2000$. The FFT length is selected to be $N_{FFT} = 2048$ points (i.e., the next power of 2). (3.2) results in:

$$\begin{aligned} Res_D &= \frac{BW_{\mathrm{FFT}}}{N_{\mathrm{FFT}}} = \frac{2 \times 10^6}{2048} = 976.5625\ \mathrm{Hz} \\ Res_C &= \frac{N|_{T=1\ \mathrm{ms}}}{N_{\mathrm{FFT}} - N_{\mathrm{Zeros}}} = \frac{1023}{2000} = 0.5115\ \mathrm{chip} \end{aligned} \qquad (3.3)$$

where:

- N_{Zeros} is the number of padded zeros

To compensate for the larger Doppler resolution than the rule of thumb, a PLL command (cf. Section § 3.2) offset by half the hardware Doppler resolution (achievable through circular shifting) is used to allow the acquisition to search these complimentary values: i.e., a first search covers $0 \pm k \cdot 976.56$ Hz, while the second pass covers $488.28 \pm k \cdot 976.56$, with index k. This leads to a ±5 kHz Doppler coverage with 21 bins of 488.28 Hz, now complying with the rule of thumb. The resulting Doppler frequency and code delay resolutions for the targeted signals, as well as the Intermediate Frequency (IF) where the RF signal is down-converted to, are presented in Table 3–I.

Considering the BeiDou signal, the achieved code resolution is slightly above one sample/chip, which could compromise the acquisition in some cases. Indeed, with 2 Msample/s, the BeiDou B1-I signal suffers a 46/2046 = 2.25% chip resolution loss, as only 2000 chip offsets, rather than 2046, can be considered. As seen later with fine increments in section § 4, the 6 dB worst case (2.5 dB average) loss associated with 1 sample/chip can be mitigated.

The 2000 averaged samples (for decimation from 60 to 2 Msample/s) must then be padded with $N_{Zeros} = 48$ zeros, although this comes at a cost. Indeed, a Single Period Zero-Padding (SPZP) algorithm processes only one code period per iteration. Zeros are added after the samples to allow a radix-2 FFT module to efficiently process power of two lengths, i.e., from 2000 to 2048. In the case of the incoming signal, the introduction of such a bundle of zeros may occur anywhere in the code period, which may not be aligned with the integration window; in the case of the replica code, it always occurs at the end of the code sequence. This process causes two partial correlation peaks to occur rather than one. For example, a 50% offset between the zero-padded signal and replica sequences generates two peaks of about half the nominal amplitude, each of which are found at $N_{FFT}/2$ and $N_{FFT}/2 \pm N_{Zeros}$, as shown in Figure 3–I. The auto-correlation of a tail zero-padded sequence should then

Table 3—I: Targeted Signals Intermediate Frequency and Resolutions Achieved with 2 Msample/s Sampling Rate

Signals	Intermediate Frequency [MHz]	Doppler Hardware Resolution [Hz]	Code Delay Resolution [chip]
GPS L1 C/A	15	976.56	0.5115
GLONASS L1OF	15 + 0.5625·[−7, 6]	976.56	0.2555
Galileo E1B	15 ±1.023	976.56	0.5115
BeiDou B1-I	15	976.56	1.0230

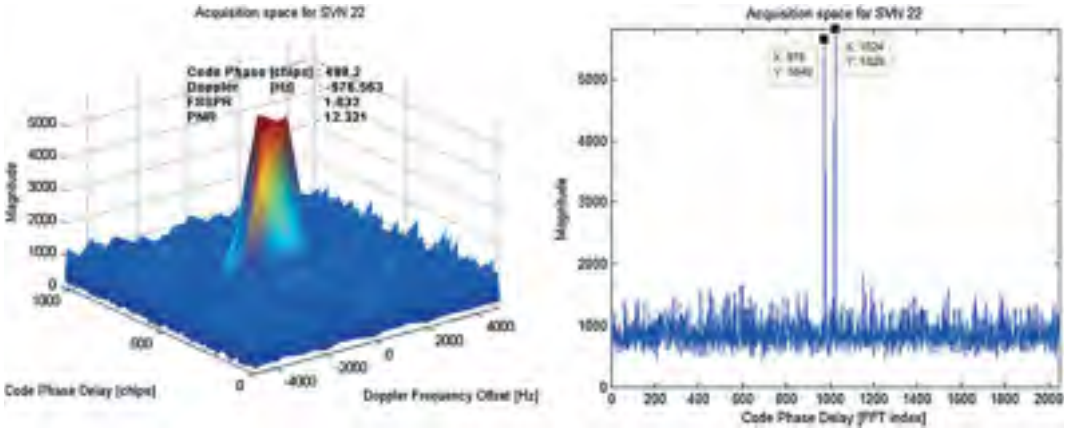

Fig. 3–I: 3D (left) and 2D (right) Acquisition Scheme with Two Partial Peaks Caused by Tail Zero-Padding in SPZP

suffer at most a 6 dB loss, i.e., a partial correlation over half its samples. Although the number of the zeros may be negligible, the partial peak they cause is quite significant in the case of SPZP as well as the navigation bit inversion issue. Hence, these partial peaks should either be detected and combined, or simply avoided all together (cf. section § 4).

An alternative to this limitation would be the DPZP, where the zeros appended at the end of two code periods always leave one full code unaltered; the other period most probably being split, as with SPZP [1], as in Figure 3–II. This analysis simplification comes at the cost of increased hardware resources and execution time as twice the samples are required, given the same chip resolution is to be achieved. As depicted in Figure 3–III, the proposed parallel code acquisition channel is composed of several modules, which are detailed in the following paragraphs.

3.1 Input Signal Quantization Module

Signal quantization is another concern in Very Large Scale Integration (VLSI) Hardware Design Language (VHDL) design: as mathematical operations proceed, the number of bits required to prevent signal loss increases. In the current case, the analog input signal (at the RF front-ends output) is conditioned by an Automatic Gain Controller (AGC) and sampled on 14 real bits, of which only 4 signed bits are retained for digital signal processing.

Given the established resources constraint, integer versus floating point operations must be decided upon. While the latter choice is expected to provide better performance, it also requires the implementation of a whole floating point Arithmetic Logic Unit (ALU). In order to save resources and time, integer operations were implemented, inducing additional noise due to truncation. These ratios are further detailed in Section 3.6.

3.2 Carrier Wipe-off Module

In the acquisition channel, a down-conversion of the incoming signal from IF to baseband is first performed. The carrier wipe-off module sine and cosine waves' frequency configuration must comply with all GNSS signals. Hence, the carrier Numerically Controlled Oscillator (NCO) must cover the frequency range defined by the union of all the considered signals, as detailed in Table 1–I. For simplicity, a full wave period is synthesized from 64 samples, each defined on 4 signed bits balanced around 0, i.e., ±7 linear amplitude levels. This standard sin/cos takes the input signal down to baseband, now quantized on 7 signed bits.

The Galileo E1 signal is CBOC modulated, where a second $6 \cdot 1.023$ MHz square sub-carrier is introduced with one tenth of the signal power of the first square sub-carrier, rated at $1 \cdot 1.023$ MHz. If Single Side Lobe (SSL) [20] were used to process either one of two main lobes of the BOC(1,1) modulation, acquisition would suffer a 3 dB loss. Also, considering either equally powered data or pilot component (another 3 dB loss), neglecting the second sub-carrier implies an additional loss of $10\log_{10}(10/11) = -0.4$ dB. The Galileo signal power admitted for a single component acquisition would thus be $-160.0 - 3.4 = -163.4$ dBW, which is

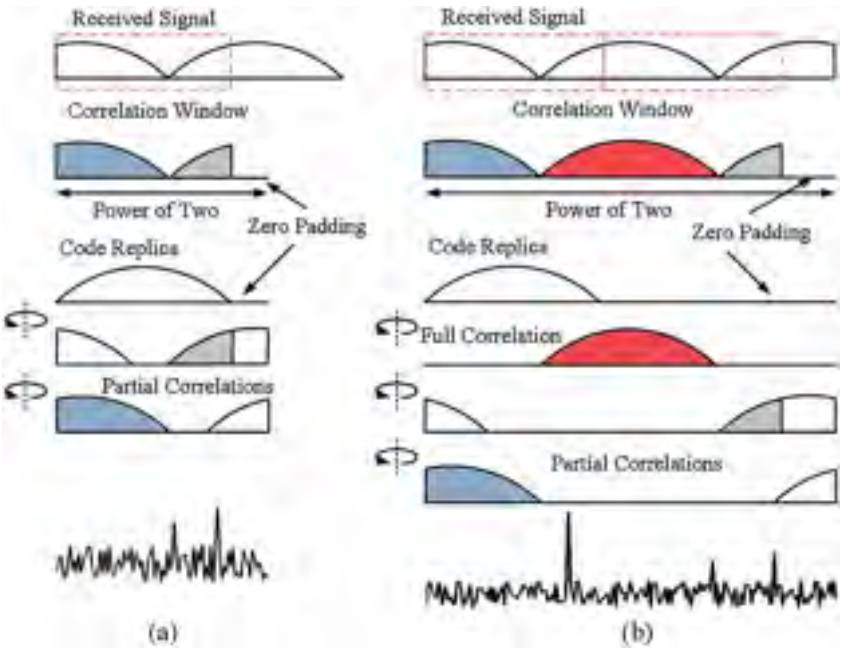

Fig. 3–II SPZP (a) and DPZP (b) Acquisition Approaches

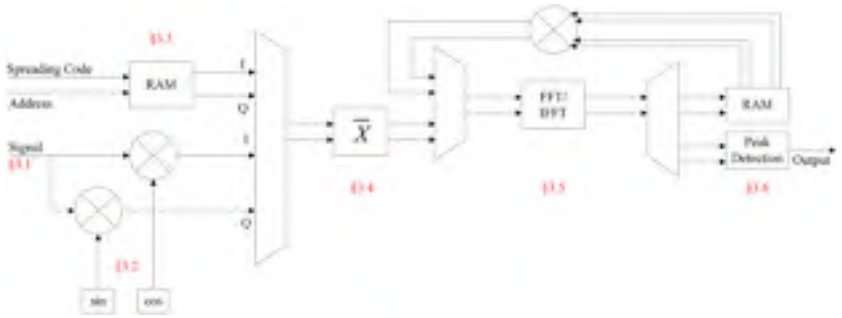

Fig. 3–III Parallel Code Acquisition Channel Schematic

almost 5 dB lower than GPS L1 C/A, i.e., – 158.5 dBW. This alone, explains why poorer performances are to be expected for the Galileo signal with the proposed acquisition approach, requiring a non-coherent integration over a few milliseconds (cf. section § 3.6.1).

3.3 Spreading Code Generation Module

In order to avoid multiplying resources for the generation of each GNSS constellation code, a common "memory code" approach is used, where the pre-computed spreading code of interest is loaded into local memory. To account for their specific chipping rates, a Delay Lock Loop (DLL) command drives a configurable code NCO, as per Table 1–I.

3.4 Averaging Module

In order to implement a reduced size I/FFT core, the baseband signal (c) is averaged over 30 consecutive samples (c_{avg}), hence decimated from 60 to 2 Msample/s, while keeping the samples on 7 bits as inputs to the FFT module, to minimize its implementation size. Averaging acts as a low-pass filter prior to decimation, thus avoiding aliasing. For performance purposes, the division by 30 is approximated by a binary shift of five positions (representing a division by 32), which raises an implementation problem: i.e., 30 consecutive positive 1-bit samples are summed and shifted, it results in 0. To avoid this, and to maximize the frequency-domain complex product, the spreading code is scaled by 5 through a look-up table, translating the memory code (cf. section § 3.3) from 0/1 to ±5, without multiplication.

$$c_{avg} = \frac{\sum_{k=1}^{30} c(k)}{32} = \left\lfloor \frac{30}{32} \right\rfloor = 0$$
$$c_{avg} = \frac{\sum_{k=1}^{30} 5 \cdot c(k)}{32} = \left\lfloor \frac{150}{32} \right\rfloor = 4 \qquad (3.4)$$

A slight loss is still suffered as the approximation results in 4 rather than 5. The signal is further altered when the averaging window straddles 2 consecutive bits.

3.5 Direct and Inverse FFT Module

One of the main design choices to be made while synthesizing Direct and Inverse I/FFT cores relates to bus sizes. In the proposed acquisition channel, the width of the signal after averaging still stands on 7 signed bit samples, which should correspond to the FFT input width. However, the input of the IFFT (which is actually the same instance of the FFT core) must also account for the result of a 15-bit complex multiplication of two complex samples. The FFT inputs and outputs were thus fixed to 16 bits, a subset of which are meaningful for the FFT computations, i.e., the 8 MSB of the FFT output are saved in RAM for subsequent computations.

Another important I/FFT core design parameter is its operation mode: burst vs. pipelined. The pipelined version represents less management, but requires a second clock domain to synchronize the signal inputs and outputs at a reduced rate (e.g., 2 MHz). The FFT takes much longer to compute as its clock domain is now 30 times slower. On the other hand, burst mode uses the 60 MHz clock domain to load the FFT samples, unload the FFT coefficients and compute the FFT. The averaging module produces samples at 2 MHz, necessitating a buffer RAM insertion, not shown in Figure 3–III. Four additional RAM blocks are needed to store the FFT complex results for both the replica and the input signals, of which only the 8 MSB are kept. This option allows non-coherent summing of several acquisition results because of its reduced computation time; the pipelined mode computation takes longer than a code period to execute.

Because of the Xilinx IP core characteristics, a 16-bit 2048-point I/FFT module is thus synthesized in burst mode. Since a single I/FFT block is used, the parallel code search algorithm must be divided into three sequential phases to allow for sharing in time for the FFT module for the following needs: the non-frequent code FFT, the repeated signal FFT, and the ongoing IFFT.

3.6 Peak Detection and Noise Computation Module

The last step in the proposed algorithm is the peak detection, which is split into four clocked operations performed by a single DSP48 [21]. First, it computes the IFFT samples squared magnitude, avoiding the computationally expensive square root operation. Each of the real and imaginary squaring operations takes one clock cycle. Then, they may be non-coherently accumulated with the previous result at the same chip offset. Note that the proposed solution does not compensate for code scaling due to Doppler, because of its associated complexity impact. On the last clock cycle, the current complex power is accumulated into the total noise measurement. This noise accumulation consists of adding the squared amplitude of every cell, including the correlation peak. By detecting the maximum cell value over the 2D search grid, the Peak to Noise Ratio (PNR) can be obtained.

$$\text{Total Power} = \sum_{d=1}^{N_{\text{Doppler}}} \sum_{c=1}^{N_{\text{FFT}}} \left(I_{d,c}^2 + Q_{d,c}^2 \right) \tag{3.5}$$

$$PNR = \frac{\left(I^2+Q^2\right)\big|_{\text{first peak}}}{\frac{\text{Total Power} - \left(I^2+Q^2\right)\big|_{\text{first peak}} - \left(I^2+Q^2\right)\big|_{\text{second peak}}}{N_{\text{Doppler}} \cdot N_{\text{FFT}} - 2}} \tag{3.6}$$

Here, the noise floor density per cell is estimated as the total cells' accumulated power as per (3.5), from which the first and second greatest peaks are removed, before being divided by the total cells' number minus the two removed peaks. This first metric could be seen as a Threshold Comparison (TC) with an adaptive threshold (Hybrid Search) [22], but considering both first and second peaks computed only once, i.e., without cell subsets.

According to the Neyman-Person lemma, TC would be optimal in maximizing the detection probability for a given False Alarm (FA) probability if the noise cells variance were known [22]. In the proposed acquisition channel, this variance is not known, and a constant threshold is used. It is yet assumed the PNR should approach the generalized likelihood-ratio test performances.

Another performance metric, a First to Second Squared Peak Ratio (FSSPR) is computed. It is used as an acquisition quality metric to further support (3.6), rather than a Ratio Detection (RD) threshold [22] in itself with lower detection performances. The second peak search neglects cells adjacent to that of the first peak.

$$FSSPR = \frac{\left(I^2+Q^2\right)\big|_{\text{first peak}}}{\left(I^2+Q^2\right)\big|_{\text{second peak}}} \tag{3.7}$$

Indeed, if multiple peaks have the same value, it means that a true correlation peak does not stand out in the search. In Figure 3–IV (left), both first and second peaks are similar in (squared) magnitude because the true Doppler is closer to -488.28 Hz, i.e., in between the hardware Doppler bins at 0 and -976.56 Hz. In Figure 3–IV (right), a 488.28 Hz offset is applied; the result really being $-976.56 + 488.28 = -488.28$ Hz, as expected.

In the case of non-coherent integrations, the IFFT operation and the Doppler search must be computed within 1 ms to allow time to compute the FFT of the

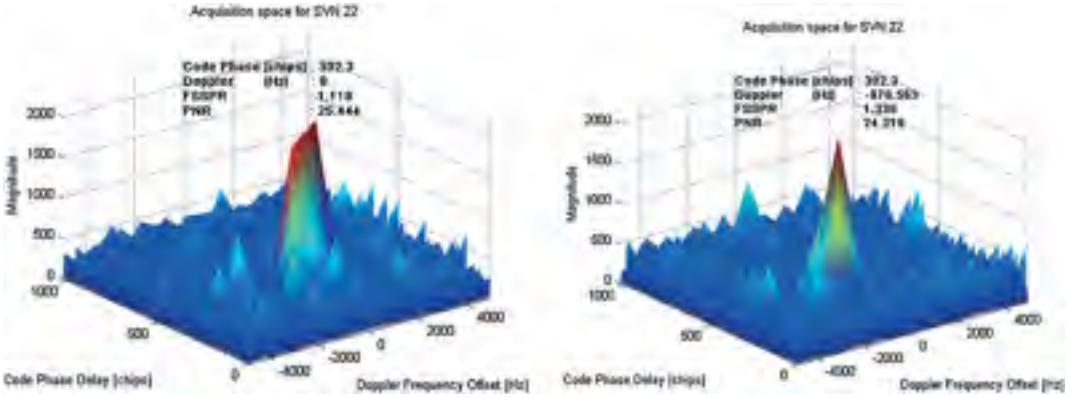

Fig. 3–IV Matlab Simulations of a GPS L1 1 ms acquisition without (left) and with (right) a 488.28 Hz compensation offset

next incoming signal epoch. Experimentation indicates that only two IFFTs – and hence two different Doppler bins – can be processed during 1 ms with extra hardware. Considering the resources constraint, the Doppler search is limited to a single bin when multiple (partial or non-coherent) integrations are required, as further analyzed in section § 3.6.1. Hence, only the following three scenarios are made available in the acquisition channel:

1. All hardware Doppler bins are covered within a single iteration (i.e., computation time < 1 ms for non-coherent integration accumulation $M = 1$)
2. Only one Doppler bin is accumulated over multiple non-coherent integrations $M > 1$ (i.e., 1 Doppler/ms)
3. Only one Doppler bin is accumulated with partial acquisition (cf. section § 3.6.1)

3.6.1 Partial Code Acquisition Methods

The basic integration time is 1 ms, which matches GPS, GLONASS, and BeiDou L1 civil signals spreading code periods, but only a quarter of the 4 ms long Galileo E1B/C primary codes. Different approaches have been investigated to consider partial code acquisition. For efficiency purposes, a reduced ±4 kHz Doppler span is used, resulting in only nine hardware Doppler bins. Also, the navigation message bit transitions do not need to be accounted for as 1 ms integrations are considered.

Initial Matlab simulations with recorded real signals have shown that correlating only a quarter of the Galileo E1B/C spreading code would not result in proper acquisition detection rates, especially with the SSL approach. Hence, four non-coherent accumulation methods are compared below and summarized. Alternatively, a maximum selection could have been used for methods 1XXX and 1111.

3.6.1.1 Method 1234. In a first attempt, four 1 ms of input signal are sequentially correlated with the four quarters of the replica code, as shown in Figure 3–V. Because of processing time constraints, the

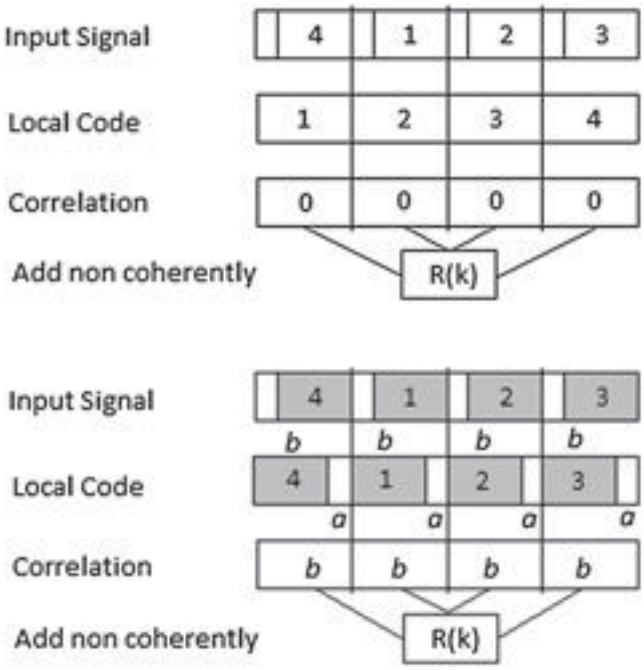

Fig. 3–V Correlation Result of a Non (top) and Partially (bottom) Aligned Galileo E1B Signal – Method 1234

acquisition channel can only process 1 ms of signal with its results accumulated non-coherently. With an unknown code alignment, this process is executed four times, each with a different code quarter offset.

In Figure 3–V, there is no correlation result when the received signal is not at least partially aligned with its replica, for each code quarter. In a 4 ms window, each replica code quarter is equally offset from the received signal; hence, their non-coherent accumulation produces a main correlation peak. Furthermore, since the FFT must be computed for every ms of input signal, the IFFT and the correlation peak search computations must all be done simultaneously with the averaging of the next ms of input signal. Thus, only one Doppler bin may be searched at a time. To cover the full ±4 kHz span, this algorithm needs to process four

different code alignments for each of the nine different hardware Doppler bins, accumulating 4 ms of correlated signal (for every Doppler bin, at every code quarter alignment).

3.6.1.2 Method 1XXX. In the 1XXX method, a single quarter of code is correlated with the received signal over several periods, as in Figure 3–VI. Since only one code quarter is used in the correlation process, the resulting idle time (NOP) can be used to search through all nine hardware Doppler bins. The total execution time for this technique is expected to be nine times lower than that of the 1234 method. However, the correlation peak amplitude should be four times smaller.

3.6.1.3 Method 1X3X. Alternately correlating two different quarters of code with the received signal led to the 1X3X method. Using half of the code results in a correlation peak twice as low as that of the 1234 method, but twice as high as that of the 1XXX method. In addition, the reduction of idle time only allows for searching within four hardware Doppler bins, resulting in an execution time slightly more than two times longer than that of the 1XXX method, but shorter than the 1234 method.

3.6.1.4 Method 1111. Finally, in order to avoid idle states, the incoming signal is correlated over four quarters of a code period, each time with the same quarter of the replica code. Since only one code quarter matches each 4 ms window of input signal, the correlation peak amplitude of this technique should be as high as the amplitude observed in the 1XXX method, while the accumulated noise should be four times greater. The idle time absence limits the Doppler search to a single bin, resulting in an execution time comparable to that of the 1234 method.

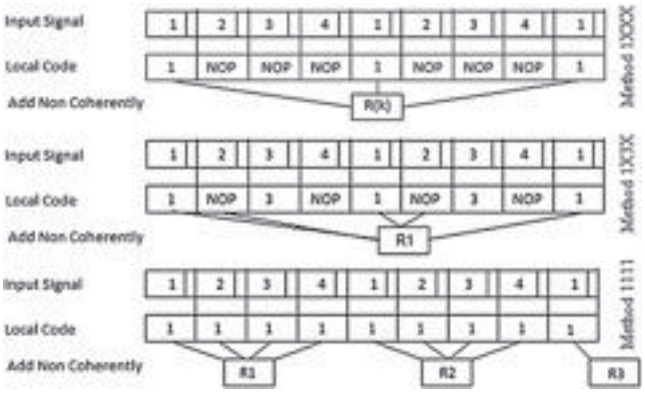

Fig. 3–VI Correlation of Replica Code Quarter(s) – Methods 1XXX (top) 1X3X (center) and 1111 (bottom)

3.6.2 Resource and Performance Comparison

The theoretical execution time has been extrapolated from VHDL simulations for the four different techniques and is presented in Table 3–II. Every algorithm has a *setup* time based on the computation of the FFT of the replica (for each code quarter used) and the averaging of the first ms of signal. Then, the *processing* time allows computing of the following: the input signal FFT, the IFFT of the frequency-domain complex multiplication results, and the correlation peak search. Note that this peak search is performed simultaneously with the IFFT of the next hardware Doppler bin or the averaging of the next ms of input signal, whichever applies. Finally, the *search* time includes the search through all nine 976.56 Hz hardware Doppler bins, for the four quarter code alignments. A negative value indicates that the last Doppler bins ended early, leaving an idle time before the next search was launched. Note that the reduction of the total Doppler span search to ± ~4 kHz (rather than ±5 kHz) greatly simplifies the computation complexity of the 1234 method.

These four methods also require different resources to store the FFT results of the different code quarters used in the correlation process. However, most RAM blocks and DSP48 slices are reused by all of them, as part of their common modules, where the common I/FFT core is obtained from the Xilinx library (made up of slices, flip flops, and 4-input Look-Up Tables or LUT), and thus kept out of Table 3–III. The replica code 16 kbit RAM remains the same, as it already supports all civil GNSS codes, except for L2CL (not considered here). Each method computes the maximum achievable Doppler bins within their idle time, which requires a single DSP48 slice in all cases.

Their resources usage may be further compared, targeting the varying number of FFT results for replica code quarters to be stored in additional RAM blocks during the correlation process. Simulations were run over the same total duration, allowing the faster 1XXX and 1X3X methods to accumulate results non-coherently with updated resources evaluation. Hence, eight DSP48 slices and 16 RAM blocks were added to the 1XXX method for accumulation results on nine hardware Doppler bins. Similarly, the 1X3X

Table 3—II: Execution Times of Four Partial Acquisition Algorithms over ±4 kHz Doppler Span

Execution time [ms]	**1234**	**1XXX**	**1X3X**	**1111**
Setup time (#quarter · time + avg. time)	4 · 1.2 + 1.0	1 · 1.2 + 1.0	2 · 1.2 + 1.0	1 · 1.2 + 1.0
Processing time (#alignment · 9/#bins · #ms)	4 · 9 · 4	4 · 1 · 4	4 · 3 · 4	4 · 9 · 4
Search time	0.2	−0.2	−3.6	0.2
Total	144.0	15.8	44.4	144.0

Table 3—III: Resources Used by Common Modules

Acquisition Module	Partial Methods (2048-point FFT)		Full Method (8192-point FFT)	
	DSP48 slices	16-kbit RAM blocks	DSP48 slices	16-kbit RAM blocks
CarrierWipe-off	3	1	3	1
Code Memory	1	1	1	4
Averaging	2	1	2	4
Signal FFT Memory	0	2	0	8
Circular Shift &Complex Multiplier	3	0	3	0
IFFT Memory	0	4	0	16
Peak Detector	1	2	1	8
Total	**10**	**11**	**10**	**41**

method requires three additional DSP48 slices and six RAM blocks to accumulate results for four distinct Doppler bins, as summarized in Table 3–IV.

Note that the resource evaluation of a "Full Method" (not implemented herein) has been appended to these two tables as a comparison benchmark. In this evaluation, it is considered that one Carrier Wipe-off module processes 4 ms worth of signal, the resulting samples being stored prior to the FFT module, where they are later processed in a burst and stored again. The IFFT produces 8192 complex samples. Equivalently, four smaller FFT modules used in parallel would require the same memory resources.

In order to get faster results, Matlab simulations were run where each algorithm accumulated their results non-coherently for 80 ms, searching only for Doppler bins over ± 4 kHz. In Table 3–V, the 1234 and 1XXX methods outperform the other two. This may be explained by fewer non-coherent integrations possible with 1X3X and increased accumulated noise (i.e. squaring losses) in the 1111 method.

From this comparison, the 1XXX method presents better performance than the 1234 (within a 80 ms limit and considering reduced resources) and should ideally be chosen. However, its 60 % resources increase is not worth its <20 % increase of both performance ratios. Finally, the 1234 method is chosen.

3.7 Justification of the Proposed Architecture

Bearing in mind that the GNSS navigation messages targeted in this paper are rated from 50 to 250 symbol/s, a slightly longer sub-optimal acquisition method may not be user perceivable; the worst case being the loss of the first data bit of a received sub-frame. This justifies resources reduction at the cost of a slightly longer Mean Time To Acquire (MTTA). These reduced resources can be compensated for by software intelligence:

1. SPZP requires synchronized triggering to minimize partial code auto-correlation losses and navigation bit inversion through a few acquisition iterations at different offsets within a 1 ms window. This reduces (and even drops) the requirement for managing two partial peaks.
2. Doppler resolution can be compensated for by a second acquisition search with a 488.28 Hz shifted Carrier NCO command. Indeed, on top of saving half the resources, a reduced computation time can be achieved: two SPZP iterations over 2000 samples, assuming the FFT is computed once for the replica and twice for the input (for both normal and shifted carrier), doesn't take as long as a single DPZP iteration over 4000 samples, assuming one FFT computation for both replica and input signals.

Table 3—IV: Resources Used by Each of the Four Partial Acquisition Methods for a ±4 kHz Doppler Span

Components	Partial Methods								Full Method	
	1234		1XXX		1X3X		1111			
	RAM	DSP	RAM	DSP	RAM	DSP	RAM	DSP	RAM	DSP
Common Components	11	10	11	10	11	10	11	10	41	10
Codes FFT Total Memory	8	0	2	0	4	0	2	0	8	0
Extra Peak Detector Resources	0	0	16	8	6	3	0	0	0	0
Total	19	10	29	18	21	13	13	10	49	10

Table 3—V: Performance of Four Partial Acquisition Algorithms over a ±4 kHz Doppler Span for an 80.0 ms execution time

Performance Ratio	1234	1XXX	1X3X	1111
FSSPR [dB]	1.6	1.8	0.8	0.2
PNR[dB]	8.7	10.2	8.8	0.3

Nevertheless, code resolution reduction from DPZP to SPZP cannot be compensated for; the worst case being a correlation peak loss of 25% in sub-chip alignment resulting in $10\log_{10}0.75 = -1.25$ dB. In order to achieve parallel multi-signal acquisition, some compromises must be made: one of them is coherent integration being limited to 1 ms as a result of unknown data bit transitions and secondary codes, when applicable.

4 TEST METHODOLOGY

In order to get a representative assessment of the acquisition channel performances, a 1000-step Monte-Carlo test was automated, providing the following numbers:

1. Detection count;
2. False-Peak count, which may be caused by detection of bad Doppler or chip alignment;
3. Miss count; and
4. Total duration.

To achieve signal detection, several criteria must be met:

1. $PNR \geq 10$;
2. $FSSPR \geq 1.5$;
3. $f_{\text{Doppler, acq}} \in f_{\text{Doppler, track}} \pm 1.5 \cdot 488.28$ Hz; and
4. $\tau_s \in \tau_{s-1} \pm \max(3, \delta_s)$ chips with code loop management and relative triggering delay compensation.

where:

τ_s is the chip delay of the acquisition step s, and
δ_s is the theoretical chip drift due to Doppler during current T_s long step.

A minimal tolerance of ±3 chips accounts for noise and timing resolution limitations. For the third criterion, it is important to consider that the full Doppler span search is split into two consecutive acquisition iterations. At high signal strength, signal detection may occur with $f_{\text{Doppler, acq}} = [-5, +5] \cdot 976.56$ Hz, even before acquisition is launched with $f_{\text{Doppler, acq}} = 488.28 + [-5, +5] \cdot 976.56$ Hz, offsetting the Doppler frequency by 488.28 Hz compared to the one seen by a dedicated tracking channel. Finally, the last criterion introduces a chip tolerance between consecutive Monte-Carlo steps. In the case of several successive iterations, the chip can be expected to vary by $\pm\delta_s$ derived in Equations (4.1) to (4.5).

$$f_{\text{code, Doppler}} = f_{\text{code}} \cdot \left(1 + f_{\text{Doppler}}/f_{\text{RF}}\right) \tag{4.1}$$

$$T_{\text{code, Doppler}} = N/f_{\text{code, Doppler}} \tag{4.2}$$

$$\Delta_{\text{chip}}\big|_{T_{code}} = \left|T_{\text{code, Doppler}} - T_{\text{code}}\right| \cdot f_{\text{code}} \tag{4.3}$$

$$\Delta_{\text{chip}}\big|_{T_{\text{I}}} = N \cdot \left|f_{\text{Doppler}}\right| / \left(f_{\text{RF}} + f_{\text{Doppler}}\right) \cdot T_I / T_{\text{code}} \tag{4.4}$$

$$\delta_s = \Delta_{\text{chip}}\big|_{T_{\text{I}}} \cdot T_s \tag{4.5}$$

where:

f_{code} is the nominal code rate,
f_{Doppler} is the Doppler frequency,
f_{RF} is the RF frequency,
$f_{\text{code, Doppler}}$ is the code rate resulting of Doppler shift,
$T_{\text{code, Doppler}}$ is the corresponding code period,
T_{code} is the nominal code period,
$\Delta_{\text{chip}}\big|_{T_{code}}$ is the chip drift after one code period,
$\Delta_{\text{chip}}\big|_{T_{\text{I}}}$ is the chip drift after one integration period, and
T_s is the duration of one Monte-Carlo step.

Furthermore, in order to compensate for the proposed identified design weaknesses, coarse/fine increments ($\Delta_{\text{coarse}}/\Delta_{\text{fine}}$) are used to delay start time in the following manner:

- Given a 60 MHz sampling frequency f_s, there are $N_{T_I} = 60\,000$ samples/ms leading to a $[0, N_{T_I}$ search span for chip alignment. Integer factors of N_{T_I} are used to impose an offset on the incoming signal window relative to a 1 ms global pulse. In fact, this allows dealing with the SPZP potential pitfall identified in Section 2.2.
- Decimating the incoming signal down to 2 Msample/s implies averaging $N_{\text{avg}} = 30$ consecutive samples into one, which could straddle two consecutive chips. In the case of GPS L1 C/A, there are $N_{T_I}/1023 = 58.651$ samples/chip. This phenomenon justifies the use of fine increments chosen in the $[1, N_{\text{avg}}[$ samples range, excluding 0 as it is tested within the preceding coarse search.
- A triggering mechanism synchronized with the 1 ms global pulse applies delayed start time with these coarse and fine increments along with the following logic, until detection is achieved:
  - The maximum PNR and FSSPR ratios are saved along with their corresponding code and Doppler bins for each coarse delay tested while the applied delay $\delta_{\text{coarse}} = i \cdot \Delta_{\text{coarse}} < N_{T_I}$, with the coarse iteration i.
  - Then the delay $\delta_{\text{coarse}}^{\max}$ at which the maximum ratios were obtained becomes the basis for the subsequent fine increment searches $\left(\delta_{\text{fine}}^{j} = \delta_{\text{coarse}}^{\max} + j \cdot \Delta_{\text{fine}}\right)$, while $j \cdot \Delta_{\text{fine}} < N_{\text{avg}}$, with the fine iteration j.
  - The code and Doppler bins associated with the maximum ratios obtained at $\delta_{\text{coarse}}^{\max} + \delta_{\text{fine}}^{\max}$ are output to the managing software for validation and statistics computation.
- Both 0 and 488.28 Hz carrier wipe-off offsets are tested along with the above procedure. Note that the second wipe-off search is only initiated after an unsuccessful 0 Hz offset search over $i_{\max} + j_{\max} = N_{T_I}/\Delta_{\text{coarse}} + N_{\text{avg}}/\Delta_{\text{fine}}$ iterations. Hence, Doppler frequencies located halfway between the hardware Doppler bins are

expected to take longer to detect, especially at low signal strengths.

- The managing software accumulates the execution duration over all the acquisition iterations $(i+j)$ of a Monte-Carlo step (s). Obviously, the more iterations that are required, the longer the acquisition step takes.

Another validation proved no detection occurred in the absence of the targeted signal. The outcome was a 129.807658 s total time for 1000 steps of the above Monte-Carlo search performed with 20 000/3 coarse/fine increments, with 0 and 488.28 Hz frequency offsets. Since no signal was found, each one of the 1000 steps performed $(i_{max}+j_{max})\cdot 2=(3+9)\cdot 2=24$ acquisition iterations. One can thus estimate 5.41 ms per acquisition iteration, assuming the replica FFT computation is performed only once at the beginning. In VHDL simulations, the FFT computation, including averaging of 1 ms worth of input signal, takes 1.259 ms. Consequently, each IFFT takes 0.259 ms and the last peak search lasts 0.136 ms. Therefore, an acquisition iteration lasts $1.259+11\cdot 0.259+0.136=4.244$ ms. Hence, the average measured acquisition iteration time corresponds to the VHDL simulations with a slight overhead due to the time to access and process the results and update commands as well as to vary the triggering time alignment (within 1 ms), thus further corroborating the design.

The results presented next are obtained from a static location, according to either of two scenarios. First, a validation is conducted through simulation (cf. section § 5). Then, real signals are acquired (cf. section § 6). In both cases, a proper inline amplification chain ensures decent signal levels reach the analog 22.3 MHz wide RF front-end, before the IF signal may be digitized.

5 ANALYSIS OF SIMULATED SIGNALS RESULTS

HEAD-start validation is conducted through Spirent GSS 7700 simulated GPS L1 C/A signals with fixed signal strength.

5.1 Coarse/Fine Search Resolution

Successive Monte-Carlo steps were launched seeking the optimal combination of coarse and fine increments in terms of execution time and detection performances. The tested coarse increments were 5, 7.5, 10, 12, 15, 20, and 30 thousands while the fine increments were 1, 2, 3, 5, 6, 10, and 15. It is expected that the coarse and fine increment combinations presenting the highest computational effort should lead to better signal detection performances, at the cost of a possibly longer execution time. The computational complexity C of coarse and fine increments (over the full span) can be defined by their worst case number of iterations.

$$C=\frac{N_{T_I}}{\Delta_{\text{coarse}}}+\frac{N_{\text{avg}}}{\Delta_{\text{fine}}}-1 \tag{5.1}$$

At first, different combinations of equivalent total complexity tests were launched to compare the impacts of these increments against one another. In Table 5–I, a computational effort of seven allows comparison of four different combinations.

In Figure 5–I, one may acknowledge the benefits of having a low Δ_{fine}, rather than a low Δ_{coarse}, as expected. While seeking the best fine increment, the coarse increment should intuitively be $N_{T_I}/3$ to overcome the SPZP limitations with the lowest computational effort. Thus, extensive simulations at constant signal strength led $\Delta_{\text{coarse, optimal}}=20\,000$ and $\Delta_{\text{fine, optimal}}=3$, resulting in a search effort of 12 (cf. Table 5–I), achieving a performance improvement over those with a search effort of seven presented in Figure 5–I. These increments remain constant for the following tests.

5.2 Optimal PNR and FSSPR Thresholds

Another series of tests were conducted to establish the $\text{PNR}_{\text{optimal}}$ and $\text{FSSPR}_{\text{optimal}}$ thresholds. The FSSPR is first assessed from 1.0 (i.e., the second peak is completely ignored) to 2; the second peak being restrained to the noise floor level at FSSPR = PNR. Then, the PNR is increased until the detection rate clearly drops.

From these results see (Figure 5–II), $\text{PNR}_{\text{optimal}}=10$, meaning the noise floor level is negligible, while maximizing robustness (i.e., reducing false peak occurrences) without significantly increasing execution time. $\text{FSSPR}_{\text{optimal}}=1.5$, as a higher value has proven to be penalizing.

5.3 Negligible Impact of Doppler Frequency Offset

In order to prove the acquisition channel performance, a simulation is conducted over the 0

Table 5—I: HEAD-start Acquisition Computational Effort Associated with Different Coarse/Fine Increments

Computational Effort [iterations]	Δ_{coarse} **[samples]**	Δ_{fine} **[samples]**
6	12 000	15
	15 000	10
	30 000	6
7	10 000	15
	12 000	10
	15 000	6
	30 000	5
...		
11	10 000	5
	30 000	3
12	7 500	6
	20 000	3

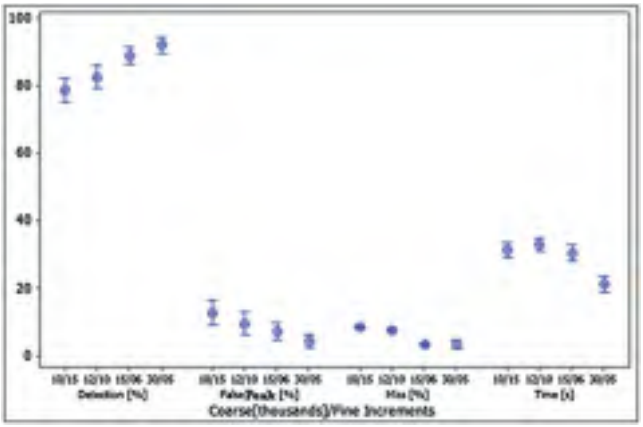

Fig. 5–I Detection Rate and Duration Statistics for a Computational Effort of 7 Legend: Detection + False Peak + Miss = 100%

to −3 kHz Doppler range with PNR = 10 or 22 and $C/N_0 = 45$ dB-Hz. From Figure 5–III, several detection drops can be observed, at the profit of false peaks. Since the signal is known to be present, this is less of a concern as the miss rate does not exceed 1%; it may hence be explained by a software misinterpretation such as a slight lack of tolerance in the detection criteria or even a zero-padding removal management issue with respect to the 1 ms global pulse. These false peaks result in a greater standard deviation for the results in a step sequence taken over a satellite course from zenith to horizon (i.e., 0 to −3 kHz Doppler range). Nevertheless, the detection statistics detailed in Table 5–II are very comforting. Also, the duration time increases from ~10 s for Doppler multiples of 976.56 Hz to ~30 s peaks for Doppler at odd multiples of 488.28 Hz. Note that this duration accounts for 1000 acquisition steps, which really corresponds to 10–30 ms per step, i.e., 2 to 6 times a 5.41 ms long iteration per step.

6 ANALYSIS OF REAL-WORLD SIGNAL RESULTS

Real signals are acquired through a passive Novatel 704 GNSS antenna located on a 1 m high pole on the flat roof with clear visibility and a 10° mask angle. For this paper's objectives, it is assumed that all satellites

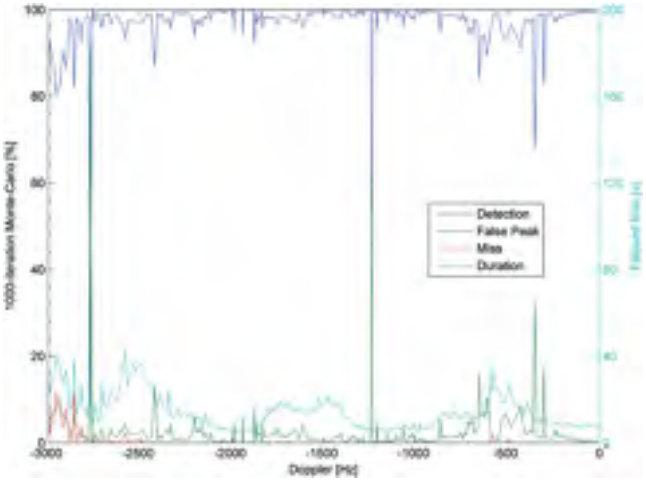

Fig. 5–III Detection Rates of Simulations over Half the Doppler Range

Table 5—II: Detection Statistics of a Simulation over Half the Doppler Range

	Detection [%]	**False Peak** [%]	**Miss** [%]	**Time** [s]
Mean	97.6	2.2	0.2	11
Std Dev.	6.6	6.3	1.3	7

of a given constellation perform equally in terms of acquisition, provided they are in the same conditions; the PRN is therefore not explicitly defined below.

From the detailed analysis performed in Section 3, the implemented solution is expected to suffer from a theoretical loss of ~6 dB, on top of the frontend noise figure and extra processing losses specific to Galileo and BeiDou signals:

- 3.5 dB current sequential acquisition losses:
  - 3.17 dB for the 22.3 MHz wide front-end Noise Figure (NF)
  - 0.29 dB for the sine approximation ($20 \cdot \log_{10}((\sum |\text{amplitude resolution}|)/64)$)
- 4.3 dB general design (sub-optimal, yet low cost generic) losses:
  - < 0.5 dB for integer (instead of float) computations
  - 1.58 dB for coarse alignment limitation (half of a third of a code alignment)

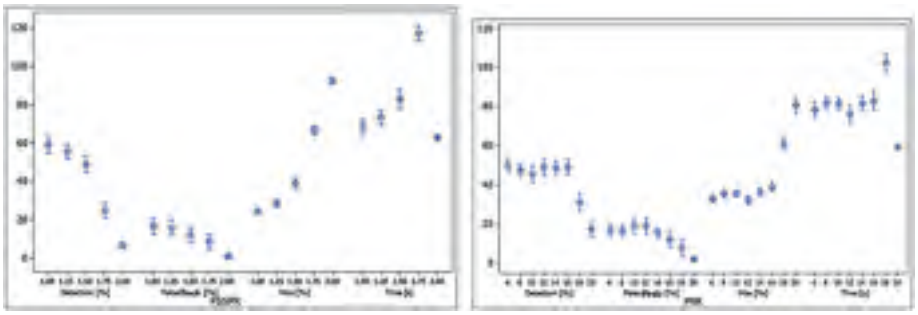

Fig. 5–II FSSPR (left) and PNR (right) Thresholds Impacts on Signal Detection Statistics at 40 dB-Hz

- ~1 dB for averaging (decimation and down-sampling)
- 0.28 dB for performing and storing FFT only on 8 MSB
- $<$ 0.87 dB for 488 Hz Doppler bin resolution

- 1.25 dB design losses for BeiDou B1-I due to chip resolution (0.75 average ACF amplitude)
- 6.4 dB design loss for Galileo E1B/C:
  - 3 dB for using either data or pilot component
  - 3 dB for SSL approach
  - 0.4 dB for neglecting its 6 MHz sub-carrier.

6.1 Zenith to Horizon Acquisitions of Real GPS L1 C/A Signals

A Monte-Carlo acquisition step, as defined in Section 4, was continuously triggered upon its completion, resulting in a massive data collection. In order to preserve its good behavior over a few hours of log, the acquisition channel was provided with an updated Doppler frequency reference obtained through an independent tracking channel assigned to the same signal. Acquisition statistics were thus logged along with the corresponding tracking channel C/N_0 for post-processing over a satellite passage from zenith to horizon, thus covering a 0 to -3500 Hz Doppler frequency span as the satellite moves away from the antenna.

In Figure 6–I, the observed false peak spikes around -1100 and -2200 Hz are not due to low signal strength, but could be due to a zero-padding removal management issue. Indeed, removing zeros as in (5.2) may introduce false peak glitches, depending on which coarse offset first meets the established detection thresholds. These signal chipping rate proportional code delay glitches have amplitude of $N_{Zeros}.{}^{N|_{T_I=1\text{ ms}}}\Big/_{(N_{IFFT}-N_{zeros})}$ chips, causing false peaks whenever greater than max(3, δ_s) chips.

One must bear in mind that the chip validation criterion is based on a given tolerance around the previous valid acquisition chip alignment. In the case of misses and false peaks, the chip drift over time between successful detections becomes underestimated; this contributes to further increasing the false detection rate, typical at lower signal strengths. Thus, in the case of the zero-padding glitches, the detection rate suffers most when the first Monte-Carlo acquisition step result (used as the reference for further chip index validation) is offset, compared to all following iterations.

Another interesting thing to point out is that the detection curve follows the C/N_0 (cf. right of Figure 6–I): the best detection scores were achieved with signal strengths above 41 dB-Hz.

6.2 Non-Coherent Integration Impact on Signal Strength Thresholds

Different non-coherent integrations of 1 ms windows drag down the minimal acquisition threshold, as seen in Figure 6–II, where 15 ms of non-coherent integration ensures 95% detection rate of signals throughout all tested signal strengths. Since the replica code length is not compensated for Doppler, increasing the total integration time will accumulate its code length offset, thus limiting acquisition sensitivity.

Although not easily applicable to the proposed solution, non-coherent integration could be taken to another level by a coherent/non-coherent hybrid approach, as is common practice for GPS L1 C/A acquisition. For example, using GPS L1 C/A with 10 ms coherent integration, one out of two (navigation bit transition free) being accumulated non-coherently would give a noticeable sensitivity boost, at the cost of longer acquisition time.

6.3 GNSS Signals Acquisition Results on L1

With a fully functional GPS L1 parallel acquisition channel, only a few adjustments are required to

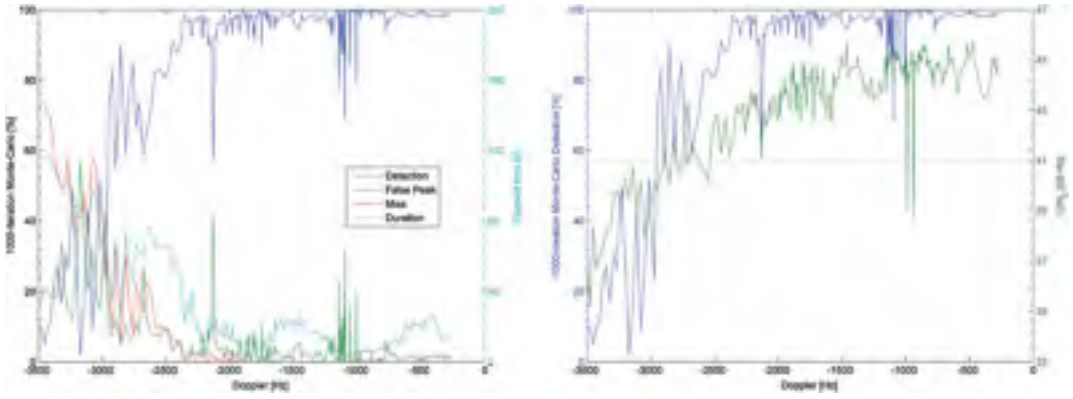

Fig. 6–I 1 ms GPS L1 Detection Rate Statistics (left) and Signal Strength (right) for Acquisitions over a Negative Doppler Span

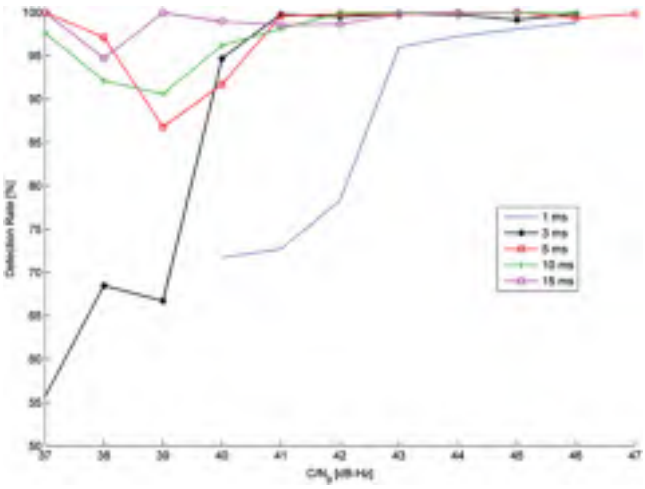

Fig. 6–II Non-Coherent Integration Impact on Detection Rate Threshold (False Peaks not considered)

accommodate other constellations' civil signals on L1, as detailed in the following paragraphs. One difference is the way to recover a chip offset from the 2048 IFFT samples. The method may be generalized as:

$$c_{peak}\big|_{T_I=1\text{ ms}} = \begin{cases} \left\lfloor (s_{peak}+1)\cdot\dfrac{N|_{T_I=1\text{ ms}}}{N_{IFFT}-N_{zeros}}\right\rfloor - 1 \leftarrow s_{peak} \leq \dfrac{N_{IFFT}-N_{zeros}}{2} \\ \left\lfloor (s_{peak}+1-N_{zeros})\cdot\dfrac{N|_{T_I=1\text{ ms}}}{N_{IFFT}-N_{zeros}}\right\rfloor - 1 \leftarrow s_{peak} > \dfrac{N_{IFFT}-N_{zeros}}{2} \end{cases} \tag{5.2}$$

where:

s_{peak} is the peak sample index, and
$c_{peak}\big|_{T_I}$ is the corresponding relative peak chip within a 1 ms coherent integration time T_I.

Another difference is the absolute chip alignment computation (relative to the global 1 ms pulse) considering different code periods, where Galileo E1 has four partial code trunks of 1023 chips/ms with the code quarter offset $\text{ms}_{\text{offset}}$ ranging from 0–3:

$$c = \left[\left(c_{peak}\big|_{T_I=1\text{ ms}} + \{\delta_{\text{coarse}}+\delta_{\text{fine}}\}\cdot\frac{N|_{T_I=1\text{ ms}}}{N_{T_I}}\right) \bmod N|_{T_I=1\text{ ms}}\right] + \text{ms}_{\text{offset}}\cdot N|_{T_I=1\text{ ms}} \tag{5.3}$$

The following paragraphs detail these other GNSS signal results.

6.3.1 GLONASS L1 Results over its FDMA Range

GLONAAS L1 has a shorter, unique code with an FDMA scheme, leading to better performance than those obtained for GPS L1 as it offers a greater chip resolution; the 12 chips worth of zero-padding still cause detection glitches, but with a lower impact in terms of chip tolerance. Different RF frequencies are managed by an adjusted IF to baseband down conversion frequency command (cf. Table 1–I), which makes this particularity transparent for the remaining of the acquisition channel architecture. The same 41 dB-Hz threshold was observed.

6.3.2 BeiDou B1-I Results with less than 1 Sample per Chip

BeiDou B1-I introduces longer codes. The 2000 averaged samples are thus slightly under-sampling the 2046 chip long spreading code. The resulting code resolution cannot be expected to have the same reliability as for GPS L1. Nevertheless, the minimal ±3 chips tolerance should have mitigated this potential limitation.

Although BeiDou B1-I shares the same 50 Hz navigation message rate as GPS L1, its 1 kchip/s secondary code is laid over the 1 ms long primary code, making it the most challenging signal to acquire with a SPZP-like approach due to phase inversion probabilities. Indeed, it prevents coherent integration over more than one 1 ms code period without prior secondary code synchronization and wipe-off. Additionally, the 48 padded zeros make initial code alignment a crucial parameter, justifying the proposed iterative coarse increments approach.

However, the miss rate is null for signal strengths above 41 dB-Hz. This corroborates a limitation in the validation method and in the chip resolution, rather than an architectural design problem. In pure acquisition, i.e., without any knowledge about the searched signal, a traditional tracking channel with early and late correlators spaced ±0.5 chip apart from the prompt correlator should handle an acquisition result with a 2046/2000 = 1.023 chip resolution in at most three (i.e., acquisition result ± 1 chip) sequential chip searches, thus mitigating this limitation.

6.3.3 Galileo E1 B Results with BOC(1,1) Approximation

In the case of the 4 ms long Galileo E1B/C spreading codes, the last term of (5.3) may not be used for validation purposes as the acquisition iterations are triggered relative to the 1 ms global pulse, without any knowledge about the input signal code start. As of December 2013, the Galileo system only bears four satellite vehicles, on top of the two GIOVE satellites [23], so signals are not as readily available as for the full GPS constellation. Furthermore, the SSL approach with BPSK simplification lowers the potential harvested satellite signal strength, leading to poorer detection rate expectations.

With these simplifications, four Galileo E1 signal variations may be tested against, i.e., data (B) and pilot (C) channels with either lower (–) or upper (+) BOC(1,1) lobes. In Figure 6–III, miss rates for a 1 ms integration time are compared to avoid

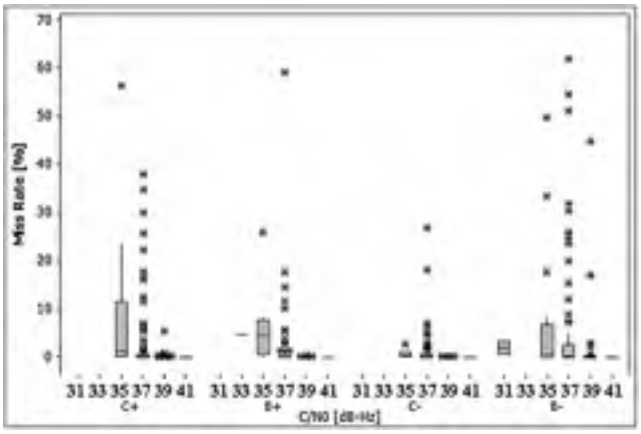

Fig. 6–III Four Galileo Variants Miss Rate with 1 ms Integration Time vs. C/N_0

beingmisled by a false peak caused by validation methodology limitations. Here are the assumptions:

- 1 ms integration window combined with coarse/fine alignment steps ensure similar acquisition conditions for all four Galileo signal variations;
- lower and upper lobes are obtained through a shifted IF to baseband frequency down-conversion command, and
- averaging at 2 Msample/s would cause the other lobes (due to subcarriers) to be filtered out.

Although it might seem that E1C– performs better, the observed variations are mostly due to acquisition validation glitches, as confirmed by the E1B– low miss rate at 30–31 dB-Hz.

7 CONCLUSION

New GNSS signals have introduced longer spreading codes' and new modulation schemes. These codes varying lengths and periods have made FFT-based acquisition algorithms more complex. This paper thus presented a generic parallel acquisition algorithm based on a constant low FFT length, accommodating at least one L1 civil signal from all GNSS constellations, where a partial code acquisition approach is taken for the longer Galileo E1B/C signal.

Several acquisition approaches were compared in terms of execution time and resources leading to the selection and implementation of a preferred method. Execution time of one acquisition iteration is ~5 ms, in line with VHDL simulations and foreseen channel management overhead. Its predicted and justified weaknesses were compensated for in software, triggering iterative searches with 20 000/3 (coarse/fine) incremented offsets until the 1-ms coherent integration period and sample averaging limitations were overcome. More specifically, samples averaged at 2 Msample/s and a 2048-point I/FFT module resulted in a 976.56 Hz frequency coefficient hardware resolution, which is not sufficient to comply with the $2/(3T_I)$ rule of thumb. When required, this is compensated for by a 488.28 Hz offset command of the frequency wipe-off module. In order to assume signal detection, a new metric combo was introduced – a 10 dB Peak to Noise Ratio (PNR) and a 1.5 First To Second Squared Peak Ratio (FSSPR) – with 95 % detection rates achieved with real signals. Experimentation showed that a 41 dB-Hz sensitivity threshold was required for 1 ms integrations while with 15 ms long non-coherent integrations, 37 dB-Hz signal strength was sufficient.

A Monte-Carlo test bench was used to determine the detection probability over a 3 kHz Doppler frequency span and a 35–45 dB-Hz signal strength range. Some validation limitations were identified and justified mathematically, leading to the scarce false peak glitches observed. Nevertheless, low miss rates were achieved throughout most experiments, demonstrating the proposed acquisition channel efficiency. The proposed generic method proved to be efficient at successfully acquiring GPS L1 C/A, GLONASS L1OF, Galileo E1B/C and BeiDou B1-I signals.

Future improvements will reuse acquisition data to perform a snapshot acquisition on other GNSS signals (on any frequency admitted by the RF front-end) with longer spreading codes at a targeted Doppler and chip offset with the 1XXX method defined for Galileo signals, while keeping the same HEAD-start acquisition channel (with triggering mechanism and different averaging ratio). This would especially be beneficial for multi-frequency acquisition of GPS L2CM being spread over 20 ms. This would make further good usage of resources on mobile devices, before it is shut down to save power. Also, transferring acquisition data to tracking channels will allow assessing the true Time To First Fix (TTFF) impact of the proposed acquisition channel. It will also be possible to extrapolate acquisition data from an L1 civil signal onto the same satellite signals on other frequencies. Also, the replica code should be compensated for Doppler in order to maximize sensitivity.

As long as the current GNSS signals will be available, this approach should remain valid and apply to most receivers, especially those embedded in mobile devices with limited space and power.

8 References

1. Tsui, J. B.-y., *Fundamentals of Global Positioning System Receivers : A Software Approach*, 2nd ed. New Jersey: John Wiley & Sons Inc., 2005.
2. Shaojun, F. and Choi Look, L., "Assisted GPS and its Impact on Navigation in Intelligent Transportation Systems," *Proceedings of the IEEE 5th International*

Conference on 2002, Intelligent Transportation Systems, 2002, pp. 926–931.
3. Strassle, C., Megnet, D., Mathis, H., and Burgi, C., "The Squaring-Loss Paradox" *Proceedings of the 20th International Technical Meeting of the Satellite Division of The Institute of Navigation* (ION GNSS 2007), Fort Worth, TX, 2007, pp. 2715–2722.
4. Global Positioning System Wing (GPSW) Systems Engineering & Integration and Space & Missiles Center (SMC) – GPSW LAAFB, "Navstar GPS Space Segment/Navigation User Interfaces," Online IS-GPS-200 Revision F, 2011.
5. Russian Institute of Space Device Engineering, "GLONASS Interface Control Document," Online GLONASS ICD, 5.1, 2008.
6. Fernandez-Prades, C., Presti, L., and Falleti, E., "Satellite Radiolocalization From GPS to GNSS and Beyond: Novel Technologies and Applications for Civil Mass Market," *Proceedings of the IEEE*, Vol. 99, 2011.
7. European Space Agency (ESA) and Galileo Joint Undertaking (GJU), "European GNSS (Galileo) Open Service: Signal In Space Interface Control Document," Online OD SIS ICD, Issue 1, 2010.
8. China Satellite Navigation Office, "*BeiDou Navigation Satellite System Signal In Space Interface Control Document Open Signal Service*," 2nd ed, 2013, p. 82.
9. Coenen, A. J. R. M., V. N. D. J. R., "New Fast GPS Code-Acquisition Technique Using FFT," *Electronics Letters* 27, 1991, pp. 158–160.
10. Borre, K., Akos, D. M., Bertelsen, N., Rinder, P., and Jensen, S. H., *A Software-Defined GPS and Galileo Receiver - A Single-Frequency Approach*, Boston: Birkha user, 2007.
11. Ziedan, N. I., *GNSS Receivers for Weak Signals*, Norwood, MA: Artech House, Inc., 2006.
12. Heckler, G. W. and Garrison, J. L., "Experimental Tests of Unaided Weak Signal Acquisition Methods Using a Software Receiver," *Proceedings of the 19th International Technical Meeting of the Satellite Division of The Institute of Navigation* (ION GNSS, Fort Worth, TX, 2006), pp. 1309–1320.
13. Li, H., Lu, M., and Feng, Z., "2010, Partial-Correlation-Result Reconstruction Technique for Weak Global Navigation Satellite System Long Pseudo-Noise-Code Acquisition," *Radar, Sonar & Navigation* [online], Vol. 5, No. 7, 2010, pp. 731–740. Available: 10.1049/iet-rsn.2010.0321.
14. Mollaiyan, K., Santerre, R., and Landry, R. J., "Acquisition of Weak Signals in Multi-Constellation Frequency Domain Receivers," *Positioning* [online], Vol. 4 No. 2, 2013, pp. 144–152. Available: http://www.scirp.org/Journal/PaperInformation.aspx?paperID=31503#.U6i5wLHm4gt
15. Sagiraju, P. K., Akopian, D., and Valio, H., "Fine Frequency Estimation in Weak Signals for GPS Receivers," *Proceedings of the 2006 National Technical Meeting of The Institute of Navigation*, Monterey, CA, 2006, pp. 908–913.
16. Sauriol, B. and Landry, R. J., "FPGA-Based Architecture for High Throughput, Flexible and Compact Real-Time GNSS Software Defined Receiver," *Proceedings of the 2007 National Technical Meeting of The Institute of Navigation*, San Diego, CA, 2007, pp. 708–717.
17. Fortin, M.-A., Guay, J.-C., and Landry, R. J., "Development of a Universal GNSS Tracking Channel," *Proceedings of the 22nd International Technical Meeting of the Satellite Division of The Institute of Navigation* (ION GNSS 2009), Savannah GA, 2009, pp. 259–272.
18. Fortin, M.-A., Guay, J.-C., and Landry, R. J., "Real-Time Low-Cost Multipath Mitigation Technique Calibrated through Real Data Repeatable Testing," *Proceedings of the 22nd International Technical Meeting of the Satellite Division of The Institute of Navigation* (ION GNSS 2009), Savannah GA, 2009, pp. 2316–2328.
19. Guay, J.-C., Sauriol, B., and Fortin, M.-A., "Real-Time Multipath Monitoring and Characterization with a Variable Spacing Correlator on a FPGA-Based Software GNSS Receiver," *Proceedings of the 21st International Technical Meeting of The Satellite Division of the Institute of Navigation* (ION GNSS 2008), Fort Worth, TX, United States, 2008, pp. 2332–2342.
20. Sun, K., "Differential Channels Combining Strategies for Composite GNSS Signals Acquisition," *Proceedings of the 2011 International Technical Meeting of The Institute of Navigation*, San Diego, CA 2011, pp. 1218–1231.
21. XtremeDSP for Virtex-4 FPGAs [online]. Available: http://www.xilinx.com/support/documentation/user_guides/ug073.pdf, 2008, pg. 121, February 21, 2011.
22. Geiger, B. C., Vogel, C., and Soudan, M., "Comparison Between Ratio Detection and Threshold Comparison for GNSS Acquisition," *IEEE Transactions on Aerospace and Electronic Systems*, Vol. 48, pp. 1772–1779, 2012.
23. European GNSS Service Center, *Constellation Information* [online]. Available: http://www.gsc-europa.eu/system-status/Constellation-Information, January 22, 2014.

APPENDIX II

PAPER #2: FORTIN AND LANDRY (2016)

This paper was published in Sensors

Fortin, Marc-Antoine and René Jr. Landry. 2016. “Implementation Strategies for a Universal Acquisition and Tracking Channel Applied to Real GNSS Signals”. *Sensors* vol. 16, no 5, pp. 624-249. doi:10.3390/s16050624. Available: http://www.mdpi.com/1424-8220/16/5/624

sensors

MDPI

Article

Implementation Strategies for a Universal Acquisition and Tracking Channel Applied to Real GNSS Signals

Marc-Antoine Fortin * and René Landry Jr.

Electrical Department, École de Technologie Supérieure (ÉTS), Montréal, QC H3C 1K3, Canada; renejr.landry@etsmtl.ca

* Correspondence: Marc-Antoine.Fortin@lassena.etsmtl.ca; Tel.: +1-514-262-9295

Academic Editor: Luis Javier Garcia Villalba

Received: 23 February 2016; Accepted: 20 April 2016; Published: 2 May 2016

Abstract: This paper presents a universal GNSS receiver channel capable of tracking any civil GNSS signal. This fundamentally differs from dedicated channels, each customized for a given signal. A mobile device could integrate fewer universal channels to harvest all available signals. This would allow securing signal availability, while minimizing power consumption and chip size, thus maximizing battery lifetime. In fact, the universal channel allows sequential acquisition and tracking of any chipping rate, carrier frequency, FDMA channel, modulation, or constellation, and is totally configurable (any integration time, any discriminator, *etc.*). It can switch from one signal to another in 1.07 ms, making it possible for the receiver to rapidly adapt to its sensed environment. All this would consume 3.5 mW/channel in an ASIC implementation, *i.e.*, with a slight overhead compared to the original GPS L1 C/A dedicated channel from which it was derived. After extensive surveys on GNSS signals and tracking channels, this paper details the implementation strategies that led to the proposed universal channel architecture. Validation is achieved using GNSS signals issued from different constellations, frequency bands, modulations and spreading code schemes. A discussion on acquisition approaches and conclusive remarks follow, which open up a new signal selection challenge, rather than satellite selection.

Keywords: GNSS; acquisition; tracking; modulation

1. Introduction

Currently, most Commercially Off The Shelf (COTS) receivers available in North America only support GPS L1 C/A, while some also support GLONASS L1OF and WAAS L1 augmentation, thanks to their integration onto a single chip [1]. As new Global Navigation Satellite Systems (GNSS) are becoming available, this trend may change. Indeed, both the Chinese and Russian governments have passed laws mandating that all receivers sold in their territories be compatible with their national systems, *i.e.*, BeiDou and GLONASS, respectively [2,3]. In parallel, mobile devices (e.g., smart phones and now wearables) have also known an exponential growth.

On the other hand, higher-end receivers also support differential correction and semi-codeless tracking of the encrypted GPS P(Y) code available on L1 and L2 for improved accuracy, such as in precision farming and land-surveying [4]. Over the last decade, dedicated resources for signal-customized channels have led to receivers with more than 200 tracking channels—not to be confused with effective acquisition channels obtained through FFT-based approaches or "fast acquisition channels"—such as Javad's [5]. These two trending markets (namely low *vs.* high end) have conflicting development paradigms: affordable battery operated *vs.* expensive and power-greedy devices.

Thanks to the modernization of GPS and GLONASS as well as the advent of Galileo and BeiDou, new signals are being broadcasted, or at least should start being transmitted shortly. These signals aim the answer the traditional GPS limitations. Indeed, higher bandwidths will help resist interferences by diluting the impact of a narrowband interference over a larger bandwidth [6]. This should also provide better positioning accuracy and resistance to multipath with a faster chipping rate [7], thus requiring a smaller correlator spacing and a higher sampling rate. Longer codes will increase signals' cross-correlation protection and their robustness in weak signal environments. The multiplication of active satellites will increase availability, while integrity should be improved through more detailed navigation messages and deployment of new control stations, as well as new generation satellites with improved on-board clocks. This context calls for implementing new robust acquisition and tracking architectures, in a compact design, that are capable of harvesting all the potential of these new signals. Indeed, considering over 530 civil GNSS RF signal components (namely data and pilot) available worldwide, half of which being visible to any ground-based user, the importance of reducing the total complexity while maximizing global robustness and precision becomes more than desirable.

This paper novelty relies on a GNSS receiver system based on a multiplicity of the proposed universal GNSS acquisition and tracking channel based on the optimal correlator approach (*i.e.*, matched filter ([8] (Chapter 10), whose aspects are further discussed herein:

1. A dual-component (AltBOC-ready) apparatus;
2. An improved Dual Estimator code discriminator;
3. A time-multiplexing code module;
4. A secondary chip wipe-off (for longer coherent integration);
5. A configurable sub-carriers and code clocks combination module derived from a single Numerically Controlled Oscillator (NCO) master clock and
6. A sub-carrier time-multiplexing with weighted sub-carriers combination module.

1.1. Survey of GNSS Signals and Receiver Architectures

This section is split into three: GNSS signals, their modulation and the resulting receiver tracking channels.

1.1.1. GNSS Signal Description

GNSS signals have undergone a noticeable evolution, multiplying constellations and signal definitions using new frequency bands, modulations as well as primary/secondary spreading code types, rates and periods. Global satellite-based navigation signals, with both open and restricted access on all frequency bands, are summarized in Table 1, where modulation families (detailed below) can be described as Binary or Quadrature Phase Shift Keying BPSK (q) or QPSK (q), Binary Offset Carrier BOC (p, q), Composite BOC CBOC $(r,\ p,\ P_r, \pm)$ and Time-Multiplexed BOC TMBOC $(r,\ p,\ w_r)$, where:

f_{ref} is the reference chipping rate, *i.e.*, 1.023 Mchip/s,
f_{c} is the current chipping rate, defined as $q \cdot f_{\text{ref}}$,
f_{s1} is the first sub-carrier rate, defined as $p \cdot f_{\text{ref}}$ and
f_{s2} is the second sub-carrier rate, defined as $r \cdot f_{\text{ref}}$,
P_r is the second sub-carrier power ratio, *i.e.*, 1/11,
w_r is the second sub-carrier weight, in terms of an occurrence ratio, *i.e.*, 4/33.

The last parameter of CBOC refers to the sign of the second sub-carrier compared to that of the first; in CBOC, data and pilot components are in phase opposition. From Table 1, one notices that GLONASS current signals are based on Frequency Division Multiplexing Access (FDMA), while modern ones will rely on Code Division Multiplexing Access (CDMA). New GLONASS and BeiDou signals are yet to be fully publically disclosed to fill out missing details. Also, GPS L2C TMBPSK modulation is based on two alternating 511.5 kchip/s spreading codes, *i.e.*, 20 ms long CM and 1.5 s long CL, resulting in a merged stream of 1.023 Mchip/s.

Table 1. GNSS Signals Survey.

System	# SV	Center Freq. (MHz)	Broadcast BW (MHz)	Signal Component	Modulation Type (f_r = 1023 kHz)	Phase (°)	Gabor (MHz)	Code Length (chip)		Code Period (ms)		MTTA (s)		Symbol Rate (symbol/s)	Data ambiguity	Forward Error Correction	Earth Power (dBW)
								Primary	Secondary	Primary	Secondary	Primary	Secondary				
GPS / WAAS	32/24 + 3/3	L1: 1575.42	24	L1C/A	BPSK(1)	90	2.046	1023	0	1	0	16	0	50	20	none	−158.50
				L1P(Y)	BPSK(10)	0	20.460	6.187E+12	0	6.05E+08	0	3.4E+28	0	50	0	none	−161.50
				L1M	sBOC(10,5)	90	30.690	undisclosed		undisclosed						FEC(½)	−158.00
				L1C-I	sBOC(1,1)	0	4.092	10,230	0	10	0	15634	0	100	1	BCH/LDPC (½)	−163.00
				L1C-Q	TMsBOC(6,1,4/33)	0	14.322	10,230	1800	10	18000	15634	4.427E+05	—	—	—	−158.25
				WAAS-L1	BPSK(1)	90	2.046	1023	0	1	0	16	0	500	2	171o; +133o	−161.00
		L2: 1227.60	24	L2CM	BPSK(½) TMBPSK (½,½)	90	2.046	10,230	0	20	0	62328	0	50	1	171o; +133o	−160.00
				L2CL	BPSK(½)	90		767,250	0	1500	0	2.6E+10	0	—	—	—	
				L2P(Y)	BPSK(10)	0	20.460	6.187E+12	0	6.05E+08	0	3E+28	0	50	0	none	−161.50
				L2M	sBOC(10,5)	90	30.690	undisclosed		undisclosed						FEC(½)	−158.00
		L5: 1176.45	24	L5-I	QPSK(10)	0	20.460	10,230	10	1	10	155	8	100	1	171o; +133o	−157.90
				L5-Q		90	20.460	10,230	20	1	20	155	61	—	—	—	−157.90
				WAAS-L5	BPSK(10)	0	20.460	10,230	0	1	0	155	0	500	1	171o; +133o	−154.00
Galileo / EGNOS	(2+4+2)/30 + 3/3	L1: 1575.42	40.92	E1B	CsBOC(6,1,1/11,+)	0	14.322	4092	0	4	0	1010	0	250	1	171o; −133o	−160.00
				E1C	CsBOC(6,1,1/11,−)	180	14.322	4092	25	4	100	1010	1899	—	—	—	−160.00
				EGNOS	BPSK(1)	90	2.046	1023	0	1	0	16	0	500	2	171o; +133o	−161.00
				E1A	cBOC(15,2.5)		35.805	undisclosed		undisclosed				100			
		E6: 1278.75	40.92	E6A	cBOC(10,5)		30.690	undisclosed		undisclosed				100			
				E6B	BPSK(5)	0	10.230	5115	0	1	0	78	0	1000	1	171o; −133o	−158.00
				E6C	BPSK(5)	180	10.230	5115	100	1	100	78	7596	—	—	—	−158.00
		E5a:1176.45	20.46	E5a-I	QPSK(10)	0	20.460	10,230	20	1	20	155	61	50	1	171o; −133o	−158.00
				E5a-Q		90	20.460	10,230	100	1	100	155	7596	—	—	—	−158.00
		E5: 1191.795	92.07		AltBOC(15,10)	8-PSK	51.150					0	0				−152.00
		E5b:1207.14	20.46	E5b-I	QPSK(10)	0	20.460	10,230	4	1	4	155	0	250	1	171o; −133o	−158.00
				E5b-Q		90	20.460	10,230	100	1	100	155	7596	—	—	—	−158.00
GLONASS / SDCM	28/24 + 2/3	L1g: 1602.00	17.5275	L1OF	BPSK(~½) - FDMA	90	8.335	511	0	1	0	8	0	100	10	none	−161.00
				L1SF	BPSK(~5) - FDMA	0	17.533	undisclosed						50			
		L1: 1575.42		L1OC	BOC(n,n)	0		undisclosed									
				L1SC				undisclosed									
				SDCM				undisclosed									−158.00
		L2g: 1246.00	15.9075	L2OF	BPSK(~½) - FDMA	90	6.710	511	0	1	0	8	0	100	10	none	−167.00
				L2SF	BPSK(~5) - FDMA	0	15.908	undisclosed						250			
		L2: 1227.60		L2OC			13.683	undisclosed									
				L2SC			13.683	undisclosed									
		L3: 1202.025		L3OC-D	QPSK(x)	0	20.460	10,230	5	1	5	155	1	200	1	171o; +133o	
				L3OC-P		90	20.460	10,230	10	1	10	155	8	—		—	
		L3: 1208.088		L3SC								0	0				
		L5: 1176.45		L5OC		0	16.368	undisclosed									

Table 1. *Cont.*

System	# SV	Center Freq. (MHz)	Broadcast BW (MHz)	Signal Component	Modulation Type (f_r = 1023 kHz)	Phase (°)	Gabor (MHz)	Code Length (chip)		Code Period (ms)		MTTA (s)		Symbol Rate (symbol/s)	Data ambiguity	Forward Error Correction	Earth Power (dBW)
								Primary	Secondary	Primary	Secondary	Primary	Secondary				
BeiDou / SNAS	(5/27 + 5/3 + 6/5) + 1/3	B1-1: 1561.098	4.092	B1-I: C/A B1-Q: military	QPSK(2)	0 90	2.046 2.046	2046	20	1 >400	20	31	61	50	1		−163.00
		L1: 1575.42			AltBOC(14,2)		2.046	2046	0	1	0	31	0	500	2		−163.00
		B1-2: 1589.74	4.092	B1-2: military	QPSK(2)	0 90	2.046 2.046	filed at ITU, although nothing is being broadcast									
		E5b:1207.14	20.46	B2-I: C/A B2-Q: military	BPSK(2) BPSK(10)	0	2.046 20.460	2046	20	1 >160	20	31	61	50	1		
		B3: 1268.52	20.46	B3-I: C/A B3-Q: military	QPSK(10)	0 90	20.460 20.460	10,230	20	1 >160	20	155	61	50	1		
		L1: 1575.42		B1-Cd B1-Cp B1d B1p	MBOC(6,1,1/11) sBOC(14,2)		14.322 32.736			OS AS				100 — 100 —		½ ½	
		B2: 1191.795		B2ad B2ap B2bd B2bp	QPSK(10) QPSK(10)	0 90 8-PSK 0 90	20.460 20.460 51.150 20.460 20.460			OS				50 — 100 —		½ ½	
		B3: 1268.52		B3 B3-Ad B3-Ap	QPSK(10) sBOC(15,2.5) sBOC(15,2.5)	0 90	20.460 35.805			AS AS				500 100 —		none ½	

Current signals and those to come have different colors; yellow cells identify memory codes.

The Mean Time To Acquire (MTTA) in Table 1 is computed per the worst case scenario represented by Equation (1) [9]:

$$MTTA = \frac{(2 - P_D)(1 + K \cdot P_{FA})}{2P_D} b \cdot M \cdot T_P \quad (1)$$

where:

P_D is the detection probability (assumed at 0.995)
P_{FA} is the false alarm probability, *i.e.*, a false positive (assumed at 0.001)
K is the false alarm weight (assumed at 2)
b is the number of search cells (combining code with 0.5 chip resolution and ±5 kHz Doppler span)
M is the non-coherent integration count (assumed at 1)
T_P is the pre-integration time (assumed to match primary code period)

In the case of the GPS L1 C/A signal, there could be 2046 code bins and 15 frequency bins, each spaced by 667 Hz assuming 1 ms integration and covering a ±5 kHz Doppler span. This sequential acquisition scheme would result in a total of $b = 30,690$ search cells. In Table 1, MTTA is applied to both primary and secondary spreading codes, although secondary code could be extrapolated from the message time stamp instead of being searched. To sum up the review of GNSS signals, there are 291 civil GNSS RF signal components (*i.e.*, considering both data and pilot components) currently available worldwide: six signal components on 32 GPS satellites + 2 × 24 for GLONASS + 6 × 6 for Galileo + 3 × 5 for BeiDou, as listed in Table 1, half of those could be visible to any ground user. Hence, in order to harvest this signal power to maximize global robustness and precision, reducing receivers' total complexity and reusing as many resources as possible becomes more than desirable. The number of signal components available will increase to more than 530 as the new satellite constellations are deployed, on top of the local and augmentation signals...

1.1.2. GNSS Signals Modulations

One of the most complex modulations involves two sub-carriers—namely SC1 & SC2—in the Multiplexed BOC (MBOC) scheme, which is defined as a spectrum (G) involving BOC $(1,1)$ and BOC $(6,1)$ in a 10 to 1 power ratio:

$$G_{\mathrm{MBOC}}(f) = \frac{10}{11} G_{\mathrm{BOC}(1,1)}(f) + \frac{1}{11} G_{\mathrm{BOC}(6,1)}(f) \quad (2)$$

This power ratio allows for a smaller bandwidth to be processed in low-end receivers, while still achieving lock. MBOC is found in two different implementations. In Galileo, the Composite BOC (CBOC) data and pilot signal components first sub-carriers end up in counter-phase, while their second carriers remain in phase, after being combined $s_{E1} = s_{E1-B} - s_{E1-C}$ [10], with:

$$\begin{aligned} s_{E1-B}(t) &= PC_{E1-B}(t) \cdot d(t) \cdot \mathrm{CBOC}(6,1,1/11,+)(t) \\ s_{E1-C}(t) &= PC_{E1-C}(t) \cdot SC_{E1-C}(t) \cdot \mathrm{CBOC}(6,1,1/11,-)(t) \end{aligned} \quad (3)$$

with the Primary Code (PC), Secondary Code (SC), navigation data (d), and:

$$\mathrm{CBOC}(6,1,1/11,\pm)(t) = \sqrt{\frac{10}{11}}\mathrm{BOC}(1,1)(t) \pm \sqrt{\frac{1}{11}}\mathrm{BOC}(6,1)(t) \quad (4)$$

In GPS, the Time-Multiplexed BOC (TMBOC) only involves the second sub-carrier in the pilot signal component, enabled four times within a 33-chip long pre-determined sequence [11]:

$$\begin{aligned} s_{L1C_D}(t) &= PC_{L1C_D}(t) \cdot d(t) \cdot \mathrm{BOC}(1,1)(t) \\ s_{L1C_P}(t) &= \sqrt{3} PC_{L1C_P}(t) \cdot SC_{L1C_P}(t) \cdot \mathrm{TMBOC}(6,1,4/33)(t) \end{aligned} \quad (5)$$

with:

$$\begin{gathered}\mathrm{TMBOC}\left(6,1,\,4/33\right)(t)=\alpha(t)\cdot\mathrm{BOC}\left(1,1\right)(t)+\beta(t)\cdot\mathrm{BOC}\left(6,1\right)(t)\\ \alpha(t)=\begin{cases}1,\ t\in 29/33\\ 0,\ t\in 4/33\end{cases}\quad and\ \beta(t)=\begin{cases}0,\ t\in 29/33\\ 1,\ t\in 4/33\end{cases}\end{gathered}\tag{6}$$

For all open signals, sub-carriers are in phase with the chip transitions, *i.e.*, sine BOC (sBOC). The only signals using cosine BOC (cBOC), with chip and sub-carriers in quadraphase, are Galileo E1A and E6A, which are respectively regulated and commercial services.

For Galileo E5, the Alternate BOC (AltBOC) modulation offers two QPSK channels symmetrically offset from a common center frequency, resulting in a 51.150 MHz wide receiver reference bandwidth encompassing the 20.460 MHz large main lobe of both open E5-A and Safety of Life (SoL) E5-B signals [10]. Processing this signal as a whole would require an even higher sampling rate (as per Nyquist), especially if secondary lobes are considered. In fact, the combination of these two signals into a single transmission primarily serves the goal of optimizing the usage of the on-board satellite power amplifier through the constant complex power envelope of a PSK-8 signal, yet with improved receiver multipath performances [12]. Anyhow, each signal component requires independent correlators. In the context of this paper, E5A and E5B are processed independently as QPSK (10) signals.

1.1.3. BOC-Ready Tracking Channels

The main complication introduced by the new signals is the ambiguous BOC Auto-Correlation Function (ACF). Indeed, the squared ACF introduces the possibility of tracking any $2n-1$ peaks separated by the sub-carrier half period T_s, with the sub-carrier to chipping rates doubled ratio $n=2\cdot f_s/f_c$. In the simplest case of BOC(1,1), there are two side peaks, whose tracking would induce a Pseudo-Range (PR) error of ~150 m. Hence, BOC ACF ambiguous tracking [13], requires adapted tracking approaches, some of which are categorized in Table 2.

Table 2. BOC Tracking Channel Architectures Classification.

Category	Main Methods	Approach
Narrow Correlators	Double-Delta (DD) [14]; High Resolution Correlator (HRC) [15]; BOC universel [16]	Narrow tracking once aligned with the main peak of the correlation curve. Weak performances in presence of noise and multipath. A complex combination of absolute values of correlators approaches the BPSK triangular ACF shape during initial alignment.
Single Lobe (~BPSK)	Single Side Lobe (SSL) [17]; Dual Sideband (DS) [18]	Independently process main lobe(s), achieving BPSK-like correlation curve.
Extra-Correlators	Bump and Jump (BJ) aka Very Early Very Late (VE-VL) [19]	Extra correlators allow monitoring secondary peaks of the correlation curve. Their location depends on the targeted modulation scheme.
Replica Spreading Code Combination	Time-Multiplexed BOC(6,1) (TM61(a)) [20]; Shaping Correlator Receiver (SCR) [21]; S-Curve Shaping [22]; Code Composite Ranging Waveform (CCRW) [23]; Strobe Correlator [24]; Autocorrelation Side-Peak Cancellation Technique (ASPeCT) [9]	Minimize secondary peaks of the correlation curve by combining different spreading codes into the local replicate signal. Despite good multipath performances, these approaches suffer from higher noise levels as they are not based on the Maximum Likelihood "Matched Filter"-like Correlator, targeting the Cramer-Rao lower bound. Furthermore, S-Curve Shaping would require a minimum sampling frequency reaching 200 MHz to track MBOC signals. ASPeCT only applies to BOC(p,p).
Extra-Loops	Sub Carrier Phase Cancellation (SCPC) [17]; Triple-Loop Dual-Estimator (TLDE) [25]	Tracking of sub-carrier on top of carrier and code, avoiding periodic signal integer uncertainty.
Frequency Response	Channel Transfer Function H(f) [26]; Symmetric Phase-Only Matched Filter (SPOMF) [27]	Frequency-domain analysis is more flexible and precise, no matter what the signal modulation is; at the extra cost (e.g., hardware resources) of direct and inverse Fourier transforms.
Loop filters	A shared Extended Kalman Filter (EKF) is used to compute the channels feedback [28,29]. VDLL could also be considered to distinguish main peak from secondary ones by eliminating solutions with larger positioning residues. EKF can also be used as individual tracking channel loop filter [30]	Vectorial DLL (VDLL) allows for inter-channel assistance, minimizing satellite loss and reacquisition occurrences by replacing independent loop filters by integrated EKF. Was successfully applied to BPSK tracking. Independent Extended Kalman Filtering (EKF) could also be used to compute the loop feedback in every channel. Both approaches could be adapted to BOC.
Time-Domain Analysis	Vision correlator [31]	Extra complex integrator measurements are taken at slightly different time offsets in order to assess the chip transition in the time-domain. This method could be applied to sub-carrier transitions as well.
Signal assistance	Combined Signals [30]	GPS L1 C/A combined with GPS L1C for enhanced tracking

2. Materials and Methods

2.1. Universal GNSS Channel Design Decisions

For a universal channel [32,33] to successfully address any signal particularity identified above, some design decisions had to be made to achieve the lowest possible design complexity. The following paragraphs detail different channel architecture aspects (*cf.* Figure 1), *i.e.*,:

1. IF to Baseband Down-conversion and Carrier (including FDMA) Wipe-off module
2. Sub-carriers and Spreading Codes Wipe-off module
3. Spreading Codes (including Time Multiplexing) Generation module
4. Correlation module
5. Data & Pilot components merging
6. Discriminator and Filters

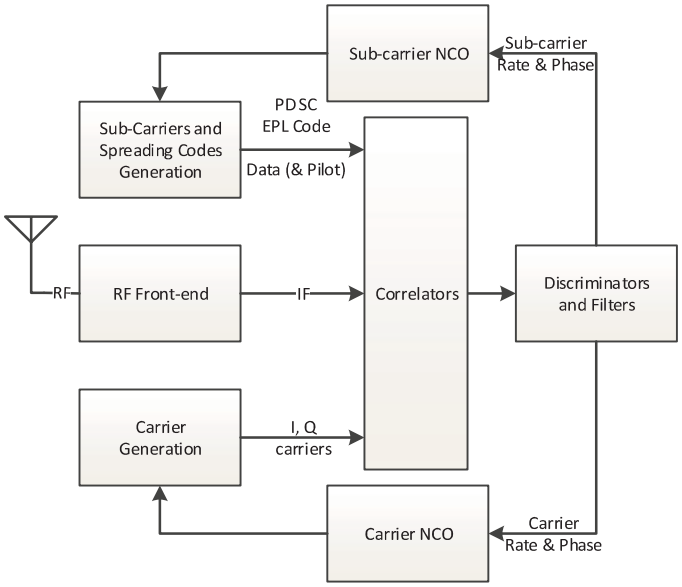

Figure 1. Tracking Channel Simplified Architecture.

An overall resource and power assessment is then presented.

2.1.1. Carrier

Assuming that all RF signals are taken down to a common Intermediate Frequency (IF), it then becomes possible to track any GNSS signal with the proposed universal channel. In order to accommodate most GNSS signals, a 30 MHz processed bandwidth appears to be a good compromise. This imposes a 60 MHz real sampling frequency and a 15 MHz Intermediate Frequency (IF), common to all RF bands. This architecture is thus compliant with all open signals.

A local carrier complex oscillator (namely a pair of sinusoidal 64-point waveforms in phase quadrature and encoded on 4 bits) is used to convert the IF signal down to baseband. Furthermore, in order to preserve a low architecture complexity, a signed multiplication optimization is proposed: Y bits $\times$ Z bits $=$ $(Y + Z - 1)$ bits. This is true only if the minimal twos complement value is never used on both operands, e.g., 0b0000 $\times$ 0b0000 would not be permitted in such 4-bit multiplications.

The flexibility offered by this frequency down-conversion allows simplifying the RF front-end. Indeed, a common RF front-end could be used to manage signals on carriers nearby one another, such as:

- Galileo E5B and Beidou B2-I (and eventually B2b) on 1207.14 MHz, as well as 1202.025 MHz for GLONASS L3 signals.
- Beidou B3 on 1268.52 MHz as well as Galileo (and QZSS) E6 signal on 1278.75 MHz:
    - In order to preserve both signals bandwidth integrity, the RF front-end would take 1273,635 MHz down to IF. Assuming IF = 15 MHz, Beidou B3 would manage 20 MHz for its QPSK (10) signal as well as 10 MHz for the Galileo E6B/C BPSK (5) signals.
    - This simplified approach could only process half of Galileo E6A BOC(10,5) and Beidou B3-Ad/Ap BOC(15,2.5) signals, considering the current 30 MHz bandwidth.
- Beidou B1-1 on 1561.098 and B1-2 on 1589.74 MHz around GPS L1 (and others) on 1575.42 MHz:
    - An alternate approach would be to implement a 14.322 MHz sub-carrier, thus dealing with both Beidou signals as sBOC $(14, 2)$, just as with Galileo E1A cBOC $(15, 2.5)$, but with a slight sensitivity loss caused by superposing these two signals, each having their spreading code providing >20 dB isolation.

More importantly, dealing with the several frequency channels of the GLONASS FDMA scheme requires a Numerically Controlled Oscillator (NCO) frequency span over several MHz, *i.e.*, $[-7,\ 6] \cdot 0.5625 = 7.3125$ MHz for L1OF and equivalently 5.6875 MHz for L2OF:

$$f_{L1OF} = 1602 + 0.5625 \cdot [-7,\ +6]\ \text{MHz}\ f_{L2OF} = 1246 + 0.4375 \cdot [-7,\ +6]\ \text{MHz} \tag{7}$$

This NCO span represents a large increase compared to the traditional ± 10 kHz required for Doppler removal for a high-dynamics receiver.

2.1.2. Sub-Carriers

As seen in Table 1, signal modulations involve up to two sub-carriers combined in different phase relations. In fact, a phase-controlled sub-carriers generation module based on a single NCO makes up a universal channel. This NCO is used to derive up to two slower periodic signals from a third one (*i.e.*, SC2); the slowest signal being used to dictate the chipping rate of the primary spreading code. By doing so, an NCO phase ambiguity issue arose, which was overcome with the introduction of a SC2 period counter used in the navigation solution algorithm.

To properly deal with signals characterized by a quarter of a cycle phase shift between chip transition and carrier rising edge (*i.e.*, cBOC), a minimalistic approach requires a source clock with twice the required rate and a dual-edge register, as depicted in Figure 2. This approach would equally apply to Galileo E1A signal with cBOC $(15, 2.5)$, where a sub-carrier six times that of the spreading code rate, both clock signals being in phase quadrature.

Another requirement brought up by the sub-carriers is their respective weight in time. Indeed, the TMBOC pilot component requires the ability to null (*i.e.*, switch off) sub-carriers in time. To be future-compliant with any periodicity length, applied on any sub-carrier, a single 16 kbit RAM block is used, achieving a maximum periodicity of 512 addresses $\times$ 32 bits/(2 components $\times$ 2 sub-carriers) = 4096. To use it efficiently, the RAM block is configured as a dual port RAM, written from the 32-bit data bus until the RAM is filled up, but only four bits are read per address to accommodate data and pilot components at once.

Furthermore, CBOC and TMBOC impose different sub-carrier amplitudes. Pursuing a matched filter approach, the replica should mimic the targeted signal as much as possible. The resulting weighing factors α for sub-carrier SC1 and β for SC2 must carry the following values: $\alpha \in [1,\ 0.95,\ 0]$ and $\beta \in [1,\ \pm 0.30,\ 0]$. The signed resolution requires a total of 6 signed bits to induce a representative ratio between one another: $\frac{\beta}{\alpha} = \frac{0.30}{0.95} = \frac{6/32}{19/32}$ with $\alpha + \beta = 25/32$, introducing a potential scaling loss. These 6-bit coefficients may be updated at every chip in this simple TMBOC implementation, as depicted in Figure 3. For example, during the sequential acquisition process, four steps are followed:

1. For each component, both 1-bit square sub-carriers are delayed to obtain Early (E), Prompt (P) and Late (L) replicas; the correlator spacing is set to $\pm T_s/4$ with the fastest sub-carrier period T_s.
2. Prompt and Differential (D = E − L) are obtained on 2 bits for each sub-carrier.
3. P & D replicas are scaled to their pre-defined constant weight through a mapping function or Look-Up Table (LUT).
4. For each component, the two scaled sub-carriers are summed.

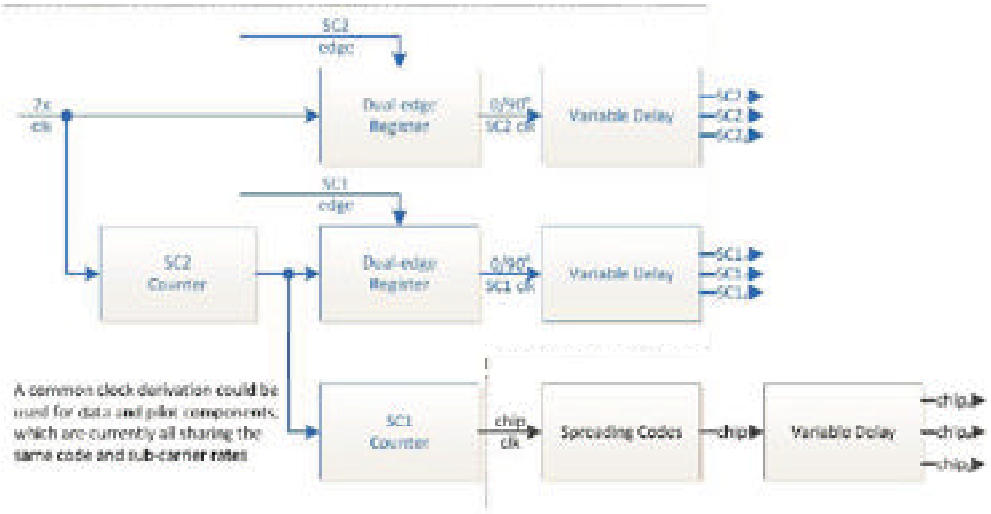

Figure 2. Sub-Carriers and Spreading Codes Module (BPSK *vs.* MBOC).

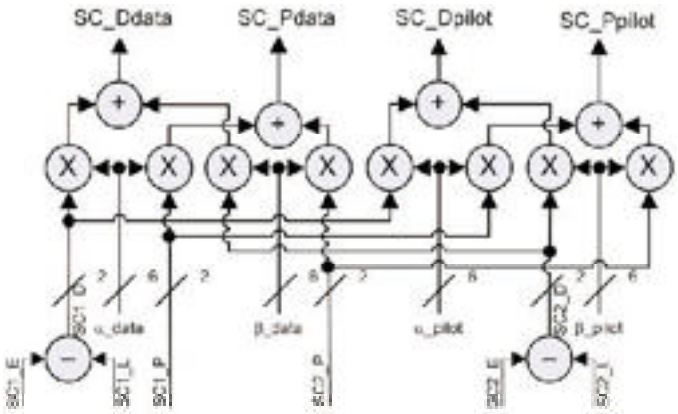

Figure 3. MBOC Sub-Carriers Multi-Bit Simplification and Combination of both Data and Pilot Components (Differential = Early − Late; Prompt)

2.1.3. Spreading Codes

As seen in Table 1, codes have different lengths and generation methods. Since all signals have their own primary (and secondary) code generation method, a universal channel would need to support them all. Linear Feedback Shift Register (LFSR) logic is definitely the best approach in the case of a dedicated signal channel. However, duplicating such resources customized for every signal becomes a burden: one channel can only track one signal at a time, resulting in many idle resources. Furthermore, considering this highly dynamic field, one may want to plan ahead. Indeed, a pre-computed memory code approach not only applies to all currently defined signals, but also allows for an easy, over-the-air, update link whenever a new Signal In Space (SIS) Interface Specification (IS) is released.

In recent GNSS signals, longer code periods also reduce the transit time integer ambiguity; the transit time for GPS satellites on L1 varies from about 66 ms (at zenith) to 80 ms (at horizon) [34]. Hence, the longer the code duration, the smaller the resulting ambiguity becomes. To further improve on this, secondary codes are laid over the primary ones, artificially making them longer (while improving the inter-correlation protection). To account for the secondary code, whose length may vary from 4 to 1800 chips, the memory codes approach is once again adopted. Another side effect of these secondary codes is the basic integration time period: they constrain the coherent integration time to the primary code period, which in turn, limits the correlation gain achieved during acquisition (at early acquisition stages, while the secondary code is still unknown).

The only civil code for which the memory code approach is not suited is GPS L2CL. Indeed, CL is 767,250-chip long, which would impose a much too high upper bound on the size of the memory dedicated to each channel, especially if we consider two such memory blocks (one for each component). A more realistic memory block size is 16 kbit (a standard size for the Virtex4 [35], on which the proposed universal channel is implemented), which is greater than 10,230—the second longest code, found on the L5, E5 and B3 signals. Hence, this requirement imposes two 16 kbit RAM blocks and a 27-register long LFSR as the minimum resources for each universal channel.

More importantly, the GPS L2C signal introduces an additional particularity, *i.e.*, the time multiplexing of two spreading codes of different lengths. The resulting merged code has twice the chipping rate compared to that of their individual sequences L2CM and L2CL, as seen in Figure 4.

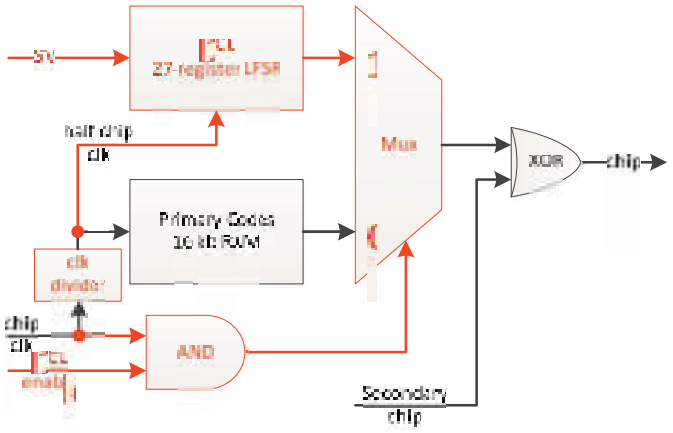

Figure 4. Spreading Codes Module (BPSK *vs.* TMBPSK Overhead).

The 1.5 s long L2CL code cannot be acquired directly at cold start. Nevertheless, its chip offset can be predicted from the satellite clock timestamp decoded through L2CM or inferred from another signal from the same satellite. A full (L2CM & L2CL) integration may then occur, harvesting twice as much signal power compared to only L2CM during the acquisition phase.

2.1.4. Correlation

In order to provide the feedback to the carrier and code NCOs, several feedback signals are required to compute the error to be compensated for. For the code, a Non-coherent Early Minus Late (NEML) discriminator requires three correlators, *i.e.*, E, P and L code replicas on both the phase (I) and quadrature (Q) branches as illustrated in Figure 5. With the current implementation based on 4 16-bit addressable registers (as opposed to dedicated RAM blocks with improved delay resolution), the different code replica offsets may belong to $P \pm 32/f_S$ samples, thus achieving a correlator spacing $\Delta = \pm\delta$ slightly larger than ±½ chip for a 1.023 Mchip/s spreading code. The resulting 6 correlators are deployed for both components of a signal.

To reduce the correlator number, the Delay Lock Loop (DLL) discriminator could only involve in-phase (carrier and eventually sub-carrier phases) measurements, thus requiring a lock on the Phase Lock Loop (PLL) (and eventually Sub-carrier Lock Loop or SLL). Such a coherent approach may not be as robust as its non-coherent equivalent [36].

Hodgart, Blunt and Unwin [37] specify that an SLL provides more precise (due to higher rate), but ambiguous (periodic clock signal) measurements compared to the DLL based on the primary code Pseudo-Random Noise (PRN). Both these estimates may be combined as:

$$\hat{\tau}^{+} = \hat{\tau}^{*} + round\left(\frac{\hat{\tau} - \hat{\tau}^{*}}{T_s}\right) T_s \tag{8}$$

where:

$\hat{\tau}^{+}$ is the combined delay estimate;
$\hat{\tau}^{*}$ is the sub-carrier delay estimate;
$\hat{\tau}$ is the code delay estimate;
T_s is the sub-carrier half-period.

To keep the correlator count as low as possible, the sub-carriers are weighted (α, β) and summed, *i.e.*, SC2 + SC1, prior correlation, avoiding an extra loop. Also, only Prompt (P) and Differential (D = E − L) instances are used to implement the NEML sub-carriers discriminator. Note that combining the sub-carriers also simplifies the discriminator, which then becomes identical as the Dual Estimator (DE), rather than the Triple Estimator (TE) extension for MBOC [25], with the same performances.

Having higher chipping rates requires greater accumulation registers. Multiplication and accumulation are performed through a DSP48 slices available in the Xilinx XC4VSX55-10FF1148 Field Programmable Gate Array (FPGA). Hence, the number of bits for these operations is not critical, as long as it remains below $48 - \log_2(60,000) \approx 32$, assuming the integration of 60,000 samples in 1 ms.

Coherent integration provides better post-correlation Signal to Noise Ratios (SNR) than non-coherent ones, where navigation bit (or secondary chip) removal introduces squaring losses [38]. The navigation data period limits the coherent integration time, thus imposing a lower limit on the sensitivity of an unaided, stand-alone receiver.

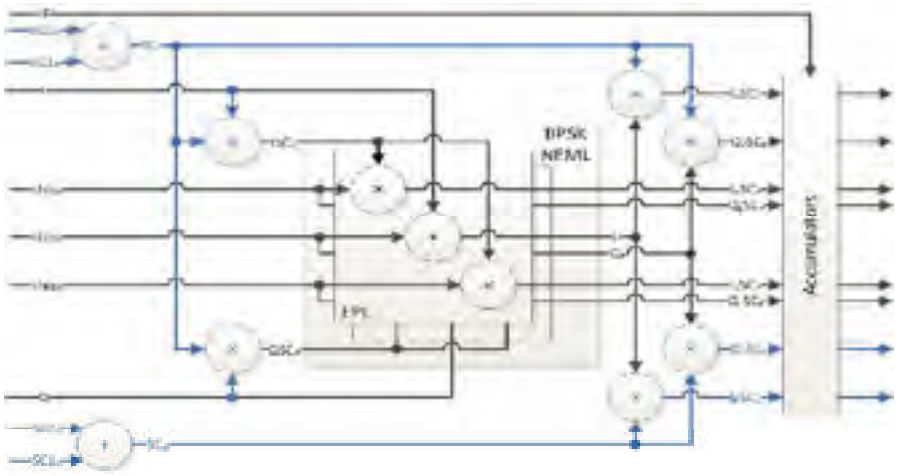

Figure 5. Single-Component Products and Correlation (BPSK *vs.* MBOC Overhead).

2.1.5. Data & Pilot Components Merging

Most new and modernized signals have two components combined in (counter-) phase or in phase quadrature, such as Galileo E1 B&C and GPS L5 I&Q, respectively. In order to deal with them, a

special design choice has to be made: either (1) each component is dealt with in a separate channel, whose correlation products are properly dealt with through a common (or distinct) discriminator; or (2) both components are integrated into one dual-component universal channel. Although more flexible, the first case would not allow for the HW reduction of the following shared resources (in the authors' opinion, when applied to the proposed architecture):

1. Memory codes address and control logic.
2. Carrier and sub-carrier NCOs direct and derived clock signals.
3. Sub-Carrier generation of Prompt (P) and Differential (D) shared by both signal components as the data and pilot chipping rates are always equal in the publically disclosed signals.
4. Sine and cosine LUTs and carrier multipliers leading to the I and Q branches.
5. 27-stage LFSR L2CL code generation implemented only once per dual component channel (*i.e.*, implementing more than 32 universal channels would waste even more resources as there should not be more than 32 L2CL codes being broadcast by the current GPS constellation).

Thus, several architectures are possible, depending on the receiver performance *vs.* cost desired ratio. Dual-component channels allow maximizing the harvested signal power, whereas single-component architectures only allow one of the following:

- Acquire and track the data component only, ignoring the pilot component available power.
- Acquire pilot component with a longer integration time for greater sensitivity and then transfer to data component tracking to extract the navigation message.
- Acquire and track both pilot and data components in independent channels.

With the dual-component channel resources available, a faster sequential acquisition also becomes possible by splitting the search space into two sets of chip offsets:

1. Dual-code delay search makes primary code acquisition two times faster and;
2. Once synchronized onto the primary code, a dual secondary chip estimation (*i.e.*, either the secondary chip changes or not) allows for an integration time over twice the primary code period by using the best of these two integration outputs.

In order to minimize power consumption in mobile devices, the pilot-related components may become idle during single-component signal tracking.

2.1.6. Discriminator and Filter

In a multi-signal receiver, the phase relationship from one signal to another may not be cancelled out as part of a common timing error and must thus be specifically accounted for. Similarly, dual-component signals are bound by their phase relationship. With a standard definition where the quadra-phase component leads the in-phase one, we have:

$$s = \sin(x) + j \cdot \cos(x) \tag{9}$$

That is to say, an in-phase (e.g., sin) signal (such as GPS L1CI) may use the I and Q correlator values, while a signal in phase quadrature (e.g., cos) with its RF carrier (such as GPS L1 C/A) should use $-Q$ and I. In the current implementation, the discriminators are programmed into the embedded MicroBlaze controller, thus allowing for great flexibility. Basically, any coherent and/or non-coherent discriminator could be used based on the signal characteristics; this is simpler than generating sinusoidal waveforms with different phases.

More precisely, considering the infinite bandwidth signal auto-correlation function, Figure 6 shows that the BOC main peak has a slope of $\pm 1.5n$ and a correlation main peak width of $\pm\frac{1}{n}$ chip, with the BOC modulation ratio $n = 2 \cdot \frac{f_s}{f_c} = 2 \cdot \frac{p}{q}$. However, the squaring involved in non-coherent

correlation steepens the peak slopes: which can be approximated by $\pm 2n$ between the correlation peak and the zero-amplitude level, separated by approximately $\pm\frac{1}{2n}$ chip. The coherent correlator spacing should not extend beyond $\pm\frac{1}{n}$ chip, above which an inversion of the EML discriminator S-curve in Figure 7 could compromise the DLL behavior (*i.e.*, it would amplify the error) [39]. Each one of the $2\,(n-1)$ side peaks in the squared BOC correlation function leads to a potential false-lock (*i.e.*, a biased discriminator output) as a result of as many side S-curves.

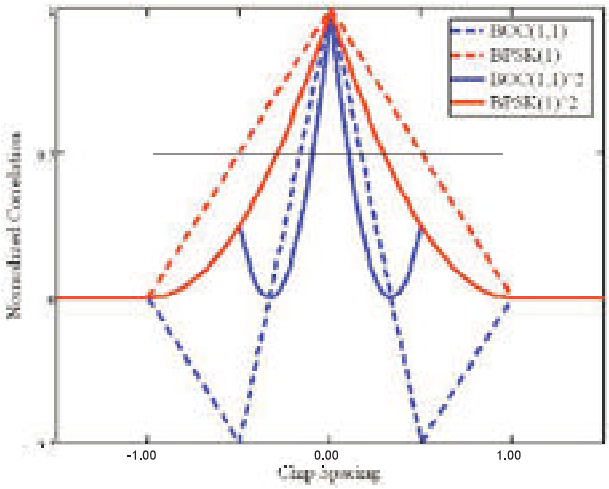

Figure 6. Infinite Bandwidth BPSK (1) and BOC(1,1) — n = 2 — Coherent and Non-Coherent Normalized Correlation Functions.

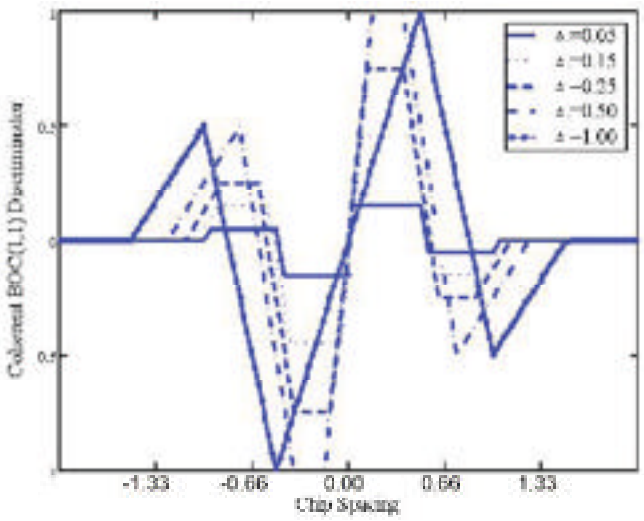

Figure 7. Effect of Correlator Spacing (■ (chip)) on a BOC(1,1) Coherent EML Discriminator (assuming an infinite front-end bandwidth).

Also, a rule of thumb imposes, neglecting dynamic stress error ([8] (Chapter 5):

$$3 \cdot \sigma_{\tau_{EMLP}} < \delta \tag{10}$$

The normalized correlation function $R\,(\tau \pm \delta)$ is estimated by its main peak positive and negative slopes: $\{1 + m\,(\tau - \delta)\}$ and $\{1 - m\,(\tau - \delta)\}$ with EML correlators spaced by $\pm\delta$ chip and a chip code delay error $|\tau| < \frac{1}{2n} - \delta$. The EML tracking architectures for BOC, should offer a code tracking improvement of m over BPSK.

In non-coherent discriminators, C/N_0 squaring losses are due to doubled random noise, while the ± 1 data is wiped off. Non-coherent processing would typically be 3 dB less sensitive than coherent processing for a given duration, although it allows for much longer integration periods, thus achieving a better overall sensitivity. This squaring loss was isolated in square brackets in the code noise jitter equations below. Hence, in non-coherent discriminators, the associated code noise may have a larger variance while preserving the same null mean. It is well known that code phase jitter performances depend on the slope of the discriminator curve (*i.e.*, better performances for steeper slopes). In fact, the code phase 1 $-\sigma$ error (m) derived from the non-coherent Early Minus Late Power (EMLP) code discriminator closed loop noise variance (squared chip periods) are defined as (extended from [12,40] to BOC derived modulations):

$$\sigma_\tau \cong c \cdot T_c \cdot \sqrt{\sigma^2_{\tau_{EMLP}}} \tag{11}$$

$$\sigma^2_{\tau_{EMLP}} \cong \begin{cases} \frac{B_L(1-0.5B_L T_P)}{2\cdot\frac{C}{N_0}} \cdot \left[1 + \frac{4}{\frac{C}{N_0}\cdot T_P\cdot(2-m\cdot\Delta)}\right] \cdot \left\{\frac{\Delta}{m}\right\}, & \pi \leqslant \Delta \cdot b \\ \frac{B_L(1-0.5B_L T_P)}{2\cdot\frac{C}{N_0}} \cdot \left[1 + \frac{4}{\frac{C}{N_0}\cdot T_P\cdot(2-m\cdot\Delta)}\right] \cdot \left\{\frac{1}{b} + \frac{b}{\pi-1}\cdot\left(\frac{\Delta}{m}-\frac{1}{b}\right)^2\right\}, & 1 < \Delta\cdot b < \pi \\ \frac{B_L(1-0.5B_L T_P)}{2\cdot\frac{C}{N_0}} \cdot \left[1 + \frac{2}{\frac{C}{N_0}\cdot T_P}\right] \cdot \left\{\frac{1}{b}\right\}, & \Delta\cdot b \leqslant 1 \end{cases} \tag{12}$$

where:

- c is the speed of light (m/s);
- T_c is the chip period, the inverse of the chipping rate f_c;
- B_L is the unilateral noise equivalent bandwidth of the code tracking loop, a.k.a. one-sided equivalent rectangular bandwidth, with the time frame of interest $\epsilon\ [1/B_L, T_{obs}]$;
- T_P is the pre-integration time (s);
- τ is the signal *vs.* replica misalignment (chip);
- Δ is the early-late correlator spacing (chip), *i.e*, $2\cdot\delta$;
- δ is the early to prompt and prompt to late correlator spacing (chip);
- $\frac{C}{N_0}$ is the Carrier power to Noise density ratio (dB-Hz);
- m is the slope of the correlation function;
- b is the normalized receiver front-end complex bandwidth $(\beta_r \cdot T_c/n)$;
- β_r is the ideal front-end complex bandwidth (with a brick-wall filter (Hz)).

In Equation (12), the term in square brackets reflects the squaring losses attributed to the non-coherent discriminator computations, while the term in braces results from approximations depending on the value of $\Delta\cdot\ b$. Given a fix front-end bandwidth and an equivalent chip spacing during tracking, the approximation mainly involves the signal modulation represented by T_c/n. The Cramer-Rao Lower band is reported by Betz *et al.* [40] to be:

$$\sigma^2_{\tau_{LB}} \cong \begin{cases} \frac{B_L(1-0.5B_L T_P)}{2\frac{C}{N_0}b^2}, b \leqslant 1 \\ \frac{B_L(1-0.5B_L T_P)}{2\frac{C}{N_0}b}, b > 1 \end{cases} \tag{13}$$

It thus becomes interesting to determine what DLL noise variance can be expected for each GNSS signal when tracked with the proposed channel. Analysis in [40] reports that for limited front-end bandwidths, the discriminator gain diminishes as the early-late correlator spacing Δ decreases, while increasing the loop bandwidth and thus the loop variance. Three discriminator regions are identified as: Spacing-Limited, Transition and Bandwidth-Limited, in accordance with Equation (12). Looking at MBOC, while assuming $\beta_r = 22.3$ MHz and $T_c/n = 1/\left(12\cdot 1.023\times 10^6\right)$, $b \approx\ 2$ for the BOC(6,1) signal component, which rapidly falls under the Bandwidth-Limited during tracking area with $\Delta \leqslant 0.5$ chip. One should bear in mind that the relative power ratio of BOC(6,1) is one tenth that of BOC(1,1), for

which $b \approx 12$, well within the Spacing-Limiting function. Looking at other GNSS signals, it appears that in the presented configuration, b ranges from 2 to 47, as depicted in Figure 8. For signals where b is high, it still is beneficial to reduce δ, also mitigating multipath errors. Nevertheless, unless dedicated RAM blocks are available for all the code phases used, a 60 MHz sampling frequency poses a 1 sample limit on δ based on delayed code phases based on the shift registers approach described above, the impact of which will vary with the GNSS signal chipping rates.

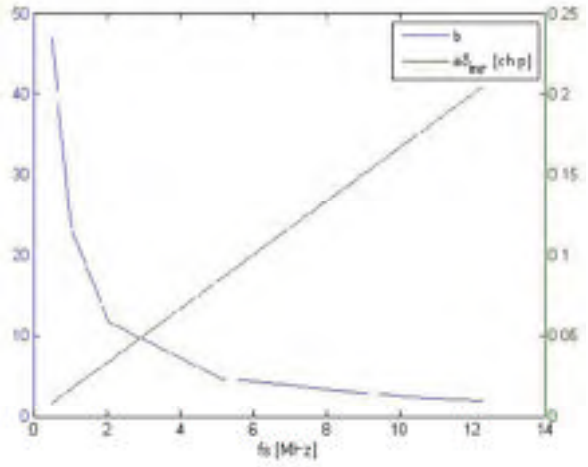

Figure 8. b and δ_{min} *vs.* $1/T_s$ with a 22.3 MHz Front-end Bandwidth at 60 MHz.

2.1.7. Power Consumption and Resource Usage

Table 3 summarizes both the power consumption, as obtained with the Xilinx ISE XPower software, and the FPGA resource usage for different tracking channel complexities, leading to the proposed universal channel. The power consumption percentages presented herein are taken relatively to the "BPSK with FDMA" reference implementation, assessing the overhead associated with the implementations derived with added feature sets.

Table 3. Universal Channel Resources for Different Feature Sets.

Resources in xc4vsx55-10ff1148	Available	BPSK w/FDMA		L2C		BOC		Single MBOC		Dual MBOC	
Dynamic Power (mW)		25.1	100%	25.1	100%	29.6	118%	33.4	133%	41.8	166%
Quiescent Power (mW)		860	100%	860	100%	860	100%	861	100%	861	100%
Total Power (mW)		885	100%	885	100%	890	101%	894	101%	903	102%
Slices	24576	651	2.6%	765	3.1%	943	3.8%	1018	4.1%	1410	5.7%
Slice Flip Flops	49152	775	1.6%	918	1.9%	1118	2.3%	1186	2.4%	1476	3.0%
4 input LUTs	49152	908	1.8%	1127	2.3%	1456	3.0%	1554	3.2%	2123	4.3%
as logic		894		1113		1436		1528		2091	
as shift registers		14		14		20		26		32	
FIFO16/RAMB16s	320	2	0.6%	2	0.6%	2	0.6%	3	0.9%	4	1.3%
DSP48s	512	11	2.1%	11	2.1%	17	3.3%	17	3.3%	29	5.7%
Max. number of single channels			37		32		26		24		17
Max. number of dual channels			18		16		13		12		17

Legend: Dynamic Power identifies 66% power consumption increase of dual MBOC compared to BPSK feature set. Each Feature Set column and Max. number of channels row are color scaled to highlight best to worst.

It can be seen that the quiescent power is relatively constant across all implementations, and may be attributed to the chip itself, leaving the dynamic power as a more meaningful comparison metric. The single-component MBOC implementation consumes 33% more power, while the dual-component (data and pilot) requires twice as much, *i.e.*, 66% increase compared to the reference BPSK implementation.

For each implementation, the absolute number of resources and associated percentage (*vs.* available) are presented. As a result, the proposed optimizations led to a dual-component MBOC universal channel of complexity comparable to that of two traditional BPSK reference channels,

but with a lot more flexibility. For flexibility and maintainability, the universal channel has been implemented with VHDL configurations that can easy be changed to enable or not several feature sets.

2.2. Universal GNSS Channel Validation

The resulting architecture of the proposed GNSS Universal Channel is presented in Figure 9, where different colors help highlight added feature sets:

- red dotted and dashed lines for L2C TMBPSK of a L2CM memory code with a locally generated L2CL code,
- blue dashed lines for MBOC sub-carriers replicas generation and feedback,
- green dotted lines for dual-component overhead (extra correlators and sub-carriers combining not shown),
- purple solid lines for the optional Variable Spacing Correlator (VSC) used to plot Auto-Correlation Function (ACF) plots.

The following sections present the different test scenarios conducted to validate the proposed architecture in terms of constellations and signals on different frequency bands, with different spreading codes and modulations. The reader should be advised that this paper focuses on available civil signals, although its architecture also applies to restricted access signals.

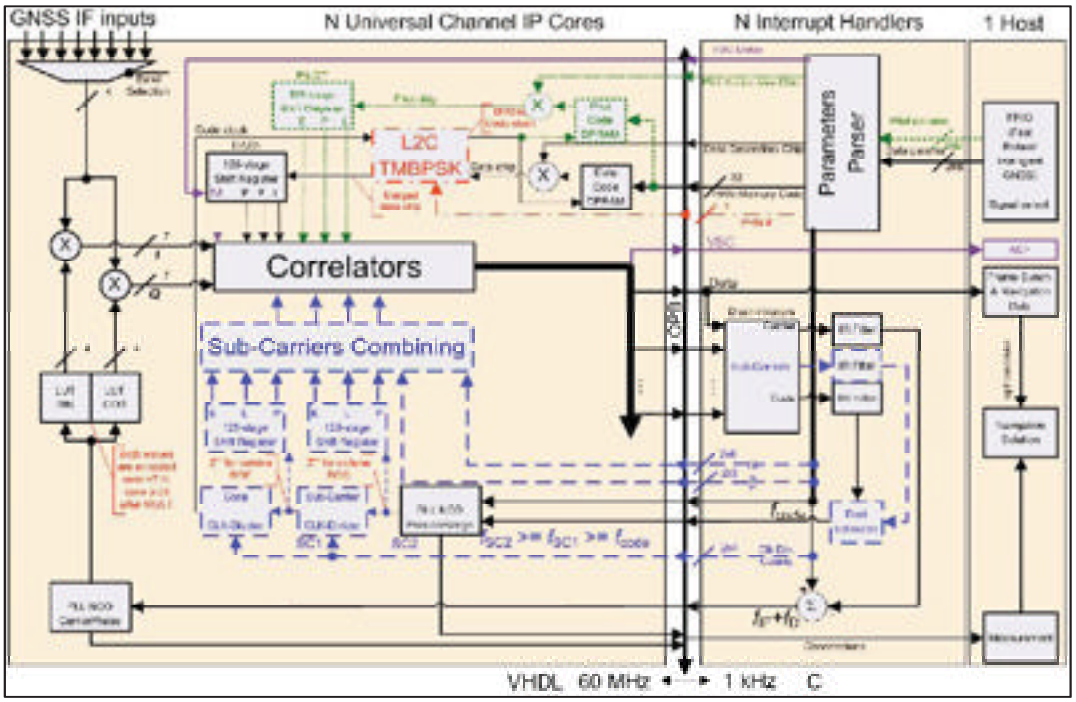

Figure 9. Proposed Universal Channel High Level Architecture.

2.2.1. Constellation Compatibility

As summarized in Table 1, the four GNSS constellations provide similar (for GNSS compatibility), yet distinctive (for GNSS interoperability) modulation characteristics. On top of that, most signals have their own navigation message definition, including preamble synchronization, parity checking, framing, interleaving and encoding, all of which are defined in their respective Interface Control Documents (ICD), or Interface Specification (IS) [10,11,41–44]. All four constellations have their own geodetic and timing systems, but provide (now or in a near future) information to relate with other GNSS. Such navigation message data fusion into a common solution add to the complexity of a

universal receiver is outside the scope of this paper, rather focused on signal processing. In order to demonstrate the proposed universal channel compatibility with all constellations, at least one signal of each is acquired and tracked.

2.2.2. Frequency Bands Compatibility

Although this is not a feature related to the universal channel per se, being able to acquire and track signals on all bands has a net advantage in terms of both frequency diversity for improved ionosphere error correction in an autonomous receiver, as well as enhanced resistance to interference. In the current implementation, a super-heterodyne RF front-end approach is used, where a configurable Local Oscillator (LO) takes the Radio-Frequency (RF) signal down to 70 MHz, which is then processed by a 24 MHz wide band-pass filter and down-converted to IF with a common 55 MHz LO. All LOs and clock are synchronized through an external 10 MHz reference clock.

2.2.3. Spreading Code Schemes Compatibility

Spreading codes are probably the greatest source of variation among all signals. Indeed, different types are currently broadcast: Gold, Weil, Maximal Length, short cycled linear patterns, *etc.* Rather than deploying dedicated logic to support all signals, a universal memory code approach is used. The remaining signal-specific configuration parameters are the code length and its chipping rate; the only exception being the GPS L2CL code generated with LFSR logic.

2.2.4. Modulations Compatibility

For compatibility sake, GNSS signals are based on a few modulation types, all derived from PSK and BOC.

2.2.5. GNSS Test Scenarios

To cover all the above signal particularities and to demonstrate the proposed universal channel, the resulting test scenarios are summarized in Table 4.

Table 4. Proposed Universal Channel Test Scenarios.

	GNSS	RF (MHz)	Signal	Primary Code	Modulation	$\pm\delta$ (Chip)	Particularity
1	GPS	1575.42	L1C	10 ms; 10,230 chips	I: sBOC(1,1); Q: TM-sBOC (6, 1, 4/33)	0.48→0.05; 0.48→0.05	L1 band; GPS; MBOC
2	GPS	1227.60	L2C	L2CM: 20 ms; 10,230 chips; L2CL: 1.5 s; 767,250 chips	TMBPSK (½, ½, ½)	0.24→0.05; off→same as L2CM	L2 band; LFSR logic; TMBPSK
3	GPS	1176.45	L5	1 ms; 10,230 chips	QPSK (10)	0.50→0.17; 0.50→0.17	L5 band; QPSK; Code rate
4	Galileo	1575.42	E1 B&C	4 ms; 4092 chips	CsBOC (6, 1, 1/11, ±)	0.48→0.05; 0.48→0.05	Galileo; MBOC; Code period
5	GLONASS	1602.00	L1OF	1 ms; 511 chips	BPSK(~½)	0.26→0.05	Δ RF in L1; GLONASS; FDMA
6	BeiDou	1561.098	B1-I	1 ms; 2046 chips	BPSK(2)	0.48→0.03	Δ RF in L1; BeiDou; Code length

One should bear in mind that GPS L2CM is first acquired without L2CL. Because of their continuous time multiplexing, the L2CM spreading code (*i.e.*, transmitted at 511.5 kchip/s) correlator spacing is limited to $\pm$0.24 chip in order to avoid being polluted by L2CL. Also, with GLONASS being transmitted at 511 kchip/s, the 60 Msample/s channel design does not allow for a correlator spacing greater than $\pm$31 samples, *i.e.*, $\pm$0.26 chip. On the other hand, GPS L5 at 10.23 Mchip/s suffers from the opposite problem: the channel sampling rate cannot achieve better than $\pm$1 sample, *i.e.*, $\pm$0.17 chip.

Unfortunately, cBOC modulation could not be formally tested without the publically undisclosed Galileo E1A and E6 spreading codes. The same applies to modernized signals that are not yet available in space, such as GPS L1C TMBOC. The test scenarios are further described in the following paragraphs.

Galileo E1 B&C

CBOC is an implementation of the MBOC spectrum, involving the two ($6\times$ and $1\times$) sub-carriers as in GPS L1Cp, but with different, yet constant amplitudes. The current implementation being based on integrations over multiples of 1 ms, a total of four partial integrations are accumulated (coherently or not) to match the full 4 ms long primary spreading code before proceeding to the next cell of the acquisition span, encompassing 4092 chips and 16 Doppler 667 Hz bins.

During acquisition, only the BOC(1,1) sub-carrier is used, with a ± 28 samples correlator spacing. This early simplification can be used since the second sub-carrier only bears a tenth of the signal power, which can be neglected. Once synchronized with a BOC(1,1) modulation, the full CBOC replica signal may be generated locally with a reduced correlator spacing of ± 3 samples.

The 12-bit un-encoded preamble may be used to synchronize onto the message frame of the data component. On the other hand, the pilot component bears a 25-bit secondary code.

GPS L1C

GPS L1C modernized signal involves BOC on the data component and TMBOC on the pilot. Although BOC(1,1) provides a similar effect than the Manchester code, TMBOC requires further thoughts. In the specific case of GPS L1Cp, BOC(1,1) and BOC(6,1) are alternatively enabled over a pre-determined 33-chip long sequence; 33 being an integer factor of the 10,230 chip long primary code length. Considering a dual-component channel (processing a total of four sub-carriers), at most 4096 chips can be saved in a 16 kbit RAM. This is insufficient to match the longest primary codes. Hence, a shorten pattern is repeatedly applied based on lower bits of the primary chip address bus, *i.e.*, modulo the shorter length. This memory is thus written via a 32-bit data bus, but read four bits at a time. A minimal set is pre-computed prior being repeated to fill out the RAM for future compliance (with the modulo operator %):

$$\frac{33 \text{ chips } \times 4 \text{ sub} - \text{carriers} \times 8 \text{ repeats}}{32 \text{ bits}} = 33 \text{ memory addresses of pre} - \text{computed pattern} \quad (14)$$

$$\text{addr}_{\text{TMBOC}} = \text{addr}_{\text{primary code}} \% 33 \quad (15)$$

The resulting enable bits are applied at step 3 of the acquisition process, defined in Section 2.1.2. Other signals are always enabled; the memory being filled with '1'.

In terms of the navigation message, CNAV-2 [11] requires a different approach than for CNAV used in both GPS L2C and L5. In fact, synchronization can be achieved on the Bose, Chaudhuri, and Hocquenghem (BCH) encoded 52-symbol Time of Interval (TOI), provided the receiver knows what to expect for the next frame. This prerequisite knowledge can be extrapolated from other signals tracked from the same broadcasted satellite. This approach is preferred over looking for "non-variable" data from sub-frame 2 that is both encoded with Low Density Parity Check (LDPC), and interleaved with sub-frame 3 using a 38 rows and 46 columns matrix.

Since GPS block III satellites (*i.e.*, the first intended to broadcast the modernized GPS L1C signal) scheduled for 2014 [45] have not been launched yet, chronograms were used to show sub-carrier weights in time for the pilot component.

GPS L2C

In the case of GPS L2C, the 10,230 chip-long L2CM code is to be generated in (nominally) 20 ms, *i.e.*, 511.5 chips per ms. To avoid partial chip every other ms, a 2 ms coherent integration approach is used. During acquisition (solely based on L2CM), 10 such 1023 chip long partial correlations are

required to parse the full L2CM code. This acquisition is performed with a correlator spacing of ±28 samples (based on 60 Msample/s), avoiding any effect from the L2CL spreading code.

The resulting search span, involving 20 ms iterations being repeated over the 10,230 different chip alignments and the 31 Doppler bins (each separated by $2/3 \times Tc = 333$ Hz), could reach up to 6342.6 s, *i.e.*, almost 2 h. To avoid this unacceptable worst case unaided sequential acquisition time, the satellite L1 C/A signal information can be extrapolated, provided its prior acquisition (the navigation bit transition being aligned with the L2CM code start), leading to the following set of Equations:

$$\text{Doppler}_{\text{L2C}} = \frac{\text{L2}}{\text{L1}} \cdot \text{Doppler}_{\text{L1 C/A}} \tag{16}$$

$$\left\lfloor \frac{c_{\text{L1 C/A}}}{2} \right\rfloor = c_{\text{L1CM}} \% 1 \text{ ms} \tag{17}$$

$$c_{\text{L2CM}} = c_{\text{L2CL}} \% \text{ 20 ms} \tag{18}$$

$$c_{\text{L1 C/A}} = c_{\text{L2CM}} = 0 \text{ whenever a L1 C/A navigation bit transition occurs} \tag{19}$$

$$c_{\text{L1 C/A}} = c_{\text{L2CM}} = c_{\text{L2CL}} = 0 \text{ whenever a L1 C/A or L2C navigation frame starts} \tag{20}$$

In fact, the universal channels are synchronized with a global 1 ms pulse, allowing for a triggering mechanism to initialize the code generation at any given chip, at a given time stamp. Equation (20) is a simplification as the 1.5 s L2CL code period starts more often than at the 6 s NAV or 12 s CNAV frames.

The CNAV navigation symbols being transmitted at 50 symbol/s, a full L2CM period must be accumulated to obtain one symbol. In order to synchronize onto the frame and to overcome its Forward Error Correction (FEC) encoding with a ½ ratio, a pattern composed of the common 8-bit preamble followed by the satellite-specific 6-bit PRN is used: Of the resulting 28 encoded symbols, the last 16 are not affected by the unknown data from the previously broadcasted frame [44]. These are then used to locate the beginning of a frame at an offset of 12 symbols. Once, the navigation data is obtained, the L2CL offset can be assessed prior to merging it with the L2CM stream, achieving a 3 dB gain with a TMBPSK match filter approach. This multiplexing requires a clock with twice the rate, *i.e.*, 1.023 Mchip/s, which is then divided down to 511.5 kchip/s for the codes generation. The same 2 ms integration time is preserved in order to keep integrating over an integer number of chips for each of L2CM and L2CL codes.

GPS L5

GPS L5 shares the same CNAV navigation data than L2C, although it is broadcasted twice as fast, allowing for the same frame synchronization scheme to be applied [41]. GPS L5 transmits 10,230 chips every 1 ms period; the chipping rate must be 10 times faster than for GPS L1 C/A, *i.e.*, 10.23 Mchip/s. Considering a 60 MHz sampling frequency, the acquisition is performed with a ±3 samples correlator spacing.

GLONASS L1OF

The RF front-end must support the 1602 MHz frequency, while the IF to baseband frequency down-conversion stage must also support the several FDMA channels, allowing them to be seamlessly tracked, independently from their different frequency offset. In fact, this frequency offset is pre-determined and associated with each PRN, relieving the universal channel from this signal type management.

Because of HW design limitations, a correlator spacing of ±31 samples is used during acquisition, which roughly corresponds to ±¼ chip. In cold acquisition, because two satellites share the same RF offset, the navigation data must be decoded (no encryption) to corroborate that the expected satellite is effectively being tracked. This information is not available in every 2 s long string, and may thus require longer decoding to find out.

BeiDou B1-I

This last signal, from the BeiDou Phase II constellation requires an RF front-end capable of processing 1561.098 MHz, with a 2046 Mchip/s. The initial correlator spacing is set to ± 14 samples during acquisition. The 11-bit un-encoded preamble may be used to synchronize onto the message frame, once the 10-bit secondary code has been wiped out.

3. Results

The proposed dual-component universal channel ends up using twice the resources of a traditional GPS L1 C/A tracking channel, in exchange for the flexibility of tracking any GNSS signal (including both pilot and data, whenever applicable). Furthermore, it has a low worst-case 42 mW/channel dynamic power consumption. This corresponds to a 66% increase compared to the reference BPSK single-component channel. Keeping in mind that a FPGA, such as the one used in the current implementation, reaches consumption as much as 12 times that of a comparable size Application Specific Integrated Circuit (ASIC) [46], an equivalent ASIC implementation power consumption would 3.5 mW/channel, or 2.1 mW/channel for the simplest BPSK implementation. These values are comparable to the consumption of the u-blox GPS L1 C/A with SBAS receiver chip specified to be 67 mW for 50 channels (1.34 mW/channel) [47].

Furthermore, the current processing bottleneck is the discriminators computation through the 1 kHz interrupt sub-routine/channel in the embedded MicroBlaze 5.0 processor, which could be resolved with a newer, more powerful, chip. Alternatively, the navigation message decoding could be performed in an external processor. Note that in all cases, except for GPS L2C, a 10 non- coherent integrations of 1 ms is performed prior to computing the DLL feedback. The resulting commands lead to a trend represented in Figure 10, where Low Significant Bit (LSB) oscillations may be observed between commands reaching up to 0.06 $\times 10^{-9}$ s/ms. These equivalent 18 m/ms jumps are smoothed out in the PVT solution, computed at up to 100 Hz.

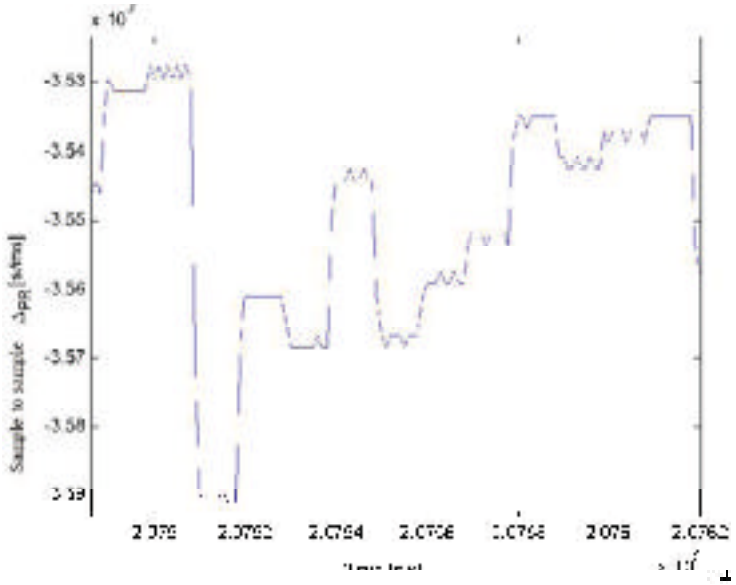

Figure 10. GPS L1 C/A LoS Variation (s) Observed every 1 ms Epoch, Based on 10 ms Non-Coherent Integration Time DLL Feedback Commands.

Another performance assessment is the instantaneous channel update mean time of 1.07 ms, allowing the receiver to rapidly adapt to its sensed environment. Finally, the 530+ civil signal components occupy a total memory codes size of ~5 MB (exception made of the L2CL code). Hence, pre-computed spreading codes may easily be stored in external memory and used on demand.

A metric to consider when seeking for the best signals to track is their pseudo-range noise. The pseudo-range being proportional to the propagation time (*cf.* Equation (21)), it should behave approximately as a parabola for a static observer, from horizon to zenith and horizon again. Its second derivative should thus tend towards a constant value. The DLL feedback can be approximated as the first derivative of the propagation time (*cf.* Equation (22)), as shown in Figure 10.

The pseudo-range noise—a random process with an order greater than 2—may then be approximated as the remaining variations of the second derivative of the pseudo-range (*cf.* Equation (23)) [48], which is generalized to a partial code within 1 ms (in Equation (24)) for the particular case for L2C (outlined in Equation (25)). At that level, only the chip index and the phase of the chipping rate clock signal, taken at 1 kHz, need to be considered ([49] (p. 264). This simplification is useful in analyzing signals, as the associated navigation message does not need to be accounted for. Moreover, multi-frequency signals being characterized by different paths, the extra time offset may then be neglected [50]. Noise is then quantified as the standard deviation of the second derivative of the pseudo-range $\sigma_{\eta_{PR}}$:

$$T_{prop.} = N_{code} \cdot T_{code} + \frac{N_{chip} + \Theta_{chip}}{f_{chip}} \tag{21}$$

$$\varepsilon_{PR} \propto \dot{T}_{prop.} = \frac{\frac{\partial}{\partial t}\left\{N_{chip} + \Theta_{chip}\right\}}{f_{chip}} \left[\frac{\mathrm{s}}{\mathrm{s}}\right] \tag{22}$$

$$\eta_{PR} \propto \ddot{T}_{prop.} = \frac{\frac{\partial^2}{\partial t^2}\left\{N_{chip} + \Theta_{chip}\right\}}{f_{chip}} \left[\frac{\mathrm{s}}{\mathrm{s}^2}\right] \tag{23}$$

$$\eta_{PR}|_{\text{partial code}} \propto \frac{\frac{\partial^2}{\partial t^2}\left\{N_{chip}\Big|_{1\text{ ms}} \,\%\left(f_{chip} \cdot 1\text{ ms}\right) + \Theta_{chip}\Big|_{1\text{ ms}}\right\}}{f_{chip}} \left[\frac{\mathrm{s}}{\mathrm{s}^2}\right] \tag{24}$$

$$\eta_{PR}|_{L2CM} \propto \frac{\frac{\partial^2}{\partial t^2}\left\{N_{chip}\Big|_{2\text{ ms}} \,\%1023 + \Theta_{chip}\Big|_{2\text{ ms}}\right\}}{511,500} \left[\frac{\mathrm{s}}{\mathrm{s}^2}\right] \tag{25}$$

where:

$T_{prop.}$ is the propagation time;
N_{code} is the number of complete code;
T_{code} is a complete code period;
N_{chip} is the chip index of the primary code;
Θ_{chip} is the phase of the chipping rate clock;
f_{chip} is the chipping rate;
η_{PR} is the pseudo-range noise.

Such a snapshot analysis is displayed in Figure 11, where the legend indicates the signal type, its average C/N_0 and its pseudo-range noise standard deviation $\sigma_{\eta_{PR}}$).

Different signals pseudo-range noise is further compared *vs.* signal strength in Figure 12, where it can be seen that WAAS L1 quality is in line with that of GPS L1 C/A (as they have the same chipping rate), while GPS L5 appears 10 times better for a given C/N_0 (with 10 times the chipping rate). Signals intrinsic phase noise can be a dominant contributor to carrier and pseudo-range measurement performance, resulting in measurement errors.

In Figure 13, a 5 Hz static GPS L1 C/A WAAS augmented solution is presented with a 15° elevation mask with 4-bit quantization. Note that the pre-computed 0-baseline reference position used has a 2 mm (95%) error.

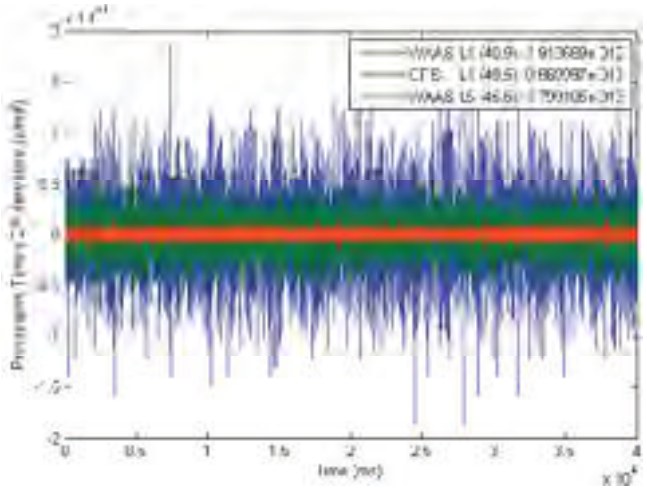

Figure 11. Propagation Time Noise During 40 sLegend: (signal type) ($\langle C/N_0 \rangle$) : (pseudo-range noise standard deviation).

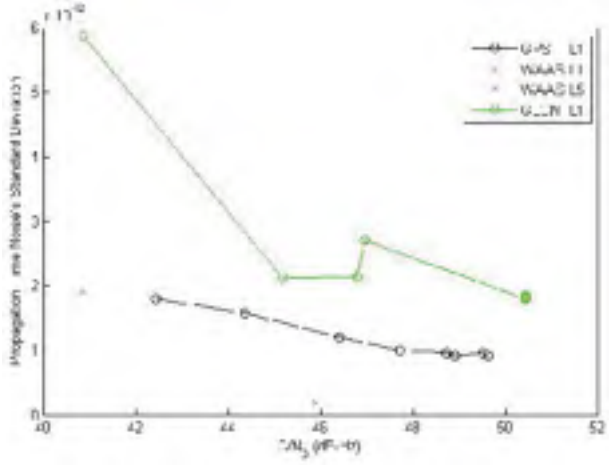

Figure 12. Different Correlator Spacing (Through Different Signals) Impact on DLL Noise *vs.* C/N_0.

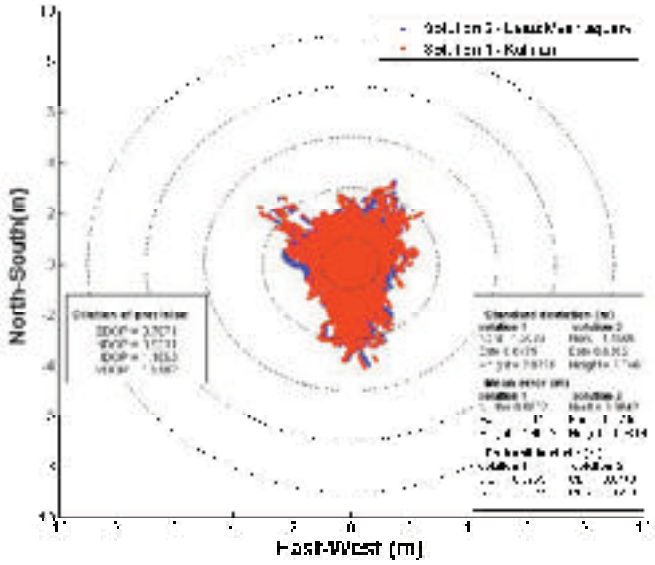

Figure 13. Relative 2D error of a GPS L1 C/A WAAS Augmented Solution.

4. Conclusions

It has been shown that with their longer codes modernized signals take longer to acquire. In order to minimize that impact, a preliminary solution based on GPS L1 C/A signals can be leveraged to reduce the search span of other signals from tracked satellites. This transition from old to new signals of any given satellite, emphasizes the need for a universal channel approach, avoiding many idle dedicated-channels. This power reduction strategy is especially critical for portable devices whose battery optimization is the challenge of the century. Moreover, a commercial application based on such a universal channel could easily introduce a pricing scheme based on available constellation and signal types. Its future compatibility would thus make it a great option for expandable design based on SW only upgrades, easily deployable into already released products.

In this paper, the GNSS signals characteristics have been identified and addressed by a universal acquisition and tracking channel, while maintaining power consumption as low as possible (by avoiding idle channels and sharing resources) and maintaining a high level of robust tracking and flexibility. As shown, the proposed architecture allows sequential acquisition and tracking of any chipping rate, carrier frequency, FDMA channel, modulation—*i.e.*, BPSK (q), QPSK (q), sin/cos BOC (p,q), CBOC $(r,\ p,\ P_r,\ \pm)$ and TMBOC $(r,\ p,\ w_r)$—or constellation, and is totally configurable (any integration time, discriminator, *etc.*) within a fast turn-around time.

Also, its dual-component architecture allows for two sequential acquisition options: (1) dual secondary chip estimation and (2) dual primary code delay (twice as fast) estimation for a single-component acquisition. Moreover, its upgradable memory codes and sub-carriers configurability (co/sine phase and α and β weights in time) make it future-compliant for any variation that could be proposed for GLONASS modernization and BeiDou phase III signals, the final description of which are yet to come.

These benefits came at the cost of increasing the tracking channel correlators number from six (NEML reference BPSK architecture) to eight for a single-component (or equivalently 16 for a dual-component) GNSS channel, thanks to the proposed resources reduction. All these GNSS signal tracking features result in a 66% power consumption increase compared to those used in a reference BPSK channel. Nevertheless, a dual-component channel requires twice the resources of a reference BPSK channel, but with twice the throughput, thus achieving an equivalent resource per channel ratio. Also, the proposed TMBOC combined with the 2 phase-controlled sub-carriers approach could be reused to implement the AltBOC sub-carrier weights with a periodicity of eight sub-chips, provided the RF front-end and sampling frequency could process a bandwidth of least 51 MHz.

Opening on Satellite Selection

The satellite selection problem has been addressed through many different approaches, leading to computationally (sub-)optimized algorithms [51]. Nevertheless, in the context of a universal channel, the challenge becomes selecting the next best signal, not only the next best satellite. Not only the number of option increases, but also does the selection algorithm complexity, thus requiring a re-spin of the existing selection algorithms. Indeed, the satellites geometry may not be sufficient anymore: frequency diversity targeting ionosphere corrections, signal effective (Gabor) bandwidth for precise pseudo-ranging measurements, signal availability in case of jamming as well as measurement ambiguity are all contributing factors to be accounted for, *i.e.*, a new research topic in itself that could address the traditional satellite navigation limitations at once.

Some thoughts on such a signal selection strategy go as follows. On cold start, all GPS L1 C/A signals are searched for in parallel to reduce as much as possible the Time To First Fix (TTFF). Once ephemerides are downloaded, known visible satellite orbits allow channels to be progressively assigned to modernized signals (most of which have dual-components, as seen in Table 1) from the same constellation, eventually on different frequency bands if the RF front-end allows, with a reduced search grid (*i.e.*, known Doppler and estimated chip alignment). Furthermore, this initial Position Velocity and Time (PVT) solution would help reducing the search span of signals on other

constellations. A key factor in resolving this signal selection challenge consists in maintaining the ideal pool of next best signals based on an adapted version of the FRIG algorithm [51]. Hence, the proposed universal channel combined with a new signal selection algorithm and a navigation data fusion strategy could become a powerful tool in cognitive receivers.

Author Contributions: Marc-Antoine Fortin conceived, designed and performed the experiments and analyzed the data; René Landry Jr. contributed the laboratory and the initial GPS L1 CA only receiver platform. Marc-Antoine Fortin wrote the paper.

Conflicts of Interest: The authors declare no conflict of interest.

References

1. U-blox AG. Standalone GNSS Chips. Available online: https://www.u-blox.com/en/gps-chips.html (assessed on 14 April 2014).
2. Sheridan, J. Russia Sticks With Glonass Mandate. 2013. Available online: http://www.ainonline.com/aviation-news/aviation-international-news/2013-01-02/russia-sticks-glonass-mandate (assessed on 11 January 2015).
3. Government Mandates Compass (Beidou) Navigation Devices on Certain Commercial Vehicles. 2013. Available online: http://www.chinaautoweb.com/2013/01/government-mandates-compass-beidou-navigation-devices-on-certain-commercial-vehicles/ (assessed on 22 May 2015).
4. Hamilton, J. GPS World Receiver Survey. 2014. Available online: http://gpsworld.com/resources/gps-world-receiver-survey/ (assessed on 7 December 2014).
5. Javad GNSS Inc. OEM Boards Compare. Available online: http://www.javad.com/jgnss/products/oem/compare.html (assessed on 13 Novembre 2014).
6. Leveson, I. Benefits of the New GPS Civil Signal—The L2C Study. *Insid. GNSS Mag.* **2006**, *1*, 42–56.
7. Thölert, S.; Erker, S.; Langley, R.; Montenbruck, O.; Meurer, M.; Temple, M.A.; Hauschild, A. A Preliminary Analysis of SVN49's Demonstration Signal. Available online: http://www.gpsworld.com/gnss-system/gps-modernization/innovation-l5-signal-first-light-8661 (accessed on 22 Februar 2010).
8. Kaplan, E.D.; Hegarty, C. *Understanding GPS Principles and Applications*, 2nd ed.; Artech House: Boston, MA, USA, 2006.
9. Julien, O.; Macabiau, C.; Cannon, M.E.; Lachapelle, G. ASPeCT: Unambiguous sine-BOC(n,n) acquisition/tracking technique for navigation applications. *IEEE Trans. Aerosp. Electron. Syst.* **2007**, *43*, 150–162.
10. European Union. *European GNSS (Galileo) Open Service Signal In Space Interface Control Document*; Galileo Joint Undertaking: Brussels, Belgium, 2010.
11. ARINC Engineering Services. *Navstar GPS Space Segment/User Segment L1C Interfaces*; En ligne IS-GPS-800; ARINC Engineering Services: Panama City, FL, USA, 2006.
12. Ries, L.; Lestarquit, L.; Armengou-Miret, E.; Legrand, F.; Vigneau, W.; Bourga, C.; Erhard, P.; Issler, J.L. A Software Simulation Tool for GNSS2 BOC Signals Analysis. In Proceedings of the 15th International Technical Meeting of the Satellite Division of The Institute of Navigation (ION GNSS 2002), Portland, OR, USA, 24–27 September 2002; pp. 2225–2239.
13. Betz, J.W. Binary Offset Carrier Modulations for Radionavigation. *J. Inst. Navig.* **2001**, *48*, 227–246.
14. Morrissey, T.N.; Shallberg, K.W.; Townsend, B. Code tracking errors for double delta discriminators with narrow correlator spacings and bandlimited receivers. In Proceedings of the 2006 National Technical Meeting of The Institute of Navigation, Monterey, CA, USA, 18–20 January 2006; pp. 914–926.
15. Burian, A.; Lohan, E.S.; Renfors, M.K. Efficient delay tracking methods with sidelobes cancellation for BOC-modulated signals. *Eurasip J. Wirel. Commun. Netw.* **2007**, *2007*.
16. Sauriol, B. *Mise en Oeuvre en Temps Réel d'un Récepteur Hybride GPS-Galileo*; École de Technologie Supérieurel: Montréale, QC, Canada, 2008.
17. Heiries, V.; Roviras, D.; Ries, L.; Calmettes, V. Analysis of non ambiguous BOC signal acquisition performance. In Proceedings of the 17th International Technical Meeting of the Satellite Division of the Institute of Navigation (ION GNSS 2004), Long Beach, CA, USA, 21–24 September 2004; pp. 2611–2622.

18. Martin, N.; Leblond, V.; Guillotel, G.; Heiries, V. BOC(x,y) Signal Acquisition Techniques and Performances. In Proceedings of the 16th International Technical Meeting of the Satellite Division of the Institute of Navigation (ION GPS/GNSS 2003), Portland, OR, USA, 9–12 September 2003; pp. 188–198.
19. Fine, P.; Wilson, W. Tracking Algorithm for GPS Offset Carrier Signals. In Proceedings of the 1999 National Technical Meeting of The Institute of Navigation, San Diego, CA, USA, 25–27 January 1999; pp. 671–676.
20. Julien, O. *Future GNSS Signal Processing I-II*; GNSS Solutions Ltd: Fort Worth, TX, USA, 2007.
21. Kim, S.; Yoon, S.; Kim, S.Y. A novel multipath mitigated side-peak cancellation scheme for BOC(kn, n) in GNSS. In Proceedings of the 9th International Conference on Advanced Communication Technology (ICACT 2007), Phoenix Park, Korea, 12–14 February 2007; pp. 1258–1262.
22. Paonni, M.; Avila-Rodriguez, J.A.; Pany, T.; Hein, G.W.; Eissfeller, B. Looking for an Optimum S-Curve Shaping of the Different MBOC Implementations. *Navigation* **2008**, *55*, 255–266.
23. Avellone, G.; Frazzetto, M.; Messina, E. A new waveform family for secondary peaks rejection in code tracking discriminators for Galileo BOC(n,n) modulated signals. In Proceedings of the 2007 National Technical Meeting of The Institute of Navigation, San Diego, CA, USA, 22–24 January 2007; pp. 246–251.
24. Sousa, F.M.G.; Nunes, F.D.; Leitao, J.M.N. Code Correlation Reference Waveforms for Multipath Mitigation in MBOC GNSS Receivers. In Proceedings of the European Navigation Conference ENC-GNSS 2008, Toulouse, France, 23–25 April 2008; Volume 1, pp. 1–10.
25. Hodgart, M.S.; Weiller, R.M.; Unwin, M. A Triple Estimating Receiver of Multiplexed Binary Offset Carrier (MBOC) Modulated Signals. In Proceedings of the 21st International Technical Meeting of the Satellite Division of the Institute of Navigation (ION GNSS 2008), Savannah, GA, USA, 16–19 September 2008; pp. 877–886.
26. Yang, C.; Miller, M. Novel GNSS receiver design based on satellite signal channel transfer function/impulse response. In Proceedings of the 18th International Technical Meeting of the Satellite Division of The Institute of Navigation (ION GNSS 2005), Long Beach, CA, USA, 13–16 September 2005; pp. 1103–1115.
27. Miller, M.; Nguyen, T.; Yang, C. Symmetric Phase-Only Matched Filter (SPOMF) for frequency-domain software GNSS receivers. In Proceedings of the 2006 IEEE/ION Position, Location, And Navigation Symposium, San Diego, CA, USA, 25–27 April 2006; pp. 187–197.
28. Pany, T.; Eissfeller, B. Use of a vector delay lock loop receiver for GNSS signal power analysis in bad signal conditions. In Proceedings of the 2006 IEEE/ION Position, Location, And Navigation Symposium, San Diego, CA, USA, 25–27 April 2006; pp. 893–903.
29. Lashley, M.; Bevly, D.M. Analysis of Discriminator Based Vector Tracking Algorithms. In Proceedings of the 2007 National Technical Meeting of the Institute of Navigation, San Diego, CA, USA, 22–24 January 2007; pp. 570–576.
30. Macchi-Gernot, F.; Petovello, M.G.; Lachapelle, G. Combined Acquisition and Tracking Methods for GPS L1 C/A and L1C Signals. *Int. J. Navig. Obs.* **2010**, *2010*.
31. Fenton, P.C.; Jones, J. The theory and performance of NovAtel Inc.'s Vision Correlator. In Proceedings of the 19 th International Technical Meeting of the Satellite Division of the Institute of Navigation (ION GNSS-2006), Long Beach, CA, USA, 26–29 September 2006; pp. 2178–2186.
32. Fortin, M.-A.; Guay, J.-C.; Landry, R.J. Development of a Universal GNSS Tracking Channel. In Proceedings of the 22nd International Technical Meeting of the Satellite Division of the Institute of Navigation (ION GNSS 2009), Savannah, GA, USA, 22–25 September 2009; pp. 259–272.
33. Landry, R.J.; Fortin, M.-A.; Guay, J.-C. Universal Acquisition and Tracking Apparatus for Global Navigation Satellite System (GNSS). Canada Patent US 8401546 B2, 2010.
34. Tsui, J.B.-Y. *Fundamentals of Global Positioning System Receivers: A Software Approach*, 2nd ed.; John Wiley & Sons Inc.: Hoboken, NJ, USA, 2005.
35. IP Processor Block RAM (BRAM) Block (v1.00a). 2011. Available online: http://www.xilinx.com/support/documentation/ip_documentation/bram_block.pdf (assessed on 3 March 2012).
36. Mao, W.L.; Lin, W.H.; Tsao, H.W.; Chang, F.R.; Huang, W.H. Acquisition of GPS Software Receiver Using Split-Radix FFT. In Proceedings of the 2006 IEEE International Conference on Systems, Man and Cybernetics, Taipei, Taiwan, 8–11 October 2006; Volume 6, pp. 4608–4613.

37. Hodgart, M.S.; Blunt, P.D.; Unwin, M. The optimal dual estimate solution for robust tracking of Binary Offset Carrier (BOC) modulation. In Proceedings of the 20th International Technical Meeting of the Satellite Division of The Institute of Navigation (ION GNSS 2007), Fort Worth, TX, USA, 25–28 September 2007; pp. 1017–1027.
38. Misra, P.; Enge, P. *Global Positioning System: Signals, Measurements, and Performance*, 2nd ed.; Ganga-Jamuna Press: Lincoln, MA, USA, 2006.
39. Betz, J.W. Design and Performance of Code Tracking for the GPS M Code Signal. In Proceedings of the 13th International Technical Meeting of the Satellite Division of The Institute of Navigation (ION GPS 2000), Salt Lake City, UT, USA, 19–22 September 2000; pp. 2140–2150.
40. Betz, J.W.; Kolodziejski, K.R. Extended Theory of Early-Late Code Tracking for a Bandlimited GPS Receiver. *J. Inst. Navig.* **2000**, *47*, 211–226.
41. ARINC Engineering Services. Navstar GPS Space Segment/User Segment L5 Interfaces. In *Interface Specification*; Navstar GPS Joint Program Office: El Segundo, CA, USA, 2005.
42. China Satellite Navigation Office. *BeiDou Navigation Satellite System Signal in Space Interface Control Document Open Signal Service*; China Satellite Navigation Office: Beijing, China, 2013.
43. Russian Institute of Space Device Engineering. *GLONASS Interface Control Document Navigational radiosignal in Bands L1, L2*; Russian Institute of Space Device Engineering: Moscow, Russia, 2008.
44. Global Positioning System Wing (GPSW) Systems Engineering & Integration. *Navstar GPS Space Segment/Navigation User Interfaces*; Global Positioning System Wing (GPSW) Systems Engineering & Integration: El Segundo, CA, USA, 2012.
45. Lockheed Martin Corporation. News Releases. 2012. Available online: http://www.lockheedmartin.com/us/news/press-releases/2012/january/0112_ss_gps.html (assessed on 28 June 2014).
46. Kuon, I.; Rose, J. Measuring the gap between FPGAs and ASICs. *IEEE Trans.Comput. Aided Des. Integr. Circuits Syst.* **2007**, *26*, 203–215.
47. U-blox AG. UBX-G6010-ST Low-Cost u-blox 6 GPS Chip. 2011. Available online: http://u-blox.com/images/downloads/Product_Docs/UBX-G6010-ST_ProductSummary_%28GPS.G6-HW-09001%29.pdf (assessed on 2 August 2012).
48. Julien, O.; Macabiau, C.; Issler, J.-L.; Nouvel, O.; Vigneau, W. Analysis and Quality Study of GNSS Monitoring Ground Stations' Pseudorange and Carrier-Phase Measurements. In Proceedings of the 19th International Technical Meeting of the Satellite Division of The Institute of Navigation (ION GNSS 2006), Fort Worth, TX, USA, 26–29 September 2006; pp. 971–980.
49. Guay, J.-C. *Récepteur SBAS-GNSS Logiciel Pour des Applications Temps-Réel*; École de Technologie Supérieure: Montréal, QC, Canada, 2010.
50. Fortin, M.-A.; Guay, J.-C.; Landry, R., Jr. Single-Frequency WAAS L1 *vs.* L5 Augmenta-tion Observations on a Ground-Based GPS L1 C/A Solution. *Positioning* **2014**, *5*, 70–83.
51. Liu, M.; Fortin, M.-A.; Landry, R.J. A Recursive Quasi-optimal Fast Satellite Selection Method for GNSS Receivers. In Proceedings of the 22nd International Technical Meeting of the Satellite Division of the Institute of Navigation (ION GNSS 2009), Savannah, GA, USA, 22–25 September 2009; pp. 2061–2071.

APPENDIX III

PAPER #3: FORTIN *ET AL.* (2014)

This paper was published in Positioning.

Fortin, Marc-Antoine, Jean-Christophe Guay and René Jr Landry. 2014. "Single Frequency WAAS Augmentation Observations (L1 vs. L5) on a Ground Based GPS L1 C/A Solution". *Positioning*, vol. 5, p. 70-83. Available: http://dx.doi.org/10.4236/pos.2014.53010

Positioning, 2014, 5, 70-83
Published Online August 2014 in SciRes. http://www.scirp.org/journal/pos
http://dx.doi.org/10.4236/pos.2014.53010

Single Frequency WAAS Augmentation Observations (L1 vs. L5) on a Ground Based GPS L1 C/A Solution

Marc-Antoine Fortin, Jean-Christophe Guay, René Jr. Landry

École de Technologie Supérieure (ÉTS), Montréal, Canada
Email: Marc-Antoine.Fortin@lacime.etsmtl.ca, Jean-Christophe.Guay@lacime.etsmtl.ca, rene.landry@etsmtl.ca

Received 12 June 2014; revised 10 July 2014; accepted 8 August 2014

Abstract

This paper presents observations on the WAAS L1 and L5 signals quality and their impact on the robustness of the navigation solution by quantifying the contributions of each broadcasted differential correction. This work is undertaken with the intent of defining performance benefits of L5 by dual frequency WAAS users and is to provide useful material for Minimum Operational Performance Standard (MOPS) development. In this perspective, a study of the WAAS signal characteristics is first carried out. The information gathered is then used to compare various GPS solutions in terms of frequency diversity, satellite diversity, pseudorange noise and different signal corrections and their impacts. These solutions are compared against a reference standalone GPS solution. All statistics are computed with respect to a post-processed Novatel Waypoint Real-Time Kinematics (RTK) GPS L1/L2 semi-codeless static solution, considered as the reference. A discussion on some simplifications with respect to specifications (*i.e.* MOPS) that could be considered by receiver manufacturers closes the paper. It is confirmed that the current WAAS navigation message definition is the same on both the L1 and L5 frequencies, the latter further being Manchester coded, thus avoiding data ambiguity. The +5 dB SNR on L5 has minor impacts in terms of reliability and continuous availability in the presented scenarios, but would become especially beneficial in hostile environments, despite a greater number of pulsed interferers. Another demonstration is that the WAAS message varies slightly from one WAAS satellite to another, even if corrections are generated centrally. Finally, it is observed that WAAS and GPS signals pseudorange noise are comparable on a "per frequency" basis.

Keywords

GPS L1, WAAS L1, WAAS L5, MOPS, Pseudorange Noise

How to cite this paper: Fortin, M.-A., Guay, J.-C. and Landry, R. Jr. (2014) Single Frequency WAAS Augmentation Observations (L1 vs. L5) on a Ground Based GPS L1 C/A Solution. *Positioning*, **5**, 70-83.
http://dx.doi.org/10.4236/pos.2014.53010

1. Introduction

The civil international aircraft industry constantly seeks for satellite navigation performance improvements. Following that thread, the first Space Based Augmentation System (SBAS), namely the Wide Area Augmentation System (WAAS), was declared operational on L1 (1575.42 MHz) in 2003, already a decade ago. It is now known that WAAS signals improve GPS signal processing by correcting ionospheric delay errors, ephemeris differential corrections (including clock bias/drift and GPS satellite position), resulting in a greater solution integrity and accuracy. Initially, SBAS was intended to improve accuracy and provide integrity assurance. In its earliest form, it did not even include differential corrections [1]. In time, the most obvious effect of SBAS became to annihilate the Selective Availability (SA), which could be differentially corrected [2]. This intended degradation of the signal quality with military purposes has been discontinued since May 2000; new GPS III satellites should no longer include SA capability, since it has been permanently deactivated [3]. Fortunately, since SA has included a voluntary clock dither error, SBAS systems still compensate for involuntary GPS clock errors due to hardware anomalies onboard Space Vehicles (SV). A complete error source assessment may be found in [4]. Because of its application in flight industry, security issues impose long validation cycles. For other applications, the latest 8-year-old Minimum Operational Performance Standard (MOPS) [5] could be re-visited in terms of general SBAS implementation rules with an up-to-date environment (e.g. considering SA has completely been deactivated and will not come back). This is important since GPS L1 cannot satisfy performance required by Federal Aviation Administration (FAA) for various phases of flight on its own, especially for approach with vertical guidance.

This assessment is even more important since WAAS has been continuously undergoing improvements and operational capability upgrades as part of its four phases [6]:

1) Initial Operating Capability (IOC) accomplished in 2003;
2) Full LPV Performance (FLP) completed in 2008;
3) Full LPV-200 Performance extended through 2013;
4) Dual Frequency Operations (DFO) planned until 2044.

Phase 1 provided high availability "in route" through non-precision approach such as Lateral and Vertical Navigation (LNAV/VNAV) service over the Conterminous United States (CONUS) as well as limited Localizer Performance with Vertical Guidance (LPV) approach service. Phase 2 provided full LPV service with a limited LPV-200 approach service availability within CONUS. Phase 3 provided robust, reliable, and sustainable LPV-200 capability and coverage throughout CONUS. This was very welcome during solar maximum, *i.e.* the 11-year cycle peak that last occurred in 2013 [7] [8]. In November 2011, the FAA approved its first Operational Specifications for Required Navigation Performance (RNP) Authorization Required (AR) using WAAS. Moreover, NAV CANADA has 180 approaches pending design and publication at 92 airports, on top of the already compliant 36 airports with a total of 57 approaches published [9]. U.S. WAAS now counts 38 ground reference stations, achieving 99 % availability over the main land. 1900 U.S. airports have commissioned 3000 LPV precision approaches and 5000 are expected by 2016. Phase 4 should implement the paradigm change where GPS L5 would replace L2 P(Y) in WAAS ionosphere computation; *i.e.* WAAS would then use L1 and L5 to generate the necessary estimates for Single Frequency Users (SFU) on L1, while Dual-Frequency Users (DFU) would calculate ionosphere induced delays directly through L1 and L5. While the current 3-GEO (Inmarsat-4GEO-PRN 133, Anik-F1R-PRN 138 and Galaxy 15-PRN 135) constellation is already dual-frequency capable, the WAAS L5 Signal In Space (SIS) is only used for line of sight ionosphere measurements. In addition, new GEO satellites are planned for procurement around 2015-2018 as current WAAS constellation leases will expire in this timeframe.

All this activity, as well as the introduction of the L5 (1176.45 MHz) civil signal on all GPS Block IIF (and newer) satellites, planned to launch on a replacement-basis, opens new possibilities for use of the WAAS system. WAAS transmissions improve system accuracy: 1) by reducing ranging measurement errors through the transmitted differential corrections for each GPS satellite and 2) by improving geometry by making their ranging signals available in addition to the set of GPS measurements. The latter is possible since the WAAS signal is synchronized with GPS system time [10]. Frequency diversity would also be very helpful in case of RF Interference (RFI) in one of the used frequency bands [11], although phase 4 includes no plans to provide for L5-only users. So once the current WAAS transmissions will be updated, there would be no more frequency diversity available in the event of RFI.

The two Aeronautical Radio Navigation Services (ARNS) L band frequencies used in WAAS, among the four Radio Navigation Satellite Services (RNSS), not only grant frequency diversity to aircrafts, but also offer GPS receiver manufacturers a lot of design choices for their future products. Hence, the purpose of this paper is to provide an overview of the actual status of WAAS signal precision and integrity on both L1 and L5, although there are no plans for a WAAS L5 service; current WAASL5 signals are not officially declared online by the FAA [12]. The WAAS signal characteristics are summarized hereafter before the measurements integration into the solution is described, and its tests methodology is defined. The following is a study of the WAAS signal quality and contents. Then, a robustness analysis of different WAAS signals is presented before a short discussion and conclusive remarks.

2. WAAS L1/L5 Signals Characteristics

There are two satellite signals currently broadcasted by the WAAS system: one on L1 and another on L5. They are both modulated with Binary Phase Shift Keying (BPSK) on their respective center frequencies, shared with GPS. As opposed to the GPS L5 civil signal, WAAS L5 has no quadrature component [13]. **Table 1** summarizes WAAS signals' general characteristics [14] [15].

The structure of the WAAS message data block is composed of an 8-bit partial preamble (of a 24-bit long preamble spread onto three consecutive data blocks), a 6-bit message type identification and a 212-bit data field, followed by a 24-bit Cyclic Redundancy Check (CRC) parity word. Each 250-bit data block is encoded through rate-½ Forward Error Correction (FEC) based on a 7-bitconstraint length, resulting in 500 symbols. It is noticeable that there is no composition difference between WAAS L1 and WAAS L5 messages at this point, apart from the WAAS L5500 sps being Manchester coded, resulting in twice the processing bandwidth at 1 kSps. This Manchester coding could also be looked at a 2-bit secondary code (*i.e.* 1.0) [16]. The occupied signal bandwidth however remains at least 20 MHz, such that at 95% of the broadcast power is contained within ±12 MHz around at the broadcast frequency. Experimentation further shows that the WAAS L1 to L5 symbols difference is below 0.1%, confirming that the same navigation message is currently being broadcasted from a given satellite simultaneously on both its WAAS signals, as mentioned in [16].

Furthermore, 63 message types are possible in WAAS L1, but only 18 are defined in its specifications ([17], p. 12). This limited message set is currently also used as a placeholder for WAAS L5 while it remains to be defined as part of the dual frequency L1/L5 MOPS development.

3. Test Methodology for WAAS L1/L5 Analyses

Initially, a post-processed zero-baseline Real-Time Kinematic (RTK) method was applied on two Novatel DL4-Plus receivers with L1/L2 semi-codeless solutions in order to establish the true reference coordinates of the antenna used for the tests presented herein. A passive Novatel-704 antenna, placed on the ÉTS roof with clear visibility, has been used with a proper inline amplification chain for all the tests. The Waypoint software provided a solution with fixed ambiguity for all samples, *i.e.* the best achievable solution quality. These reference coordinates (*i.e.* 45.494035˚ latitude, −73.562770˚ longitude and 10.445 m elliptical height obtained with sub-millimeter standard deviation) are later used to compute all the statistics presented in this paper.

A research prototype of a universal GNSS receiver (RxGNSS) was used to conduct the tests presented in the following sections. Currently, 12 channels can be seamlessly configured to acquire and track any civil GNSS or

Table 1. General characteristics of WAAS signals.

WAAS signals		L5	L1
Carrier frequency	(MHz)	1176.45	1575.42
Code length	(chips)	10230	1023
Code rate	(Mcps)	10.230	1.023
Code duration	(ms)	1	1
Data rate	(bps)	250	250
Encoded symbol rate	(sps)	500	500
3-dB Bandwidth	(MHz)	20	20

SBAS signal [18]. The RxGNSS further includes three configurable RF front-ends connected to a Lyrtech VHS-ADAC board with 8 ADCs and 1 XC4VSX55-10FF1148 FPGA (with an embedded MicroBlaze processor) as well as an external computer [19]-[22]. In order to appreciate the impacts of WAAS corrections, a GPS L1 C/A code solution with carrier smoothing is considered as the performance benchmark.

All three WAAS satellites are visible from the antenna location, as described in **Table 2**. As a final note, the reader should be aware that slow, fast and ionospheric corrections were applied to the GPS L1 C/A signals being tracked, for all WAAS solutions presented below. All logs are described as the tests below are defined.

4. Analysis of the WAAS L1 and L5 Signals Characteristics

Tests were performed with the RxGNSS to compare WAAS signals on L1 and L5 in terms of C/N_0, navigation message contents, pseudorange noise and resulting navigation solution performances.

4.1. C/N0 Impacts Analysis

MOPS states that it is often sufficient to choose the WAAS satellite with the greatest elevation angle, but warns that it may not be the best [23]. At the time the tests were conducted, PRN 133 (with highest elevation angle) was declared Non Precision Approach (NPA); PRN 138 was therefore used by default as it provided higher signal strength. The transmitted power level is mainly determined by the satellite Equivalent Isotropically Radiated Power (EIRP), although there could be spatial variation between the L1 and L5 arrays. A detail worth noting is the WAAS L5 signal strength for PRN 138 was witnessed to be more than 4dB higher than on L1, which differs from previous findings where both frequencies showed similar C/N_0 (within ±1 dB-Hz) [24]. This also goes against the Signal In Space (SIS) power levels contained in the WAAS Technical Specifications for GEO 5/6/7 Service Lease where the maximum transmitted power is 2.5 dB higher on L5 compared to L1 [15]. One could have expected higher L5 signal power to help fight against the known pulsed interference environment L5 resides in. Indeed, Distance Measuring Equipment (DME), Tactical Air Navigation (TACAN), Joint Tactical Information Distribution System (JTIDS) and Multifunctional Information Distribution System (MIDS) all represent a higher worldwide pulsed threat than in the other 3 RNSS L bands [25].

From the same test performed on June 20, 2012 used in the previous paragraphs, a C/N_0 statistical analysis was also conducted, the results of which are summarized in **Table 3**.

The ~5.44 dB-Hz increase of L5 over L1 for PRN 138 has multiple advantages, such as in tracking loops performance (*i.e.* reduced code and phase thermal noise provides better solution accuracy, assuming their pseudoranges were included in the solution), as well as a greater navigation message successful decoding ratio (*i.e.* fewer tracking losses).

Furthermore, MOPS receivers are required to have no worse than a 0.05% message loss rate at the minimum power level; *i.e.* the end-to-end SIS service reliability must be greater than 99.95% in any one hour interval [5]. In the RxGNSS, the CRC pass rate translates into a successfully received messages ratio. In the present case, a

Table 2. WAAS satellite relative location (from Montréal, Canada).

PRN	C/N_0 (dB-Hz)		Elevation (˚)	Azimuth (˚)
	L1	L5		
133[a]	40.0	42.0	35.5	213.7
135	37.4	39.4	12.5	247.3
138	40.9	46.1	28.2	223.3

a. PRN 133 is Non-Precision Approach (NPA) on June 19th, 2012.

Table 3. C/N0 statistics for satellite PRN 138.

Signal	Mean	Std.	Min.	Max.
L1	40.8	0.2	40.1	41.5
L5	46.2	0.4	44.9	47.0

CRC pass rate of 99.6% was achieved on L1, and 100% on L5. Isolated discontinuities on L1 were caused by tracking losses due to lower signal strength. In order to maximize reliability, the following tests are only conducted with WAAS L5 corrections, tracked with high signal strength.

The WAAS navigation message is composed of two symbols per data bit, resulting in 500 sps. The RxGNSS samples at each 1 ms long spreading code period, providing exactly two samples per symbol. Hence, a samples pair (even and odd) is obtained for every encoded WAAS symbol transmitted.

In the case of WAAS L1, a 1 kSps stream error is defined as different even and odd samples within a symbol. As expected, the error count increases as the signal strength falls under 40 dB-Hz, most probably due to tracking losses. Nevertheless, such a stream error rate $\left(\overline{x} \pm 3\sigma\right)$ of 1.1% ± 2.0% at 38 dB-Hz would still remain acceptable, considering that Viterbi decoding resists to 15 distributed errors per 500-symbol data blocks (*i.e.* 3 % of all symbols), 78.55 % of the time, as simulated in [26]. Note that these numbers do not account for FEC gains, which would result in greater error rate tolerance at a given bit energy per noise density $\left(E_b/N_0\right)$. Indeed, the Word Error Rate (WER) is specified to be 1×10^{-3} [5]. On the other hand, GPS L1 C/A stream errors can easily be averaged out over 20 consecutive samples. Such stream errors (here defined as different samples within a 20 sample long bit) were not witnessed on the RxGNSS at signal strengths above 41.5 dB-Hz, which is consistent with observations on the WAAS signals. In the case of GPS L5, the secondary code may still be mapped to one of its two polarity, whichever is closest to the one observed, once synchronization is achieved.

Considering that two 1 kSps samples represent one 500 sps WAAS symbol (for both WAAS L1 and L5), a common WAAS decoding approach is to consider only one sample out of two. For such an approach to work, both alignments (odd and even) need to be tested in order to achieve initial alignment. This simple approach allows maintaining complete frequency diversity with the current WAAS signal definition. It has thus been applied to the following tests.

4.2. Analysis of the WAAS Navigation Message

Figure 1 displays a navigation stream auto-correlation. This 3-second periodicity is partly due to the WAAS 24-bit preamble being distributed over 8-bit preambles on three consecutive 1-s long data blocks. However, 8 bits out of 250 may not be sufficient to justify normalized correlation levels larger than 50%. The occurrence of each message type occurrence is bounded by its maximum update interval, defined as a multiple of 60 s in most cases. The User Differential Range Error Index (UDREI) data, bared by message types 2 - 6 and 24, is the only one with a 6 s maximum update interval; a 3 s repeat period would thus seem to be a safe operation mode, providing a more probable reason for the witnessed 3 s periodicity of the navigation message.

WAAS satellites may broadcast messages from any WAAS Master Station (WMS). In general, each GEO broadcasts information from a different WMS. However, there are times when one WMS may be broadcasting

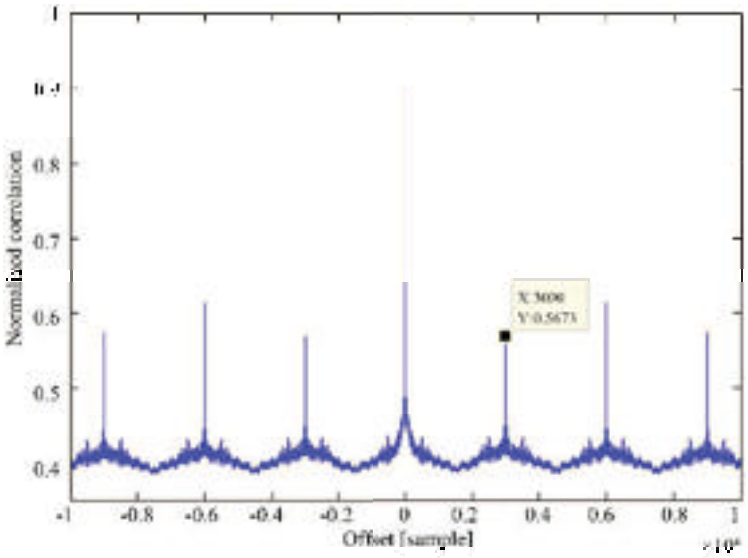

Figure 1. Zoom on a partial auto-correlation showing a 3 s periodicity.

through more than one GEO. Also, all three master stations have the same input data and therefore the message content among the WMSs is very similar, but not necessarily identical. We formulated the hypothesis that different WAAS satellites transmitting different contents could influence the resulting navigation solution. In order to evaluate the impact of WAAS corrections provided by different satellites, two other tests were realized, both performed on June 20, 2012. For each test, all the three WAAS satellites were assigned to a tracking channel and their sampled 1kSps stream were compared. More precisely, the encoded navigation message symbols are >45% different from one satellite to another. Although Forward Error Correction (FEC) provides a data decoding robustness, it also propagates a small data difference over several symbols [27].

This falsely increases the contents difference ratio when comparing symbol streams from different satellites. Bearing in mind that message types 9, 12 and 28, respectively for the broadcasting satellite ephemerides, clock and their covariance, will vary from one satellite to another (over the complete data field and thus on the CRC too) [28], a smaller symbols difference ratio was expected. Indeed, these message types maximum update intervals are respectively 120, 300 and 120 s, which is rather slow compared to those of other message types. These other message types should be similar in contents, although they could be transmitted in a different order or at a different time.

Also, because of the navigation message structure, missing a data block could have noticeable consequences. For example, if the Ionospheric Grid Point (IGP) Mask Message Type 18 (defining the way to interpret the following Ionospheric Delay Corrections Messages Type 26) first reception was missed, ionospheric corrections would not be available until a new Ionospheric Mask Issue of Data (IODI) is received. The IODI changes very infrequently (less than once a year) so a non-aviation user could apply an even longer time out and ensure that the ionospheric corrections are properly decoded based on previous data. In cold-start mode, an extra augmentation setup delay could last up to a maximum update interval of 300 s for Message Type 18. In the long run, this threat is minimized through the Message Type 18 time out interval of 1200 s. Indeed, after first successful reception, such an outage would imply Message Type 18 is missed four times in a row. Note that aviation procedures are interrupted whenever outages last more than 4 s.

Similarly, in cold start mode, missing the first PRN Mask Message Type 1 could cause an outage lasting up to 120 s for all of the following message types (assuming a missed change in IOD PRN (IODP) mask) [28]:

- Fast Corrections (Message Types 2 - 5 and 24);
- Integrity Information (Message Type 6);
- Acceleration Information (Message Type 7);
- Long-term Corrections (Message Type 25);
- Clock-ephemeris Covariance (Message Type 28).

Again, in the long run, one would need to miss five consecutive Message Type 1 data blocks to suffer such an outage.

4.3. Pseudorange Noise Analysis

Another useful metric to consider when seeking for the best WAAS signal to use is the pseudorange noise. The pseudorange being proportional to the propagation time (4.1), it should behave approximately as a parabola, from horizon to zenith and horizon again. Its second derivative should thus tend towards a constant value. The pseudorange noise—a random process with an order greater than 2—could then be approximated as the remaining variations of the pseudorange second derivative (4.2) [29]. At that level, only the chip index and the phase of the chipping rate clock signal, taken at 1 kHz, need to be considered for a static receiver ([26], p. 264). This simplification is useful in analyzing WAAS signals, as the associated navigation message does not provide a readily available transmission time such as the GPS Time of Week (TOW); SBAS plans for time information in message type 12, which was not transmitted by WAAS satellites in 2012. Fixed ambiguity may be solved for WAAS pseudorange based on a pre-existing navigation solution, and remains valid as long as the WAAS signal is continuously pursued. Combined with GPS L1 C/A signals, it is however possible to extrapolate that information since both data blocks are synchronized, although WAAS time is offset with respect to GPS time. Moreover, L1 and L5 being characterized by different paths, an extra time offset is to be considered [23]. Noise is then quantified as the standard deviation of the pseudorange second derivative $\sigma_{n_{PR}}$:

$$T_{prop.} = N_{code} \cdot T_{code} + \frac{N_{chip} + \Theta_{chip}}{f_{chip}} \left[\mathrm{s}\right] \tag{4.1}$$

$$n_{PR} \propto \ddot{T}_{prop.} = \frac{\frac{\partial^2}{\partial t^2}\left\{N_{chip} + \theta_{chip}\right\}}{f_{chip}} \left[\mathrm{m/s^2}\right] \tag{4.2}$$

where:

$T_{prop.}$ is the propagation time;
N_{code} is the number of complete code;
T_{code} is a complete code period;
N_{chip} is the chip index, within a code;
θ_{chip} is the phase of the chipping rate clock;
f_{chip} is the chipping rate;
n_{PR} is the pseudorange noise;

A snapshot analysis shows the second derivative of the propagation time (*C.f.* **Figure 2** where the legend indicates the signal type, its average C/N_0 and its noise standard deviation).

The lower propagation time noise is due to the WAAS L5 chipping rate being 10 times faster, thus allowing for 10 times narrower correlator spacing. Indeed, it is well known that code phase jitter performance depends on the slope of the discriminator curve and the SNR. More precisely, the Delay Lock Loop (DLL) has a closed loop 1-sigma error defined as [30] [31]:

$$\sigma_\varepsilon \approx \frac{c}{f_c}\sqrt{\frac{2 \cdot B_L \cdot T_P \cdot R_n(0)}{K^2}} \left[\mathrm{m}\right] \tag{4.3}$$

where:

c is the speed of light (*i.e.* 299, 792, 458 m/s);
B_L is the loop bandwidth;
T_P is the integration time (*i.e.* 1 ms);
$R_n(0)$ is the noise correlation at null offset between the incoming and the replicate codes;
K is the discriminator slope $\equiv \langle S \rangle / \tau$;
S is the useful signal;
τ is the offset between input signal and replica.

The impact of correlator spacing on different signals are compared in **Figure 3**. Note that the chipping rates are 1.023 Mcps for GPS L1 C/A and 0.511 Mcps for GLONASS. The correlator spacing is set to ±0.5 chip during acquisition (not shown) and 0.05chip during tracking for all L1 signals, but to ±0.17 chip for WAAS L5, due to

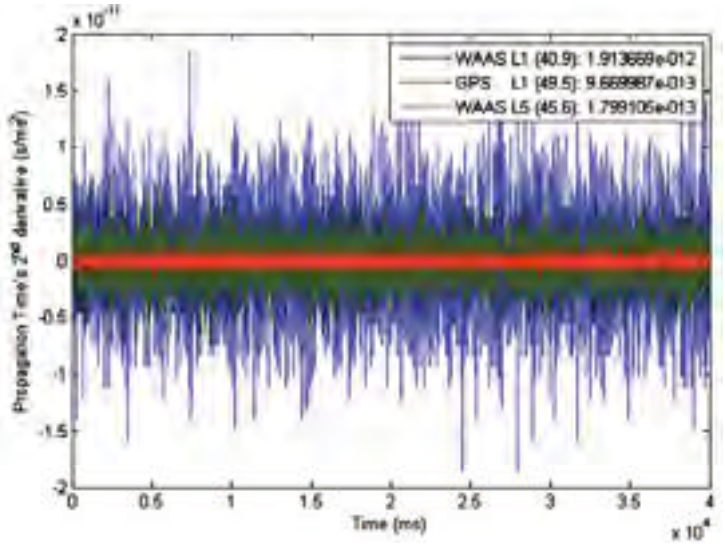

Figure 2. Propagation time noise during 40s (Legend ⇒ <signal type> (<C/N_0>): <noise standard deviation>).

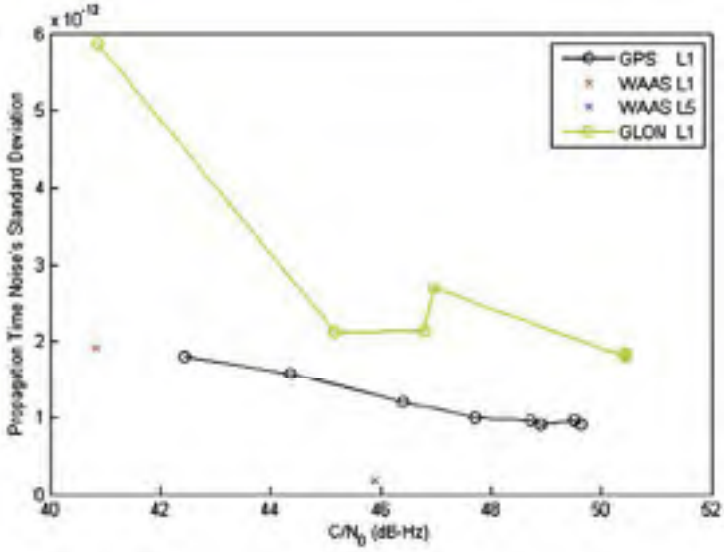

Figure 3. Correlator spacing impact on DLL noise vs. C/N_0.

a 60 MHz sampling frequency limitation. From the figure, it can be seen that WAAS L1 quality is in line with that of GPS L1 C/A, while WAAS L5 appears 10 times better for a given C/N_0. Considering that the signals intrinsic phase noise can be dominant contributor to carrier and pseudorange measurement performance and that carrier tracking error may also contribute to measurement errors, it appears that WAAS signal pseudorange noise are similar with that of GPS signals on L1 and L5 [32] [33]. Indeed, WAAS has specified an end-to-end SIS single-sided phase noise vs. frequency offset from the nominal carrier [15], which provides better performance relative to the MOPS specifications of 0.1 radian error in 10 Hz tracking loop.

4.4. Navigation Solution Performance Analysis for Different WAAS Satellites

Two logs were taken in order to compare the WAAS satellite corrections impact on the receiver performances for a static user; no test was performed on satellite PRN 133 as it was NPA at the time the tests were conducted [34]. Test #1 was performed on June 22, 2012 and lasted 24 hours, where a WAAS L5 channel was configured to track satellite PRN 138. Meteorological observations [35] for that day at the Montréal Dorval Airport, Canada (YUL)—14.9 km away from the antenna as the crow flies—were a broken sky condition with an average temperature of 23.5˚C. Test #2 was performed on June 23, 2012 and lasted 24 hours, where a WAAS L5 channel was configured to track satellite PRN 135. The sky conditions were scattered with an average temperature of 21.5˚C. Both tests started at 8 A.M. It can be noticed that PRN 138 has a greater elevation angle than PRN 135 relative to the antenna position, and thus its C/N_0 is consequently stronger (*C.f.* **Table 2**).

Table 4 highlights some of the statistical results. The performance differences are considered negligible: only a few centimeters difference which could be explained by a change in weather between the two tests. Hence, it can be concluded that, despite not exactly the same, WAAS message lead to equivalent, comparable differential positioning performances. Because of the stronger C/N_0, satellite PRN 138 has been chosen for the following tests aimed at quantifying the positioning impact of differential corrections on different WAAS signals.

5. Differential Correction Comparison through WAAS L1 and L5

Now that the WAAS signals have been characterized, different static tests are realized to analyze the robustness of a GPS solution with different WAAS options. All the 15 message types defined for WAAS L1 are decoded (from either WAAS L1 or L5 identical transmissions) and most of their data is applied after Carrier Smoothing (CS) of the raw GPS L1 C/A measurements, if they are to be significant, *i.e.* not buried in code measurement noise [26]. Basically, slow and fast corrections are respectively applied to GPS satellites clock and ephemerides, as well as to the raw pseudorange measured by the receiver, while ionospheric corrections replace the GPS broadcasted Klobuchar ionospheric model. These corrections should be extrapolated in time with degradation

parameters. However, now that SA has been deactivated, Rapid Rate Corrections (RRC) can be removed in ground receivers (where integrity is not as critical as for air-born receivers) as it introduces 12 s periodic noise [2], and is thus not applied. In the navigation solution presented herein, WAAS almanacs and ephemerides are only used to populate the sky plot; their pseudoranges and the SBAS UTC data blocks are thus not used. Also, integrity is achieved by bounding the pseudorange measurements; out-of-bound measurements being discarded while others are weighted in the Kalman solution. Prior to analyzing the metrics below, positioning performance improvements in these conditions were assessed to be comparable to those obtained with a Novatel DL4-Plus receiver hooked up to the same RF setup.

In the following paragraphs, horizontal statistics are compared, *i.e.* standard deviations, mean errors, CEP and R95. More precisely, three sets of tests were conducted: WAAS corrections from L1 vs. L5; day vs. night and slow vs. fast corrections.

5.1. WAAS L1 vs. L5 Corrections Impacts on Positioning

Although the navigation message contents have been shown to be identical on both WAAS frequencies, which can be continuously tracked on PRN 138, 24 hour-long tests with WAAS L1 or WAAS L5 were compared against a GPS with CS to quantify and compare their impacts. These three tests were run on different days with the conditions defined in **Table 5**.

Satellites may fail to maintain coherency between the broadcast code and carrier. However, this threat has never been observed on the GPSL1 signal, but has been observed on WAAS geostationary satellite signals (over 24-hour cycles) and on the GPS L5 signal. Because of different receiver averaging windows, this error cannot be differentially corrected [4]. Nevertheless, L1 vs. L5 Code-Carrier Coherence (CCC) can be mitigated using Code Minus Carrier corrected for the Ionosphere (CMCI) [15]. Anyhow, only GPS L1 C/A pseudoranges are used in the solution, the CCC error associated with this diurnal variation should thus not impact the performance comparison presented in **Table 6** (horizontal 2D error relative to the static antenna position obtained with post-processed RTK) and **Table 7** (improvements obtained for the different WAAS solutions compared to that of GPS CS). These augmented solutions mean errors may seem very high compared to other performance evaluations and is thus only used as a relative comparison. It can be seen that there are important improvements of both WAAS solutions over GPS CS. However, the differences between the two WAAS solutions are not noticeable because the order of magnitude difference is only a few centimeters, which could be attributed to external causes such as diurnal variations.

Hence, these observations corroborate the current WAAS implementation where both WAAS frequencies currently transmit exactly the same data. However, the message content on L5 is expected to be revised as part of the dual frequency operations capability. Meanwhile, since the overall performances are comparable for both

Table 4. Static position performances with WAAS corrections.

PRN	C/N_0 (dB-Hz)	Probability Circles (m)	
		R95[a]	CEP[b]
135	~ 40.0	1.35	0.45
138	~ 46.5	1.38	0.48

a. R95 stands for 95% Radius. b. CEP stands for Circular Error Probability (at 50%).

Table 5. Characteristic of the solutions obtained with WAAS corrections from satellite PRN 138 (24H).

Solution	Date	Meteorological observation [35]	RxGNSS channels configuration	WAAS C/N_0 (dB-Hz)
GPS CS	June 19, 2012	Overcast 25˚C clear visibility	−12 GPS L1 C/A	N/A
GPS CS-WAAS L1	June 21, 2012	Scattered 28˚C clear visibility	−11 GPS L1 C/A −1 WAAS L1	N/A 41.0
GPS CS-WAAS L5	June 22, 2012	Broken 23.5˚C clear visibility	−11 GPS L1 C/A −1 WAAS L5	N/A 46.5

Table 6. Solution horizontal statistics (GPS, WAAS L1 and WAAS L5 solutions).

	Standard deviation (m)			Mean error (m)			Probability circle (m)	
	North	East	Height	North	East	Height	CEP	R95
GPS CS	1.183	1.007	2.747	0.681	−0.206	6.470	0.795	2.434
WAAS L1	0.809	0.481	1.568	0.191	−0.105	2.006	0.475	1.367
WAAS L5	0.792	0.488	1.533	0.269	−0.124	1.740	0.482	1.376

Table 7. Solution horizontal improvement statistics (WAAS solutions over GPS CS).

	Standard deviation (m)			Mean error (m)			Probability circle (m)	
	North	East	Height	North	East	Height	CEP	R95
WAAS L1	0.374	0.526	1.179	0.490	−0.101	4.464	0.320	1.067
WAAS L5	0.392	0.518	1.214	0.412	−0.082	4.730	0.313	1.059

WAAS frequencies, the following analyses are performed with correction data only obtained from WAAS L5. Similar results can be expected for L1, provided its C/N_0 is strong enough to allow continuous tracking. The next paragraph quantifies the ionospheric positioning error.

5.2. Day vs. Night WAAS L5 Impact

It is known that the atmosphere ions interfere more with the signals during the day, when they are polarized by the sun [36]. In order to estimate the greatest contribution of WAAS corrections further, 8-hour subsets of the previous solutions are analyzed; approaching the solar solstice,16 hours of sun and 8 without are expected. Analyzing the impact of ionospheric corrections for a single location over eight hour periods does not allow for general conclusions, as very different result could be obtained for different times and locations. Nevertheless, the intent here is to weight their relative contributions to the augmented solution considered above, *i.e.* a day vs. night comparison at the same location within a given 24-hour period. Hence, "day" test was extracted from June 22, 2012 8 A.M. to 4 P.M. (broken sky conditions at 25˚C) while the "night" test was extracted from 9 P.M. to 5 A.M. (scattered sky at 21.5˚C). **Table 8** presents the improvements obtained for different WAAS solutions over GPS CS. As expected, GPS CS performs better at night than during the day, as the ionospheric delays are less harmful. Despite these results, WAAS corrections always improve the solution, but with a greater impact during the day. This allows assessing the ionospheric delays as the greatest threat, accounting for ~30 cm of CEP. The next paragraph looks at the impact of slow and fast corrections

5.3. Impact of Slow and Fast Corrections

It has been shown that fast corrections needed to be applied on top of the slow corrections for them to be significant [23]. With SA discontinued, it is interesting to validate these corrections impact as they now uniquely apply to the real residual satellite clock error, *i.e.* the difference between the time of the actual clock and the one already modelled by the GPS Control Segment (CS) [37]. To measure the magnitude of their contribution, a 24-hour test was run on July 11th, 2012 at 7h15, a day with a few clouds, clear visibility and an average temperature of 23.5˚C [35]. **Table 9** presents detailed performance metrics and improvements achieved by applying the WAAS L5 corrections to the GPS L1 C/A solution with fast corrections over the one without. Although fast corrections magnitude is not as big as for ionospheric (~30 cm CEP) or slow corrections (~15 cm CEP), they still provide a solution improvement (~3 cm CEP).

6. Discussion

It has been shown that one 1 kSps sample out of two is identical on both WAAS frequencies. This would also wisely provide a true message frequency diversity feature in the WAAS design, *i.e.* a frequency redundancy as proposed in [38], useful in case of RF interference in one of the used bands, were a WAAS L5-only capability

Table 8. Standard deviation & mean error improvements (Day and Night WAAS L5 over GPS CS).

	Standard deviation (m)			Mean error (m)			Probability circle (m)	
	North	East	Height	North	East	Height	CEP	R95
Day	0.464	0.475	0.952	0.721	0.081	5.514	0.453	1.346
Night	0.409	0.179	1.183	0.101	−0.002	3.840	0.125	0.754

Table 9. Solution horizontal statistics (with and without Fast corrections).

Fast corrections	Standard deviation (m)			Mean error (m)			Probability circle (m)	
	North	East	Height	North	East	Height	CEP	R95
Yes	0.792	0.488	1.533	0.269	−0.124	1.740	0.482	1.376
No	0.959	0.524	1.757	0.161	−0.115	1.561	0.509	1.663
Gain	0.168	0.035	0.224	−0.108	0.009	-0.179	0.027	0.287

provided. Ultimately, the L5 broadcast will provide a new service and require different messages. Anyhow, the current required MOPS message loss rate is sufficiently low as to offer little benefit from repeating messages on both frequencies. Thus, this important advantage will be partly or totally lost when the L5 WAAS message will evolve differently from the L1 WAAS message. An alternative would be to upgrade the current WAAS L1 message to support integrity and precision on both L1 and L5, while still transmitting a duplicate of that message on WAAS L5. This would however imply to drop the SBAS service provider objective for backward compatibility with legacy L1—only users.

In terms of robustness, the WAAS signal to be tracked should be the one with the greatest C/N_0 available, which may not correspond to the one with the greatest elevation angle, as prescribed in the MOPS [23]. It can also be concluded that, granted such a WAAS signal is being tracked; an additional WAAS signal would not cause a positive impact on the GPS L1 C/A PVT in terms of the navigation message as all WAAS signals achieve the same performances. Nevertheless, in terms of noise performance and mitigating multipath effects, the WAAS L5 higher chipping rate sharpens the auto-correlation peak by a factor of ten, making it a better signal than WAAS L1 from a raw pseudorange standpoint. It also appears that missing a data block announcing the new indices of the upcoming data blocks does not induce noticeable differences (except maybe at cold start); either way, it could be circumvented if the indices were overlooked and RRC were applied, although this behavior is not supported by the MOPS [5].

This paper does not assess whether WAAS pseudorange should be used in the solution as this was already presented in previous work [13] [39]. This being said, despite their lower efficiency, WAAS L1 observables could be included into the solution in severe environments or when too few satellites are visible [24]; this would come at a lower cost than for WAAS L5, as the same sampling rate and front-end could be used, although WAAS L5 would indeed be a more promising alternative with its higher signal strength and lower DLL noise.

Until Direct RF Sampling as well as Software Defined Radio (SDR) become widely accessible through lower price, it may not be worthwhile to support a second front-end solely for WAAS L5, especially since only four GPS satellites are currently broadcasting on that band. The only exception to this would be for Safety of Life (SoL) applications, such as in the flight industry where high reliability is critical as lives are at stake. For such services, as well as for automated agriculture and car guidance applications, WAAS L5 offers a positive impact over L1 in terms of robustness due to its higher C/N_0, avoiding scarce discontinuities. All of this, while providing full frequency diversity in cases of signal deterioration due to jamming or unintentional interference, as long as L1 and L5 WAAS messages will remain the same.

7. Conclusions

In this paper, most results were related to the WAAS signal characteristics, the navigation message and the integration of the provided corrections, as opposed to previous work focused on the inclusion of WAAS pseudoranges in the navigation solution found in [13] [39], or to the WAAS L5 used in a L5-only PVT solution in [16].

It has been confirmed that, for the time being, WAAS navigation messages are identical on both satellite frequencies, at the time the experiments were conducted (*i.e.* 2012). On top of different spreading codes and rates, WAAS L5 uses Manchester coding to provide sufficient density of transitions to ensure low receiver clock drift likelihood due to lengthy strings of constant bits, while also avoiding data ambiguity; *i.e.* the spreading code period matches that of the transmitted symbol, thus enhancing symbol synchronization in the receiver [38]. It was also demonstrated that the broadcasted information was strongly correlated from one satellite to another and offered similar positioning performances, assuming the same tracking conditions. Speaking of which, WAAS PRN 138 provides a higher signal power on L5 over L1 by ~5.5 dB-Hz, which is enough to avoid the isolated tracking losses witnessed with other WAAS satellites. Nevertheless, measured C/N_0 from the three WAAS satellites was not proportional to their elevation, as seen in **Table 2**, differing from previous findings [24]. Another displayed metric is that the WAAS L1 signal quality, in terms of pseudorange noise, is as good as for GPS L1 C/A, for the same C/N_0. WAAS L5 PRN 138 pseudorange noise is 10 times lower than that of GPS L1 C/A (at the same C/N_0), in conformity with GPS signals [32] [33].

For single frequency receivers, WAAS L1 provides a 50% error reduction, distributed over the ionospheric, slow and fast corrections in a decreasing order of magnitude. A greater impact of WAAS corrections was noticed during the day, although WAAS corrections are still beneficial during the night, due to slow and fast corrections being required all around the clock. Hence, even if mobile devices may need to rationalize their power consumption, a single WAAS channel should be kept active at all times, although a reduced set of features could be considered.

The results presented herein should remain valid until the year 2020. By then, all GPS satellites should broadcast the GPS L5 and new L1C MBOC civil signals, while the GALILEO constellation, providing E1 MBOC and E5A signals among others, should be fully operational. WAAS L5 should then be updated to better support these new signals, hopefully preserving frequency diversity.

Up-coming research will continue assessing WAAS signals' improvement as they are deployed during Phase 4.

References

[1] Braff, R. and Shively, C. (1986) GPS Integrity Channel. *Navigation*, *Journal of the Institute of Navigation*, **32**, 334-350. https://ion.org/publications/abstract.cfm?articleID=100431

[2] Kim, E., Walter, T. and Powell, J.D. (2006) Optimizing WAAS Accuracy/Stability for a Single Frequency Receiver. *Proceedings of the* 19*th International Technical Meeting of the Satellite Division of the Institute of Navigation* (*ION GNSS* 2006), Fort Worth, September 2006, 962-970.

[3] National Coordination Office for Space-Based Positioning Navigation and Timing (2012) Selective Availability. http://www.gps.gov/systems/gps/modernization/sa/

[4] Walter, T., Blanch, J., Phelts, R.E. and Enge, P. (2012) Evolving WAAS to Serve L1/L5 Users. *Navigation*, **59**, 317-327. http://dx.doi.org/10.1002/navi.21

[5] RTCA (2006) Minimum Operational Performance Standards for Global Positioning System/Wide Area Augmentation System Airborne Equipment. Document Number: DO-229D.

[6] Lawrence, D., Bunce, D., Mathur, N.G. and Sigler, C.E. (2007) Wide Area Augmentation System (WAAS)—Program Status. *Proceedings of the* 20*th International Technical Meeting of the Satellite Division of the Institute of Navigation* (*ION GNSS* 2007), The Institute of Navigation, 892-899.

[7] Hathaway, D.H. (2012) The Sunspot Cycle. http://solarscience.msfc.nasa.gov/SunspotCycle.shtml

[8] Gannon, M. (2013) Sun's 2013 Solar Activity Peak Is Weakest in 100 Years. Online. http://www.space.com/21937-sun-solar-weather-peak-is-weak.html

[9] Federal Aviation Administration (2012). Navigation Services—WAAS—News. http://www.faa.gov/about/office_org/headquarters_offices/ato/service_units/techops/navservices/gnss/waas/news/

[10] Fernandez-Prades, C., Presti, L.L. and Falletti, E. (2011) Satellite Radio Localization from GPS to GNSS and Beyond: Novel Technologies and Applications for Civil Mass Market. *Proceedings of the IEEE*, **99**, 1882-1904. http://dx.doi.org/10.1109/JPROC.2011.2158032

[11] Jan, S.-S. (2002) Analysis of a Three-Frequency GPS/WAAS Receiver to Land an Airplane. *Proceedings of the* 15*th International Technical Meeting of the Satellite Division of the Institute of Navigation ION GPS* 2002, Oregon Convention Center, Portland, 24-27 September, 2002, 2576-2586.

[12] Murfin, T. (2012) ION Nashville 2012 Round-Up. GPS World.

http://www.gpsworld.com/ion-nashville-2012-round-up/

[13] Rho, H. and Langley, R.B. (2008) Evaluation of the New WAAS L5 Signal. *Proceedings of ION GNSS* 21*st International Technical Meeting of the Satellite Division of the Institute of Navigation*, Savannah, 16-19 September 2008, 1667-1678.

[14] Hsu, P.-H., Cheung, L. and Grewal, M. (2004) Prototype Test Results of L1/L5 Signals of Future GEO Satellites. *Proceedings of ION GNSS* 17*th International Technical Meeting of the Satellite Division*, Long Beach, 21-24 September, 1359-1366.

[15] Federal Aviation Administration (2011) WAAS Technical Specifications for GEO 5/6/7 Service Lease. Department of Transportation, Vol. WAAS100232, 45.

[16] Chen, Y.H., Juang, J.C., De Lorenzo, D.S., Seo, J., Lo, S., Enge, P., *et al.* (2011) Real-Time Dual-Frequency (L1/L5) GPS/WAAS Software Receiver. *Proceedings of the* 24*th International Technical Meeting of the Satellite Division of the Institute of Navigation* (*ION GNSS* 2011), Oregon Convention Center, Portland, Oregon, 20-23 September 2011, 767-774.

[17] Federal Aviation Administration (2008) Global Positionning System Wide Area Augmentation System (WAAS) Performance Standard. 1st Edition, Department of Transportation, 28.
http://www.gps.gov/technical/ps/2008-WAAS-performance-standard.pdf

[18] Landry, R.J., Fortin, M.A. and Guay, J.C. (2010) Universal Acquisition and Tracking Apparatus for Global Navigation Satellite System (GNSS). Canada Patent No 12/767,773.

[19] Fortin, M.A., Guay, J.C. and Landry, R.J. (2009) Development of a Universal GNSS Tracking Channel. *Proceedings of the* 22*nd International Technical Meeting of the Satellite Division of the Institute of Navigation ION GNSS* 2009, Savannah, GA, 22-25 September 2009, 259-272.

[20] Fortin, M.A., Guay, J.C. and Landry, R.J. (2009) Real-Time Low-Cost Multipath Mitigation Technique Calibrated through Real Data Repeatable Testing. *Proceedings of the* 22*nd International Technical Meeting of the Satellite Division of the Institute of Navigation ION GNSS* 2009, Savannah, Georgia, 22-25 September 2009, 2316-2328.

[21] Guay, J.C., Sauriol, B. and Fortin, M.A. (2008) Real-Time Multipath Monitoring and Characterization with a Variable Spacing Correlator on a FPGA-Based Software GNSS Receiver. *Proceedings of the* 21*st International Technical Meeting of the Satellite Division of the Institute of Navigation ION GNSS* 2008, Savannah, 16-19 September 2008, 2332-2342.

[22] Sauriol, B. and Landry, R.J. (2007) FPGA-Based Architecture for High Throughput, Flexible and Compact Real-Time GNSS Software Defined Receiver. *Proceedings of the* 2007 *National Technical Meeting of the Institute of Navigation*, San Diego, 22-24 January 2007, 708-717.

[23] Radio Technical Commission for Aeronautics Special Committee 159 (2001) Minimum Operational Performance Standards for Global Positioning System/Wide Area Augmentation System Airborne Equipment. RTCA.
http://www.rtca.org/store_product.asp?prodid=817

[24] Langley, R.B. and Rho, H. (2009) Innovation: The WAAS L5 Signal. GPS World.
http://www.gpsworld.com/gnss-system/innovation-the-waas-l5-signal-7047

[25] Issler, J.L., Ries, L., Bourgeade, J.M., Lestarquit, L. and Macabiau, C. (2004) Probabilistic Approach of Frequency Diversity as Interference Mitigation Means. *Proceedings of the* 17*th International Technical Meeting of the Satellite Division of the Institute of Navigation* (*ION GNSS* 2004), Long Beach, CA, 21-24 September 2004, 2136-2145.

[26] Guay, J.C. (2010) Récepteur SBAS-GNSS logiciel pour des applications temps-réel. École de technologie supérieure, Montréal.

[27] Todd, K.M. (2005) Error Correction Coding: Mathematical Methods and Algorithms. Wiley Series Edition, John Wiley & Sons Inc., New Jersey. ISBN: 978-0-471-64800-0.

[28] Federal Aviation Administration (2001) Specification for the Wide Area Augmentation System (WAAS). Department of Transportation, 156.
http://www.faa.gov/about/office_org/headquarters_offices/ato/service_units/techops/navservices/gnss/library/documents/media/waas/2892bC2a.pdf

[29] Julien, O., Macabiau, C., Issler, J.L., Nouvel, O. and Vigneau, W. (2006) Analysis and Quality Study of GNSS Monitoring Ground Stations' Pseudorange and Carrier-Phase Measurements. *Proceedings of the* 19*th International Technical Meeting of the Satellite Division of The Institute of Navigation* (*ION GNSS* 2006), Fort Worth Convention Center, Fort Worth, TX, 26-29 September 2006, 971-980.

[30] Betz, J.W. (2000) Design and Performance of Code Tracking for the GPS M Code Signal. *Proceedings of the* 13*th International Technical Meeting of the Satellite Division of the Institute of Navigation ION GNSS* 2000, Salt Lake City, UT, 19-22 September 2000, 2140-2150.

[31] Ries, L., Lestarquit, L., Armengou-Miret, E., Legrand, F., Vigneau, W., Bourga, C., Erhard, P. and Issler, J.L. (2002) A

Software Simulation Tool for GNSS2 BOC Signals Analysis. *Proceedings of the* 15*th International Technical Meeting of the Satellite Division of the Institute of Navigation ION GNSS* 2002, Institute of Navigation, Portland, OR, 24-27 September 2002, 2225-2239.

[32] ARINC Engineering Services (2005) Navstar GPS Space Segment/User Segment L5 Interfaces. *Interface Specification*, Navstar GPS Joint Program Office, El Segundo, California, 95.

[33] Global Positioning System Wing (GPSW) Systems Engineering & Integration (2010) Navstar GPS Space Segment/ Navigation User Interfaces. Los Angeles Air Force Base, El Segundo, California, 185. http://www.losangeles.af.mil/shared/media/document/AFD-100813-045.pdf

[34] Federal Aviation Administration (2012) Satellite Position and WAAS Status. http://www.nstb.tc.faa.gov/RT_WaasSatelliteStatus.htm

[35] Oolman, L. (2012) Surface Observations. http://weather.uwyo.edu/surface/meteorogram/

[36] El-Rabbany, A. (2002) Introduction to GPS: The Global Positoning System. Mobile communications Series, Boston.

[37] Jan, S.S. (2003) Aircraft Landing Using a Modernized Global Positioning System and the Wide Area Augmentation System. Doctor of Philosophy Thesis, Aeronautics and Astronautics, Stanford University, Stanford.

[38] Van Dierendonck, A.J., Hegarty, C., Niles, R., Morrissey, T. and Reddan, P. (2005) Next Generation Satellite Based Augmentation System (SBAS) Signal Specification. *Proceedings of the* 2005 *National Technical Meeting of the Institute of Navigation*, San Diego, CA, 24-26 January 2005, 371-384.

[39] Schempp, T., Burke, J. and Rubin, A. (2008) WAAS Benefits of GEO Ranging. 21*st International Technical Meeting of the Satellite Division of the Institute of Navigation ION GNSS* 2008, Savannah, GA, 16-19 September 2008, 2000-2007.

BIBLIOGRAPHY

Aarmo, K. A., A. Rinnan, and B. Forsell. 1996. "Method for dissemination of DGPS corrections by FM-RDS and tests of some GPS receivers". In *Proceedings of ION GPS*. (Kansas City, MO, USA 1996), p. 1745-1751. Institute of Navigation, Alexandria, VA, USA.

ARINC Engineering Services. 2013. *Navstar GPS Space Segment/User Segment L1C Interfaces*. online IS-GPS-800D.

Avellone, G., M. Frazzetto, and E. Messina. 2007. "A new waveform family for secondary peaks rejection in code tracking discriminators for Galileo BOC(n,n) modulated signals". In *Institute of Navigation National Technical Meeting, NTM 2007, Jan 22-24 2007*. p. 246-251. Institute of Navigation, Fairfax, VA 22030, United States.

Badke, B. 2009. "Carrier-to-Noise Density and AI for INS/GPS Integration". *Inside GNSS Magazine*, p. 20-24.

Barker, B. C., J. W. Betz, J. E. Clark, J. T. Correia, J. T. Gillis, S. Lazar, K. A. Rehborn, and J. R. Straton. 2000. "Overview of the GPS M Code Signal". <http://www.mitre.org/work/tech_papers/tech_papers_00/betz_overview/betz_overview.pdf>.

Barmettler, A. 2015. "Global Navigation Satellite System GNSS (GPS/GLONASS)". <https://www.calsky.com/cs.cgi/Satellites/12?obs=9418275354346>.

Beaulieu, N. C., A. S. Toms, and D. R. Pauluzzi. 2000. "Comparison of Four SNR Estimators for QPSK Modulations". *IEEE Communications Letters*, vol. 4, n° 2, p. 43-45.

Bello, P. A. and R. L. Fante. 2005. "Code Tracking Performance for Novel Unambiguous M-Code Time Discriminators". In *Institute of Navigation - NTM ION 2005 National Technical Meeting*. p. 293-298. Institute of Navigation, Fairfax, VA 22030, United States.

Benedicto, J., S. Dinwiddy, G. Gatti, R. Lucas, and M. Lugert. 2000. *GALILEO : Satellite System Design and Technology Developments*. Technical report.

Bensky, A., 2008. *Wireless Positioning Technologies and Applications*. 317 p.

Betz, J. W. 2000. "Design and Performance of Code Tracking for the GPS M Code Signal". In *Institute of Navigation - 13th International Technical Meeting of the Satellite Division, ION GNSS 2000*. p. 2140-2150. Institute of Navigation, Fairfax, VA 22030, United States.

Betz, J. W. 2001. "Binary Offset Carrier Modulations for Radionavigation". *Journal of The Institute of Navigation*, vol. 48, n° 4, p. 227-246.

Betz, J. W. and K. R. Kolodziejski. 2000. "Extended Theory of Early-Late Code Tracking for a Bandlimited GPS Receiver". *Journal of The Institute of Navigation*, vol. 47, n° 3, p. 211-226.

Bhola, N., J. Lee, M. Srivastav, and A. G. Dempster. 2006. "The Application of GPS Multipath Mitigation Techniques in BOC Signals". In *Proceedings of IGNSS*.

Bickerstaff, J., R. Frayling-Cork, and T. Haddrell. 2006. "Capture, analysis and mitigation of multipath in a high sensitivity GPS receiver". In *Proceedings of the Institute of Navigation - 19th International Technical Meeting of the Satellite Division, ION GNSS 2006*. (Fort Worth, TX, United States 2006), p. 1696-1705. Institute of Navigation, Fairfax, VA 22030, United States.

Blackroc Technology. 2015. "The GNSS Market". <http://www.blackroc-technology.com/technologies/gnss/market/>.

Blanchard, A., 1976. *Phase-locked loops: Application to coherent receiver design*.

Blunt, P. 2007. "Advanced Global Navigation Satellite System Receiver Design". Doctor of philosophy thesis, University of Surrey, 226 p.

Borre, K. 2001. "Positioning Based on GPS Pseudoranges". <http://old.gps.aau.dk/downloads/dipoli.pdf>.

Bourdeau, F. 2011. *Conception d'une méthode d'acquisition rapide et universelle pour les signaux GNSS*. Technical report.

Burian, A., E. S. Lohan, and M. K. Renfors. 2007. "Efficient delay tracking methods with sidelobes cancellation for BOC-modulated signals". *Eurasip Journal on Wireless Communications and Networking*, vol. 2007, p. 72626.

Chapron, V. 2010. *Développement d'un banc d'essai automatisé d'analyse des performances d'un récepteur GNSS*. Technical report.

Chen, A., D. De Lorenzo, G. X. Gao, P. Enge, and S. Lo. 2007. "GNSS Over China: The Compass MEO Satellite Codes". *Inside GNSS Magazine*, vol. 2, n° 5, p. 36-43.

Chen, Y.-H., J.-C. Juang, D. S. De Lorenzo, J. Seo, S. Lo, P. Enge, and D. M. Akos. 2011. "Real-Time Dual-Frequency (L1/L5) GPS/WAAS Software Receiver". In *Proceedings of the 24th International Technical Meeting of The Satellite Division of the Institute of Navigation (ION GNSS 2011)*. (Oregon Convention Center, Portland, Oregon 2011), p. 767-774. Institute of Navigation.

Chibout, B., C. Macabiau, A.-C. Escher, L. Ries, J.-L. Issler, S. Corrazza, and M. Bousquet. 2007. "Comparison of Acquisition Techniques for GNSS Signal Processing in Geostationary Orbit". In *Proceedings of the 2007 National Technical Meeting of The Institute of Navigation*. p. 637-649.

China Satellite Navigation Office. December 2013. "BeiDou Navigation Satellite System Signal In Space Interface Control Document".

Civil Aviation Authority. 2003. *GPS Integrity and Potential Impact on Aviation Safety*. Technical report.

Constantinescu, A. 2007. "Radiocommunications Spatiales". <https://cours.ele.etsmtl.ca/academique/sys836/>.

Coursey, D. 2009. "Air Force Responds to GPS Outage Concerns". <http://abcnews.go.com/Technology/AheadoftheCurve/story?id=7647002&page=1>.

C/S2ESC - Software & Systems Engineering Standards Committee. 1990. *IEEE Standard Glossary of Software Engineering Terminology*. Technical report. 84 p.

Côté, D. 2010. *Migration, optimisation et développement de nouveaux outils intégrés au logiciel d'interface du Récepteur universel de Systèmes Globaux de Navigation Satellitaire (RxGNSS)*. Technical report.

Côté, D. and M. Andrianarison. September 6th, 2013 2013. *RF Head and related components status*. Technical report. Montréal : École de technologie supérieure.

De Castro, D., J. Diez, A. Fernandez, and J.-M. Sleewaegen. 2006. "A new unambiguous low-complexity BOC tracking technique". In *Institute of Navigation - 19th International Technical Meeting of the Satellite Division, ION GNSS 2006, Sep 26-29 2006*. p. 1830-1835. Institute of Navigation, Fairfax, VA 22030, United States.

Delaporte, T. 2009. "Real-Time Kinematic software using robust Kalman filter and dual-frequency GPS signals for high precision positioning". Memorandum, École de technologie supérieure, Montréal, 155 p.

Diessongo, H. T., H. Bock, T. Schüler, S. Junker, and A. Kiroe. 2012. "Expoiting the Galileo E5 Wideband Signal for Improved Single-Frequency Precise Positioning".

Dovis, F., P. Mulassano, and L. Lo Presti. 2005. "A novel algorithm for the code tracking of BOC(n,n) modulated signals". In *18th International Technical Meeting of the Satellite Division of The Institute of Navigation, ION GNSS 2005, Sep 13-16 2005*. p. 152-155. Institute of Navigation, Fairfax, VA 22030, United States.

Ducharme, M.-A. 2010. *Conception d'un banc d'essais pour le décodage des messages de navigation des systèmes GNSS*. Technical report.

Dussart, S. 2012. *Intégration de signaux Galileo GIOVE-B dans un récepteur GNSS*. Technical report.

El Hatimi, I. 2011. *Mise en œuvre en temps réel d'une solution de navigation GLONASS/GPS*. Technical report.

Enge, P. and F. van Diggelen. 2014. "GPS: An Introduction to Satellite Navigation, with an interactive Worldwide Laboratory using Smartphones". <https://www.coursera.org/course/gpslab>.

European Space Agency. June 2012a. "GLONASS Signal Plan". <http://www.navipedia.net/index.php/GLONASS_Signal_Plan>.

European Space Agency. February 2012b. "NeQuick Ionospheric Model". <http://www.navipedia.net/index.php/NeQuick_Ionospheric_Model>.

European Space Agency. March 2013. "GNSS Basic Observables". <http://www.navipedia.net/index.php/GNSS_Basic_Observables>.

European Space Agency. December 3rd, 2014 2014. "Galileo Satellite Recovered and Transmitting Navigation Signals". <http://www.esa.int/Our_Activities/Navigation/Galileo_satellite_recovered_and_transmitting_navigation_signals>.

European Space Agency. March 13th, 2015 2015. "Sixth Galileo Satellite Reaches Corrected Orbit". <http://www.esa.int/Our_Activities/Navigation/The_future_-_Galileo/Launching_Galileo/Sixth_Galileo_satellite_reaches_corrected_orbit>.

Falletti, E., M. Pini, and L. Lo Presti. 2010. "Carrier-to-Noise Algorithms". *Inside GNSS Magazine*, vol. January-February, p. 22-27.

Fang, H.-r. and D. P. O'Leary. 2006. "Modified Cholesky Algorithms: A Catalog with New Approaches". <http://www.cs.umd.edu/~oleary/tr/tr4807.pdf>.

Fante, R. L. 2003. "Unambiguous Tracker for GPS Binary-Offset-Carrier Signals". In *Institute of Navigation - ION 59th Annual Meeting*. p. 141-145. Institute of Navigation, Fairfax, VA 22030, United States.

Federal Space Agency - Information-analytical centre. 2010. "GLONASS constellation status". <http://www.glonass-center.ru/en/GLONASS/>.

Finck, B. août 2011. "La Russie suspend les vols de Soyouz". <http://www.lapresse.ca/sciences/astronomie-et-espace/201108/25/01-4428754-la-russie-suspend-les-vols-de-soyouz.php?utm_categorieinterne=trafficdrivers&utm_contenuinterne=cyberpresse_B2_sciences_265_accueil_POS1>.

Fine, P. and W. Wilson. 1999. "Tracking Algorithm for GPS Offset Carrier Signals". In *Proceedings of the Institute of Navigation National Technical Meeting, NTM 1999*. p. 671-676. Institute of Navigation, Fairfax, VA 22030, United States.

Fortin, M.-A. and R. J. Landry. 2016. "Implementation Strategies for a Universal Acquisition and Tracking Channel Applied to Real GNSS Signals". *Sensors*, vol. 16, n° 5, p. 624.

Fortin, M.-A., J.-C. Guay, and R. J. Landry. 2009a. "Real-Time Low-Cost Multipath Mitigation Technique Calibrated through Real Data Repeatable Testing". In *Proceedings of the 22nd International Technical Meeting of the Satellite Division of the Institute of Navigation ION GNSS 2009*. (Fort Worth, TX, United States 2009), p. 2316-2328. Institute of Navigation, Fairfax, VA 22030, United States.

Fortin, M.-A., J.-C. Guay, and R. J. Landry. 2009b. "Development of a Universal GNSS Tracking Channel". In *Proceedings of the 22nd International Technical Meeting of the Satellite Division of the Institute of Navigation ION GNSS 2009*. (Fort Worth, TX, United States 2009), p. 259-272. Institute of Navigation, Fairfax, VA 22030, United States.

Fortin, M.-A., I. Ilie, D. Fortin, K. Mollaiyan, and R. J. Landry. 2010. "Wideband Dual-Channel RF Record and Playback for Multi-Constellation Analysis". In *Proceedings of the 23rd International Technical Meeting of the Satellite Division of the Institute of Navigation ION GNSS 2010*. (Fort Worth, TX, United States 2010), p. 879–891. Institute of Navigation, Fairfax, VA 22030, United States.

Fortin, M.-A., J.-C. Guay, and R. J. Landry. 2014. "Single Frequency WAAS Augmentation Observations (L1 vs. L5) on a Ground Based GPS L1 C/A Solution". *Positioning*, vol. 5, p. 70-83.

Fortin, M.-A., F. Bourdeau, and R. J. Landry. 2015. "Implementation Strategies for a Software-Compensated FFT-based Generic Acquisition Architecture with Minimal FPGA Resources". *Journal of The Institute of Navigation*, vol. 62, n° 3, p. 171–188.

Gannon, M. 2013. "Sun's 2013 Solar Activity Peak Is Weakest in 100 Years". <http://www.space.com/21937-sun-solar-weather-peak-is-weak.html>.

Gao, G. X. 2008. "Towards Navigation Based on 120 Satellites: Analyzing the New Signals". Online ph. d. thesis, Stanford University, Stanford. <http://gracegao.ae.illinois.edu/publications//GraceThesiswithSignatureSep122008.pdf>, 161 p.

Garin, L., F. van Diggelen, and J. Rousseau. 1996. "Strobe & Edge Correlator Multipath Mitigation for Code". In *Proceedings of ION GPS–96*. p. 657-664. Institute of Navigation, Fairfax, VA 22030, United States.

Garin, L. J. Munich, July 19-22, 2005 2005. "The "Shaping Correlator", Novel Multipath Mitigation Technique Applicable to GALILEO BOC(1,1) Modulation Waveforms in High Volume Markets". In *Proceedings of the European Navigation Conference GNSS 2005*. p. 16.

Gernot, C., S. K. Shanmugam, K. O'Keefe, and G. Lachapelle. 2007. "A Novel L1 and L2C Combined Detection Scheme for Enhanced GPS Acquisition". In *Proceedings of the 20th International Technical Meeting of the Satellite Division of The Institute of Navigation (ION GNSS 2007)*. p. 219-230. Institute of Navigation, Fairfax, VA 22030, United States.

Gibbons, G. 2009. "GPS SVN49 and L5 Signal: A Success with Problems". <http://www.insidegnss.com/node/1478>.

Gibbons, G. 2012. "Fractured GNSS Fairy Tales". *Inside GNSS*, vol. 7, n° 5, p. 12.

Global Positioning System Wing (GPSW) Systems Engineering & Integration. September 24, 2013. "Navstar GPS Space Segment/Navigation User Interfaces". <http://www.gps.gov/technical/icwg/>.

Gold, R. 1967. "Optimal binary sequences for spread spectrum multiplexing (Corresp.)". *Information Theory, IEEE Transactions on*, vol. 13, n° 4, p. 619-621.

GPS World. 2014. "Activation of Pre-Operational CNAV Message Set for April 28". <http://gpsworld.com/activation-of-pre-operational-cnav-message-set-for-april-28/>.

Guay, J.-C. 2010. "Récepteur SBAS-GNSS logiciel pour des applications temps-réel". Mémoire de maîtrise, École de technologie supérieure, Montréal, 283 p.

Guay, J.-C., B. Sauriol, and M.-A. Fortin. 2008. "Real-Time Multipath Monitoring and Characterization with a Variable Spacing Correlator on a FPGA-Based Software GNSS Receiver". In *Proceedings of the 21st International Technical Meeting of the Satellite Division of the Institute of Navigation ION GNSS 2008*. (Fort Worth, TX, United States 2008), p. 2332-2342. Institute of Navigation, Fairfax, VA 22030, United States.

Hathaway, D. H. 2010. "The Solar Cycle". *Living Revisions*, vol. 7, p. 1-65.

Heiries, V., D. Roviras, L. Ries, and V. Calmettes. 2004. "Analysis of non ambiguous BOC signal acquisition performance". In *17th International Technical Meeting of the Satellite Division of the Institute of Navigation, ION GNSS 2004, Sep 21-24 2004*. p. 2611-2622. Institute of Navigation, Fairfax, VA 22030, United States.

Heiries, V., D. Roviras, V. Calmettes, and L. Ries. 2006. "An enhanced correlation processing multipath mitigation technique for BOC signals". In *2006 IEEE/ION Position, Location, and Navigation Symposium, Apr 25-27 2006*. p. 342-347. Institute of Electrical and Electronics Engineers Inc., Piscataway, NJ 08855-1331, United States.

Hodgart, M. S. and P. D. Blunt. 24 February 2015. *Receiver of binary offset carrier (BOC) modulated signals*. US8964813 B2. Google Patents. <http://www.google.com/patents/US8964813>.

Hodgart, M., P. Blunt, and M. Unwin. 2007. "The optimal dual estimate solution for robust tracking of Binary Offset Carrier (BOC) modulation". In *Proceedings of the 20th International Technical Meeting of the Satellite Division of the Institute of Navigation ION GNSS 2007*. (Fort Worth, TX, United States 2007), p. 1017-1027. Institute of Navigation, Fairfax, VA 22030, United States.

Ilie, I., D. Fortin, A. Leblanc, and M.-A. Fortin. 2008. "Low Cost IF/RF Navigation Validation Platform with Integrated Traffic Message Channel Simulation". In *International Symposium on GPS/GNSS 2008*. p. 407-413. Organization Commitee of International Symposium on GPS/GNSS 2008.

Ilie, I., D. Fortin, and M.-A. Fortin. 2009a. "Multi-channel Record and Playback System for GNSS RF/IF Receivers' Design Validation and Fine-Tuning". In *Proceedings of the 22nd International Technical Meeting of the Satellite Division of the Institute of Navigation ION GNSS 2009*. (Fort Worth, TX, United States 2009), p. 2265-2275. Institute of Navigation, Fairfax, VA 22030, United States.

Ilie, I., D. Fortin, R. J. Landry, and M.-A. Fortin. 2009b. "Real-World Interferences' Impacts Analysis using High Dynamic Range GNSS RF/IF Signals Record and Playback". In *Proceedings of the 22nd International Technical Meeting of the Satellite Division of the Institute of Navigation ION GNSS 2009*. (Fort Worth, TX, United States 2009), p. 38-48. Institute of Navigation, Fairfax, VA 22030, United States.

Ioannides, R. T., L. E. Aguado, and G. Brodin. 2006. "Coherent integration of future GNSS signals". In *Proceedings of the Institute of Navigation - 19th International Technical Meeting of the Satellite Division, ION GNSS 2006*. (Fort Worth, TX, United States 2006), p. 1253-1268. Institute of Navigation, Fairfax, VA 22030, United States.

Irsigler, M. and G. W. Hein. 2005. "Development of a real-time multipath monitor based on multi-correlator observations". In *Proceedings of the 18th International Technical Meeting of the Satellite Division of The Institute of Navigation, ION GNSS 2005, Sep 13-16 2005*. p. 2626-2637. Institute of Navigation, Fairfax, VA 22030, United States.

Julien, O., C. Macabiau, M. E. Cannon, and G. Lachapelle. 2007. "ASPeCT: Unambiguous sine-BOC(n,n) acquisition/tracking technique for navigation applications". *IEEE Transactions on Aerospace and Electronic Systems*, vol. 43, n° 1, p. 150-162.

Kaplan, E. D. and C. Hegarty, 2006. *Understanding GPS principles and applications*. Artech House mobile communications library. ed. Second. Elliott D. Kaplan, ed. ill., Boston, Mass. : Artech House, 680 p.

Kim, S., S. Yoon, and S. Y. Kim. 2007. "A novel multipath mitigated side-peak cancellation scheme for BOC(kn, n) in GNSS". In *9th International Conference on Advanced Communication Technology, ICACT 2007, Feb 12-14 2007*. p. 1258-1262. Institute of Electrical and Electronics Engineers Inc., New York, NY 10016-5997, United States.

Lamontagne, G. 2009. "Conception et Mise en Oeuvre d'une Tête de Réception à Échantillonnage Direct RF pour les Signaux de Radionavigation par Satellite". Mémoire de maîtrise, École de technologie supérieure, Montréal.

Landry, R. J. 1997. "Techniques de robustesse aux brouilleurs pour les récepteurs GPS". Thèse de doctorat en génie, École nationale supérieure de l'aéronautique et de l'espace, Toulouse. <http://books.google.ca/books?id=N3HRNwAACAAJ>, 292 p.

Landry, R. J., M.-A. Fortin, and J.-C. Guay. 26 April 2010. *Universal Acquistion and Tracking Apparatus for Global Navigation Satellite System (GNSS)*. US 8401546 B2. USPTO. <http://www.google.com/patents/US8401546>.

Langley, R. B. and H. Rho. May 2009. "Innovation: The WAAS L5 Signal". *GPS World*.

Lanigan, C. A., K. Pflieger, and P. K. Enge. 1990. "Real-time Differential Global Positioning System (DGPS) data link alternatives". In *Proceedings of ION GPS*. (Colorado Springs, CO, USA 1990), p. 599-606. Publ by Inst of Navigation, Washington, DC, USA.

Lavoie, D. 2013. "Validation et augmentation du réalisme d'un simulateur de constellation GPS LI et évolution vers un simulateur GNSS". Mémoire de maîtrise électronique, École de technologie supérieure, Montréal, 232 p.

Lavoie, P. 2012. "Système de navigation hybride GPS/INS à faible coût pour la navigation robuste en environnement urbain". Mémoire de maîtrise, École de technologies supérieure, Montréal, 314 p.

Lee, Y. C. 2002. "Compatibility of the New Military GPS Signals with Non-Aviation Receivers". In *Institute of Navigation - ION 58th Annual Meeting*. p. 581-597. Institute of Navigation, Fairfax, VA 22030, United States.

Liang, C. and W. Jie. 2012. "Research of Ambiguity Fast Resolution in GPS Orientation Determination". In *The 2nd International Conference on Computer Application and System Modeling*. (Paris, France 2012), p. 1356-1359. Atlantis Press.

Lim, D., S. Moon, C. Park, and S. Lee. April 2006. "L1/L2CS GPS Receiver Implementation with Fast Acquisition Scheme". In *Position, Location, And Navigation Symposium, 2006 IEEE/ION*. p. 840-844. Institute of Navigation, Fairfax, VA 22030, United States.

Liu, M., M.-A. Fortin, and R. J. Landry. 2009. "A Recursive Quasi-optimal Fast Satellite Selection Method for GNSS Receivers". In *Proceedings of the 22nd International Technical Meeting of the Satellite Division of the Institute of Navigation ION GNSS 2009*. (Fort Worth, TX, United States 2009), p. 2061-2071. Institute of Navigation, Fairfax, VA 22030, United States.

Lohan, E. S., A. Lakhzouri, and M. Renfors. 2006. "Feedforward Delay Estimators in Adverse Multipath Propagation for Galileo and Modernized GPS Signals". *EURASIP Journal on Applied Signal Processing*, vol. 2006, p. 1-19.

Martin, N., V. Leblond, G. Guillotel, and V. Heiries. 2003. "BOC(x,y) Signal Acquisition Techniques and Performances". In *Proceedings of the 16th International Technical Meeting of the Satellite Division of the Institute of Navigation ION GPS/GNSS 2003*. p. 188-198. Institute of Navigation, Fairfax, VA 22030, United States.

McGraw, G. A. and M. S. Braasch. 1999. "GNSS Multipath Mitigation Using Gated and High Resolution Correlator Concepts". In *Proceedings of the US Institute of Navigation NTM*. p. 333-342. Institute of Navigation, Fairfax, VA 22030, United States.

Miller, M., T. Nguyen, and C. Yang. 2006. "Symmetric Phase-Only Matched Filter (SPOMF) for frequency-domain software GNSS receivers". In *Record - IEEE PLANS, Position Location and Navigation Symposium*. (San Diego, CA, United States 2006), p. 187-197. Institute of Electrical and Electronics Engineers Inc., Piscataway, NJ 08855-1331, United States.

Misra, P. and P. Enge, 2006. *Global Positioning System: Signals, Measurements, and Performance*. ed. 2e édition. Lincoln, Massachussetts : Ganga-Jamuna Press, 570 p.

Montenbruck, O., M. Garcia-Fernandez, and J. Williams. 2006. "Performance comparison of semicodeless GPS receivers for LEO satellites". *GPS Solutions*, vol. 10, n° 4, p. 249-261.

Morrissey, T. N., K. W. Shallberg, and B. Townsend. 2006. "Code tracking errors for double delta discriminators with narrow correlator spacings and bandlimited receivers". In *Institute of Navigation, National Technical Meeting 2006, NTM, Jan 18-20 2006*. p. 914-926. Institute of Navigation, Fairfax, VA 22030, United States.

Narbaïts-Jauréguy, D. 2009. *Développement d'une tête RF multi-fréquentielle permettant l'acquisition des signaux GNSS par FFT en temps réel*. Technical report.

National Coordination Office for Space-Based Positioning Navigation and Timing. 2001. "Frequently Asked Questions About Selective Availability". <http://www.gps.gov/systems/gps/modernization/sa/faq/>.

National Coordination Office for Space-Based Positioning Navigation and Timing. 2015a. "Space Segment". <http://www.gps.gov/systems/gps/space/>.

National Coordination Office for Space-Based Positioning Navigation and Timing. 2015b. "New Civil Signals". <http://www.gps.gov/systems/gps/modernization/civilsignals/>.

Office of Space Commercialization. 2008. "Public Notice on Continued Support for Semi-Codeless GPS Access Through 2020". <http://www.space.commerce.gov/public-notice-semi-codeless-gps-access-2020/>.

Pany, T. and B. Eissfeller. 2004. "Code and Phase Tracking of Generic PRN Signals with Sub-Nyquist Sample Rates ". *NAVIGATION, Journal of the Institute of Navigation*, vol. 51, p. 143-160.

Pany, T., M. Irsigler, and B. Eissfeller. 2005. "S-curve shaping: A new method for optimum discriminator based code multipath mitigation". In *18th International Technical Meeting of the Satellite Division of The Institute of Navigation, ION GNSS 2005, Sep 13-16 2005*. p. 2139-2154. Institute of Navigation, Fairfax, VA 22030, United States.

Paonni, M., J. A. Avila-Rodriguez, T. Pany, G. W. Hein, and B. Eissfeller. Winter 2008-2009. "Looking for an Optimum S-Curve Shaping of the Different MBOC Implementations". *NAVIGATION, Journal of The Institute of Navigation*, vol. 55, n° 4, p. 255-266.

Pivel, T. 2012. *Démodulation de signaux GPS pour un récepteur GNSS Universel avionique*. Technical report.

PosiTim. May 2010. "Navigation Systems". <http://www.positim.com/compass_overview.html>.

Proakis, J. G. and D. G. Manolakis, 2007. *Digital signal processing*. ed. 4th. 1084 p.

Psiaki, M. L., D. M. Akos, and J. T. Thor. 2005. "A comparison of direct radio frequency sampling and conventional GNSS receiver architectures". *Navigation. Journal of the Institute of Navigation*, vol. 52, n° 2, p. 71-81.

Psiaki, M. L. 2004. "FFT-based acquisition of GPS L2 civilian CM and CL signals". In *Proceedings of the 17th International Technical Meeting of the Satellite Division of the Institute of Navigation, ION GNSS 2004*. (Long Beach, CA, United States 2004), p. 457-473. Institute of Navigation, Fairfax, VA 22030, United States.

Ries, L., L. Lestarquit, E. Armengou-Miret, F. Legrand, W. Vigneau, C. Bourga, P. Erhard, and J. Issler. 2002. "A Software Simulation Tool for GNSS2 BOC Signals Analysis". In *Institute of Navigation - 15th International Technical Meeting of the Satellite Division, ION GNSS 2002*. p. 2225-2239. Institute of Navigation, Fairfax, VA 22030, United States.

Romain, B. 2012. *Analyse de la robustesse d'une solution GPS-WAAS L1 et L5*. Technical report. Montréal : École de technologie supérieure.

Russian Institute of Space Device Engineering. 2008. "GLONASS Interface Control Document Navigational radiosignal in Bands L1, L2". <http://www.spacecorp.ru/upload/iblock/1c4/cgs-aaixymyt%205.1%20ENG%20v%202014.02.18w.pdf>.

Sauriol, B. 2008. "Mise en oeuvre en temp-réel d'un récepteur hybride GPS-Galileo". Mémoire de maîtrise, École de technologies supérieure, Montréal, 329 p.

Sharpe, T., R. Hatch, and F. Nelson. 2000. "John Deere's StarFire System: WADGPS for Precision Agriculture". In *Proceedings of the 13th International Technical Meeting of the Satellite Division of The Institute of Navigation (ION GPS 2000)*. p. 2269-2277. Institute of Navigation, Fairfax, VA 22030, United States.

Siala, M. and R. B. Gibert. 1999. "Semi-blind maximum a posteriori multipath fast fading channel estimation for TDMA systems". In *Vehicular Technology Conference, 1999. VTC 1999 - Fall. IEEE VTS 50th*. p. 466-470.

Simsky, A. juillet-août 2006. "Three's the charm: Triple Frequency Combinations in Future GNSS". *Inside GNSS*, vol. 1, n° 5, p. 38-41.

Sousa, F. M., F. D. Nunes, and J. M. Leitao. 2006. "Strobe pulse design for multipath mitigation in BOC GNSS receivers". In *2006 IEEE/ION Position, Location, and Navigation Symposium, Apr 25-27 2006*. p. 348-355. Institute of Electrical and Electronics Engineers Inc., Piscataway, NJ 08855-1331, United States.

Sousa, F. M. G., F. D. Nunes, and J. M. N. Leitao. 2008. "Code Correlation Reference Waveforms for Multipath Mitigation in MBOC GNSS Receivers". In *Proceedings of the European Navigation Conference ENC-GNSS 2008*. (Toulouse 2008), p. 1 - 10.

Spilker, J. J. and B. W. Parkinson, 1996. *Global Positioning System: Theory and Applications*, volume 1. 823 p.

Spirent Federal Systems. 2014. *Testing Multi-GNSS in an R&D Environment*. Technical report. 26 p.

Thibodeau, G. 2010. *Validation de la mise en forme et du décodage de tous les signaux GNSS civils*. Technical report.

Townsend, B. and P. Fenton. 1994. "A practical approach to the reduction of pseudorange multipath errors in a L1 GPS receiver". In *Proceedings of the 7th International Technical Meeting of The Satellite Division of the Institute of Navigation. Part 1 (of 2), Sep 20-23 1994*. p. 143-148. Inst of Navigation, Alexandria, VA, USA.

Trimble Navigation Limited. 2007. "Error correction". <http://www.trimble.com/gps_tutorial/howgps-error2.aspx>.

Trimble Navigation Limited. 2014. "OmniSTAR HP". <http://www.omnistar.com/>.

Tsui, J. B.-y., 2005. *Fundamentals of global positioning system receivers : a software approach*. Wiley series in microwave and optical engineering. ed. 2nd. New Jersey : John Wiley & Sons Inc., xvi, 352 p.

Urlichich, Y., V. Subbotin, G. Stupak, V. Dvorkin, A. Povalyaev, and S. Karutin. 2011. "Innovation: GLONASS.Developing Strategies for the Future". <http://www.spacecorp.ru/upload/iblock/a57/glonass_eng.pdf>.

U.S. Department of Defense. 2007. "DoD Permanently Discontinues Procurement Of Global Positioning System Selective Availability". <http://www.defense.gov/releases/release.aspx?releaseid=11335>.

U.S. Department of Homeland Security. 2015. "GPS CONSTELLATION STATUS FOR 04/02/2015". <http://www.navcen.uscg.gov/?Do=constellationstatus>.

van Dierendonck, A. J. 2014. "Benefits and Limitations of New GNSS Signal Designs". In *International Technical Symposium on Navigation and Timing*. p. 15. Ecole Nationale de l'Aviation Civile.

van Dierendonck, A. J., P. Fenton, and T. Ford. 1992. "Theory and performance of narrow correlator spacing in a GPS receiver". *Navigation*, vol. 39, n° 3, p. 265-283.

van Diggelen, F., 2009. *A-GPS: Assisted GPS, GNSS, and SBAS*. 399 p.

van Nee, R. D. J., J. Siereveld, P. C. Fenton, and B. R. Townsend. 1994. "Multipath estimating delay lock loop: approaching theoretical accuracy limits". In *Proceedings of the 1994 IEEE Position Location and Navigation Symposium, Apr 11-15 1994*. p. 246-251. IEEE, Piscataway, NJ, USA.

Ávila Rodríguez, J. n. 2014. "MBOC Modulation". <http://www.navipedia.net/index.php/MBOC_Modulation>.

Wallner, S., J.-A. Avila-Rodriguez, G. W. Hein, and J. J. Rushanan. 2007. "Galileo E1 OS and GPS L1C Pseudo Random Noise Codes - Requirements, Generation, Optimization and Comparison". In *Proceedings of the 20th International Technical Meeting of the Satellite Division of The Institute of Navigation (ION GNSS 2007)*. (Fort Worth, TX 2007), p. 1549-1563. Institute of Navigation.

Ward, P. W. 2004. "A design technique to remove the correlation ambiguity in binary offset carrier (BOC) spread spectrum signals". In *Proceedings of the Institute of Navigation, 2004 National Meeting, NTM 2004, Jan 26-28 2004*. p. 886-896. Institute of Navigation, Alexandria, VA 22314, United States.

Xu, G., 2007. *GPS: Theory, Algorithms and Applications*. ed. 2. 340 p.

Yang, C. 2005. "Joint Acquisition of CM and CL Codes for GPS L2 Civil (L2C) Signals". In *Proceedings of the 61st Annual Meeting of The Institute of Navigation* . p. 553-562. Institute of Navigation, Fairfax, VA 22030, United States.

Yang, C. and M. Miller. 2005. "Novel GNSS receiver design based on satellite signal channel transfer function/impulse response". In *Proceedings of the 18th International Technical Meeting of the Satellite Division of The Institute of Navigation, ION GNSS 2005*. (Long Beach, CA, United States 2005), p. 1103-1115. Institute of Navigation, Fairfax, VA 22030, United States.

Yang, C., M. Miller, T. Nguyen, and D. Akos. 2006. "Generalized frequency-domain correlator for software GPS receiver: Preliminary test results and analysis". In *Institute of Navigation - 19th International Technical Meeting of the Satellite Division, ION GNSS 2006, Sep 26-29 2006*. p. 2346-2360. Institute of Navigation, Fairfax, VA 22030, United States.

Zhou, T. 2006. "Modified LLL algorithms". Master's thesis, McGill University, Montreal. <http://digitool.Library.McGill.CA:80/R/-?func=dbin-jump-full&object_id=99356&silo_library=GEN01>.